IMPROVEMENTS RELATING TO ATOMIC SPECTROSCOPIC METHODS AND APPARATUS INCORPORATING AN INDUCTIVELY COUPLED PLASMA

by

STANLEY GREENFIELD. M.I.M., C.Chem., F.R.I.C.

Doctoral Thesis submitted in partial fulfilment of the requirements for the award of Doctor of Philosophy of the Loughborough University of Technology. 17th September, 1979.

Supervisors:

Internal.	(Department of Chemistry)	Professor D. Thorburn Burns, January 1974 to October 1975.
		Professor R. F. Phillips, October 1975 to September 1979.
External.	(Albright & Wilson Ltd.)	Sector Chairman, Mr. H. T. Searle.

ACKNOWLEDGEMENT

The work described in this thesis is entirely original except where due reference is made. No part of it has been previously submitted for any other degree. The work was carried out in the laboratories of the Analytical Services Section of the Specialities Sector of Albright & Wilson Ltd., between January 1974 and September 1979.

I would like to take this opportunity to thank Professor D. Thorburn Burns, whose idea it was that I should attempt a Ph.D. thesis, who was my initial supervisor and has been my mentor throughout. In addition I am most grateful to Professor R. F. Phillips for his constant encouragement and kindness. My thanks are also due to my colleagues at Albright & Wilson, particularly to Hugh McGeachin and Peter Smith for technical assistance and many hours of discussion, Len Brierley, Ernest Hobbs and Arthur Hill for skilled workshop assistance, Peter Sutton and Fred Chambers for standing in when more than two hands were needed, Fred Tromans for help with the drawings and Mary Bodley for the enormous task of typing, and re-typing, the manuscript.

I am grateful to Albright & Wilson Ltd., for financial assistance and the provision of facilities, obtained through the good offices of Mr. H. T. Searle, Sector Chairman, and Mr. K. L. Lloyd, Regional Personnel Manager, who thus made it all possible.

Chapter 5. THE CRITERIA TO BE USED FOR COMPARING PLASMA TORCHES.

Summary.

5.1 The Relationship Between the Net Signal, Net and Gross Signal to Background Ratios and the P.M. tube Amplification and Dark Current.

5.1.1 Intrinsic Merit.

5.1.2 Conditions for Maximum Net Signal (General Case).

5.1.3 Special Case 1. (Any straight line).

5.1.4 Special Case 2. (Straight Line Through the Origin).

5.1.5 Special Case 3. (Horizontal Straight Line).

5.2 Detection Limits.

5.2.1 General Case. Necessary Conditions for the Better Plasma to Give the Better Detection Limit.

5.2.2 General Case. Sufficient Conditions for the Better Plasma to Give Better Detection Limits.

5.2.3 (Linear Cases).

5.2.4 General Case (Same Gain).

5.2.5 The Effect of the Background Factor on the Critical Value of the Dark Current.

5.2.6 Other Factors Affecting the Detection Limit. (Effect of Dark Current).

5.2.7 (Effect of Gain).

5.2.8 (Effect of Sensitivity).

5.2.9 Criterion When Maximum Gain is Used.

5.2.10 Special Case 1. Dark Current versus Gain is a Straight Line Through the Origin.

5.2.11 Special Case 2. Dark Current versus Gain is a Horizontal Straight Line.

Chapter 10. A COMPARISON OF PLASMAS VARIOUSLY PRODUCED.

10.1 Optimisation Using the Signal Divider.

10.1.1 Sodium Results with the Scott Torch.

10.1.2 Sodium Results with the Greenfield Torch.

10.1.3 Sodium Results with the Scott Torch and a New Meinhard Nebuliser.

10.1.4 Sodium Results with the Greenfield Torch and a New Meinhard Nebuliser.

10.1.5 Summary of the Results Obtained on Both Torches and Nebulisers for the Sodium 5896Å line.

10.1.6 Caesium Results with the Scott Torch and Nebuliser No. 1.

10.1.7 Caesium Results with the Greenfield Torch and Nebuliser No. 1.

10.1.8 Caesium Results with the Scott Torch and Nebuliser No. 2.

10.1.9 Caesium Results with the Greenfield Torch and Nebuliser No. 2.

10.1.10 Summary of the Results Obtained on Both Torches and Nebulisers for the Caesium 4555Å line.

10.1.11 Barium Results with the Scott Torch and Nebuliser No. 1.

10.1.12 Barium Results with the Greenfield Torch and Nebuliser No. 1.

10.1.13 Barium Results with the Scott Torch and Nebuliser No. 2.

10.1.14 Barium Results with the Greenfield Torch and Nebuliser No. 2.

10.1.15 Summary of the Results obtained on Both Torches and Nebulisers for the Barium 4554Å line.

10.1.16 Aluminium Results with the Scott Torch and Nebuliser No. 1.

10.1.17 Aluminium Results with the Greenfield Torch and Nebuliser No. 1.

CHAPTER 1

INTRODUCTION

1.1 Plasmas as Excitation Sources

The limitations of flames as excitation sources in spectrochemical analysis are well known and can be placed on a rational basis in the following manner. Since the energy of flames is derived from combustion processes, their temperatures are mainly limited by the heats of combustion of the gases used. The comparatively low temperatures which can be obtained can result in poor sensitivity, which in cases where the line of interest is difficult to excite can be vanishingly small; in addition molecules or radicals containing the analyte atoms may not be dissociated, so that chemical interferences and further loss in sensitivity may be serious. Even the exotic fuel mixtures to which the quest for higher temperatures has led are not hot enough to eliminate these drawbacks. A flame has a maximum achievable temperature reached when the energy released in the combustion process is used solely to heat the products of combustion. In practice this temperature can never be achieved because of energy losses due to radiation and conduction to the surrounding atmosphere. A source where the amount of energy supplied is independent of the mass of gas it heats is not subject to the limitation that each gram of gas has a certain amount of energy available, so that, in principle at least, very much higher temperatures can be obtained. Plasma sources are of this type and the search for higher temperatures was and is the reason for their development and application.

A plasma is a gas, ionised sufficiently for its properties to depend significantly on the ionisation, while macroscopically remaining electrically neutral overall. The plasma state is widespread, occurring in devices as different as fluorescent lamps, nuclear fusion

reactors and stellar atmospheres. Much of the early work on plasmas is reported in the astophysical literature. In the field of spectrochemical analysis the most commonly encountered plasma is the discharge column of any arc no matter how produced. The important property of a plasma as a spectroscopic source is that electric energy can be imparted to the electrons, which can be transferred, by collisions, to the other particles and thereby heating them. In the case of low pressure plasmas electrons can travel relatively long distances when the pressure is low before colliding with an atom and can gain enough energy from the electromagnetic field to produce ions by knocking off an electron, or at least excite the atom to produce light. Therefore these plasmas make excellent light sources as most of the energy is used to produce light rather than heat. An example is the fluorescent tube. With high pressure plasmas, the mean free path is much smaller and there are many times more collisions per atom per second. There are enough collisions to distribute the kinetic energy uniformly among the electrons, atoms and ions. In a high pressure plasma the atoms are therefore not only excited and ionised, but the kinetic energy they possess means that the gas is hot. This is the fundamental difference between high and low pressure plasmas: in the latter the gas temperature is low because of insufficient collisions to distribute the kinetic energy of the electrons. In the DC arc the electrons gain their energy by acceleration in the electric field between the electrodes: in the inductively-coupled plasma sources discussed herein the electrons gain their energy from the high-frequency magnetic field produced by a work-coil energised by a high-frequency power generator.

In a system in thermodynamic equilibrium, the distribution of the kinetic energies of the particles is given by Maxwell's law, the distribution of the populations of the different excited states of the atoms is given by Boltzmann's law, the ionisation equilibrium by Saha's law and the energy distribution of the radiation by Planck's law: the same value of temperature occurs in all these equations. Complete thermodynamic equilibrium[1] never occurs in any observable system but the conditions of local thermodynamic equilibrium, LTE, sometimes do. In LTE, Maxwell's, Boltzmann's and Saha's laws apply to small volumes with the same value of temperature T, but Planck's law is no longer valid. In a further relaxation of conditions it is found that fairly close to LTE, Maxwell's, Boltzmann's and Saha's laws still apply, but with different values of T : Maxwell's law applies to the atoms and heavy ions with a particular value of temperature, the gas or kinetic temperature, Tg, and to the electrons with another value, the electron temperature, Te. The populations of excited levels of different atoms are described by Boltzmann's law with different values of excitation temperature, T_{ex}. For sensitivity in spectrochemical analysis a high excitation temperature is required while for freedom from chemical interferences a high kinetic temperature is needed. The kinetic temperature is always lower than the excitation and electron temperatures unless the system is in LTE when, by definition, they are identical. The principal advantage of using a source in LTE is that such a source would be expected to have a high kinetic temperature and hence a relative freedom from chemical interferences. In small plasmas

1. J. Richter in "Plasma Diagnostics" W. Lochte-Holtgreven, Editor, p.45, North Holland Publishing Co., 1968.

such as those used in the laboratory for spectroscopic sources LTE occurs at high (usually atmospheric) pressure, since then the collision rate is high enough to ensure adequate transfer of energy from the electrons to the heavier particles. In low-pressure plasmas collisions between electrons and atoms are rare, so that the electron temperature is higher than the gas temperature.

All the sources reviewed here have certain features in common. The energy is derived from a high-frequency power oscillator operating at a frequency typically in the range 5 - 50 MHz and with power outputs which can range from a few hundred watts to 15 kW. A work-coil, which usually has two or three turns, but occasionally more, surrounds a quartz tube through which flows a stream of gas. When the work-coil is powered by the oscillator, a strong magnetic field is set up in the tube and any free electrons in the gas absorb energy from the field. Electrons may be produced by the use of a Tesla coil, or by introducing an isolated conductor which when heated by the field, emits electrons. These electrons absorb sufficient energy to produce further electrons by impact ionisation of the gas and a self-sustaining brilliant discharge is set up.

The oscillator and its output circuit may contain only one tuned circuit; in this case a change in the impedance of the plasma alters the frequency of operation but it can be shown both theoretically and practically to have very little effect on the power transferred to the plasma[2]. Alternatively, there may be more than one tuned circuit[3].

2. S. Greenfield, I. Ll. Jones, H. McD. McGeachin and P. B. Smith Analytica Chimica Acta, (1975) 74, 231.

3. U.K. Pat. No. 1,109,602, Fig. 2, 1968.

or there may be a tuned output circuit with a crystal-controlled oscillator[4]. When the frequency of oscillation is controlled by a crystal a change in plasma impedance can only result in a variation of power. A similar effect occurs when there are two tuned circuits unless they are very tightly coupled, i.e. the coefficient of coupling approaches unity.

Argon is the most commonly used gas for plasma generation. A monatomic gas requires less power than a diatomic gas since no dissociation is necessary to achieve a plasma state. Many designs of torch in which the plasma is produced use two or three independently controlled gas streams and diatomic gases are sometimes used in one stream. Helium has been used occasionally but because of its high ionisation potential it is difficult to form a stable discharge in helium unless a high power, high frequency generator is available.

An important reason for the use of more than one gas stream is the control of the shape of the plasma, which is of importance both for sensitivity and stability. If one gas stream is used so that the sample aerosol is mixed with the working gas in which the plasma is formed, emission from the sample atoms occurs throughout the whole volume of the discharge, which is a prolate spheroid. The large volume in which the sample atoms are excited causes the emission from the sample atoms per unit area of surface to be low and results in low sensitivity. A further factor against the use of a single stream is that the presence of sample atoms in the discharge causes changes in its electrical properties, which results in changes in the power dissipated in and hence the stability of the plasma.

4. F. E. Terman "Radio Engineering" McGraw Hill, New York, 1954.

The introduction of a second stream (called the coolant) flowing tangentially round the plasma gas stream modifies the shape of the spheroidal discharge, flattening its base. This makes it easier for a third stream, containing the sample aerosol, to be injected up the axis of the plasma, whose shape is changed to an annulus. The difficulty of injecting an aerosol into a spheroidal plasma is well-known and has been explained in terms of magnetohydrodynamic (M.H.D.) thrust[5]. Measurements of the radial distribution of the magnetic field in the plasma, by means of magnetic probes, have shown it to be at its greatest near the tube walls falling to a low value in the centre. Similarly the magnetic pressure (which is the force exerted on electrically charged particles by the magnetic field) exhibits this drop towards the centre. This drop from the boundaries to the axis will lead to an inward radial flow of plasma by "magnetic pumping". This will build up the kinetic pressure at the axis and cause an axial flow of plasma to both ends from where it will return to the outer boundaries. In this way vortex rings will be formed superimposed on the main axial flow and the thermal expansion of the gas, as is shown in Fig. 1. The use of a coolant makes the injection easier.

5. J. D. Chase, J. Appl. Phys., 1969, 40, 318.

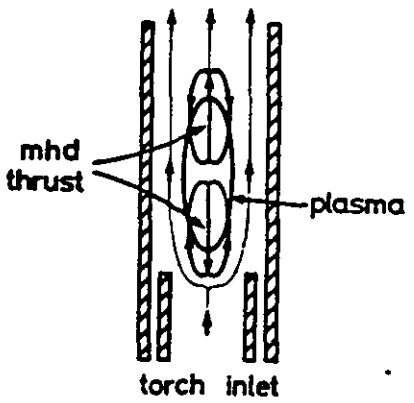

Fig. 1. Showing how the M.H.D. thrust has to be overcome in order to form an annular plasma.

In principle the value of the discharge frequency should influence the ease with which an annular plasma is formed. In high-frequency induction heating of a conductor, the magnetic field falls to a value $^1/_e$ of that at the surface in a distance known as the skin depth, and most of the power absorbed by the conductor is dissipated in this outer layer[6]. The skin depth is inversely proportional to the square root of the frequency, so that the higher the frequency, the more power is dissipated in the outer layer and the formation of a central cooler tunnel becomes easier. In practice, however, some workers have found that the design of the torch and the gas flows are of greater importance than frequency in achieving an annular plasma.

6. P. G. Simpson "Induction Heating" McGraw Hill, New York, 1960.

The shape possessed by an annular plasma confers several advantages. The sample atoms are confined to the central tunnel. Because of the skin effect most of the power is dissipated in the outer layers, whose electrical conductivity is unaltered by the presence of the sample atoms in the tunnel. The power dissipated in the plasma is therefore substantially independent of the nature and concentration of the sample which leads to improved stability. The tail-flame, as the gas stream emerging from a plasma is known, is short, wide and diffuse from a spheroidal plasma; in contrast that from an annular plasma is long, narrow and sharply bounded. The emission per unit surface area is therefore high and sensitivity, signal to concentration ratio, is good when the tail-flame is used as the spectroscopic source. The tail-flame is heated by radiation and conduction from the fire-ball. Since the tail-flame, unlike the plasma fire-ball, emits very little continuum radiation, the background is low and the signal to noise ratios are high.

Since the tunnel of an annular plasma is cooler than the surrounding discharge some of the advantages of a high temperature in breaking up refractory species and so reducing or eliminating chemical interferences may be lost. In practice, however, it is found that if readily attainable powers are employed, the temperature in the tunnel is sufficient to overcome, for example, the formation of a refractory compound between calcium and phosphorus, which results in a diminution of calcium signal[7].

7. S. Greenfield, I. Ll. Jones and C. T. Berry, Analyst., (1964) 89, 713.

1.2 Historical Development of High-Frequency Inductively Coupled Plasma

In any study of inductively coupled plasmas the first papers of interest are those of Babat, who in 1942 published the results of his researches into the properties of electrodeless discharges[8]. This work became more widely known from a later paper[9], which describes and distinguishes between capacitive electrodeless discharges excited by the electric field, and eddy electrodeless discharges excited by the alternating magnetic field. The first type, in which the elementary conductance currents are not closed and are continued by dielectric currents, (i.e. currents which appear to flow through capacitors) were termed "E discharges" : the second type with elementary conductance currents in the form of closed curves were termed "H discharges". It was stated that this distinction was meaningful only if the wave-length of the exciting oscillations exceeded the dimension of the cell containing the plasma. Babat also noted that the higher the frequency of the generator the lower is the current and power consumption required to form a stable plasma and that the tighter the coupling between the inductor and the "gaseous turn" then again the lower the current and power consumption for stability.

This work was followed up by Reed[10] who described an inductively coupled plasma torch (I.C.P.) operating at atmospheric pressure on argon gas and argon mixtures, powered by a 10 kW high frequency 4 MHz power supply.

8. G. I. Babat, Ventn. Elektroprom., 1942, No.2,1; No.3.2.
9. Idem, J. Inst. Elec. Engrs. (London), 1947, 94.
10. T. B. Reed, J. Appl. Phys., 1961, 32, 821.

The torch consisted of a quartz tube with a brass base having one tangential gas entry, placed within the work coil of the generator (Fig. 2). The torch is pointed downwards because it was used for crystal growing.

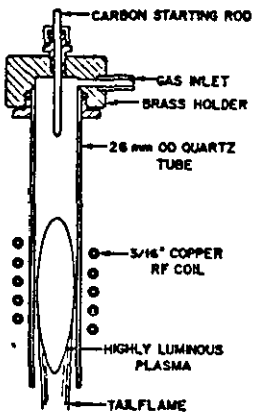

Fig. 2. Early Torch of Reed. Ref. 10.

A pilot plasma was formed by the temporary insertion of a carbon rod into the torch thus producing thermal electrons by heating the carbon in the alternating magnetic field. These electrons provided the initial ionisation of the argon gas enabling coupling to occur between coil and gas, and a plasma to be formed. Reed considered that a tangential gas entry was necessary, in order to create a vortex in the gas stream which would cause some of the plasma to flow counter-current to the stream, and so maintain the plasma. It was found that equally stable plasmas were produced by cylindrical or flat so-called pancake coils, but with the latter system greater emission was obtained. The plasma was operated in argon, and argon mixtures containing 20% air, helium, or hydrogen, or 50% oxygen and was found to be in LTE.

Later in the same year Reed[11] described a torch with three concentric quartz tubes with a centre powder feed for use in crystal growing (Fig. 3).

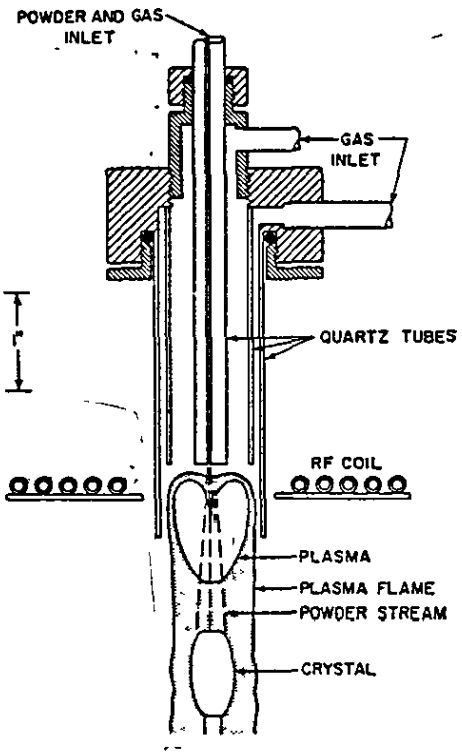

Fig. 3. Torch used by Reed for Crystal Growing. Ref. 11.

Each tube had an independent gas flow : the outermost flow was at high velocity, to recirculate the plasma and to keep the hot discharge away from the outer quartz tube; the plasma was formed in the intermediate gas flow at low velocity; the powder was carried in the innermost, high-velocity, flow. More heat transfer to the powder being volatilised was obtained when mixtures with diatomic gases and helium were used. The main physical properties of these plasmas were described and their possible application as spectral sources for solid samples suggested[12].

11. T. B. Reed, J. Appl. Phys. 1961, 32, 821.

12. T. B. Reed, International Science and Technology, June 1962, 42.

Only brief mention in these papers and in a subsequent patent[13] was made to an annular plasma, formed at a frequency of 100 MHz, with the implication that this shape was undesirable. Although it was claimed possible to inject solid particles into the solid plasma used, it would seem most likely that almost all the material went round the outside of the plasma, forming a broad tail-flame.

A patent application was made in 1963 (issued later as U.K.[14] and U.S.[15] patents) by the present author and his colleagues for a torch adapted for use as a spectroscopic source. This device consisted of three concentric tubes, (Fig. 4). The two outer quartz tubes were used to contain the plasma and the inner tube of borosilicate glass was used to inject an aerosol through the plasma, once it had been formed.

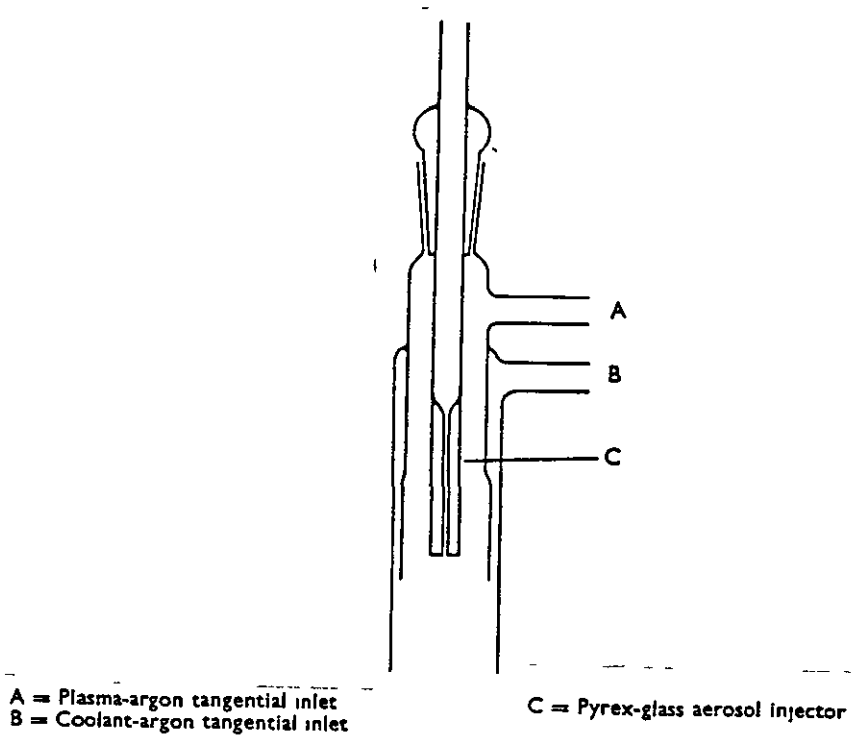

Fig. 4. Early Torch of Greenfield.
Ref. 7.

13. U.S. Pat. 3,324,334, 1967.

14. U.K. Pat. 1,109,602, 1968.

15. U.S. Pat. 3,467,471, 1969.

The torch was concentric with the work-coil of the generator, which in the initial studies was a 2.5 kW, 36 MHz generator. Argon gas was fed tangentially into the inner quartz tube (A) the H.F. field applied by the work coil and a pilot plasma produced by a Tesla coil or by use of a graphite rod as described by Reed[10]. Once the plasma formed, argon gas was introduced tangentially into the outer tube (B) to stabilise the plasma and keep it away from the walls of the cell. A hole was then punched through the flattened base of the plasma by the introduction, through the injector (C) of a sample-containing aerosol in argon gas. The aerosol entered the torch, passed through a tunnel of plasma, and the long narrow tail-flame which resulted was used as the spectroscopic source. Although used initially with the tail-flame pointing downwards it was later inverted and used with the tail-flame issuing upwards.

The use of this device was described in 1964[67]; this is the earliest reference to the application of such a cell with an annular plasma and the utilization of the emission from the tail-flame, remote from the intense and continuous emission from the plasma. The merits of this torch stem from the annular shape of the plasma which, as mentioned in section 1.1, gives excellent stability and sensitivity. Orders of magnitude for unoptimised detection limits indicated that the source was capable of high sensitivity. Further it was also established that the source exhibited freedom from matrix effects; for example, the well known interference of phosphorus and aluminium on the emission of calcium found in normal flames, was completely eliminated. The introduction of gases, vapours, aerosols, liquids, powdered solids and slurries were all shown to be possible.

In 1965 Wendt and Fassel[16] described an inductively coupled plasma torch (I.C.P.) (Fig. 5) with laminar flow for which was claimed

16. R. H. Wendt and V. A. Fassel, Anal. Chem., 1965, 37, 920.

the advantages of less turbulance and greater stability than was obtained with vortex flow. This device was used with a 3.4 MHz, 5 kW generator.

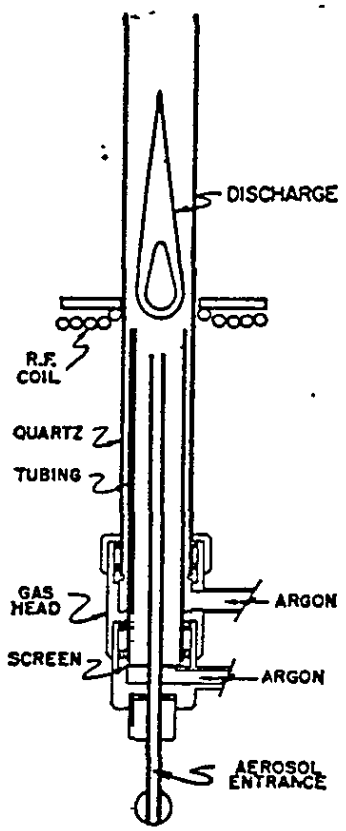

Fig. 5. Torch of Wendt and Fassel. Ref. 16.

It was stated that whereas tangential entry of the gases tended to cause sample particles to be thrown onto the walls of the cell, because of the vortex formed in the gas stream, laminar flow did not. This effect is understandable for the solid type of plasma which they studied, where the sample aerosol flows round the outside of the plasma. In this study the emission was viewed through the quartz tube, from a part of the plasma not in contact with the atmosphere and it was suggested that this reduced the N_2^+ radiation. The detection limits quoted were very low.

In view of the solid type of plasma employed it is probable that their use of an ultrasonic nebuliser contributed greatly to achieving such low detection limits.

The present author and co-workers at that time[17] described the effect of different gases, gas-flows and generator power on the emission observed with their system with annular plasma. It was found that the intensity decreased with the injector gas in the order Ar > N_2 > Air > O_2. Oxygen, if used, had the advantage of removing C-C bands. The intensity decreased as the plasma gas was changed in the order Ar/N_2 > O_2/Ar > He> Ar. It was also noted that only a limited quantity of a diatomic gas, which requires to be dissociated, could be used with the power then available (2.5 kW) and it was concluded that a bigger generator was desirable, to enable a plasma to be run on nitrogen. High speed cine films of the plasma demonstrated that, in the absence of smoothing in the rectification circuit, the plasma was extinguished in every half cycle of the mains frequency. This effect was potentially helpful in that it was used instead of a chopper to allow a.c. amplification of the photo-transistor signals in a simple filter photometer. It was suggested that several of these simple monitors could be grouped around a plasma to allow the simultaneous non-dispersive determination of a number of elements. A further suggestion was that a stroboscope could be used to select one stage in the growth of the plasma and hence possibly select a particular source temperature.

Later, in 1965, the present author et al published[18] preliminary studies made with a larger generator (6.0 MHz, 25 kW) using a similar

17. S. Greenfield, I. Ll. Jones, C. T. Berry and L. G. Bunch, Proc., Soc., Anal. Chem., 1965, 2, 111.

18. S. Greenfield, C. T. Berry and L. G. Bunch, Spectroscopy with a High Frequency Plasma Torch, Radyne Publication, 1965.

cell and plasma configuration to that previously described. It was observed that the spectra changed from those expected from a flame to those normally obtainable from a spark as the power in the plasma, measured by a calorimetric method[19], was increased up to 6.4 kW. The detection limits obtained for a number of elements were one or two orders of magnitude better than those obtained with a D.C. arc and Hilger & Watts Large Quartz Spectrograph. A variation in sensitivity with observation height in the tail-flame was noted. Analyses of industrial materials were reported for the first time; these were the determination of aluminium in a phosphate rock using a 3 kW, 36 MHz generator and an Optica CF4N1 spectrophotometer and the determination of phosphorus in phosphate rock using a 25 kW, 6 MHz generator and a Hilger & Watts Large Quartz spectrograph. Coefficients of variation (C.O.V.) of 5%, for aluminium at a level of 0.9% w/w, and 2.75%, for phosphorus at a level of 15% w/w were obtained.

Dunken and Pforr[20] used a three tube torch with a 1-2 kW, 40 MHz generator and an ultrasonic nebuliser. Liquids and solids were introduced into the plasma in an argon stream but the shape of the plasma was not described. Both atomic and ionic lines of the introduced elements were found in the spectrum and each showed very good signal to background ratios. The only spectra observed without a sample were atomic argon lines, one OH band and four CN bands.

The torch described by Britske et al[21] consisted of a single tube with branch pieces with quartz windows, powered by a 4 kW, 40 MHz generator.

19. British Standard Specification, B.S. 1799 : 1952.

20. H. Dunken and G. Pforr, Z. Chem., 1966, 6, 278.

21. M. E. Britske, V. M. Borisov and Yu. S. Sukach, Zavodsk. Lab., 1967, 33, 252.

This torch had the disadvantage of fixed viewing positions and therefore optimisation of viewing position is not possible. As shown in Fig. 6.

1) Torch body.
2) Work Coil.
3) Quartz Windows.
4) Nebuliser.
5) Spray Chamber.

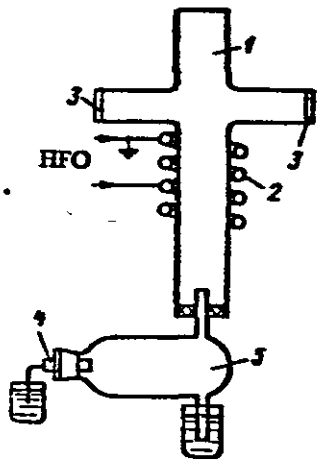

Fig. 6. Torch of Britske. Ref. 21.

The plasma was described as a long 'filament' (15 cm) surrounded by a weak glow; when the power was reduced the filament disappears and the glow filled the tube uniformly. Only readily excited lines were observed in the glow, while lines corresponding to high excitation energies were observable in the 'filament'. This discharge differs markedly from most I.C.P. and was later[22] compared with capacitive discharge. The stability of emission intensity was reported to be 1-2%, but the analytical sensitivity was low.

22. M. E. Britske and Yu. S. Sukach in Primen, Plazmatrona Spektrosk., Mater. Vses. Simp. 1968. Zh. Zheenbaev Ed., p.96, "Ilim" Frunze USSR, 1970.

An ultrasonic nebuliser with a facility for rapid and easy sample changing was used in conjunction with a 2.5 kW, 36 MHz generator and plasma torch of three tube design, by Hoare and Mostyn[23]. The sample vessel incorporated several cells which could be rotated in turn to connect automatically with the sample injection gas flow and to locate automatically in the focussed ultrasonic beam. Shown in Fig. 7.

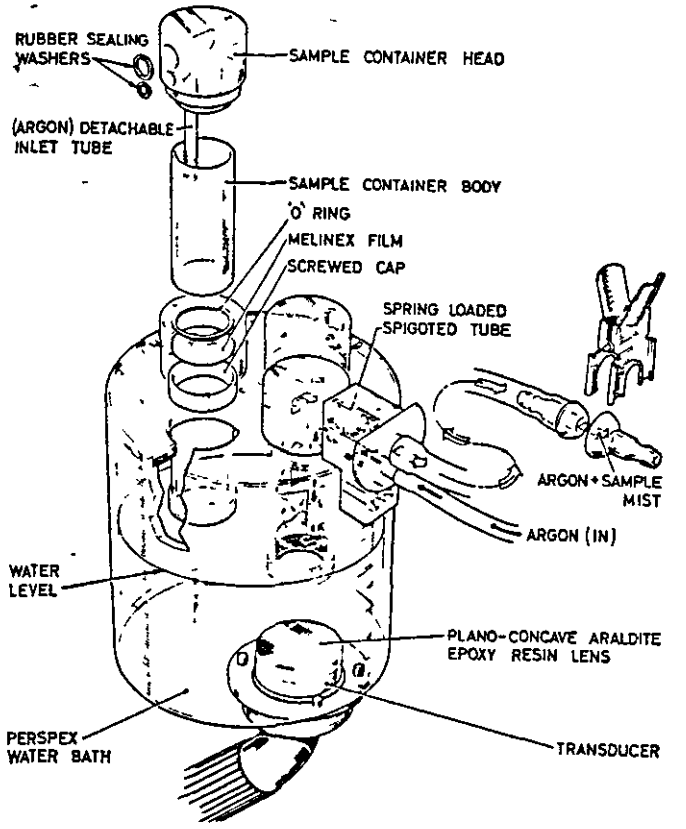

Fig. 7. Ultrasonic Nebuliser. Ref. 23.

There was no interruption of the plasma discharge during sample changeover and a highly reproducible sample flow rate was claimed. A powder injection system was also described ; the injector gas flow

23. H. C. Hoare and R. A. Mostyn, Anal. Chem. 1967, 39, 1153.

was capable of carrying solid material from a vibrated container to the plasma, Fig. 8, The powder system whilst very effective for qualitative work did not give quantitative results.

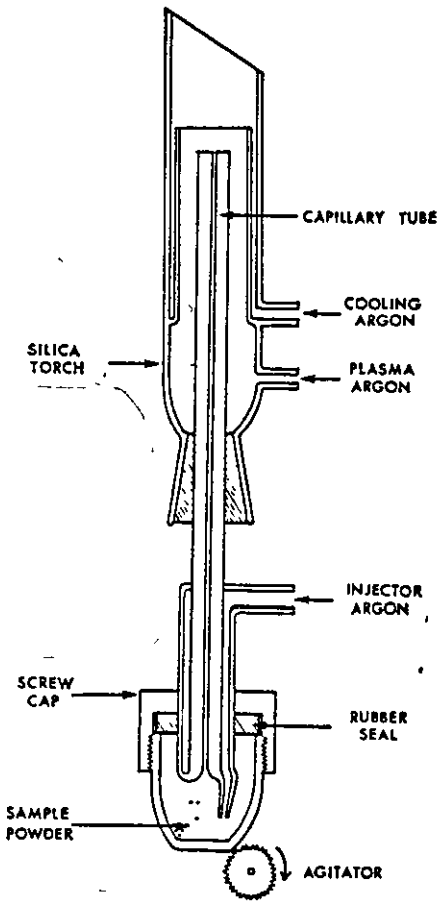

Fig. 8. Powder Injection System. Ref. 23.

Freedom from matrix effects were reported for both solid and solution samples. Boron and zinc in nickel alloys were determined after suitable disolution. It was claimed that cutting the top of the quartz discharge tube at an angle of 45° (to improve the view of part of the plasma) also led to improved stability in the plasma flame.

An early practical application was by Pforr [24] using a previously described torch[19], Fig. 9.

1) Coolant Gas.
2) Plasma Gas.
3) Aerosol Injection.

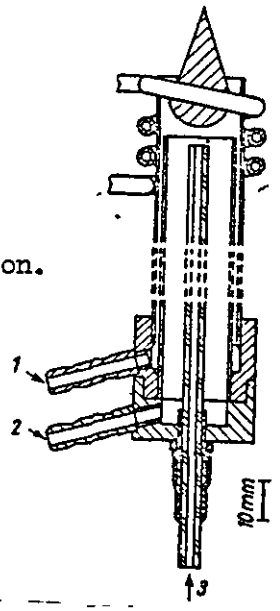

Fig. 9. Torch used by Dunken and Pforr. Ref. 20.

He found that the stability of the emission depended on the gas flows and that it was not possible to vary these completely independently if stability was to be maintained. In particular the carrier gas flow had to be kept small. This compromised the efficiency of nebulisation so that a system was devised using a high flow of carrier gas in the nebuliser and subsequently diverting part of it from the torch. The application was to the analysis of oil and a motor driven syringe was used to supply the sample to the nebuliser, thereby reducing the effects of the viscosity of the sample. Aluminium, iron and nickel were determined. From the diagram (Fig. 9) it appears that the plasma was not annular in shape.

24. G. Pforr, 9th International Symposium, Leipzig, Lubricants, Lubrication and Bearing Techniques, 1967.

A two tube torch was used by Mermet and Robin[25] Fig. 10 who demonstrated that greater sensitivity was obtained when an aerosol was injected into the plasma by means of an injector, rather than when fed into the plasma gas stream. The injector was water cooled.

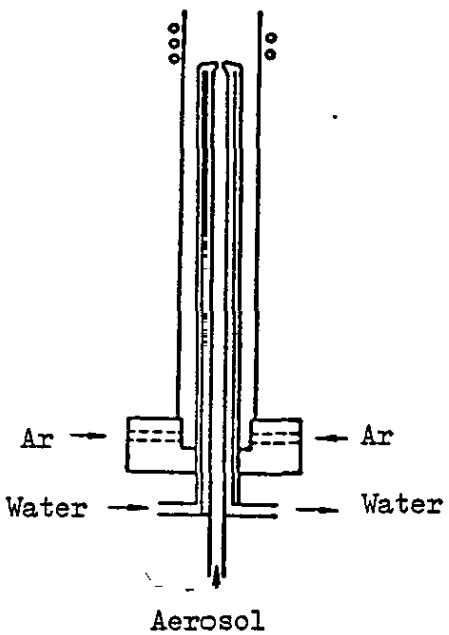

Fig. 10. Torch of Mermet and Robin. Ref. 25.

At low injector gas velocities, the aerosol was entrained on the periphery of the plasma, whilst at higher velocities it penetrated the discharge to give a darker zone at the centre apparently forming an annular plasma. This can be explained in terms of difficulty of injection into a plasma which has been already mentioned and discussed in terms of M.H.D. thrust. It was noted that the amount of aerosol influenced the electrical properties of the plasma so that the power dissipated in it was dependent on the rate of generation of aerosol. This effect would not be expected if the aerosol passed through a tunnel in an annular plasma.

25. J. M. Mermet and J. Robin; Proc. Colloq. Spectrosc. Int. 14th., 1967, 2, 715.

The present author considers that there are two factors which might explain this apparent anomaly. Firstly the frequency used (1.6 MHz) is unusually low so that the skin depth is relatively large and hence the tunnel therefore may not be electrically screened. The second factor is that at an injector-gas flow rate of less than 0.8 ℓ/min., all the aerosol flowed round the outside of the plasma, at 1.0 ℓ/min. the dependence of power on aerosol uptake was very marked but at 1.5 ℓ/min. it was much less so. It is thus suggested herein that at these particular injector-gas flow rates, only part of the aerosol traverses the tunnel and the rest flows round the outside, and that still higher injector-gas flow rate is required to ensure that all the aerosol traverses the tunnel.

Veillon and Margoshes[26] were the first to report matrix effects using a plasma torch. A two tube torch similar to that of Fassel[16] was used, Fig. 11. The central injector was omitted which it was claimed, did not affect the performance of the torch. The advantages of an annular plasma were not appreciated and it now seems likely that the explanation of the apparent matrix effects was that the electrical properties of the discharge were modified by the sample aerosol flowing round it, thereby altering the power dissipated and hence the temperature. In addition it is probable that the temperature encountered in the external path was insufficient to dissociate refractory species.

26. C. Veillon and M. Margoshes, Spectrochim, Acta, 1968, 23B, 503.

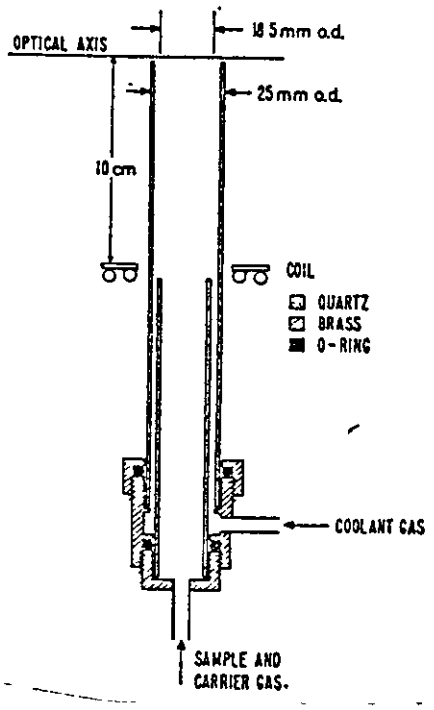

Fig. 11. Torch of Veillon and Margoshes. Ref. 26.

An account of the ultrasonic nebulisation of molten metal into a previously described torch[16], Fig. 12, was given by Fassel and Dickinson[27] but with a variable frequency generator, operating at 30 MHz, 2.5 kW nominal. Arsenic and copper in tin-base solders were determined.

27. V. A. Fassel and G. W. Dickinson, Anal. Chem., 1968, 40, 247.

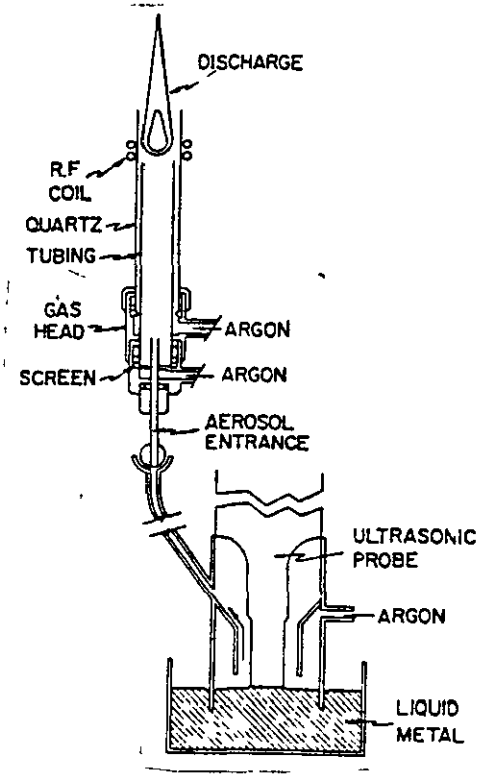

Fig. 12. Ultrasonic Nebuliser, for Liquid Metal, and High Frequency Torch of Fassel, Ref. 27.

In 1969 Dickinson and Fassel[28] gave an account of their continuing investigations into the analytical applications of plasma torches. At this stage they had recognised the importance of an annular plasma[7, 14, 15] and suggested that increasing the frequency of the generator used should produce an annular plasma because of the skin depth effect. It was also suggested that the introduction of material into a plasma produces a mismatch between the plasma and generator, thus decreasing the amount of power transferred to the plasma. The use of a coupling unit was

28. G. W. Dickinson and V. A. Fassel, Anal. Chem. 1969, 41, 1021.

advocated; the use of this device enabled the introduction of three times as much material as was previously possible through the plasma. The matrix effects reported by Veillon and Margoshes were ascribed to the experimental conditions used by these workers. More detailed comments were recently made[29] and the work of the present author et al[6] on freedom from matrix effects confirmed.

An innovation was made by Kleinmann and Svoboda[30] using a low power (120 - 220 W) generator at 40 MHz and a single-tube torch, Fig. 13 with separate vaporisation of the sample. Later it was demonstrated[31] that this low power plasma, electron density 4×10^{14} cm^{-3} was not in local thermodynamic equilibrium, the electron temperature (11,400 K) being much higher than the gas temperature (about 2,200 K).

29. G. F. Larson, V. A. Fassel, R. H. Scott and R. N. Knisely, Ibid., 1975, 47, 328.

30. I. Kleinmann and V. Svoboda, Ibid., 1969, 41, 1021.

31. I Kleinmann and J. Cajko, Spectrochim. Acta., 1970, 25B, 657.

1) Graphite support.
2) Tantalum holder.
3) Quartz tube.
4) Copper cone.
5) O-ring.
6) Brass mantle.
7) Gas port.
8) Teflon gaskets.
11)
9) Cable lug.
10) Cooling water
12) ports.
13) Auto-transformer.

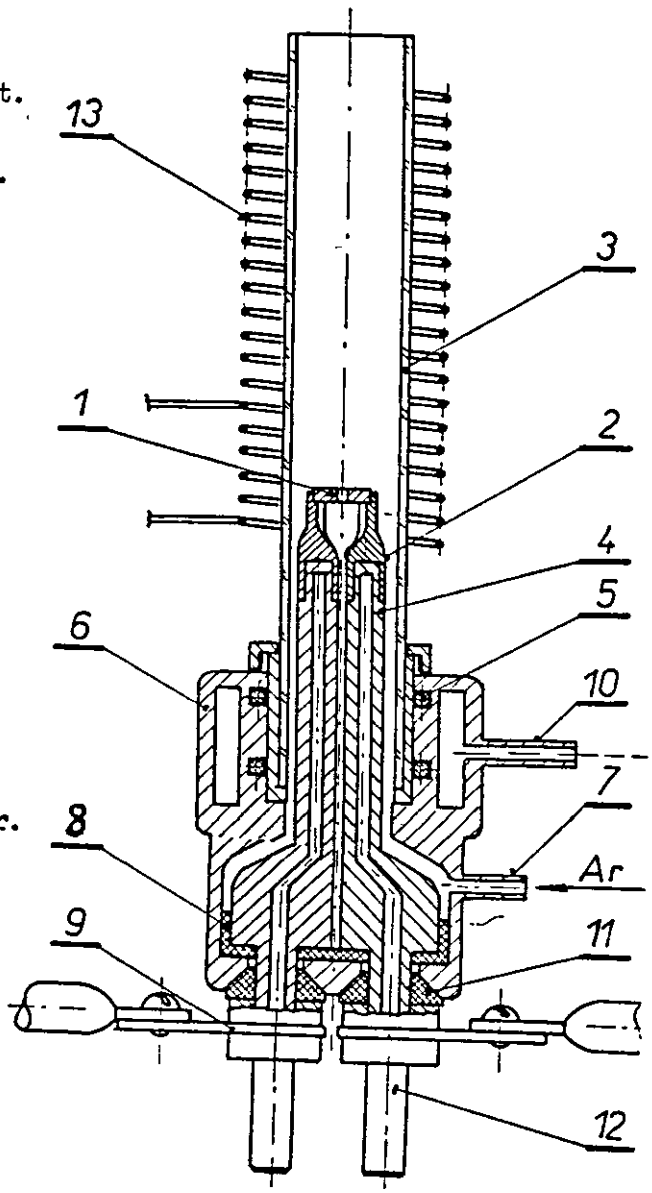

Fig. 13. Plasma Torch with separate Vaporisation of Sample. Kleinmann & Svoboda, Ref. 30.

Truitt and Robinson[32, 33], described the introduction of organic material into a torch similar to that of Wendt and Fassel [16] but with a much longer outer tube, Fig. 14 under a number of plasma conditions.

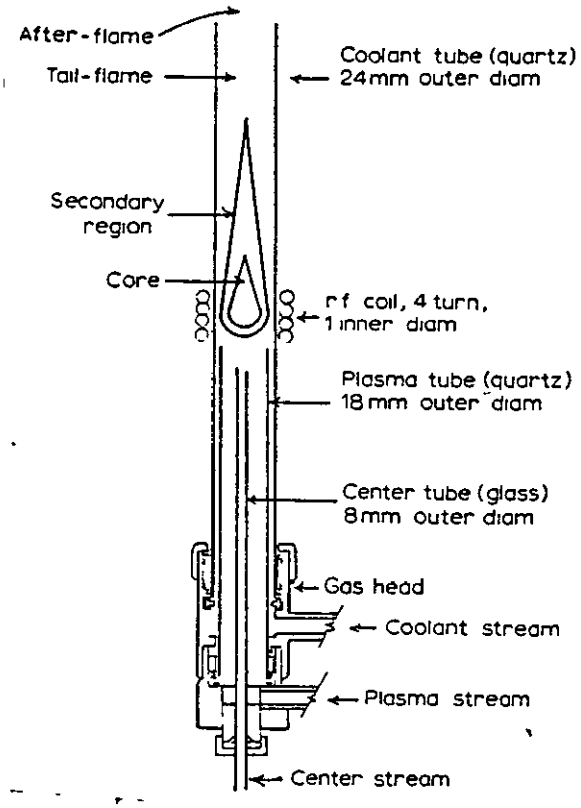

Fig. 14. Torch of Truitt and Robinson. Ref. 32, 33.

32. D. Truitt and J. W. Robinson, Anal. Chim. Acta. 1970, 49, 401.

33. Idem. ibid., 1970, 51, 61.

It was claimed that the torch gave a lower continuum and greater freedom from spectral band structure than that of the present author et al[7]. This was later disputed on the basis of experimental spectra recorded using various length torches[34]. It was suggested that the results described by Truitt and Robinson[32, 33], were probably peculiar to the equipment used; the plasma did not appear to be annular and it was reported that the wall of the torch melted if power above 1.7 kW were used, probably as a consequence of its length. In the earlier paper[32], OH bands at 3064 and 2800A, Balmer series H lines, N^+, NO, N_2^+ were found in the spectra. In the later paper, following the introduction of typical hydrocarbons, four molecular fragments C, H, C_2 and CN were found in the spectra; the point of introduction of the sample made no difference to the emission. The addition of nitrogen increased the CN and decreased the C intensity, oxygen diminished CN and C_2 intensities because of oxidation to CO or CO_2. However, when CO or CO_2 was added their emission bands were not observed. As well as the expected increase in emission from atomic C and Ar, the intensities of the CN and C_2 band system also increased with power; this is unusual since increased power usually causes increased dissociation of molecular species.

Pforr and Aribot[35] studied the introduction of solids and viscous liquids to a plasma torch. Rods of metallic materials were unsuitable samples to introduce directly into the plasma because of their high thermal conductivity, but rods of glass and quartz could be used as samples for the determination of major components, but much greater sensitivity was obtained by blowing powdered samples into the plasma. Calcium, magnesium, titanium, iron and aluminium were determined in quartz powders at concentrations of a few parts per million.

34. S. Greenfield and P. B. Smith, Anal. Chim. Acta. 1971, 57, 209.
35. G. Pforr and O. Aribot, Z. Chem. 1970, 10, 78.

Borms et al[36] compared a I.C.P. with flame emission. Despite difficulty in operating their I.C.P. due to lack of stability, they reported detection limits for a number of elements of 0.01 to 1 ppm; they found the analytical curves were linear over three orders of magnitude, that 1,000 ppm of aluminium, sodium and phosphate did not mutually interfere and that a 1,000 fold excess of calcium gave enhancement for some elements.

A table of spectra observed with a plasma torch operating with nitrogen, argon and oxygen coolant gases was given in a review[37] with the relative exposure times to give comparable background in parts of the spectrum free from banding for the different coolant gases these were nitrogen 60 secs., oxygen 30 secs. and argon 7.5 secs. Under favourable conditions C.O.V. of the order of 0.3% are obtainable.

A demountable, laminar flow torch using nitrogen as coolant was described by Dagnall et al[38], Fig. 15 for use in experiments with the injection of powders into annular plasmas.

36. A. G. J. Borms, G. R. Kornblum and L. DeGalan, Proc. Third Int. Congr. At. Absorption. At. Fluorescence Spectrom. Paris 1971, Vol. 1, p.53, Hilger, London, 1973.

37. S. Greenfield, Metron, 1971, 3, 224.

38. R. M. Dagnall, D. J. Smith, T. S. West and S. Greenfield, Anal. Chim. Acta. 1971, 54, 397.

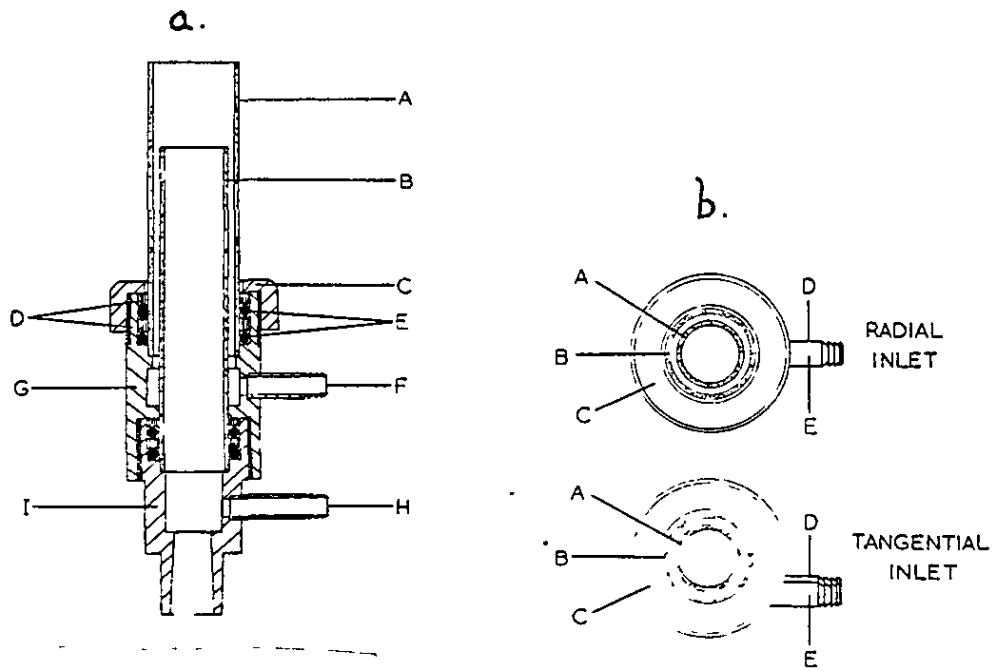

a. Demountable plasma torch (A) Outer silica tube (B) inner silica tube, (C) locking cap, (D) spacer ring, (E) rubber "O" ring, (F) coolant gas inlet, (G) upper body (H) plasma gas inlet, (I) lower body with B14 socket

b. Radial and tangential injection of plasma and cooling gases (A) Inner silica tube, (B) outer silica tube, (C) torch body, (D) plasma gas inlet, (E) coolant gas inlet

Fig. 15. Demountable Plasma Torch. Ref. 38.

It was reported that only one direction of winding of the work coil, the opposite to that of the gas vortex, would allow of coupling with the H.F. field.

Kleinmann and Polej[39] reviewed capacitively coupled and inductively coupled high frequency plasma torches and microwave torches, from the point of view of the requirements of a source and the type of discharge obtained. In commenting on tangential and laminar flow systems they, like earlier workers[16], overlooked the fact that particles would not be thrown onto the torch walls by vortex flow, if they are fed through the centre of an annular plasma.

39. I. Kleinmann and B. Polej, Chem. Listy, 1971, 65, 1.

Triche et al[40] introduced powders into a single-tube torch, Fig.16. Results were not quantitative and difficulty was experienced in penetrating the solid plasma. An attempt was made to relate the position of maximum emission to the ionization potential of the element under examination, but it was necessary to take into account the excitation potentials as well. Later the effect on the emission of varying the quantity of liquid sample aspirated was examined[41].

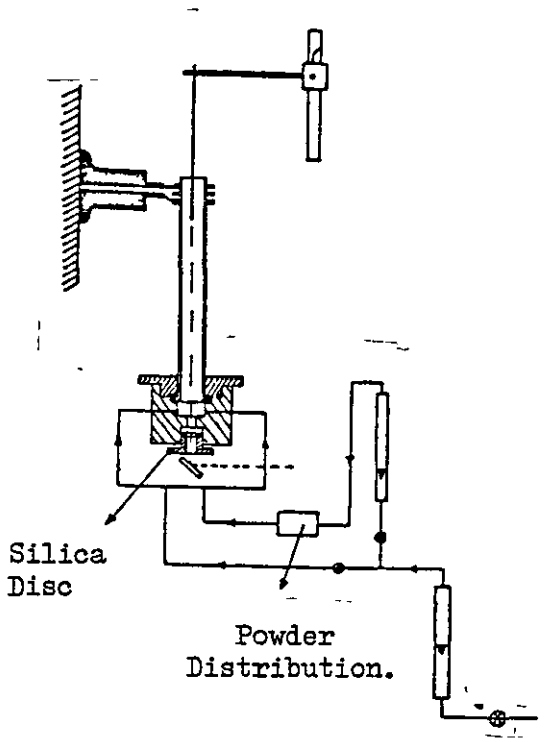

Fig. 16. Torch of Triche. Ref. 40, 41.

40. H. Triche, A. Saadate and J. Besombes-Vailhe Methodes Physiques D'Analyse, 1972, 8, 26.

41. H. Triche, A. Saadate, B. Talayrach and J. Besombes-Vailhe. Anulusis, 1972, 1, 413.

A 6.6 kW, 5.4 MHz generator with a three-tube torch and a water-cooled metal injector Fig. 17 was used by Souilliart and Robin[42] to determine rare earths in an iron matrix. Having been troubled by changes in resistivity of their plasma when an aerosol was introduced they employed an infrared desolvation furnace followed by a condenser to remove water from their ultrasonically generated aerosol. The present author would expect such changes in resistivity unless an annular plasma is used.

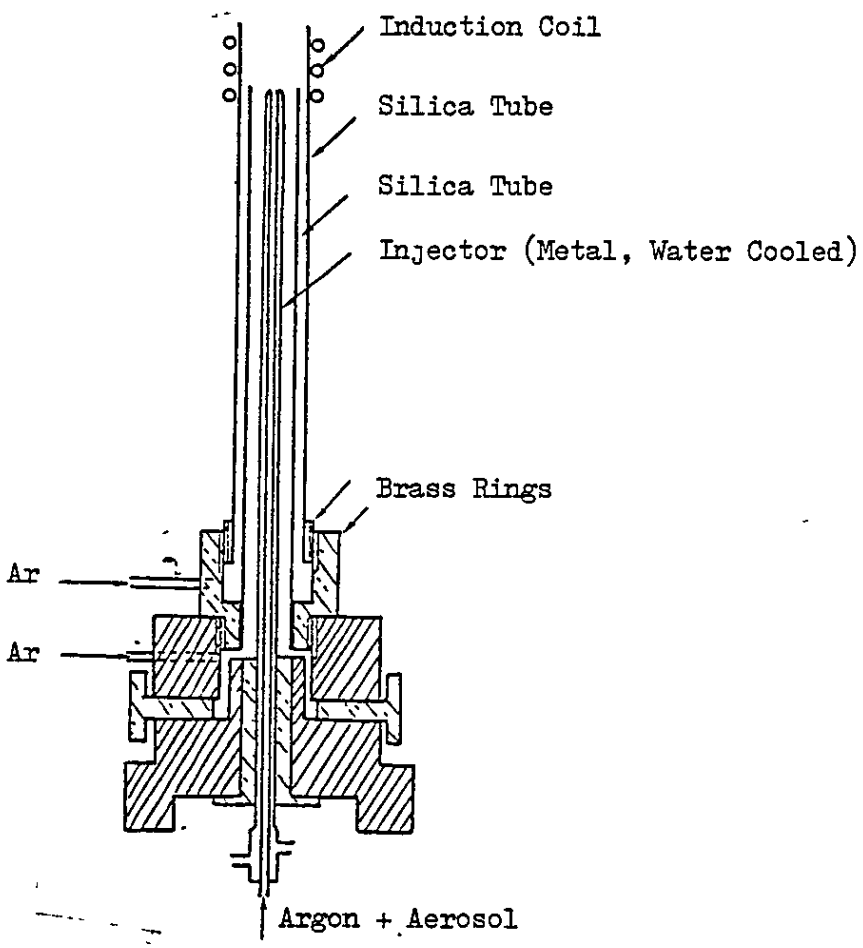

Fig. 17. Torch of Souilliart. Ref. 42.

42. J. C. Souilliart and J. P. Robin, Analusis, 1972, 1, 413.

The extreme sensitivity and versatility of the I.C.P. was further demonstrated by the present author and Smith[43], when it was shown that determinations at the ppm level could be carried out on micro-litre quantities of sample. Limits of detection for barium, 1.7×10^{-10} g, and aluminium, 1.1×10^{-9} g were obtained with precisions between 3 - 5% relative. Examples were given of applications to the determination of trace elements in oil, organic compounds and blood.

Boumans and de Boer[44] compared an I.C.P. . Fig. 18 with a nitrous oxide - acetylene flame and gave detection limits for an argon plasma.

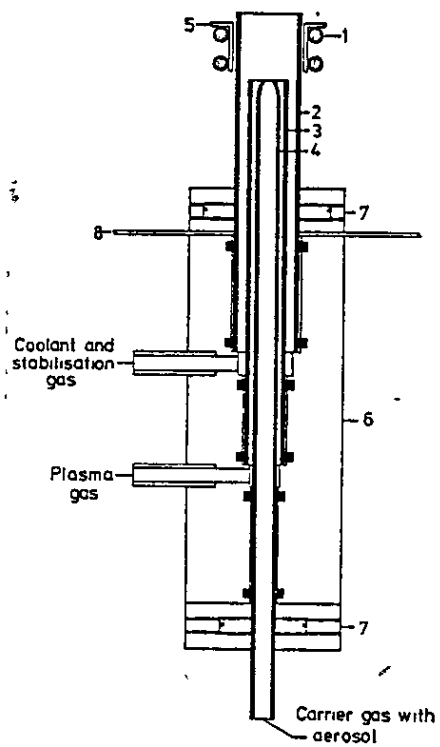

Fig. 18. Plasma tube assembly (schematic).
1. Two-turn, water-cooled induction coil;
2. Coolant tube; 3. Plasma tube;
4. Aerosol tube; 5. Quartz collar;
6. Plexiglass base; 7. Centering screws;
8. Bottom of plasma torch chamber. Ref. 44.

43. S. Greenfield and P. B. Smith, Anal. Chim. Acta. 1972, 59, 341.

44. P. W. J. M. Boumans and F. J. de Boer, Spectrochim. Acta., 1972, 27B, 391.

The stability of the plasma with this system was found to be comparable with that of the flame. It was stated that the lowest detection limit was not always associated with the operating conditions that gave the highest line-to-background ratio. For certain elements it was found that both line-to-background ratio and the noise level decreased when the observation zone was lower in the tail-flame. Since a decrease in line-to-background ratio and a decrease in noise level have opposite effects on the detection limit it is consistent that observed detection limit of the elements considered did not vary markedly with the location of the observation zone. Limits of detection were defined by representing the analytical curve in the vicinity of the detection limit as a straight line.

The application of plasma torches to non-metals (where the best lines have short wavelengths which are absorbed by air) has been made by using a monochromator with a nitrogen path between it and a plasma torch, Fig. 19. Kirkbright et al[45] were able to obtain D.L. for sulphur at a wavelength of 2149A of 1.7 ppm and 0.15 ppm respectively. The linear range for both extended over five orders of magnitude, to beyond 1,000 ppm. The analysis of soil extract for phosphorus was reported, coefficients of variation were 3-7%.

45. G. F. Kirkbright, A. F. Ward and T. S. West, Anal. Chim. Acta. 1972, 62, 241.

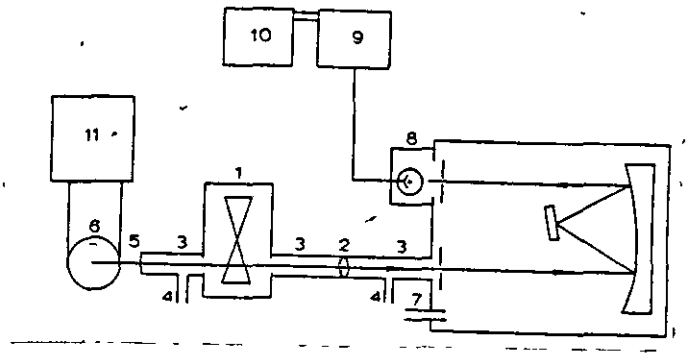

Fig. 19. Instrumental assembly employed. (1) Rotating chopper unit. (2) 62.5 mm. focal length silica lens. (3) 25 mm. o.d. glass tubes. (4) 8 mm o.d. glass side tube for nitrogen inlet. (5) 25 mm. diameter silica window. (6) Plasma torch and work coil. (7) 6.5 mm o.d. copper tube for nitrogen inlet to monochromator. (8) Photomultiplier. (9) Amplifier. (10) Chart recorder. (11) Radiofrequency power supply. Ref. 45.

Fassel[46] reviewed what he called "Electrical Flames" and concluded that the detection limits which could be obtained with the I.C.P. were, with few exceptions, comparable with or greatly superior to the best which could be obtained with flame atomic spectroscopy in any mode be it atomic absorption, emission or fluorescence. It was also confirmed that an annular plasma similar in configuration to that of Greenfield[15], and later his own, was free from the matrix effects experienced by Veillon and Margoshes[25].

46. V. A. Fassel, XVI Coll. Spect. Intern. Heidelberg, 1971, Plenary Lecture, p.63, Hilger, London, 1972.

Extending their previous work[45] Kirkbright et al[47] determined iodine, mercury, arsenic and selenium, all of which exhibit emission at wavelengths shorter than 200 nm. Spectral interferences from a variety of ions were investigated and sometimes found. A chemical interference when oxidising agents were present was noted in the determination of iodine as was blocking of the nebuliser.

Alder and Mermet[48], using a demountable, Fig. 20, three-tube torch and a 6 kW generator observed all the expected ArI lines but no ArII lines. The highest energy-level from which radiation was observed was about 15.4 eV.

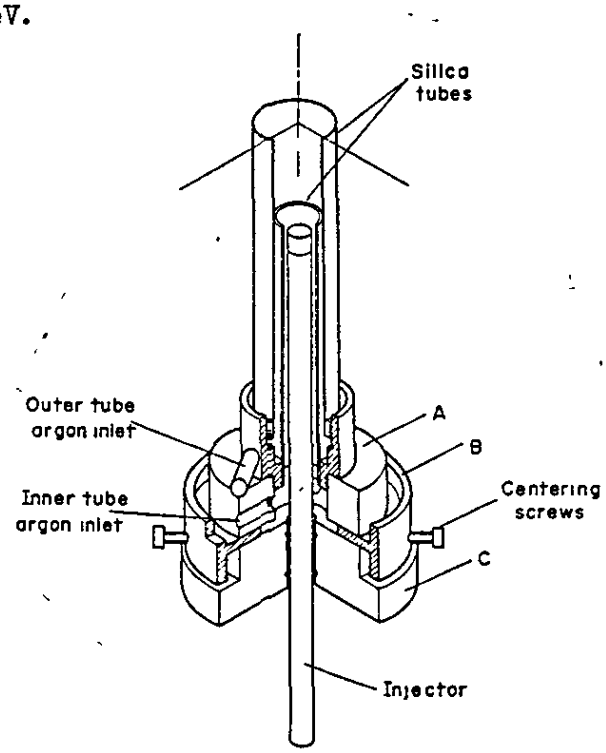

Fig. 20. Two tube plasma torch with central injector. Part A is fixed to part B and B is free to move over C. Ref. 48.

47. G. F. Kirkbright, A. F. Ward and T. S. West, Anal. Chim. Acta. 1973, 64, 353.

48. J. F. Alder and J. M. Mermet, Spectrochim. Acta. 1973, 28B, 421.

When methane was injected atomic C and H were observed together with C_2 and CN but no emission from CO or CH (cf refs. 32, 33). C_2 was noted in cooler regions of the tail flame but not in the hot regions (cf ref. 18) indicating decomposition of this molecule. It was suggested that since the bond strength of C_2 is 6.25 eV and that of CH 3.47 eV, the latter may be too unstable to survive. No enhancement of zirconium or hafnium emission was found in an argon-methane plasma compared with one of pure argon; which implies that reduction of the oxides by atomic carbon does not take place and that the temperature and enthalpy of the plasma are alone sufficient to break strong oxide bonds. Similarly when lanthanum was introduced into an argon plasma bands due to lanthanum oxide were not observed. Qualitative studies were made on the emission from sulphur, bromine, chlorine and phosphorus.

Scott et al[49] used a three-tube torch which is shown diagramatically in Fig. 21 with vortex stabilisation without a "plasma gas" in what is described as a compact system. The aerosol was produced by a pneumatic nebuliser and prior desolvation was not used. With an input power of 1.3 kW one might presume a power in the plasma of between 650 and 900 watts. Temperatures of 5000 K were reported, 18 mm above the load coil and linear calibration curves were obtained over five decade concentrations.

49. R. H. Scott, V. A. Fassel, R. N. Kniseley and D. E. Nixon, Anal. Chem. 1974, 46, 75.

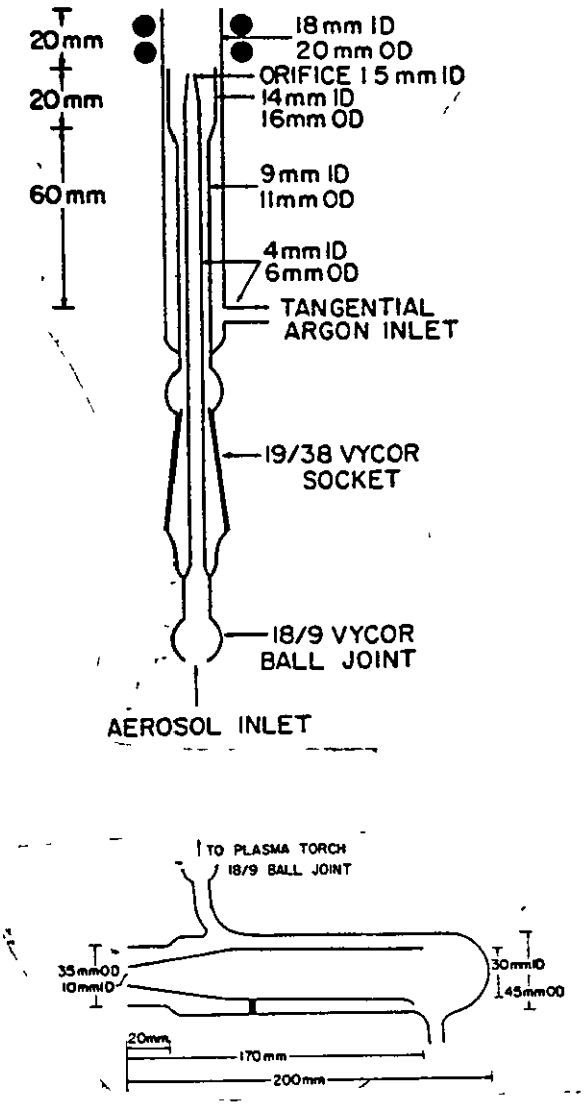

Fig. 21. Torch and Spray Chamber of Scott. Ref. 49.

Using a generator and torch similar to those of Boumans and de Boer[43], Kornblum and de Galan[50] measured the axial and radial distributions of temperature, electron concentration and element concentration. The bore of the tip of the injector tube (6.25 mm)

50. G. R. Kornblum and L. de Galan, Spectrochim. Acta. 1974, 29B, 249.

was much wider than that used by most workers. The plasma was operated in a horizontal configuration, Fig. 22 as it was claimed this made the experiments easier. The power used was 2 kW : unusually, for this power, desolvation was necessary to prevent the plasma being extinguished.

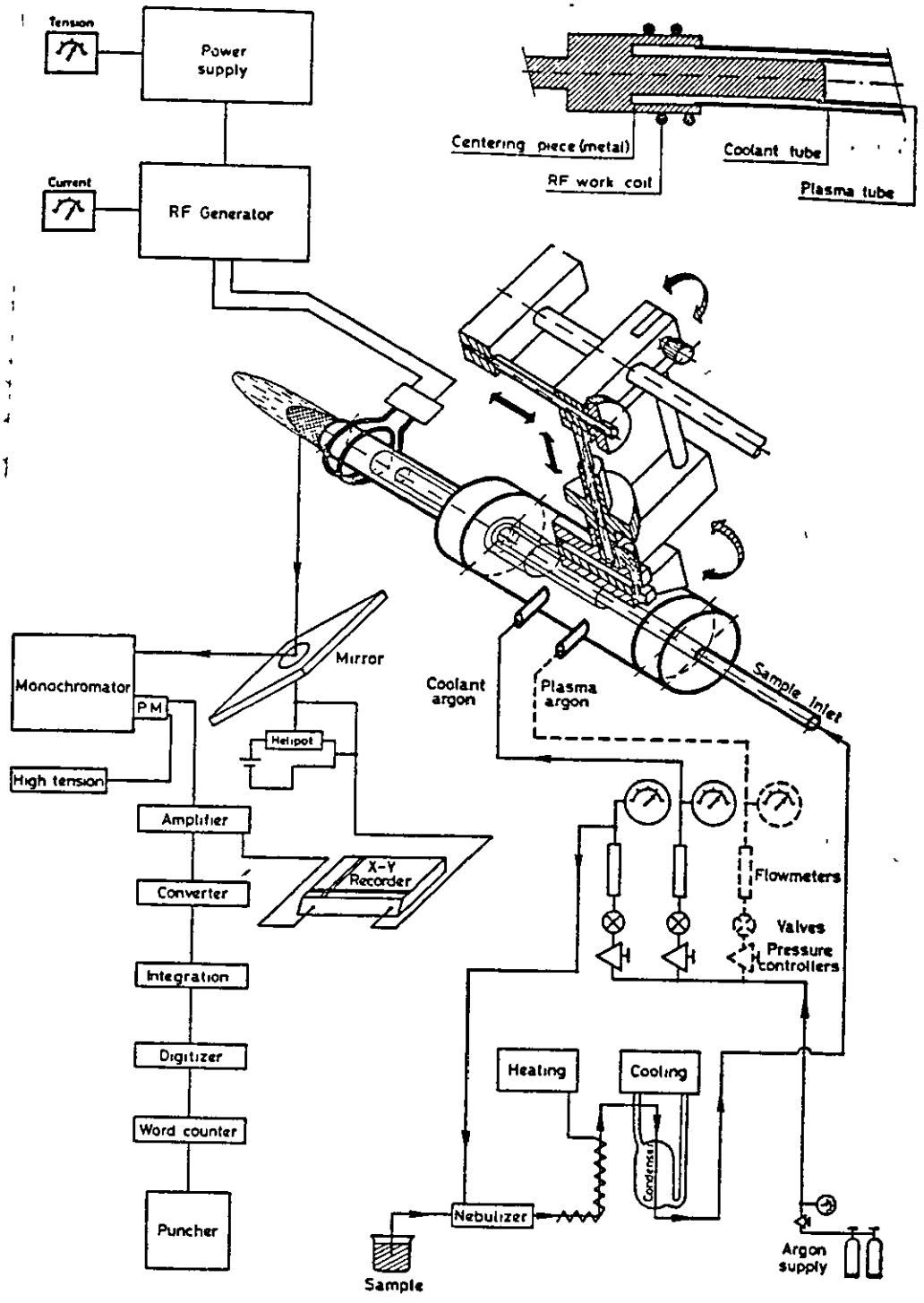

Fig. 22. Block diagram of the complete apparatus. Insert at the top right shows the work coil with the centering piece to position the coolant and plasma tubes in the centre of the coil. Ref. 49.

Dreher and Frank[51] describe a demountable torch Fig. 23 operating at atmospheric pressure in argon, which was used for emission spectroscopy in the vacuum ultraviolet.

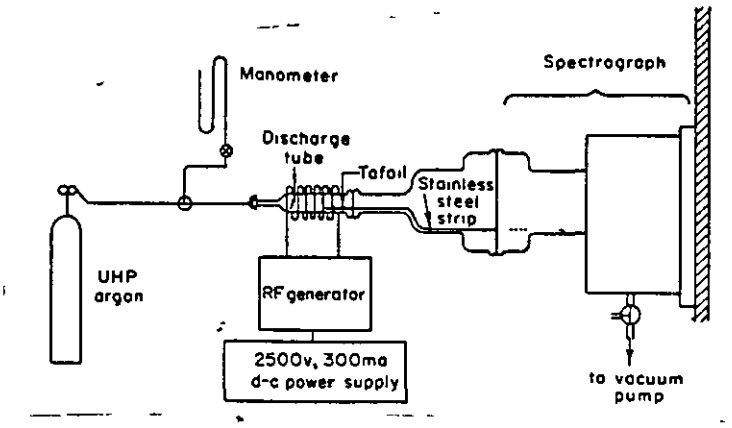

Fig. 23. Diagram of induction-coupled radio-frequency discharge source of Dreher and Frank. Ref. 51.

The source was totally enclosed. The power was very low (250 W) and the cell had to be dismantled and cleaned after each exposure.

Kirkbright and Ward[52] attempted to explain some properties of inductively coupled plasmas and of flames by examining idealised models Fig. 24. The much greater linear range of the plasma is ascribed to higher temperature which causes the overall neutral particle densities to be somewhat less because of expansion and ionization, the fraction of these in the ground state to be much less because of increased excitation, and the Doppler widths to be greater. The higher sensitivity is also a consequence of the higher temperature. Other deductions made were that the maximum energy supplied to the analyte particles for their

51. G. B. Dreher and C. W. Frank, Appl. Spectry. 1974, 28, 191.

52. G. F. Kirkbright and A. F. Ward, Talanta, 1974, 21, 1145.

model was 2.3 J for the plasma and .001 J for a typical flame, was that a plasma can handle a concentration range of five or six orders of magnitude against three for the flame and that concentration ranges for the plasma can be increased by reducing sample uptake rates. Cu, Fe, Mg, Mn, Ti and Zn were determined in aluminium alloys with a flame and with a plasma;

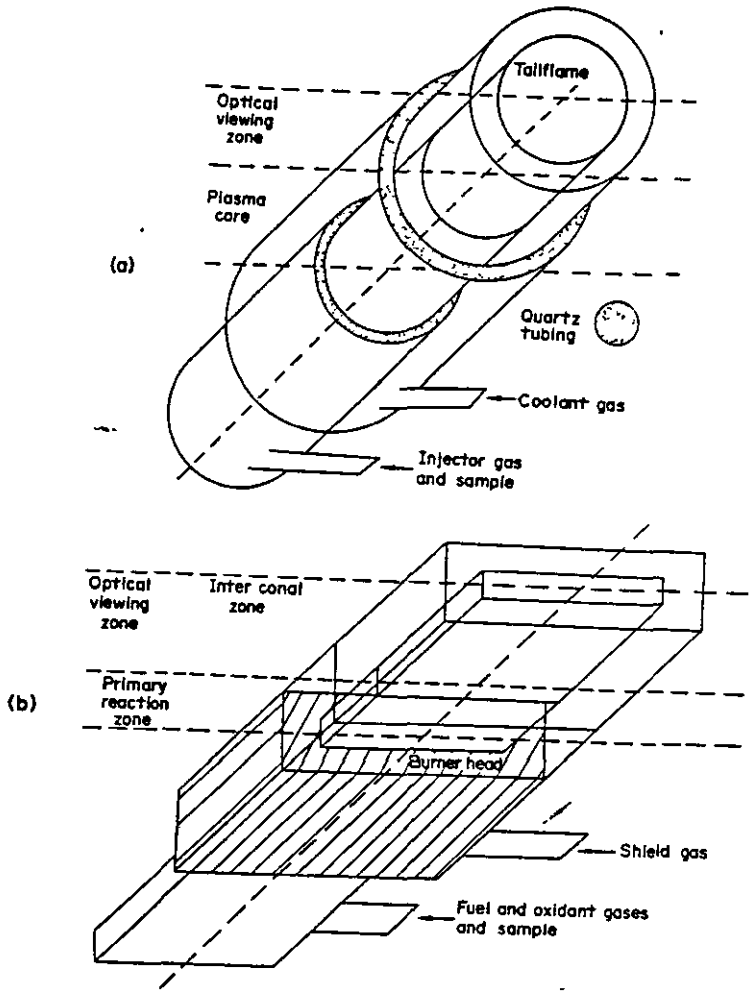

Fig. 24. Diagrammatic representation of ideal plasma and flame models (a) plasma (b) flame. Ref. 52.

non-linear calibration curves were obtained when using a flame without dilution, and precisions of the order of 5% were obtained with the plasma as against 10% with a flame. Kirkbright reported this work at a later date in lecture form[53].

Fassel and Kniseley[54] made a re-assessment of emission spectroscopy with I.C.P. as against flame-excited atomic absorption, fluorescence and emission spectroscopy, and concluded that I.C.P. were superior on most counts agreeing with Boumans and de Boer[44] that the I.C.P. - optical emission spectrometer system "constitutes a most promising excitation source for simultaneous multi-element analysis of solutions".

Such a system had been in everyday use for practical analysis in an industrial laboratory for over four years, based on an I.C.P. coupled to a 30-channel direct-reading spectrometer with fully automatic sequential sampling and read-out[2]. The torch is shown in Fig. 25. Important points in its design were discussed. The data are processed by an off-line computer.

53. G. F. Kirkbright, Proc. Anal. Div. Chem. Soc. 1975, 12, 8.

54. V. A. Fassel and R. N. Kniseley, Anal. Chem. 1974, 46, 1110A, 1155A.

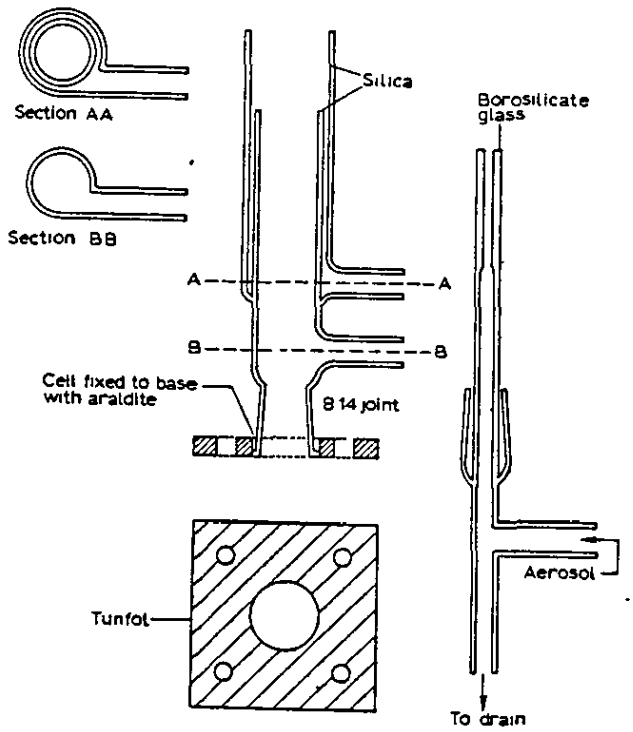

Fig. 25. The Plasma Torch of Greenfield. Ref. 2.

With this system simultaneous multi-element analysis at both trace and assay levels is possible on each exposure. A survey of commercial samples analysed in one three month period shows that a wide variety of concentrations of different elements can be determined simultaneously from the same solution, and that many elements with concentrations in the sample of less than 10 ppm can be determined.

Boumans and de Boer[55] made a further assessment of high-frequency plasmas for the multi-element analysis of solutions and reported some "reconnaissances in the field of applications". These gave rise to optimism on the possibility of general analysis of solutions. They made comparisons with analysis by the d.c. arc and by atomic absorption using both flames and furnaces; the comparisons favoured the inductively coupled plasma source, which was also found to be superior to the

55. P.W.J.M.Boumans and F.J. de Boer, Proc. Anal. Div. Chem. Soc. 1975, 12, 140.

capacitively coupled microwave source and to the d.c. plasma jet. The detection limits which were obtained under compromise conditions on pure aqueous solutions of 32 elements were low, typically 0.01 - 1 ng per ml of solution. The effect of a matrix was typically only to double these, provided that the matrix concentration in the solution was less than 0.5%, this upper limit being set by the nebulising and desolvating assembly. After including a factor to account for possible interferences, which are discussed at some length, they predicted typical detection limits under real conditions to lie in the range 0.1 - 10 μg per gram of sample.

Scott and Kokot[56] applied the inductively-coupled plasma to the determination of Cu, Zn, Ni, Co and Pb in soil samples. Comparison of the results with those obtained from atomic absorption showed that there was good agreement for Cu and Zn but discrepancies for Ni and Co which were probably due to enhancement effects in the atomic absorption measurements. Discrepancies for Pb were due to spectral interferences by Mg and Ca.

Scott and Strasheim[57] determined trace quantities of Fe, Mn, Cu, Al, B and Zn in orchard leaves, using one composite synthetic standard under compromise conditions. Good or acceptable results were obtained for all elements except zinc, where a significant low bias was found to be due to depression of the spectral background because of the presence of K and Ca in the samples. It was found that this bias could be reduced to a tolerable level by buffering the standard.

Butler, Kniseley and Fassel[58] gave a further assessment of the potentialities of the inductively coupled plasma: this application was to

56. R. H. Scott and M. L. Kokot, Anal. Chim. Acta. 1975, 75, 257.

57. R. H. Scott and A. Strasheim, Anal. Chim. Acta. 1975, 76, 71.

58. Constance C. Butler, R. N. Kniseley and V. A. Fassel, Anal. Chem. 1975, 47, 825.

the analysis of low and high alloy steels. They showed that the presence of an iron matrix had little effect on the detection limits of 12 alloying elements and that no chemical concentration was necessary to determine them at low levels. Since a long linear range in the calibration curves was obtained, both major and trace elements could be determined from a single dilution level. Results for 5 typical alloying constituents showed good agreement with certified values. Coefficients of variation of about 1 - 3% were derived from measurements obtained over a period of four months. Although the results obtained are promising for the analysis of real samples, their claims that the 12 elements can be determined at fractional ppm levels without prior chemical concentration, and that their results on NBS Standard Reference Samples all fall in the range reported by NBS, are not supported by the figures quoted.

A new informal monthly publication, ICP Information Newsletter[59] made its first appearance. The objective of this publication is "to encourage the rapid and impartial distribution of current information and opinions related to the inductively coupled plasma discharge source for spectrochemical analysis in a single location".

59. I.C.P. Information Newsletter, Edited R. M. Barnes, Univ. Mass. 1975.

1.3 Raison D'Etre

Although spectroscopists are beginning to recognise that inductively coupled plasma torches constitute excitation sources for emission spectroscopy with quite exceptional properties, there is by no means universal agreement, by the experts in the field, on such matters as equipment, operating parameters and excitation mechanisms.

One such problem area is the question of the wattage necessary to do useful analytical work and the optimum requirement which is discussed in Chapter 5. As the power in a plasma is increased so is its temperature. According to the Boltzmann equation an increase in temperature results in an increase in the populations of the excited atomic levels. Hence it can be expected that the emission from a given atomic energy level will continue to increase until a stage is reached where further increases in temperature will excite more and more atoms to higher energy atomic levels and high ionisation states and there will be no further increase in emission, with temperature, from the given level. Further increase of temperature causes a decrease in emission and the temperature at which maximum emission occurs is the so called "norm temperature". Saha's equation[60] can be used to plot the variation in particle density of the different ionised species with temperature. This is a form of the law of mass action and gives the equilibrium K_p for the reaction $A \rightleftharpoons A^+ + e$. In a practical form it is written :-

$$\log K_p = -5040\ X/T + 5/2 \log T + \log Z^+ - \log Z - 6.1816$$

where X is the ionisation energy (in ev) of the neutral atoms and Z and Z^+ the partition functions of the neutral atoms and atomic ions respectively. The partition functions are calculated from the statistical weights and energy levels. The variation of particle density with temperature calculated by means of the Saha equation is shown for calcium in Fig. 26.

60. M.N.Saha, Phil Mag. 1920, 40, 472.

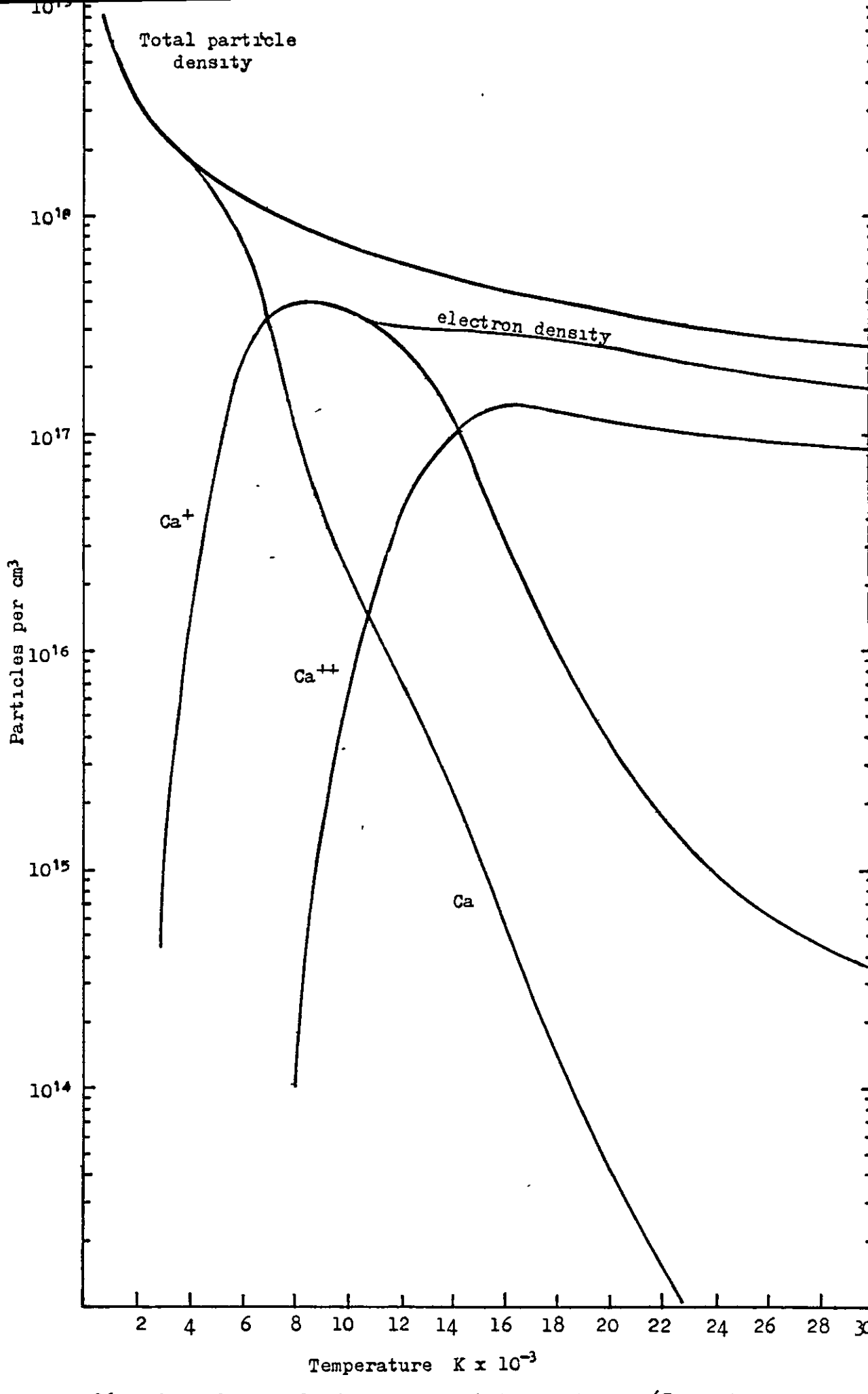

Fig. 26. Plot of particle densities with temperature. (Ionisation states higher than Ca^{++} are ignored).

Thus one benefit that can be expected from the use of high powered plasmas is an increase in the signal to concentration ratio or sensitivity, up to the power which gives the norm temperature. However, as the temperature of the plasma increases so will the number of free electrons and hence the continuum or background emission so that the signal to background ratio and hence the signal to noise ratio may be reduced with deleterious effect on the detection limits attainable. However, since the emission is normally measured in the tail-flame of the plasma, remote from the "fire-ball" itself, this may not in practice be an insurmountable problem.

Any spectrometric analysis system using an inductively coupled plasma as an excitation source consists of a number of parts which in any comparison of low powered (< 2 kW) and high powered (> 2 kW) plasmas must be kept unchanged apart from the source if the comparisons are to be meaningful. Only the torches, generators and possibly the gases should be changed. The analysis solutions and nebuliser should be the same in all cases. Not only will changes in concentration obviously affect the signal but matrix changes may alter the uptake rate of the nebuliser and may also cause chemical interference. No two apparently identical nebulisers give precisely the same result, they differ in uptake rate, droplet size and distribution, gas flow and some are followed by desolvation.

Net signal is of no value in comparing different torches on different systems and neither are net signal to net background ratios, since the entrance and exit slits, dispersion and resolution will vary from instrument to instrument and these features will determine the amount of background radiation incident on the photomultiplier tube.

Unless these are standardised, intersource as opposed to intersystem comparisons cannot be made. A further important point to be made is that the optical system will look at different areas of the tail-flame of the plasma. Since plasmas are non-uniform sources one instrument may see relatively more background than another.

The stability and electronic noise at various amplification levels, and the degree of amplification of the electronics associated with the detectors and integrators will also vary from instrument to instrument which again implies these should be the same for intersource comparisons. Since detection limits are generally defined as some factor times the standard deviation of the measured overall background (generally 2σ) expressed as concentration, the electronic noise level at high amplification is a major factor in total noise and hence detection limits cannot validly be used to compare torches on different overall systems.

The object of the present work was to study the emitted light intensities of elements possessing high and low excitation potentials, and thus from various energy levels, using low and high powered plasmas on the same spectrophotometric system and with the same nebuliser and solutions, but with different generators, torches and gases. The elemental and background emission has been measured at various heights in the tail flame in order to locate optimum operating conditions.

CHAPTER 2.

INITIAL EXPERIMENTAL EQUIPMENT.

The equipment described herein was developed and used in the Analytical Section of the Specialities Sector of Albright and Wilson Ltd., Oldbury. The author is Manager of these laboratories.

2.1 Generators

Model.	Type.	kW	Frequency MHz
Radyne S.C.15	Free running. Power control by capacitive tuning of the output circuit.	2.5 nominal.	36.0
Radyne R.D.150.	Free running. Power control by varying the H.T. on the valve.	15.0 nominal.	7.0

(The above kilowattages refer to the rating of the generator; hereafter the kilowattages quoted refer to the actual power in the plasma and were determined calorimetrically)[19,61].

2.2 Torch, Injector and Work Coil.

These were identical for both generators and are shown diagrammatically in Figs. 27-29.

2.3 Gas Flows, Control and Measurement

Plasma 6.0 to 14.0 litres/min.$^{-1}$ argon.
Coolant 20 to 67.5 litres/min.$^{-1}$ nitrogen
Nebuliser 2.0 to 4.2 litres/min.$^{-1}$ argon

} Controlled and measured by Brooks "Sho-Rate" flow meters.

2.4 Nebuliser

Pneumatic. Unicam S.P.900 nebuliser operating at 13 lbs./□" instead of the more normal 30 lbs./□" specified by the manufacturers, since this pressure would give too high a flow of injector gas.

61. S.Greenfield and H.McD.McGeachin, Analytica Chimica Acta 1978, 100, 101

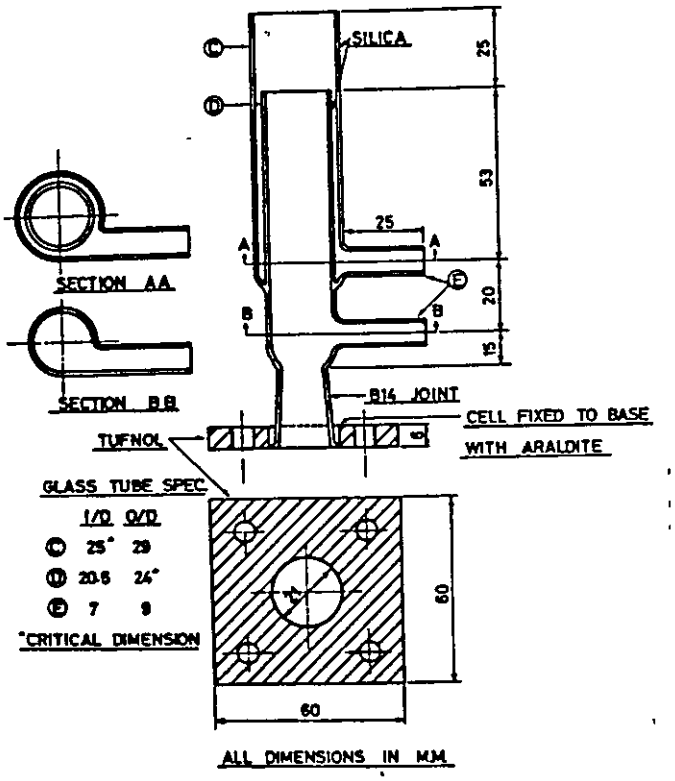

Fig.27. Plasma Cell.

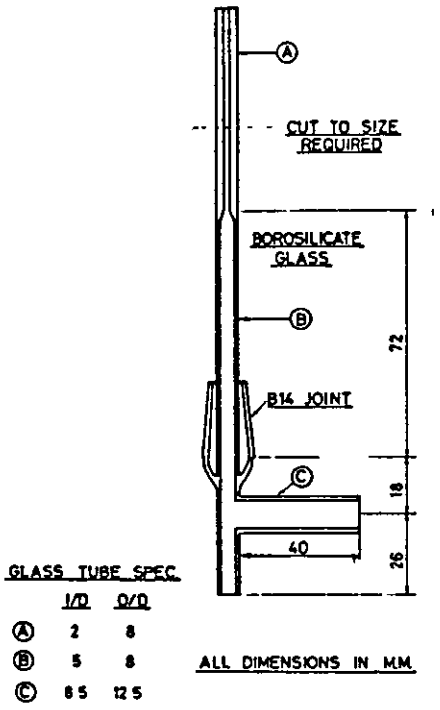

Fig.28. Injector.

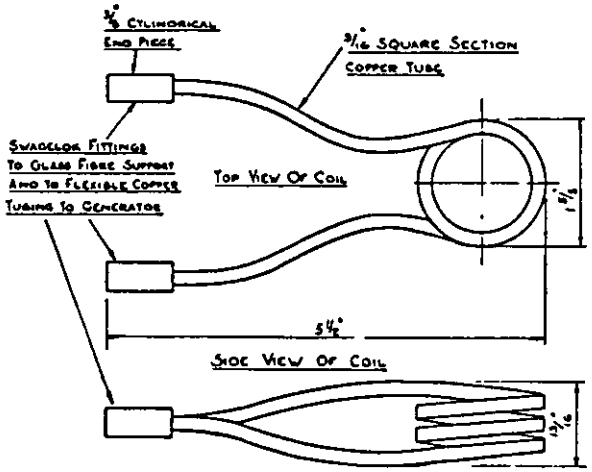

Fig.29. Work Coil.

2.5 The Spectrometer

The direct reading spectrometer employed was a 30-channel Hilger and Watts F.A.19 Polychromator; this uses a concave grating of 3-m. radius of curvature and gives a dispersion of 0.173 mm A^{-1} (A = A°) in the first order. Radiation from the source was focussed on the entrance slit, as shown in Fig. 30, and then reflected by a plane mirror on to the grating. The different wavelengths in the resulting spectrum are focussed at different points on a circle where a series of carefully adjusted exit slits passes the wavelengths of interest. The radiation transmitted by an exit slit is focussed by a concave mirror to fall, after reflection from a plane mirror, on the cathode of a photomultiplier (P.M.). There are thirty slits and photomultipliers, E.M.I. Types 6256, 9789QB and one RL6256B.

When radiation strikes a P.M., a current flows, proportional to the intensity of radiation. The current from each P.M. charges a capacitor for the duration of each exposure so that the voltages on the capacitors provide measures of the integrated intensities. It is to be noted that the response of the P.M. also varies with the wavelength of the radiation.

2.6 Entrance Optics

The optical arrangements whereby the two generators and torches may be used independently on the same spectrometer are shown in Fig.30.

2.7 Mechanical Wedge

V shaped wedge placed between the lens and the entrance slit and capable of being moved vertically by a rack and pinion mechanism. It was used as a stop to reduce the amount of radiation entering the Polychromator when this was required.

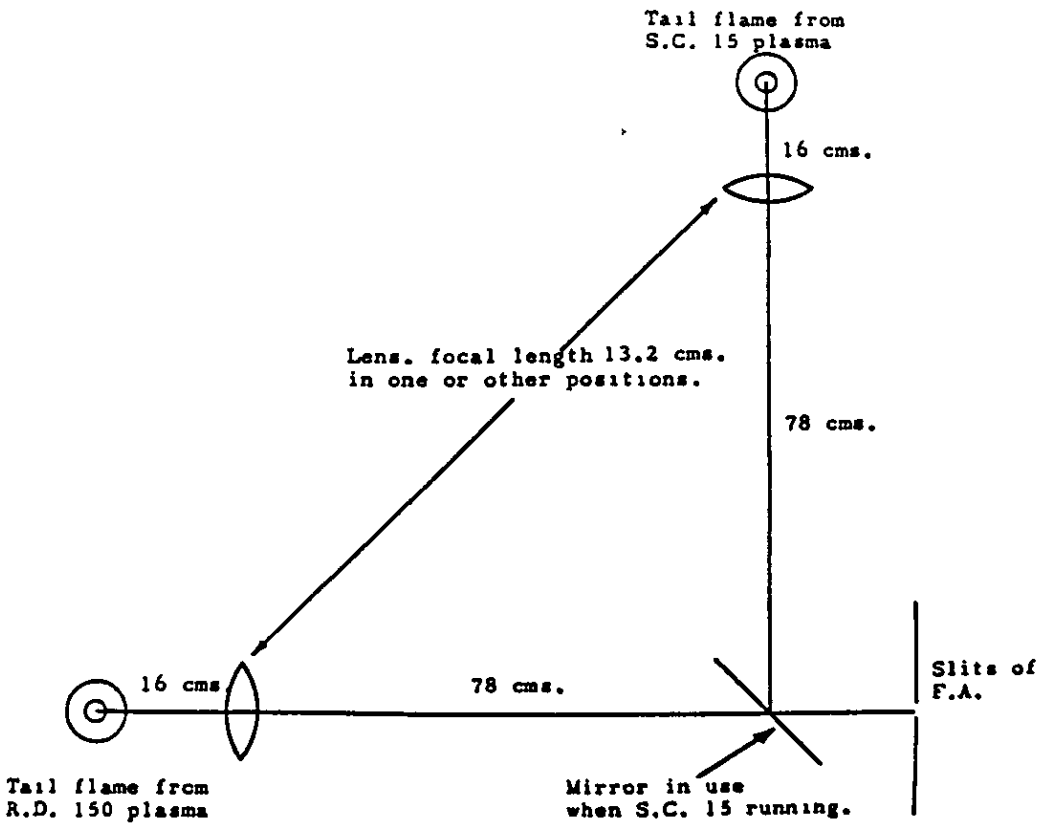

Fig.30. Entrance Optics.

2.8 Measuring Set

The basic measuring units are the comparator and counter. The former serving to convert the integrated potential appearing across the integrator capacitor into a train of pulses, the number of pulses in the train being linearly related to the capacitor potential, the number of pulses is recorded by a 4-decade counter.

The method used in converting the potential into a train of pulses may be followed by reference to Fig. 31. In this diagram, V701 is a double cathode follower valve which compares the potentials applied to its two control grids. The capacitor potential to be measured is injected into the first control grid, via a resistor R704. The corresponding cathode potential changes by an amount almost equal to the control grid change. (R704 is a 1 Megohm resistor to limit the current

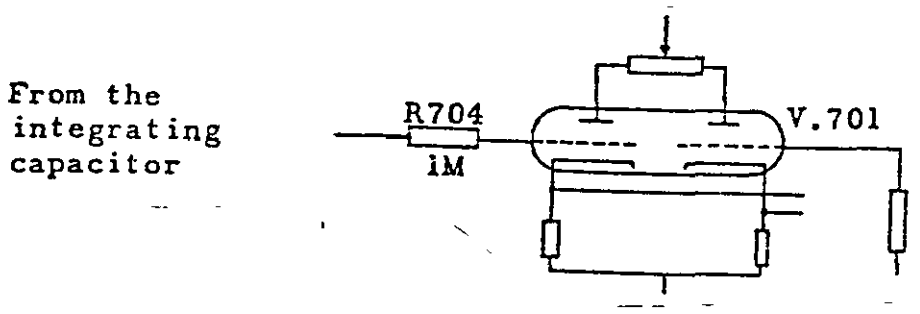

Fig. 31. Schematic diagram of Measuring set.

drawn from the integrating capacitor and hence to reduce to a minimum the potential change on the capacitor when measurement is made). The second grid is connected to a source of variable potential, changes in which are followed by a corresponding change in cathode potential. Initially, there is no input signal, the two grids are arranged to be at similar potentials and the valve balances, so that the two cathodes are at equal potentials. At the start of the measurement cycle, the capacitor potential to be measured is injected from the integrator to grid 1 of valve V701, thus unbalancing the two cathodes.

After a short delay, a linear potential sweep is initiated and applied to the second control grid of valve V701. The capacitor potential is negative and the sweep is negative going, and hence as the run-down of grid 2 progresses valve V701 tends towards balance, ultimately reaching a level at which the two cathode potentials are equal.

As the run-down continues further, the cathode potentials will again be unbalanced, the polarity of this inbalance being opposite of that at the start of the run down. Since the potential sweep applied to valve V701 is linear, the time interval between the initiation of the

sweep and the instant at which the valve is again in balance is directly proportional to the potential across the integrating capacitor. This time interval is measured by allowing the counter to run at a fixed frequency from the instant at which the potential sweep is initiated until valve V701 again becomes balanced, terminating the count at this instantaneous balance point.

2.9 The Profile Meter

This device enables an instantaneous measurement to be made of the current being produced by a particular P.M. tube. The current generated by the P.M. tubes flows through the 1 Megohm resistor, R701, to earth as shown in Fig. 32.

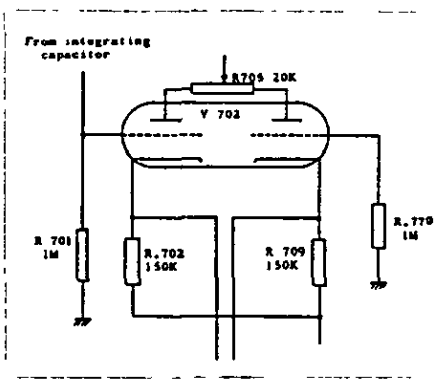

Fig. 32. Profile Meter.

The potential developed across resistor R701 is injected into control grid 1 of valve V702 and (as for valve V701 previously mentioned) fixes the cathode potential. The other cathode potential is fixed by the grid leak resistor R.770.

In the no signal condition the two grid potentials and hence the two cathode potentials are equalised by varying the plate potentials on the two halves of the valve via resistor R705. When a signal is injected to

number 1 grid an inbalance occurs and if a microammeter is connected between the two cathodes current flows. The magnitude of this current is linearly related to the potential on the grid and hence to the current generated in the P.M.

The nomenclature for the various resistors and valves is those used in the manufacturers handbook as the Measuring Set and Profile Meter are standard items supplied with the instrument.

2.10 "Modulog"

Inter-Cole System's multiplexing, integrating digital voltmeter with fast paper tape output. Used for the acquisition of data.

CHAPTER 3.

PRELIMINARY EXPERIMENTS

The first element to be examined was sodium. This is an easy element to excite and the U_1 line at 5890Å has an excitation potential of 2.1 e.v. (For a neutral atom the most sensitive line is indicated by U_1 and other lines by U_2, U_3 etc. in order of decreasing sensitivity. For the singly charged atomic ion the corresponding designations are V_1, V_2, etc.). The intensities at various heights in the tail flame were recorded using the profile meter. The height was measured from the flattened base of the spheroidal plasma. The position of the base remains reasonably constant whereas the plasma increases in length with power and the position of the top is difficult to locate.

3.1 Sodium Results

A solution of sodium chloride containing 1,000 ppm sodium ion was aspirated and the emission of various heights and powers measured. The Height/Power/Emission data are given in Table 1 and shown diagramatically in Figs. 33 and 34. The dashed lines are extrapolations.

The Polychromator gain was set at 1 throughout but the wedge was used to give a five-fold attenuation of the emission when the torch and high power generator was used. In order to make a comparison between the two sets of results all readings obtained for the RD150 generator were multiplied by five. Background measurements were too low relative to the intense sodium emission to be measured with any significant precision.

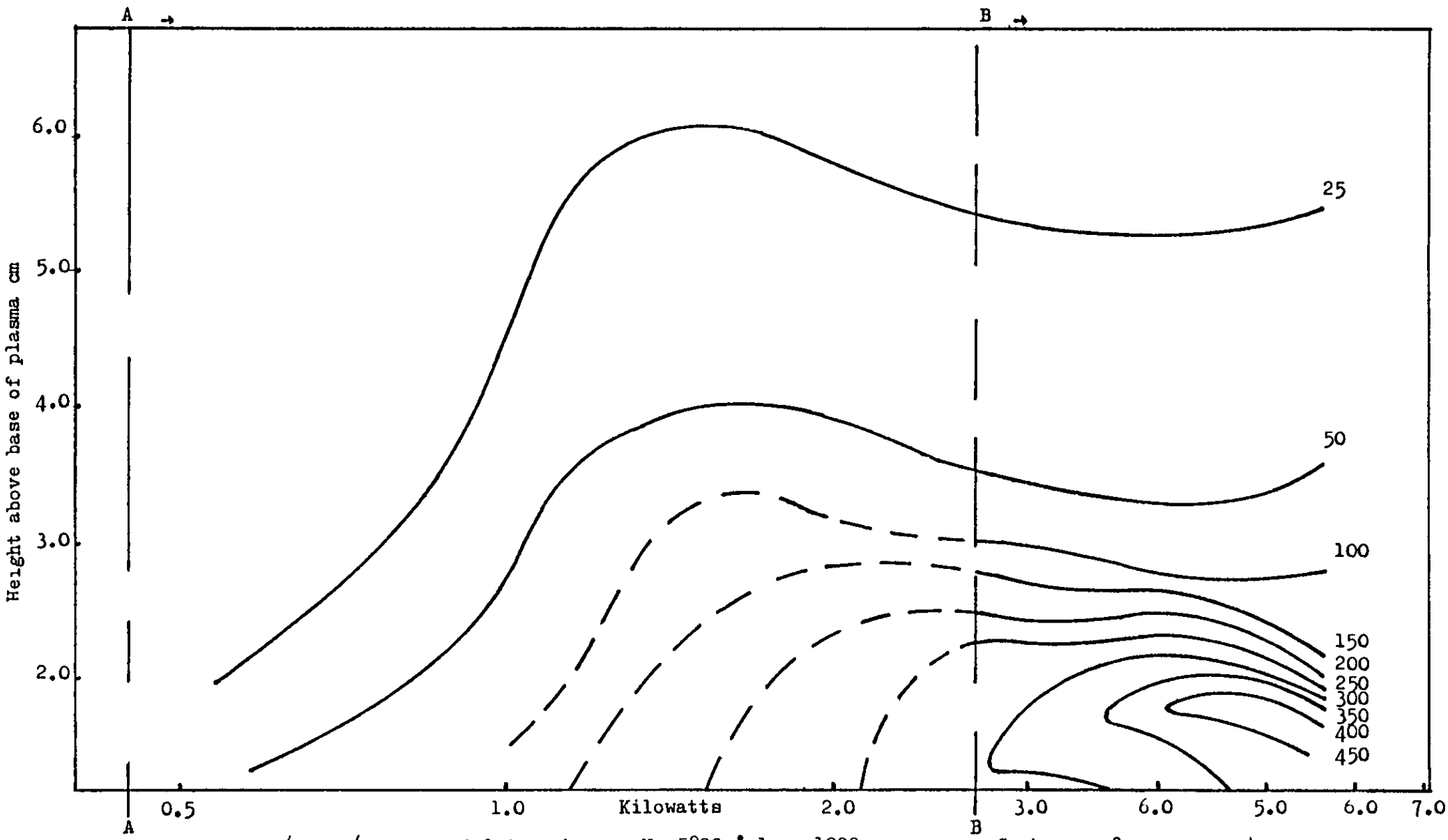

Fig. 33. Height/Power/Emission Relationships. Na 5890 Å line 1000 p.p.m. Contours of emission at intervals of 50 μa with one at 25 μa.

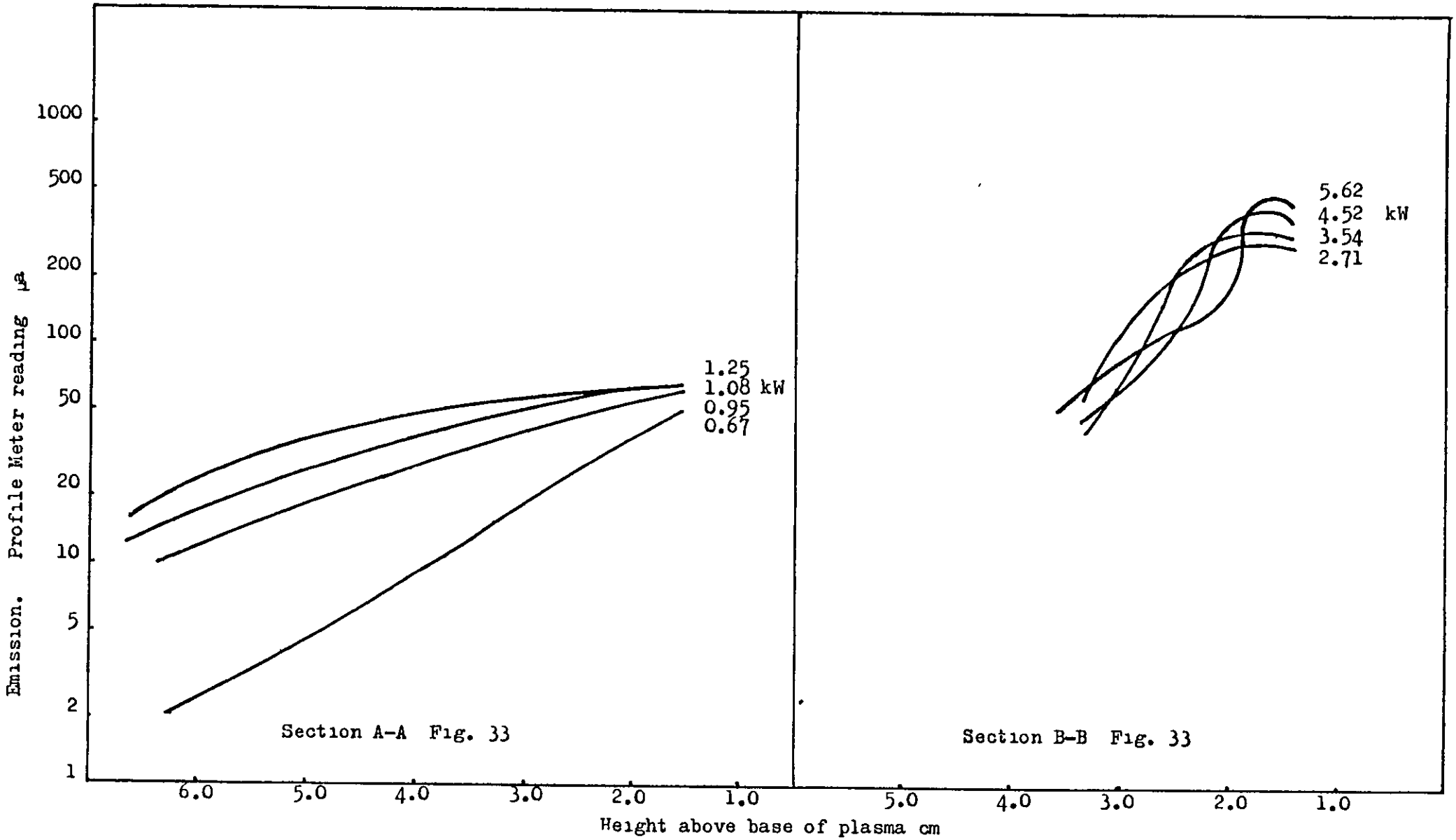

Section A-A Fig. 33

Section B-B Fig. 33

Fig. 34. Height/Power/Emission Relationships. Na 5890 Å line 1000 p.p.m. Plot of log emission in µa.

Table 1. Height/Power/Emission Relationships.

Sodium 5890Å line. Profile Meter Readings.

Plasma gas flow	6.0ℓ/min. Ar.	S.C.15 Generator.
Nebuliser gas flow	2.6ℓ/min. Ar.	Concentration of sodium.
Coolant gas flow	20.0ℓ/min. N_2.	1000 p.p.m.

Height	Gross Signal in μa at :-			
cm.	0.67 kW	0.95 kW	1.08 kW	1.26 kW
1.56	52	61	63	63
2.24	32	55	58	60
2.74	23	45	52	57
3.24	16	39	47	54
3.74	11	31	40	51
4.24	7	24	32	45
4.74	5	18	27	39
5.24	4	17	23	33
5.74	2	13	19	29
6.24	*	11	15	20
6.74	*	9	13	21
7.24	*	8	11	18

Plasma gas flow	7.5ℓ/min. Ar.	R.D.150 Generator.
Nebuliser gas flow	2.0ℓ/min. Ar.	Concentration of sodium.
Coolant gas flow	20.0ℓ/min. N_2.	1000 p.p.m.

Height	Gross Signal in μa at :-			
cm.	2.71 kW	3.54 kW	4.52 kW	5.62 kW
1.40	280	310	370	435
1.58	295	335	390	450
1.83	290	345	405	350
2.08	280	320	330	160
2.58	190	170	100	115
3.08	95	65	65	85
3.58	40	40	45	50
4.08	*	*	*	35
4.58	*	*	*	30

* Unreliable readings. With excessively high fractional error.

The next element investigated was boron. The U_1 line at 2.497.7Å with an excitation potential of 4.9 e.v. was chosen for examination since this would be more difficult to excite than the sodium U_1 line at 5890.0Å.

Section 3.2 Boron Results

Height/Power/Emission data was obtained as before. With the low powered plasma, using a solution containing 1000 p.p.m. of boron present as boric acid, it was necessary to turn the gain on the P.M. tubes up to five (x 16) whereas with the high power generator a gain of one was used and the wedge was introduced attenuating the signal by 7.57. Thus all readings on the profile meter, when using the high power generator, were multiplied by 121 (i.e. 7.57 x 16) in order for a meaningful comparison to be made between the two sets of results. Where possible the background was recorded, as was the gross signal to gross background ratio. Net backgrounds could not be measured due to the insensitivity of the profile meter which precluded the measurement of the dark current. Some net signals were recorded. The data is summarised in Table 2.

Table 2. Height/Power/Emission Relationships.

Boron 2497.7Å line. Profile Meter Readings.

Plasma gas flow 6.0ℓ/min. Ar. S.C.15 Generator.

Nebuliser gas flow 2.3ℓ/min. Ar. Concentration of boron.

Coolant gas flow 20.0ℓ/min. N_2. 1000 p.p.m.

Height	Gross Signal in μa at :-			
cms.	0.73 kW	0.90 kW	1.10 kW	1.20 kW
1.56	24	44	56	87
2.24	18	35	26	49
2.74	10	18	15	31
3.24	8	12	12	21
3.74	8	10	11	15
4.24	-	10	11	12
4.74	-	-	-	12
	Gross Background			
1.56	3	4	4	5
2.24	*	4	3	4
2.74	*	3	3	3
3.24	*	3	3	3
3.74	*	3	3	3
4.24	*	3	3	3
4.74	*	*	*	3
	Net Signal			
1.56	21	40	54	82
2.24	18	31	23	45
2.74	10	15	12	28
3.24	8	9	9	18
3.74	8	7	8	12
4.24	-	7	8	9
4.74	-	-	-	9
	Gross Signal/Gross Background			
1.56	8	11	14	17
2.24	*	9	9	12
2.74	*	6	5	10
3.24	*	4	4	7
3.24	*	3	4	5
4.24	*	3	4	4

Plasma gas flow	7.5ℓ/min. Ar.	R.D.150 Generator.
Nebuliser gas flow	2.0ℓ/min. Ar.	Concentration of boron.
Coolant gas flow	20.0ℓ/min. N_2.	1000 p.p.m.

Height	Gross Signal in μa at :-			
cm.	2.71 kW	3.50 kW	4.49 kW	5.64 kW
1.40	3267	5203	6897	10164
1.58	2783	4477	6171	9196
1.83	-	3630	5203	8470
2.08	1573	3146	4961	9075
2.58	1210	2904	4961	10890
3.08	1210	2662	4840	9196
3.58	1210	2299	3872	6050
4.08	1089	1936	2904	3872
4.58	847	1452	2057	2420
5.08	726	1210	1573	1936
	Gross Background			
1.40	*	847	1694	3267
1.58	*	242	968	2178
1.83	*	*	242	968
2.08	*	*	121	484
2.58	*	*	*	363
3.08	*	*	*	242
3.58	*	*	*	121
4.08	*	*	*	*
4.58	*	*	*	*
5.08	*	*	*	*
	Net Signal			
1.40	*	4356	5203	6897
1.58	*	4235	5203	7018
1.83	*	*	4691	7502
2.08	*	*	4840	8591
2.58	*	*	*	10527
3.08	*	*	*	8954
3.58	*	*	*	5929
4.08	*	*	*	*
4.58	*	*	*	*
5.08	*	*	*	*
	Gross Signal/Gross Background			
1.40	*	6	4	3
1.58	*	18	6	4
1.83	*	*	25	9
2.08	*	*	41	19
2.58	*	*	*	30
3.08	*	*	*	38
3.58	*	*	*	50

* Unreliable readings for reasons stated.

At this stage it became apparent that the profile meter was probably not sensitive enough for this application although it was convenient and fast in use. However, two more experiments were made, one with an aluminium solution and another with a vanadium solution.

Section 3.3 Aluminium and Vanadium Results

Aluminium has a V_2 line at 2816Å with an excitation potential of 17.7 e.v. which is thus fairly difficult to excite. Using a solution containing 1000 p.p.m. of aluminium present as aluminium chloride, the difficulty of excitation was confirmed by the data tabulated in Table 3.

Table 3. Height/Power/Emission Relationships.

Aluminium 2816Å line. Profile Meter Readings.

Plasma gas flow	6.0ℓ/min. Ar.	S.C.15 Generator.
Nebuliser gas flow	2.3ℓ/min. Ar.	Concentration of Aluminium.
Coolant gas flow	20.0ℓ/min. N_2.	1000 p.p.m.

Gross Signal in μa at :-

1.3 kW

Nil (maximum gain (x 1024)). (Integration using the Measurement Set gave 73 counts for a 10 sec. exposure).

Plasma gas flow	7.5ℓ/min. Ar.	R.D.150 Generator.
Nebuliser gas flow	2.0ℓ/min. Ar.	Concentration of element.
Coolant gas flow	20.0ℓ/min. N_2.	1000 p.p.m.

Gross Signal in μa at :-

6.66 kW

13 (gain of 7 (x 64)).

Vanadium has a V_2 line with an excitation potential of 11.2 e.v. at 3093.108Å. Data obtained, using a solution containing 1000 p.p.m. of Vanadium present as metavanadate, are shown in Table 4.

Table 4. Height/Power/Emission Relationships.

Vanadium 3093Å line. Profile Meter Readings.

Plasma gas flow 6.0ℓ/min. Ar. S.C.15 Generator.

Nebuliser gas flow 2.3ℓ/min. Ar. Concentration of vanadium.

Coolant gas flow 20.0ℓ/min. N_2. 1000 p.p.m.

Gross signal in μa at :-

0.9 kW

58 (gain of 4(x 48))

Section 3.4 Observations on Preliminary Experiments

At the conclusion of the preliminary experiments with sodium the following observations were made :

1) The gross signal increased with increasing power.

2) The maximum gross signal for each power occurred at a position nearer to the plasma as the power was increased. As the plasma increases in length as the power is increased all the measurements on the high power plasmas were made from positions in the plasma.

3) With the low powered plasma the emission at each power showed no maximum only a decrease in emission as the viewing position moved out away from the plasma. In contrast, definite maxima occurred at various positions along the tail-flame in the high power plasma experiments.

4) At a fixed height all readings increased with increasing power when using the small generator. With the high power plasmas maxima occurred at lower powers than that which gave the highest gross signal. (In two instances maxima was followed by a minima, this may be due to the inaccuracies of measurement). These results demonstrate that the optimum position for viewing depends both on power and on height.

Boron behaved in a similar fashion but with some interesting differences, namely :

1) All signals increased with increasing power, however, at a certain position the signal increased faster than the background as was evidenced by an increasing gross signal/gross background ratio.

2) The position of maximum net signal moves nearer to the plasma as the power is increased and then moves away as the power is further increased. This could be due to the norm temperature having been reached; any further increase in temperature will cause the signal to decrease and so putting the position of maximum intensity further away out of the plasma.

The increase in gross signal following a decrease at 5.64 kW is considered to be probably due to the increasing continuum.

3) With the exception of the readings at 5.64 kW there was no maxima along the tail-flame.

4) At a fixed height all signals increased with increasing power i.e. no maxima was observed.

5) The gross signal/gross background ratios are considered inconclusive because it was apparent, at this stage of the investigation, that the profile meter was too insensitive for accurate measurements to be made of the dark current and of the background signals. These data could be important for reasons which are given and discussed in detail in Chapter 5. However, it was first necessary to consider the types of noise inherent in the detectors and associated electronics of the Polychromator.

CHAPTER 4.

NOISE IN MEASURED SIGNALS.

Many workers, for example, Boumans et al.[62, 63], state that the relative standard deviation of the measured emission signal over a wide range of concentration is constant. This type of noise, proportional to the signal rather than its square root, has been observed in several kinds of spectroscopic systems[64]. In electronics it is known as "pink noise" since its low frequency components dominate in its power spectrum, in contrast to the more familiar "white noise", where all components have the same amplitude.

A peculiar property of a system with pink noise is that increasing the integration time will not improve the signal/noise ratio. This is almost a paradox, for doubling the integration time is in many ways equivalent to taking the mean of two readings, which normally improves the precision. The explanation, appears to lie in the noise spectrum. With white noise, the signal can jump from one value to another with great freedom, so that a high value is likely to be followed by a low one and two readings is therefore likely to be better than a single reading. With pink noise, however, where low frequency components dominate, a high reading will require many of these components to be positive. Since they are low frequency, a relatively long time must elapse before they change sufficiently to allow a low reading to occur. Thus in consecutive readings high values tend to follow high values and so a mean of two shows little, if any, improvement over a single value.

62. P.W.J.M.Boumans and F.J.de Boer, Spectro-Chim. Acta. 1972, 27B, 391.

63. Idem. Ibid. 1975, 30B, 309.

64. J.O.Ingle, Jun., Anal. Chem. 1977, 49, 339.

Section 4.1 Fourier Analysis.

Experiments were carried out, using a plasma source without analyte, where readings of the photo-multiplier output from the sodium 5890Å channel were punched at a rate of about 14 per second for about a minute. This was achieved by feeding the output of the photomultiplier into the "Modulog" data logger and thence into a high speed paper tape punch. Plasma conditions were not recorded as they were not considered to be important.

The resulting plot indicated that there might be some periodicity. A Fourier analysis was carried out. The algorithum for performing this assumes that the set of readings corresponds to half a period, so that the assumed period is two minutes and the fundamental frequency is $^{1}/_{120}$ per second i.e. 0.0083 Hz. The first hundred harmonics were calculated, Table 5.

TABLE 5.

Fourier Analysis of Photomultiplier Signals

	Cosine Values	Frequency Hz	Mean of Moduli
1.	100.139596	0.0083	
2.	66.342120		
3.	40.296473		
4.	39.823253		
5.	4.976448		
6.	16.920285		
7.	-2.766459		
8.	-40.812485		
9.	-1.191430		
10.	-16.589949	0.083	32.9
11.	8.663648		
12.	21.017252		
13.	18.663982		
14.	-9.456564		
15.	1.229285		
16.	10.033206		
17.	16.973824		
18.	-16.882899		
19.	-0.656687		

TABLE 5 (contd)

	Cosine Values	Frequency Hz	Mean of Moduli
20.	-14.041261	0.166	11.7
21.	-10.678848		
22.	15.945893		
23.	-7.445489		
24.	-10.212133		
25.	11.682048		
26.	-4.820914		
27.	-11.482011		
28.	-3.987730		
29.	-17.578028		
30.	5.088432	0.249	9.8
31.	8.111728		
32.	-6.853823		
33.	-4.595546		
34.	-33.250046		
35.	-2.460208		
36.	7.513333		
37.	-10.504395		
38.	-9.912675		
39.	-3.566708		
40.	2.602825	0.332	8.9
41.	20.555519		
42.	11.169309		
43.	-12.563534		
44.	6.541921		
45.	-6.594364		
46.	-13.604203		
47.	-4.476244		
48.	-1.968937		
49.	5.790979		
50.	0.072564	0.415	8.3
51.	-13.498690		
52.	11.425497		
53.	7.794419		
54.	2.340794		
55.	-2.227517		
56.	13.501519		
57.	5.616568		
58.	-4.182845		
59.	0.461633		
60.	12.238667	0.498	7.3
61.	5.344566		
62.	-3.367399		
63.	-6.106444		
64.	-19.306985		
65.	5.250138		
66.	16.135496		
67.	-1.242266		
68.	-8.997971		
69.	-0.257131		

TABLE 5 (contd)

	Cosine Values	Frequency Hz	Mean of Moduli
70.	2.046067	0.581	6.8
71.	1.643273		
72.	0.348404		
73.	-2.203385		
74.	6.463187		
75.	2.307185		
76.	4.291800		
77.	11.595497		
78.	3.627345		
79.	-2.674324		
80.	6.159507	0.664	4.1
81.	4.861743		
82.	-5.046484		
83.	1.464889		
84.	7.248294		
85.	0.703679		
86.	-6.861671		
87.	0.327370		
88.	8.151172		
89.	5.908400		
90.	-0.856781	0.747	4.1
91.	-0.537233		
92.	-0.925972		
93.	-1.585038		
94.	5.047474		
95.	-8.997994		
96.	-0.572437		
97.	1.202327		
98.	-1.670502		
99.	-1.181177		
100.	6.622380	0.83	2.8

The largest amplitudes are associated with the lowest frequencies, and although the amplitudes fluctuate individually, it can be seen, from calculating the mean of the module in ten successive groups of ten, that the mean amplitude is decreasing with frequency (32.9, 11.7, 9.8, 8.9, 8.3, 7.3, 6.8, 4.1, 4.1, 2.8). This is, at least qualitatively, characteristic of pink noise.

Section 4.2 Relative Standard Deviation of the Signal.

In another experiment, the signal obtained from an aerosol of water injected into the plasma was measured on a number of channels of the Polychromator, at various heights in the plasma, in order to obtain a range of signals from different P.M. tubes. Plasma conditions were again, not recorded.

The signal due to continuum and any molecular emission from the water was measured in the Na, Mo, Ba and Mn channels (at gains 9, 5, 11 and 7 respectively) at height counter readings of 900, 1000, 1100, 1200, 1250, 1300 and 1350. One hundred counts represented a distance, in a vertical direction, of one centimeter. (At height 1350 only the Mo and Mn channels were used, the others being overloaded). Ten replicate readings were taken (four being rejected from height 1100 because of the likelihood of air having been entrained, since the solution sampling beak was subsequently observed to have jammed). Standard deviations were calculated and listed with the mean signals as shown in Table 6.

TABLE 6.

Readings of Signal and Standard Deviations.

x	σ	x	σ
152	2.1	1638	28.5
162	3.7	1670	35.4
167	2.9	2167	95.4
186	4.0	2318	22.2
241	3.8	3952	65.5
358	9.4	3962	89.0
412	5.4	4298	113.2
441	52.6	6684	104.3
495	21.9	7936	93.5
658	10.5	11704	143.6
783	43.8	13397	82.8
1479	53.0	19234	152.2
1517	68.2	24693	572.8

These are shown plotted on log-log paper in Fig. 35. The logarithms of x and σ were used to calculate by least squares the best straight line. The slope, i.e. regression coefficient, was 0.90 and the relation between σ and x was

$$\sigma = 0.04\ x^{0.90}$$

This line is shown superimposed on the data points in Fig. 35.

The standard deviation of the value regression coefficient 0.90 is ± 0.07 which for 95% confidence limits is ± 0.14.

The closeness of 0.90 ± 0.14 to unity serves as a justification for believing that the noise in the background is proportional to the background and not to its square root, the noise is therefore best described as pink.

The conclusions of the previous experiment were tested in a different manner. An iron solution containing 1 p.p.m. of iron was nebulized into the plasma. The plasma conditions were arbitrary and were not recorded. The wavelength used was 2599Å. Ten replicate readings were taken at ten seconds exposure and at one hundred seconds exposure.

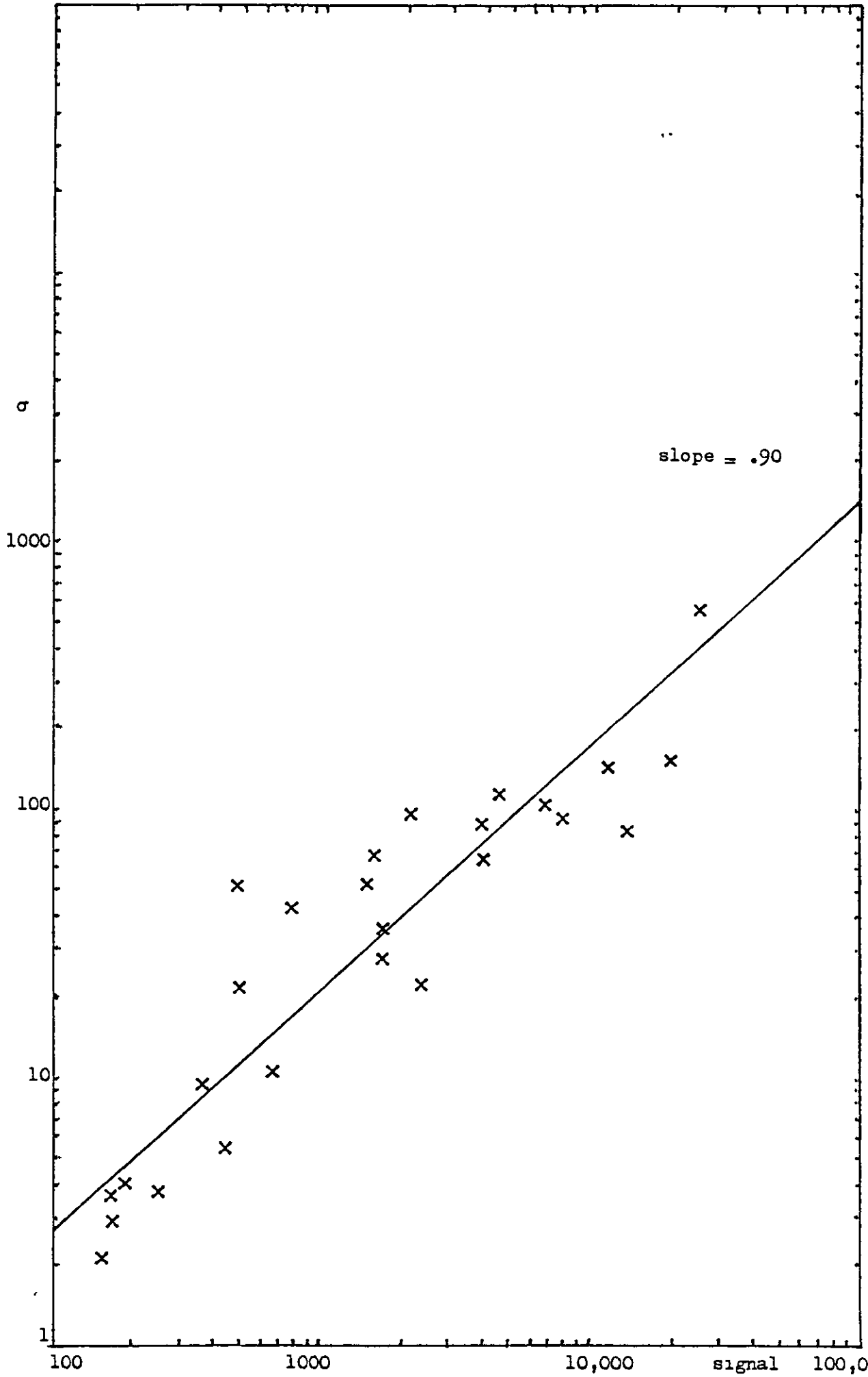

Fig. 35. Plot of standard deviation (σ) versus signal.

The experiment was repeated using a 0.1 p.p.m. solution. The results are shown in Table 7.

TABLE 7.

Replicate Readings of 1.0 and 0.1 p.p.m.

Solutions of Iron.

Iron conc. p.p.m.	1.0	1.0	0.1	0.1
Exposure time, secs.	100.0	10.0	100.0	10.0
Mean ($\bar{x}$)	37,204.0	3774.5	21,629.0	2207.4
Std. Dev. (σ)	256.9	37.6	295.3	29.5

For standard deviations of two sets of data σ_1 and σ_2 the confidence limits of the ratio σ_1/σ_2 are tabulated[65]. For 95% confidence the lower limit is (for 9 degrees of freedom in each) $0.50\ \sigma_1/\sigma_2$ and the upper limit is $2.01\ \sigma_1/\sigma_2$.

Then $\frac{256.9}{37.6} = 6.839$ and the limits are 3.42 and 13.7.

Similarly for $\frac{295.3}{29.5} = 9.99$ the limits are 5.00 and 20.1.

Thus neither set includes the ratio $\sqrt{10} = 3.16$; but both include the ratio 10. Thus a square root dependance on the signal for the noise is excluded. Linear dependance is compatible with both sets of results.

Having established that the noise is proportional to the signal it was now possible to examine the signals coming from the plasma from the point of view of deciding that criteria which could be properly used to compare one torch with another.

65. O.L.Davies, Statistical Methods in Research and Production, 3rd Ed., Oliver and Boyd 1958. Table H.

CHAPTER 5.

THE CRITERIA TO BE USED FOR COMPARING PLASMA TORCHES.

Summary

In this chapter the concept of the intrinsic merit of a plasma is introduced. This is defined for present purposes as the ratio of the spectral radiancy of a spectroscopic line to that of the background at the same wavelength. Spectral radiancy is a function of the plasma alone, independent of the spectrometer and measuring system. The consequent independence of the intrinsic merit of a plasma on spectrometer and measuring system is a justification for its name.

In practice, of course, signals can be utilised only after passing through the spectrometer and measuring system. They thus have a contribution from the dark current. Experiments have shown that with the apparatus used in this laboratory, dark currents are in general related hyperbolically to the gain while net signals are related linearly to the gain. Because of the difference of these effects, any quantities depending on measured signals will also depend on the gain. Such quantities discussed in this chapter are the maximised net signal, i.e. the net signal obtained when the gross signal fills the measuring scale, and the gross signal to background ratio, on which, it is shown, the detection limit depends when the noise of the background is proportional to the background. A different ratio, but involving the same quantities is appropriate when the noise depends on the square root of the background.

Much of the chapter is concerned with the discussion of whether the better (in the intrinsic sense) of two plasmas will always yield the better detection limit when the spectrometer and measuring system are taken into account. It will become apparent that if the dark current is zero, the better plasma does in fact always give the better detection limit, but if the dark current is not negligible, the better plasma may or may not give the better detection limit, because the rate at which a non-negligible dark current degrades the detection limit depends on the plasma.

Criteria to decide whether the better plasma gives the better detection limit are derived. These are of two types. The first type is a necessary criterion in the sense that if it is satisfied then the better plasma certainly gives the better D.L. and if it is not satisfied the better plasma certainly gives the poorer D.L. It will be shown that such criteria are not useful in practice because of the impossibility of evaluating a factor which occurs in them. The second type can be called a sufficient criterion. This is more restrictive than the first kind but involves only measurable quantities. If it is satisfied then the better plasma certainly gives the better D.L; if it is not satisfied then the better plasma may or may not give the better D.L.

Sometimes it has been found experimentally that the relation between dark current and gain, in general hyperbolic, simplifies to a linear dependence. Two special cases of this kind are treated, namely, when the relation is a straight line through the origin, which is the same relation as for a signal, and when the dark current is constant with respect to gain. These special cases have simpler criteria.

The case where maximum useful gain is used, so that the measuring scale is filled by the gross signal, is treated, since with the apparatus used in this laboratory detection limits improve with gain. The criteria derived in this case are reported only for the special cases of linear dependence of dark current on gain, because of the excessive complexity of the general hyperbolic case.

The conclusion can be drawn that detection limits, necessarily involving the spectrometer and measuring system, need not always be reliable indicators of the intrinsic merit of a plasma.

In Section 1.3 the object of the present work was given as the study of the emitted light intensities of elements using high and low power plasmas to determine the optimum wattage necessary to do useful analytical work. It was shown that valid intersource comparisons could only be made on the same system. What was not specified were the criteria to be used in any such comparisons.

Of the generally accepted criteria used in comparisons of atomic spectroscopic techniques,[55] those appropriate to the proposed intersource comparison are :-

1) Limits of detection.

2) Convenience of operation. Particular points are the ability to accept high salt concentration without extinguishing the plasma, minimisation of the effects of impedance changes consequent on the introduction of material into the plasma and freedom to work with gases other than argon. These are effects depending on energy density or electron density and when these are both high, as they are when the power is high, a given change causes a smaller fractional change.

3) Dissociation of Molecules. A high degree of molecular dissociation prevents chemical matrix effects which are due to the formation of refractory species and in addition gives a reduction of background effects from molecular bandheads.

4) Ionisation. Unless the power density is such as to produce a substantial electron density due to the ionisation of the gases, the introduction of an easily ionised material will make a marked difference to the electron density thus perturbing the ionisation equilibria.

It can readily be seen that an increase of power will be favourable to criteria 2, 3 and 4. Criterion 1 is subject to the most controversy. Initially it seemed attractive to use detection limits as a measure of the merit of a plasma. It will be shown later in this chapter that detection limits involve the noise on the background and hence, as discussed in Chapter 4, the magnitude of the background. In many cases in this laboratory the background consists almost entirely of the dark current so that the detection limit depends strongly on the dark current; thus it depends on the measuring system of the spectrometer and not solely on the plasma. It became desirable, therefore, to deduce a quantity depending on the plasma alone by which two plasmas could be compared. It is shown that the ratio of the net signal to the net background is such a quantity, giving a measure of the ratio of spectral radiances of line and background. The relation between detection limit and this ratio is examined to see under what circumstances the plasma with the highest ratio gives the best detection limit.

First it is necessary to examine the relationship governing the signals received from the plasma and the spectrometer; these are shown diagramatically in Fig. 36.

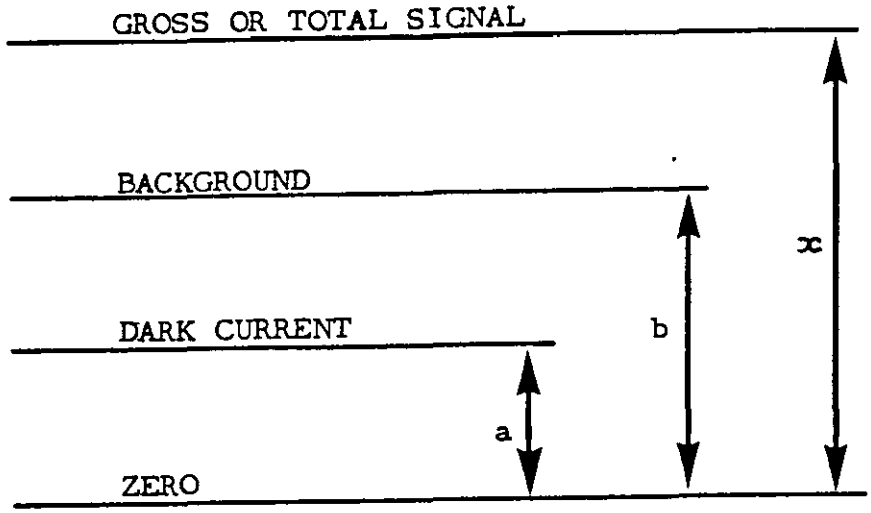

Fig. 36. Signals Obtained from the Spectrometer.

The dark current mainly arises either from thermal electrons leaving the photocathode, in which case the current will increase with the voltage applied to the PM tube, or, from current leakage at the anode in which case the value will not increase markedly with gain or voltage[66]. In both cases if the applied voltage is increased beyond a certain value a glow discharge from the ionisation of the gas in the tube occurs and the dark current increases rapidly. These effects are shown in Fig. 37 obtained from data from the P.M. tubes of the Polychromator.

Each line represents the response curve for a single PM tube. The DVM readings are plotted logarithmically. The gains are the readings of the sensitivity knobs; advancing these knobs by one position doubles the sensitivity, so that the horizontal axis too is effectively logarithmic in the factors by which signals are multiplied. The "expected slope" is a line showing how a signal due to incidental light increases with gain.

66. Photomultiplier Tubes. EMI Electronics Ltd. Brochure P001/FP 70. 1970.

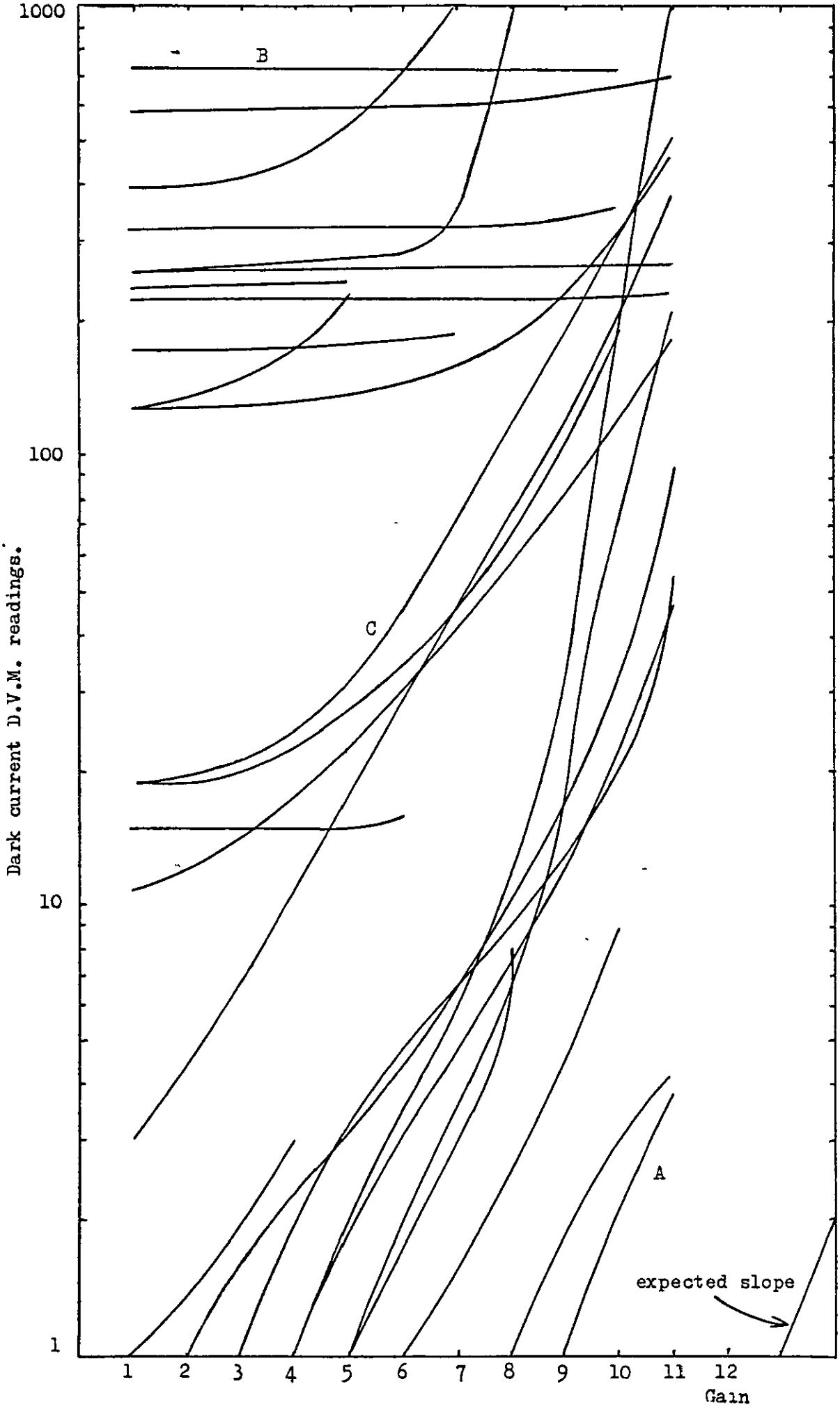

Fig. 37. Plot of dark currents versus gain for 29 P.M. tubes.

It will be seen that the dark currents fall into three classes: A, the dark current arising from electrons emitted thermally from the cathode; B, the dark current arising from anode leakage; and C, a mixture of A and B. Examples of these are suitably labelled in Fig.37.

Until the glow occurs, all the variations in dark current measured in this laboratory have been found to fit a hyperbolic function

$$a = \frac{P_1 g + R_1}{1 + Q_1 g}$$

An example of the fit obtained (for the data of Channel 4) is shown in Table 8.

Table 8. Observed and Calculated Values of Dark Currents.

Gain Factor.	Observed dark current.	Calculated dark current.
1	131	131.4
2	132	131.8
4	133	132.7
8	135	134.5
16	139	138.1
32	147	145.1
64	158	158.9
128	184	185.6
256	232	235.4
512	326	322.8
1024	460	460.6

The values of P_1, Q_1 and R_1 obtained for the thirty channels of the spectrometer from least squares fitting are listed in Table 9. There was no photomultiplier in Channel 19. It may be noted that Channels 3, 5, 12, 22 and 28 have negative values of Q_1 and channel 12 has in addition a negative value of P_1. It will appear later that

certain conclusions can be drawn if P_1, Q_1 and R_1 are not negative, so that it is desirable to examine whether the negative values obtained are significantly different from zero. Estimation of confidence limits of P_1, Q_1 and R_1 is complicated. Instead, the relevant experimental data are plotted in Fig. 38. It will be seen that deviations from straight lines are small and on this basis it seems permissable in each case to take Q_1 as zero (so that the hyperbolae reduce to straight lines) and replace the calculated hyperbolae by straight lines with slopes and intercepts which are positive or zero. We can then claim that, in this experiment, P_1, Q_1 and R_1 never take negative values.

Table 9. Values of P_1, Q_1 and R_1 in the equation $a = \frac{P_1 g + R_1}{1 + Q_1 g}$ relating dark current to gain.

Channel	P_1	Q_1	R_1
0	.0417	.00015	226.4
1	.0330	.00062	.90
2	.0440	.0113	.75
3	.0655	- .00072	176.1
4	.498	.00038	130.9
5	.0394	- .00012	1.40
6	26.34	.0360	736.7
7	0	0	15.0
8	.437	.00019	9.64
9	0	0	0
10	.0162	.0032	.27
11	.0082	.0011	.43
12	- .567	- .0018	325.8

Table 9 (contd)

Channel	P_1	Q_1	R_1
13	22.30	.0746	256.9
14	.0763	.00062	1.47
15	.368	.0011	15.9
16	.0605	.00019	261.5
17	.0793	.0057	.57
18	.0040	.00014	.32
19	-	-	-
20	.702	.00082	598.1
21	38.52	.156	240.4
22	9.974	- .0011	387.3
23	.438	.00043	19.2
24	.864	.19	.51
25	.764	.00006	20.8
26	6.03	.0033	124.1
27	0	0	1.0
28	.0539	- .0021	.92
29	0	0	1.0

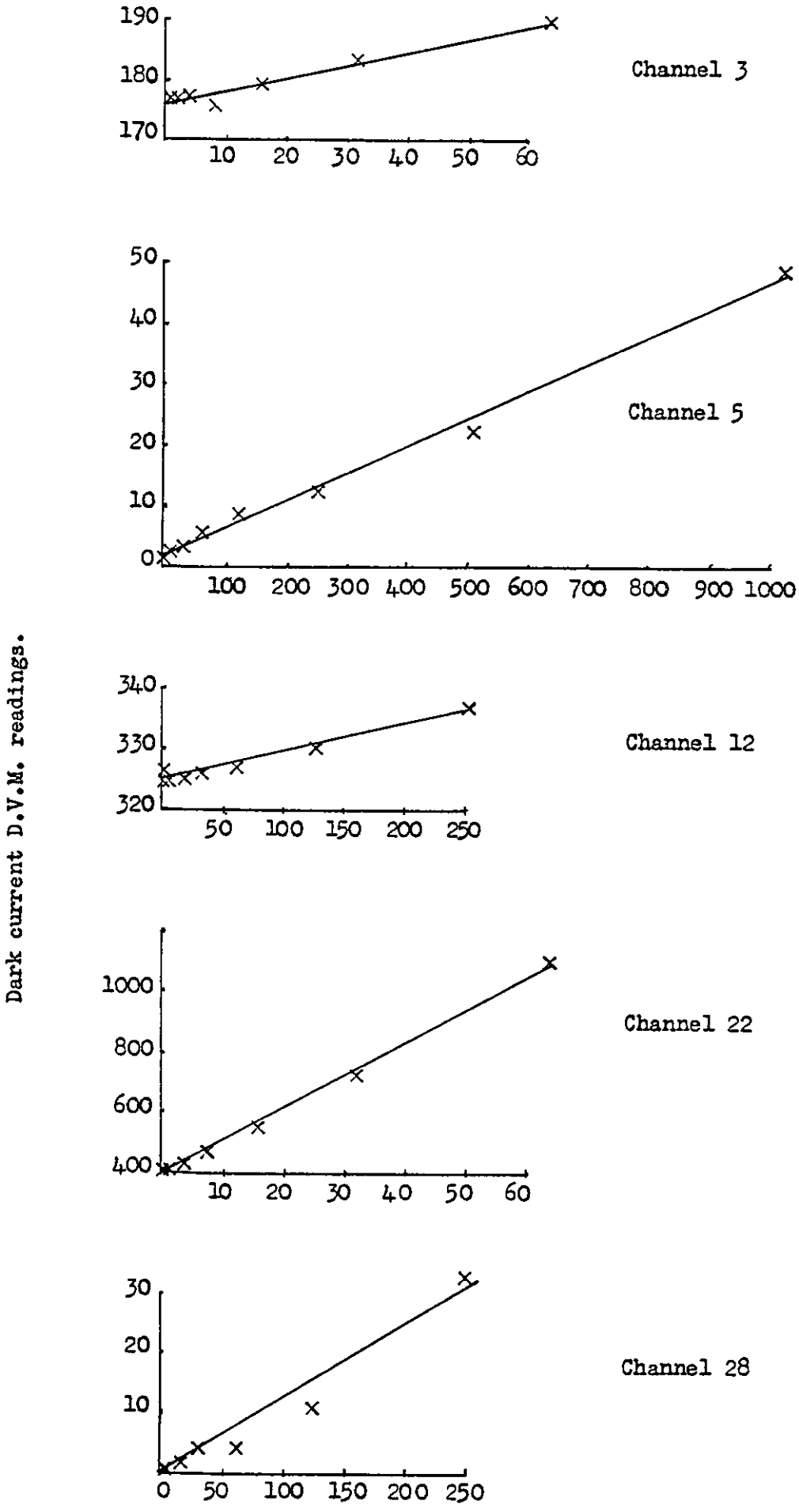

Fig. 38. Linear plot of dark current against gain for selected channels.

Section 5.1 The Relationship Between the Net Signal, Net and Gross Signal to Background Ratios and the P.M. tube Amplification and Dark Current.

5.1.1 Intrinsic Merit.

Let p and q be the spectral radiances (the energies emitted in watts per sq.cm. per steradian per Angstrom) corresponding to net signal and net background emitted by the plasma. The ratio p/q, depending on the plasma alone, can be taken as defining the "intrinsic merit" of the plasma. The intensities reaching the photomultipliers will depend not only on p and q but also, since the dimensions of p and q are watts per sq.cm. per steradian per A, on the area of the appropriate part of the plasma, on the solid angles used, and on the wavelength range passed by the exit slits.

If the plasma is focussed on the plane of the entrance slit, the only area of the plasma which produces light entering the spectrometer is that which produces the part of the image defined by the area of the slit. This part of the plasma is thus responsible for both signal and background and anything happening elsewhere in the plasma is therefore not observed.

The useful solid angle is defined by the useful aperture of the lens, which in its turn is defined by the solid angle subtended by the ruled part of the grating at the entrance slit as is shown in Fig. 39.

Any solid angle in excess of this will not contribute to the signal, but may, by scattering stray light, add to the background, if the masking is not adequate.

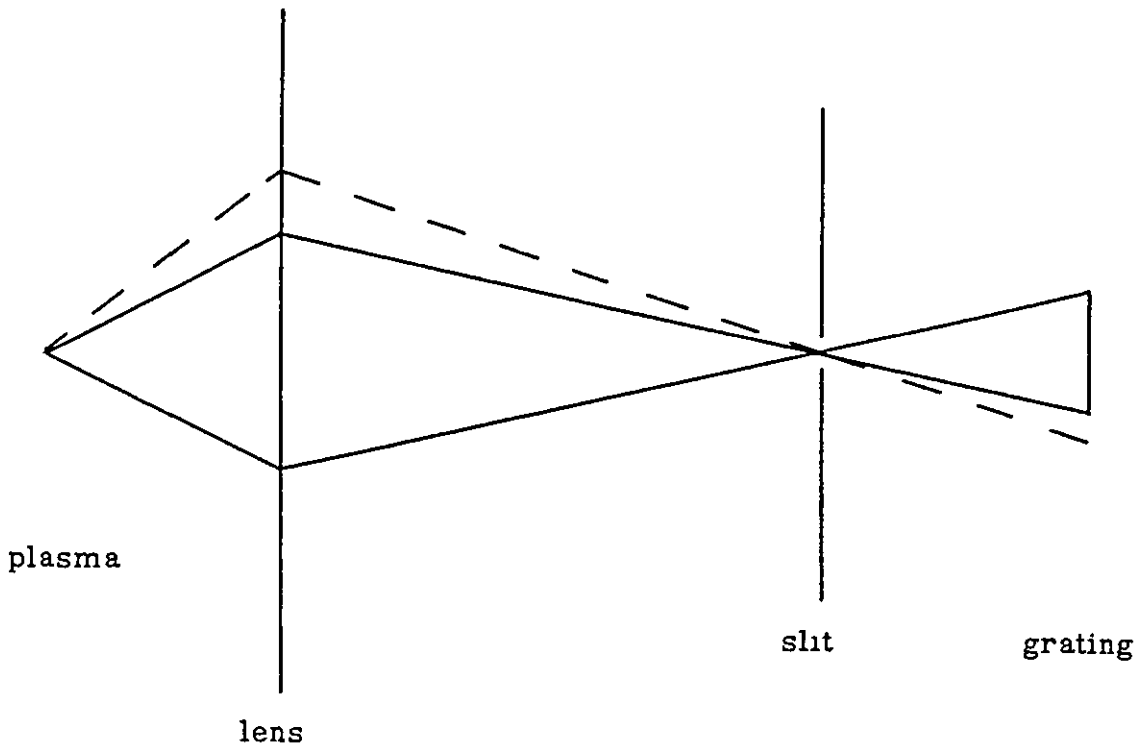

Fig. 39. Useful Solid Angle of the Entrance Optics.

The resolution of the spectrometer in practice is likely to be defined by the angle subtended by the width of the entrance slit at the grating. The width of the exit slit should be wide enough to include only the image of the spectral line. If it is wider than this, the exit slit will pass background radiation in a wavelength range greater than necessary, thereby increasing the background without affecting the signal of analytical interest.

Thus as a consequence of the units (watts per sq.cm. per steradian per Angstrom) in which the radiances p and q are expressed, the factors by which p and q have to be multiplied to give the energy per unit time incident at the photo cathode will depend first, on the area of the plasma observed, second on the useful solid angle and third, on the wavelength range passed by the exit slit, that is on the width of the exit slit.

Let u be the factor for the signal radiancy p and v that for the background radiancy q.

Thus $u = u_1\ u_2\ u_3$.

u_1, the area of the plasma observed, is given by the area of the entrance slit divided by the magnification of the entrance optics.

u_2 is the solid angle subtended by the ruled part of the grating at the entrance slit (see Fig. 39).

In the case of the signal the wavelength range passed by the exit slit is not directly the quantity of interest. A spectral "line" observed at the exit slit is in fact an image (usually at unit magnification) of the entrance slit formed with radiation of the wavelength of the line. The quantity of interest is the fraction of this image which is transmitted by the exit slit. u_3 is defined as this fraction, which cannot of course, exceed unity: when the complete line profile is accepted, the signal cannot be increased by further widening of the exit slit.

The factor v by which q has to be multiplied to give the background energy depends similarly on three factors

$v = v_1\ v_2\ v_3$.

v_1 is identical to u_1, since the same part of the plasma is observed both for signal and background.

The useful solid angle is likewise the same for the signal and that part of the background radiation which is dispersed by the grating. The background may have components due to scattered light in addition however and these can be taken account of in a formal way by allowing v_2 to exceed u_2.

As the exit slit is widened there is no limitation on the increase in background radiation transmitted. The appropriate value for v_3 is therefore the wavelength range passed by the exit slit.

The difference in treatment of signal and background is due to the difference between the continuous nature of the background and the narrow profile of a line. The energy of the background radiation in a range of 10A is ten times that in a range of 1A (more or less). The energy in a spectral line will be the same in both cases (provided the line width is less than 1A).

If there are other properties of the spectrometer affecting the signal and background that this discussion overlooks they will involve other factors u_n and v_n.

The important point is that the factors which determine u and v are properties of the spectrometer alone, namely the focal length and aperture of the lens in the entrance optical system and the dimensions of entrance slit, exit slit and grating. They are not dependent on the plasma.

The gross signal arriving at the photocathode is thus (up + vq) and the background is vq. These will then be amplified by the photomultiplier, which is the sole amplifier in the system used. The dark current, which may or may not be amplified, dependent on its origin, is added. For unit amplification, the gross signal is

$$x_1 = up + vq + a_1 \quad - - - - - - - - - - - - - \quad 1$$

and the gross background

$$b_1 = vq + a_1 \quad - - - - - - - - - - - - - \quad 2$$

This is shown schematically in Fig. 40.

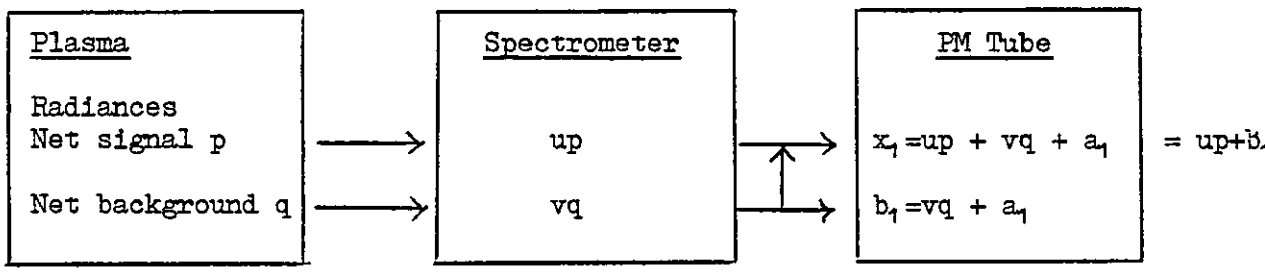

Fig. 40. Signals arriving at the PM Tube

$$\text{Now } q = \frac{b_1 - a_1}{v} \qquad \text{----------} \quad 3$$

$$\text{and } p = \frac{x_1 - b_1}{u} \qquad \text{----------} \quad 4$$

$$\text{Therefore } \frac{p}{q} = \frac{v}{u} \cdot \frac{x_1 - b_1}{b_1 - a_1} \qquad \text{----------} \quad 5$$

$$\text{i.e. } \frac{x_1 - b_1}{b_1 - a_1} = \frac{u}{v} \cdot \frac{p}{q} \qquad \text{----------} \quad 6$$

so that for a given value of $\frac{u}{v}$, $\frac{x_1 - b_1}{b_1 - a_1}$ is proportional to $\frac{p}{q}$

For gains other than unity, where the dark current a_1 is amplified by a factor f when the signal is amplified by gain g,

$$a = fa_1 \qquad \text{----------} \quad 7$$

$$x = g(x_1 - a_1) + fa_1 \qquad \text{----------} \quad 8$$

$$b = g(b_1 - a_1) + fa_1 \qquad \text{----------} \quad 9$$

x and b are the values at any gain g; x_1 and b_1 at $g = 1$.

Note that in general the factor f by which the dark current is amplified is not the same as the signal amplification g.

$$\text{Then } \frac{x - b}{b - a} = \frac{g(x_1 - a_1) + fa_1 - g(b_1 - a_1) - fa_1}{g(b_1 - a_1) + fa_1 - fa_1}$$

By cancellation

$$\frac{x - b}{b - a} = \frac{x_1 - b_1}{b_1 - a_1} \qquad \text{----------} \quad 10$$

and from equation 6

$$\frac{x - b}{b - a} = \frac{u}{v} \cdot \frac{p}{q} \qquad \text{----------} \quad 11$$

Thus the ratio of net signal to net background (hereafter called the "net ratio") is proportional to p/q, regardless of gain.

This ratio is also independent of the nature of the dark current, and indeed of its magnitude, for if a is increased to a + d, x is increased to x + d and b to b + d so that the new ratio $\frac{(x + d) - (b + d)}{(b + d) - (a + d)}$ keeps its value $\frac{x - b}{b - a}$.

5.1.2 Conditions for Maximum Net Signal (General Case).

Given a series of readings of x, b and a, it is of interest to predict which set corresponds to the largest value of net signal when amplification is applied to fill the scale of the measuring instrument, of length A.

To fill the scale A with the gross signal x we must amplify by a factor C, the maximum useful amplification, defined as that value of g which produces a gross signal of magnitude A.

Then $C(x_1 - a_1) + fa_1 = A$ ---------- 12

so that $C = \frac{A - fa_1}{x_1 - a_1}$ ---------- 13

and the amplified values of the net signal and net background are

$$\frac{A - fa_1}{x_1 - a_1}(x_1 - b_1) \quad \text{and} \quad \frac{A - fa_1}{x_1 - a_1}(b_1 - a_1)$$

These two quantities add up to $A - fa_1$, the available scale length.

It was shown previously that it had been found by experiment that the dependence of dark current on gain could be expressed as a hyperbolic function, provided the gain was not so large as to cause ionisation glowing in the PM tube.

Thus $$a = \frac{P_1 g + R_1}{1 + Q_1 g} \qquad \text{---------- 14}$$

It is now convenient to write $a = fa_1$ where a_1 is the value of a when $g = 1$, namely $\frac{P_1 + R_1}{1 + Q_1}$

Then $$f = \frac{a}{a_1} = \frac{P_1 g + R_1}{1 + Q_1 g} \cdot \frac{1 + Q_1}{P_1 + R_1} \qquad \text{------- 15}$$

$$= \frac{\frac{P_1(1 + Q_1)g}{P_1 + R_1} + \frac{R_1(1 + Q_1)}{P_1 + R_1}}{1 + Q_1 g} \qquad \text{----- 16}$$

$$= \frac{Pg + R}{1 + Qg} \qquad \text{---------- 17}$$

where P, Q and R are defined by the relations

$$P = \frac{P_1(1 + Q_1)}{P_1 + R_1} \qquad \text{---------- 18}$$

$$R = \frac{R_1(1 + Q_1)}{P_1 + R_1} \qquad \text{---------- 19}$$

$$Q = Q_1 \qquad \text{---------- 20}$$

It was found that, in the experiments carried out, P_1, Q_1 and R_1 were never significantly negative. It follows that P, Q and R are never significantly negative, so that they can be taken as positive or zero.

Then $$a = fa_1 \qquad \text{---------- 21}$$

$$= \frac{Pg + R}{1 + Qg} \cdot a_1 \qquad \text{---------- 22}$$

Since the value of a when $g = 1$ is a_1, it follows that

$$P + R = 1 + Q \qquad \text{---------- 23}$$

The maximum amplification C is now obtained from equation 13 by substituting the appropriate value of f, namely that corresponding to amplification C.

Then $$C = \frac{A - \frac{PC + R}{1 + QC} \cdot a_1}{x_1 - a_1} \qquad \text{---------- 24}$$

i.e. $$C(x_1 - a_1) = \frac{A + AQC - PCa_1 - Ra_1}{1 + QC} \qquad \text{---------- 25}$$

i.e. $$C(x_1 - a_1) + QC^2(x_1 - a_1) - A - AQC + PCa_1 + Ra_1 = 0 \qquad \text{------ 26}$$

i.e. $$C^2.Q(x_1 - a_1) + C(x_1 - a_1 - AQ + Pa_1) + Ra_1 - A = 0 \qquad \text{------ 27}$$

This is a quadratic equation with two roots,

$$C = \frac{-(x_1 - a_1 - AQ + Pa_1) \pm \sqrt{\{(x_1 - a_1 - AQ + Pa_1)^2 + 4Q(x_1 - a_1)(A - Ra_1)\}}}{2Q(x_1 - a_1)} \qquad \text{-- 28}$$

The appropriate root is that with the positive sign, as shown by the following argument.

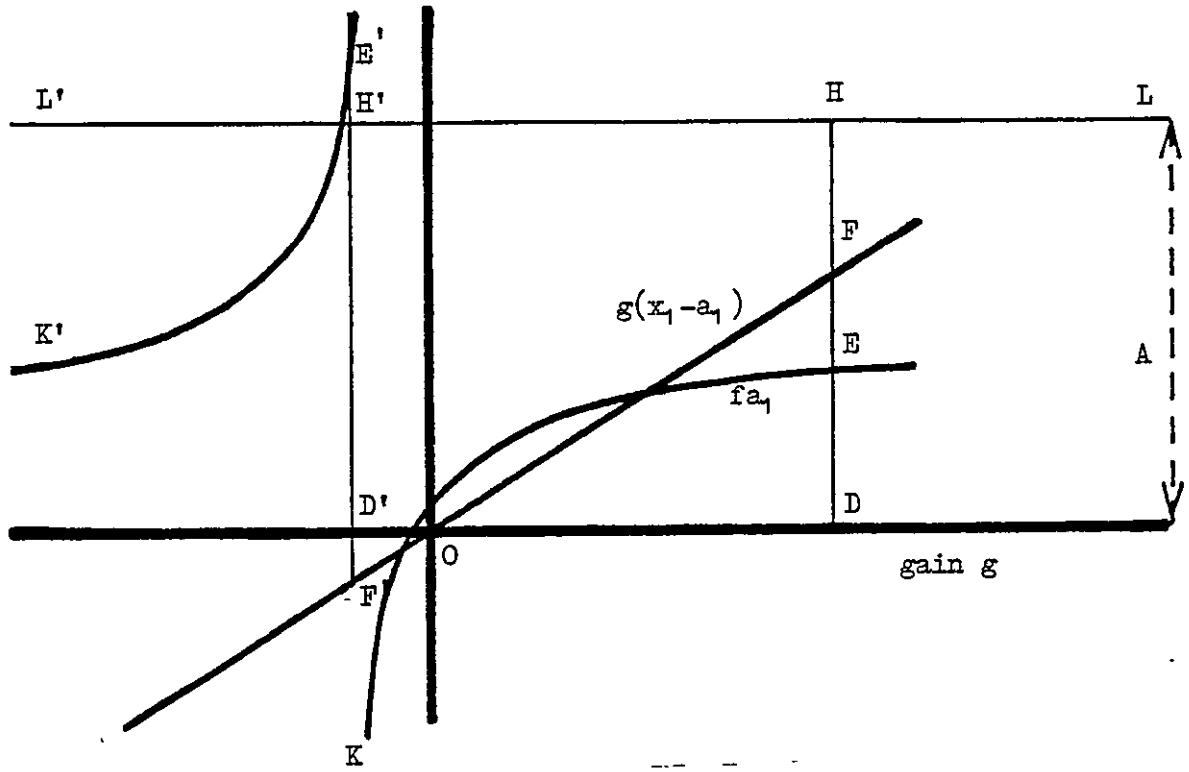

Fig. 41. Dependence of components of gross signal on gain.

The gross signal x is given by

$$x = g(x_1 - a_1) + fa_1 \qquad \text{(equation 8)}$$

If the two terms in this equation are plotted separately against g, the first is a straight line through the origin (OF in Fig. 41) while the second (because f has a hyperbolic dependence on g) is a hyperbola, which formally must have two branches (KE and K'E' in Fig. 41). Since the gain g in reality must be positive, only the right-hand branch KE is of physical importance. For two values of g the sum of the two terms will fill the scale length A (represented by LL'). These values of g are represented by OD, such that DE + DF = DH and OD', such that D'E' + D'F' = D'H'. In the second case OD' and D'F' are negative and the solution, involving a negative value of gain, is purely conceptual. Thus of the two solutions of the quadratic in the maximum amplification C, one is positive and one negative and the required solution, necessarily positive, must be given by taking the positive sign in the expression for the root. (Had both roots been positive and hence physically possible, a more complicated argument would be required to choose the appropriate one).

The value of the net signal when the gross signal fills the scale is thus $C(x_1 - b_1)$

$$= \frac{1}{2Q}\frac{x_1 - b_1}{x_1 - a_1}\left[\sqrt{\{(x_1 - a_1 - AQ + Pa_1)^2 + 4Q(x_1 - a_1)(A - Ra_1)\}} - (x_1 - a_1 - AQ + Pa_1)\right] \quad --- 29$$

The quantities involved in this equation can all be obtained by measurement.

Despite effort, it does not seem possible to simplify the expression. It had been hoped that a simple criterion could be obtained, so that from measurements made in experiments where the

scale was not filled, the conditions under which the highest net signal would be obtained when the scale was filled, could be deduced. It does not seem possible to achieve this aim for the general case where the dark current is related hyperbolically to the gain. However simpler criteria are obtained if the dark current is related linearly to gain.

5.1.3 Special Case 1. (Any straight line).

If the value of Q is zero, the hyperbolic function becomes a straight line with slope P and intercept R.

When Q = 0, equation 27 reduces to

$$C = \frac{A - Ra_1}{x_1 - a_1 + Pa_1} \qquad \text{------- 30}$$

Since P + R = 1 + Q (equation 23), in this case P + R = 1 so that

$$C = \frac{A - Ra_1}{x_1 - Ra_1} \qquad \text{------- 31}$$

The maximised net signal, that is, the net signal obtained when the scale length A is filled by the gross signal x, is then given by

$$\frac{A - Ra_1}{x_1 - Ra_1} \cdot (x_1 - b_1) \qquad \text{------- 32}$$

$$= \frac{A - Ra_1}{x_1 - b_1 + b_1 - Ra_1} \cdot (x_1 - b_1) \qquad \text{------- 33}$$

$$= \frac{A - Ra_1}{1 + \dfrac{b_1 - Ra_1}{x_1 - b_1}} \qquad \text{------- 34}$$

which is maximised when $\frac{x_1 - b_1}{b_1 - Ra_1}$ is maximised.

Two simple special cases are for R = 0 and R = 1.

5.1.4 Special Case 2. (Straight Line Through the Origin).

If R = 0 then P = 1 and we have for the dependence of dark current on gain a straight line through the origin, so that the dark current is amplified like a signal, $a = ga_1$. Under these circumstances the maximum in the ratio x_1/b_1 will indicate the conditions for maximum net signal.

5.1.5 Special Case 3. (Horizontal Straight Line).

If R = 1 then P = 0 and the line is horizontal so that dark current is independent of gain, $a = a_1$. For these circumstances it is the ratio $\frac{x_1 - b_1}{b_1 - a_1}$ which indicates the conditions to give maximum net signal.

In the discussions it has been tacitly assumed that the required amplification can be obtained.

Section 5.2 Detection Limits.

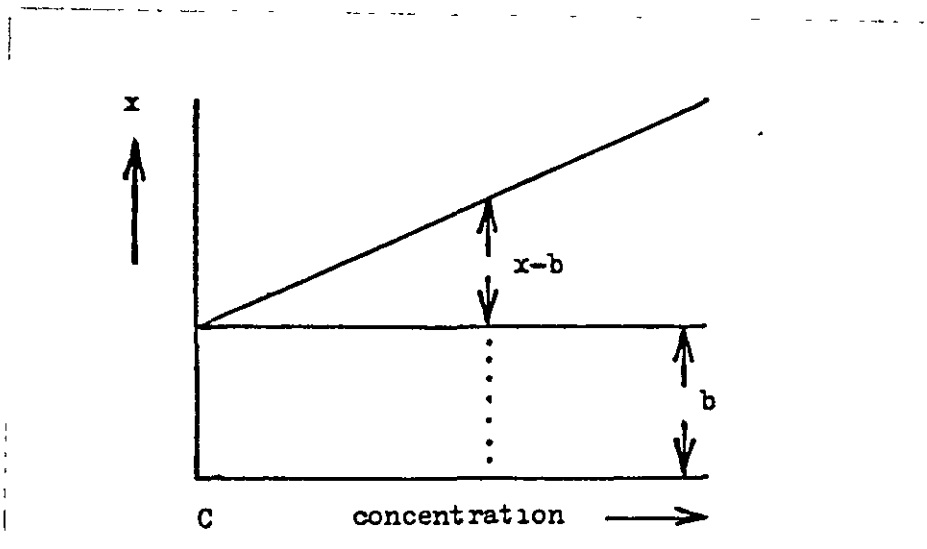

Fig. 42. Schematic Representation of Detection Limits.

In Fig. 42 the slope of the calibration curve is $m = \frac{x-b}{c}$, i.e. the net measured signal divided by the concentration which produces it. This is the sensitivity. An unknown concentration is found from $c = \frac{x-b}{m}$.

The Detection Limit (D.L.) is defined as the concentration giving a net signal twice (or some other factor n) the noise of the background.

i.e. for D.L. $x-b = 2\sigma(b)$ ----- 35

so that D.L. $= \frac{2\sigma(b)}{m} = 2\sigma(b).\frac{c}{x-b}$ ----- 36

where the net signal x-b is produced by a concentration c.

Now sensitivity m for an exposure of time t is m = N.t. where N is net counts per sec. per p.p.m. and $\sigma(Bt) = \sqrt{Bt}$ <u>if the noise in the background is given by the square root of the background</u>. (B is gross background in counts per sec.).

If R is defined as the signal to background ratio N/B, then $B = \frac{N}{R}$

and D.L. $= \frac{n\sqrt{Bt}}{Nt} = \left(n\sqrt{\frac{Nt}{R}}\right).\frac{1}{Nt}$ --- 37

$= \frac{n}{\sqrt{NtR}}$ --- 38

Thus for a square root dependence, exposure time must be taken into account.

For the case (as in the system under study) where the noise in the background is <u>proportional</u> to the background, $\sigma(b) = kb$.

Then D.L. $= \frac{2kbc}{x-b} = \frac{2kc}{\frac{x}{b}-1}$ --- 39

This is the smallest when x/b is a maximum. Thus to optimise the D.L. we have to maximise x/b. Note that this is the gross ratio.

If the dark current was very much less variable than the net background, then the noise in the gross background might be taken to be proportional to the net background (b-a). In this event

$$D.L. = \frac{2kc(b-a)}{x-b} \qquad \text{-------- 40}$$

and the D.L. would be minimised when the net ratio $\frac{x-b}{b-a}$ is maximised. This net ratio is proportional to p/q, the ratio of the spectral radiances of the plasma for signal and background, so that the plasma with the better value of p/q would always give the smaller D.L. Comparison of stabilities is a very difficult and tedious experiment. From a limited range of experiments no significant evidence was found that the dark current is more stable than the net background, so that the gross ratio x/b should be used to optimise the D.L.

Since the D.L. is inversely related to the gross ratio x/b it will depend not only on the plasma but also on the spectrometer system. The ratio p/q can be taken as a measure of the "intrinsic merit" of a plasma. The question arises "of two plasmas with different figures of merit under what conditions does the better always produce the lower detection limit?"

5.2.1 General Case. Necessary Conditions for the Better Plasma to Give the Better Detection Limit.

First a relation between x/b and the radiances p and q is obtained. This involves the gain g and the dark current at unit amplification a_1.

$a = fa_1$ (equation 7)

$x = g(x_1 - a_1) + fa_1$ (equation 8) $x_1 = up + vq + a_1$ (equation 1)

$b = g(b_1 - a_1) + fa_1$ (equation 9) $b_1 = vq + a_1$ (equation 2)

$$\frac{x}{b} = \frac{g(x_1 - a_1) + fa_1}{g(b_1 - a_1) + fa_1} \qquad \text{-------- 41}$$

$$= \frac{gup + gvq + fa_1}{gvq + fa_1} \qquad \text{-------- 42}$$

$$= \frac{gup}{gvq + fa_1} + 1 \qquad \text{-------- 43}$$

The way in which x/b varies with the dark current at unit amplification a_1, is illustrated for two different sets of conditions in Fig. 43. It is seen that the curves cross and it will be shown that the value of a_1 where the curves cross is a quantity of significance. This value of a_1 is derived as follows :

The curves cross when

$$\frac{x_1}{b_1} - \frac{x_2}{b_2} = \frac{g_1 up_1}{g_1 vq_1 + f_1 a_1} - \frac{g_2 up_2}{g_2 vq_2 + f_2 a_1} = 0 \qquad \text{--- 44}$$

i.e. when $g_1 g_2 uvp_1 q_2 + g_1 up_1 f_2 a_1 = g_1 g_2 uvp_2 q_1 + g_2 up_2 f_1 a_1$ --- 45

or after cancelling u,

$$g_1 g_2 v(p_1 q_2 - p_2 q_1) + a_1 (g_1 f_2 p_1 - g_2 f_1 p_2) = 0 \qquad \text{--- 46}$$

hence when

$$a_1 = \frac{- g_1 g_2 vq_1 q_2}{f_2 g_1 p_1 - f_1 g_2 p_2} \left(\frac{p_1}{q_1} - \frac{p_2}{q_2} \right) \qquad \text{--- 47}$$

$$= \frac{- g_1 g_2}{f_1 f_2} \cdot \frac{vq_1 q_2}{\frac{g_1 p_1}{f_1} - \frac{g_2 p_2}{f_2}} \left(\frac{p_1}{q_1} - \frac{p_2}{q_2} \right) \qquad \text{--- 48}$$

Since $\frac{x}{b} = \frac{gup}{gvq + fa_1} + 1$ (equation 43)

the value of x/b decreases as a_1 increases. Since a_1 cannot be negative, the maximum value of x/b is $\frac{up}{vq} + 1$, occurring at $a_1 = 0$.

Thus for zero dark current the better plasma (having the larger value of p/q) gives the larger value of x/b and hence the better D.L. The effect of a non-zero dark current is to degrade the value of x/b and hence the D.L. The rate of change of x/b with a_1 is dependent on the spectral radiances p and q, so that different plasmas will have different rates of change. This is why the curves of x/b against a_1 cross at the critical value of a_1 given by equation 48. There are two cases depending on whether this critical value is positive or negative.

Suppose the critical value is positive (Fig 43.1). Then if a_1, the actual dark current at unit amplification, is less than this critical value the plasma which has the higher value of x/b at $a_1 = 0$ will still have the higher value of x/b, so that the better plasma, though its D.L. is degraded more rapidly than the poorer one, still gives the better D.L. If, however, a_1 exceeds the critical value, the more rapid degradation of the D.L. of the better plasma results in a poorer D.L.

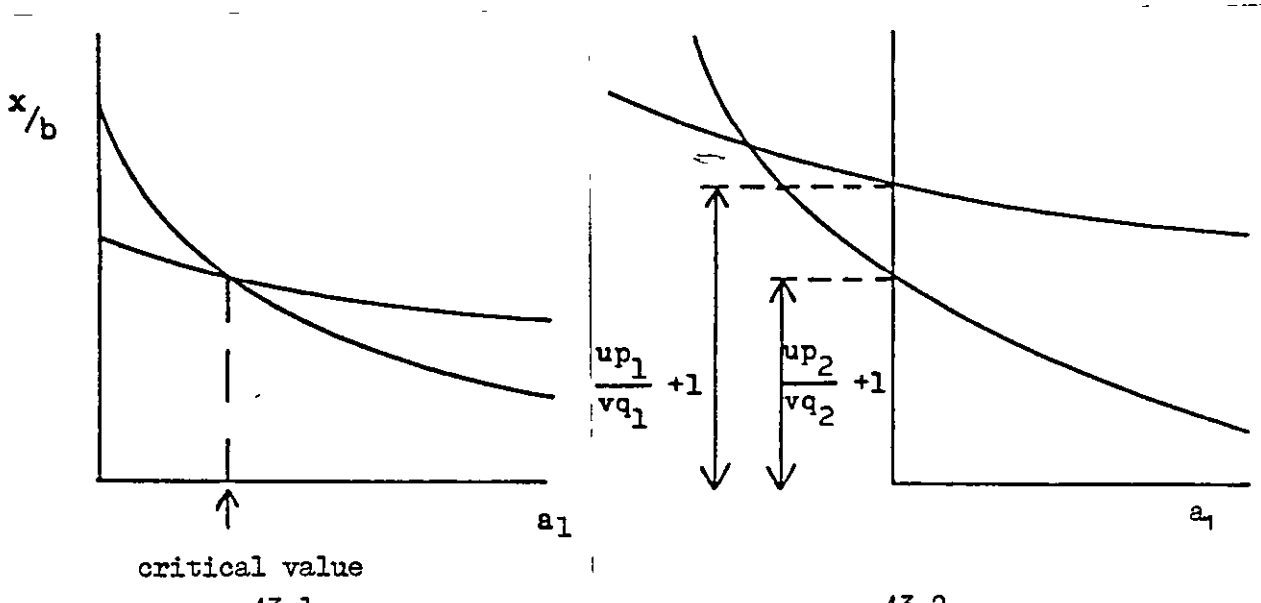

Fig. 43. Plot of x/b versus a_1 for Two Different Plasmas when the Critical Value of a_1 is (1) Positive, and (2) Negative.

The second case is when the critical value of a_1 is negative. In practice of course a_1 (as distinct from the critical value) cannot be negative so in this case a_1 always exceeds the critical value. However, as before, the better plasma is the one which gives the greater value of x/b when $a_1 = 0$ and, as can be seen from Fig. 43.2, this plasma will give the greater value of x/b for all positive values of a_1

It is not possible to evaluate the critical value of a_1, because it involves v, the factor relating the background measurement to the spectral radiancy of the background, and v cannot be estimated reliably. It is, therefore, not possible to use this criterion, namely that, if the critical value of a_1 is positive, the better plasma gives the better D.L. if the measuring system has a dark current at unit gain a_1 which is less than the critical value, while if a_1 exceeds the critical value the better plasma gives the poorer D.L. This is particularly unfortunate as the criterion is of the type which can be described as a necessary condition in the sense that if it is satisfied the result holds, and if it not satisfied the result does not hold. Conditions which use measurable quantities are therefore sought : it will be seen that such conditions are not necessary, in the sense just discussed, but can be called sufficient, in the sense that if they are satisfied the result certainly holds, but if they are not satisfied the result may or may not hold.

5.2.2. General Case. Sufficient Conditions for the Better Plasma to Give Better Detection Limits.

If the curves cross at a negative value of a_1, as shown in Fig.43.2, the better plasma always gives the better D.L. If plasma 1 is better than plasma 2, so that $p_1/q_1 > p_2/q_2$, a negative value for the crossing point (Equation 48) is obtained if $g_1 p_1/f_1 > g_2 p_2/f_2$.

This is thus an appropriate sufficient condition. If it is satisfied then the better plasma gives the better D.L. If it is not, then the critical value of a_1 is positive and the better plasma will give the better D.L. if the actual value of a_1 is less than the (unknown) critical value, and the poorer D.L. if the actual value of a_1 is greater, as in Fig. 43.1. The sufficient condition is thus seen to be more restrictive than necessary, ignoring the possibility that the critical value is positive and greater than the actual dark current.

The condition for a negative value of the crossing point is $g_1 p_1/f_1 > g_2 p_2/f_2$.

From equation 17

$$f = \frac{pg + R}{1 + Qg}$$

Hence
$$\frac{g_1 p_1}{f_1} - \frac{g_2 p_2}{f_2} = \frac{g_1 p_1 (1 + Qg_1)}{Pg_1 + R} - \frac{g_2 p_2 (1 + Qg_2)}{Pg_2 + R} \quad ---- \quad 49$$

$$= \frac{1}{(Pg_1+R)(Pg_2+R)} \left[Pp_1 g_1 g_2 + Pp_1 g_1^2 g_2 Q + Rg_1 p_1 + Rg_1^2 p_1 Q \right.$$
$$\left. -Pp_2 g_1 g_2 - Pp_2 g_1 g_2^2 Q - Rg_2 p_2 - Rg_2^2 p_2 Q \right] -- \quad 50$$

$$= \frac{1}{(Pg_1+R)(Pg_2+R)} \left[Pg_1 g_2 (p_1 - p_2) + PQg_1 g_2 (g_1 p_1 - g_2 p_2) \right.$$
$$\left. + R(g_1 p_1 - g_2 p_2) + RQ(g_1^2 p_1 - g_2^2 p_2) \right] \quad ---- \quad 51$$

$$= \frac{1}{(Pg_1+R)(Pg_2+R)} \left[Pg_1 g_2 (p_1 - p_2) + (PQg_1 g_2 + R)(g_1 p_1 - g_2 p_2) + RQ(g_1^2 p_1 - g_2^2 p_2) \right]$$
$$---- \quad 52$$

Hence $g_1 p_1/f_1 > g_2 p_2/f_2$ if $p_1 > p_2$ and $g_1 p_1 > g_2 p_2$ and $g_1^2 p_1 > g_2^2 p_2$. Under these conditions, if $p_1/q_1 > p_2/q_2$, the critical value of a_1 is negative. If any of these conditions is not satisfied, predictions cannot be made.

Physically $p_1 > p_2$ means that plasma 1 is "brighter" in the sense that the net spectral radiancy of plasma 1 is greater than that of plasma 2. The condition $g_1 p_1 > g_2 p_2$ can be re-written $g_1 up_1 > g_2 up_2$, which, since gup is the net signal (x-b), implies that the net signal from plasma 1, measured at a gain of g, is greater than the net signal from plasma 2, measured at gain g_2. The physical interpretation of the criterion $g_1^2 p_1 > g_2^2 p_2$ which occurs only for the general non-linear case, is not easily visualised.

5.2.3 (Linear Cases).

If the dark current depends linearly on the gain, Q = 0 and the conditions for a negative value of a_1 become less restrictive, namely $p_1 > p_2$ and $g_1 p_1 > g_2 p_2$. The conditions for the two special cases treated earlier are simpler still. If $a = ga_1$, then $f = g$ and the condition $\frac{g_1 p_1}{f_1} > \frac{g_2 p_2}{f_2}$ becomes $p_1 > p_2$. If $a = a_1$, $f = 1$ and the condition becomes $g_1 p_1 > g_2 p_2$.

5.2.4 General Case (Same Gain).

If the same gain is used for both plasmas, then the single criterion $p_1 > p_2$ is sufficient to ensure that the critical value of a_1 is negative both for linear and for hyperbolic dependence of dark current on gain.

5.2.5 The Effect of the Background Factor on the Critical Value of the Dark Current.

The critical value of a_1 is proportional to v, so that a larger range over which the relatively better detection limit is obtained from the intrinsically better plasma could be obtained by increasing v, for example by using wider exit slits. This, however, would lower the value of x/b and so the absolute value of the detection limit would be degraded.

5.2.6 Other Factors Affecting the Detection Limit. (Effect of Dark Current.

(x/b) depends hyperbolically on a_1

$$\frac{x}{b} = \frac{gup}{gvq + fa_1} + 1 \qquad \text{(Equation 43)}$$

The detection limit is given by

$$D.L. = \frac{2kc}{\frac{x}{b} - 1} \qquad \text{(Equation 39 if n = 2)}$$

where k is a constant and c the concentration which produces the observed value of x/b.

Hence $$D.L. = 2kc\,\frac{gvq + fa_1}{gup} = 2kq\,\frac{cv}{pu} + \frac{2k}{gu} \cdot \frac{c}{p}\, fa_1 \qquad ------ 53$$

so that the detection limit depends linearly on the dark current.

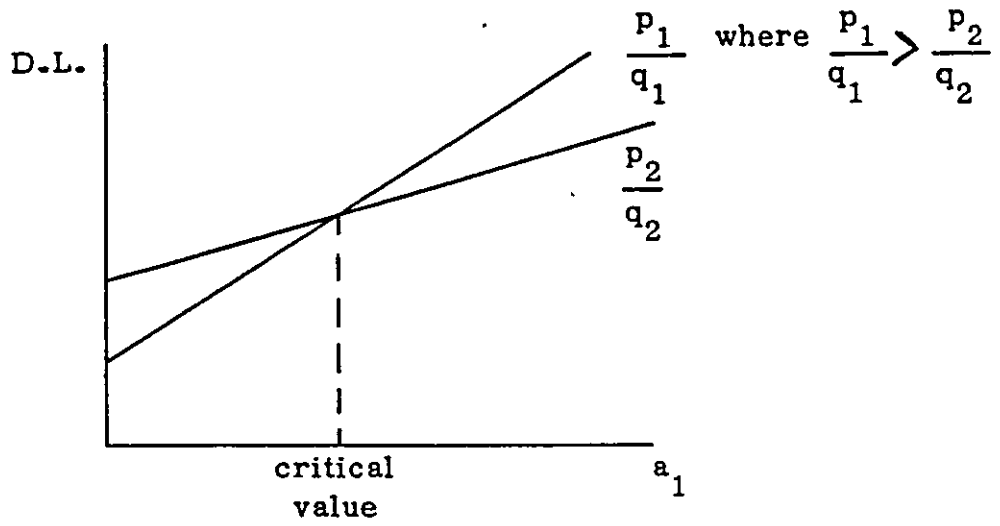

Fig. 44. Detection Limit plotted against Dark Current for Two Plasmas.

The best (i.e. the lowest) value of detection limit is obtained with zero dark current. It can be seen from equation 53, that the plasma with the larger value of p/q gives the smaller D.L. for zero dark current as is shown in Fig. 44. It is again seen that if a_1 exceeds the critical value, the poorer detection limit is obtained from the intrinsically better plasma.

5.2.7 (Effect of Gain).

Equation 53 also indicates that a small value of f/g is desirable in order to keep small the rate at which the D.L. is degraded with dark current. This ratio decreases as g increases, since for the type of hyperbola found (with P, Q and R all positive) the slope, while always positive, decreases as g increases, so that f grows more slowly while g grows at a constant rate. More rigorously, if the ratio f/g is differentiated with respect to g, the rate of increase is found to be negative :

Since $$f = \frac{Pg + R}{1 + Qg} \qquad \text{(Equation 17)}$$

$$\frac{f}{g} = \frac{Pg + R}{g + Qg^2} \qquad \text{---------- 54}$$

So that $$\frac{d(f/g)}{dg} = \frac{P}{g + Qg^2} - \frac{Pg + R}{(g + Qg^2)^2} \cdot (1 + 2Qg) \text{ --- 55}$$

$$= \frac{Pg + PQg^2 - Pg - 2PQg^2 - R - 2RQg}{(g + Qg^2)^2} \qquad \text{----- 56}$$

$$= \frac{- R - 2RQg - PQg^2}{(g + Qg^2)^2} \qquad \text{---------- 57}$$

Thus d(f/g)dg is negative for P, Q and R all positive, so that f/g decreases as g increases.

Thus in general a large value of g is advantageous, so that the effect of dark current on D.L. is kept small. For a given dark current the effect of g on the D.L. is shown in Fig. 45. The exceptional case, where the D.L. is independent of gain occurs when $\frac{d(f/g)}{dg}$ is zero.

When none of P, Q or R is negative, this condition can only occur (since from equation 23, P + R = 1 + Q) for P = 1, Q = 0, R = 0, which is the case in which the dark current is amplified proportionally, like a signal.

5.2.8 (Effect of Sensitivity).

From equation 53 it can be seen that the lowest detection limit (with $a_1 = o$) depends on a large value of $\frac{u}{v} \frac{p}{cq}$. This can be thought of as $\frac{u}{vq}$ times the plasma sensitivity p/c, that is, the spectral radiancy for the analytical signal divided by the concentration producing it. A small value of the slope in Fig.44 is desirable and this is obtained with a large value of gup/cf, indicating again the desirability of high sensitivity.

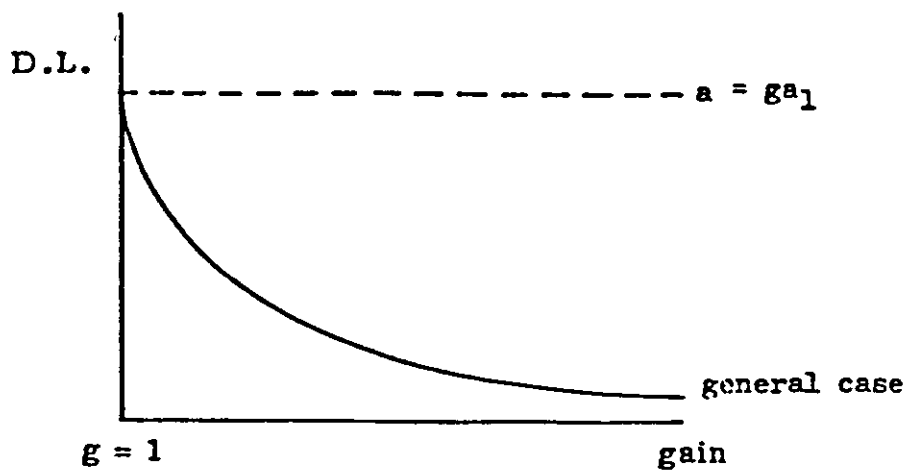

Fig. 45. Dependence of Detection Limit on Gain.

5.2.9 Criterion When Maximum Gain is Used.

Fig. 45 shows that, apart from the exceptional case when dark current behaves like a signal, the D.L. improves as the gain increases. Since it is not always known how the dark current depends on gain it is therefore desirable always to use the gain which will fill the scale where this is possible. These gains depend on the nature of the dark current, and are obtained by equating the gross signal x to the scale length A.

The maximum gain has already been derived (equation 28); it is a rather cumbersome expression which does not seem capable of simplification in the general hyperbolic case. It was shown in equation 31, however, that when the dark current depended linearly on the gain so that $a = (Pg + R)a_1$, that

$$C = \frac{A - Ra_1}{x_1 - Ra_1}$$

where, since a has the value a_1 at $g = 1$, $P + R = 1$. There were two particular cases of interest, $P = 1$, $R = 0$ corresponding to $a = ga_1$ and $P = 0$, $R = 1$ corresponding to $a = a_1$.

5.2.10 Special Case 1. Dark Current versus Gain is a Straight Line Through the Origin.

In this case the dark current is amplified like a signal ($a = ga_1$) and $R = 0$.

The maximum gain C is thus given by $C = A/x$, (from equation 31), and by the use of equation 1,

$$C = A/(up + vq + a_1) \qquad \text{----------} \quad 58$$

However in this case x and b are both proportional to the gain (equations 8 and 9) so that x/b is independent of gain. It follows that, for two plasmas, the critical value of a_1 at which the curves of x/b versus a_1 cross remains constant, regardless of the value of the gain.

This critical value is obtained from equation 48 by putting $f_1 = g_1$ and $f_2 = g_2$.

$$a_1 = - \frac{vq_1 q_2}{p_1 - p_2} \cdot \left(\frac{p_1}{q_1} - \frac{p_2}{q_2} \right) \qquad \text{---------- 59}$$

If, as before, the dark current at unit amplification is less than this critical value, the better plasma gives the better D.L. It should be noted too, that if plasma 1 is better than plasma 2 (so that $p_1/q_1 > p_2/q_2$) and if plasma 1 has a higher spectral radiancy than plasma 2 (so that $p_1 > p_2$), then the critical value of a_1 is necessarily negative. This corresponds to the conditions of Fig. 43.2 showing the in real conditions where the dark current cannot be negative, the better plasma (which gives the better D.L. for zero dark current) always gives the better D.L.

5.2.11 Special Case 2. Dark Current versus Gain is a Horizontal Straight Line.

In this case the dark current is constant, $a = a_1$ and $R = 1$ so that the maximum amplification C is given by

$$C = (A - a_1)/(x_1 - a_1)$$

and hence by using equation 1

$$C = (A - a_1)/(up + vq) \qquad \text{---------- 60}$$

From equation 43,

$$\frac{x}{b} = \frac{gup}{gvq + a_1} + 1 \qquad \text{---------- 61}$$

so that at maximum amplification C

$$\frac{x}{b} = \frac{A - a_1}{up + vq} \cdot \frac{up}{\left(\frac{A-a_1}{up + vq} \right) \cdot vq + a_1} + 1 \qquad \text{------ 62}$$

Multiply top and bottom by up + vq

$$\frac{x}{b} = \frac{A - a_1}{up + vq} \cdot \frac{up(up + vq)}{(A-a_1)vq + a_1(up+vq)} + 1 \qquad \text{------ 63}$$

Cancel and multiply out brackets :

$$\frac{x}{b} = \frac{(A-a_1)up}{Avq - a_1 vq + a_1 up + a_1 vq} + 1 \quad \text{-------} \quad 64$$

Cancel :

$$\frac{x}{b} = \frac{(A-a_1)up}{Avq + a_1 up} + 1 \quad \text{-------} \quad 65$$

If the better plasma gives the better D.L., $x_1/b_1 - x_2/b_2$ should have the same sign as $p_1/q_1 - p_2/q_2$.

Then

$$\frac{x_1}{b_1} - \frac{x_2}{b_2} = (A - a_1)\left[\frac{up_1}{Avq_1 + a_1 up_1} - \frac{up_2}{Avq_2 + a_1 up_2}\right] \quad \text{----} \quad 66$$

$$= (A-a_1)\frac{Aup_1 vq_2 + a_1 u^2 p_1 p_2 - Aup_2 vq_1 - a_1 u^2 p_1 p_2}{(Avq_1 + a_1 up_1)(Avq_2 + a_1 up_2)} \quad \text{----} \quad 67$$

$$= \frac{(A - a_1)Auv(p_1 q_2 - p_2 q_1)}{(Avq_1 + a_1 up_1)(Avq_2 + a_1 up_2)} \quad \text{----} \quad 68$$

$$= \frac{(A - a_1)Auv(p_1/q_1 - p_2/q_2)q_1 q_2}{(Avq_1 + a_1 up_1)(Avq_2 + a_1 up_2)} \quad \text{----} \quad 69$$

This always has the same sign as $(p_1/q_1 - p_2/q_2)$. Thus for dark current independent of gain, if the maximum amplification is used, the better plasma always gives the better D.L.

5.2.12 Noise Proportional to Square Root of the Background.

The previous results all apply to the case where the noise in the background is proportional to the background, which, by experiment, was shown in Chapter 4 to be true for our system. Other workers have reported a similar result [61,62]. However, cases where the noise is determined by the square root of the background have also been reported[67].

67. A. Danielsson and E. Soderman, I.C.P. Information Newsletter, 1977, 2, 267.

In these cases, as was pointed out in Section 5.2, the detection limit is a function of the exposure time. For a given exposure time it will be proportional to $\sqrt{b}/(x-b)$. It will then be optimised when $b/(x-b)^2$ is minimised, and this squared ratio is more tractable for mathematical manipulation.

5.2.13 General Case (Necessary and Sufficient Conditions).

As before,

$$a = fa_1 \quad \text{(equation 7)}$$

$$b = g(b_1 - a_1) + fa_1 \quad \text{where } b_1 = vq + a_1 \quad \text{(equations 9 and 2)}$$

$$x = g(x_1 - a_1) + fa_1 \quad \text{where } x_1 = up+vq+a_1 \quad \text{(equations 8 and 1)}$$

so that $x-b = g(x_1 - a_1 - b_1 + a_1) = g(x_1 - b_1) = gup$ ------- 70

Then $$\frac{b}{(x-b)^2} = \frac{gvq + fa_1}{g^2u^2p^2} \qquad \text{------- 71}$$

Just as previously the crossing point of two curves of x/b plotted against a_1 was of interest (Section 5.2.1), now the crossing point of two curves of $b/(x-b)^2$ is derived as the value of a_1 for which $b_1/(x_1-b_1)^2 = b_2/(x_2-b_2)^2$.

$$\frac{b_1}{(x_1-b_1)^2} - \frac{b_2}{(x_2-b_2)^2} = \frac{g_1vq_1 + f_1a_1}{g_1^2u^2p_1^2} - \frac{g_2vq_2 + f_2a_1}{g_2^2u^2p_2^2} \qquad \text{--- 72}$$

$$= \frac{v}{u^2}\left(\frac{q_1}{g_1p_1^2} - \frac{q_2}{g_2p_2^2}\right) + \frac{a_1}{u^2}\left(\frac{f_1}{g_1^2p_1^2} - \frac{f_2}{g_2^2p_2^2}\right) \qquad \text{--- 7}$$

This is zero when, re-arranging the second bracket,

$$a_1\left(\frac{f_1g_2^2p_2^2 - f_2g_1^2p_1^2}{g_1^2g_2^2p_1^2p_2^2}\right) = -v\cdot\left(\frac{q_1}{g_1p_1^2} - \frac{q_2}{g_2p_2^2}\right) \qquad \text{--- 74}$$

i.e. when $$a_1 = \frac{vg_1^2g_2^2p_1^2p_2^2}{f_1g_2^2p_2^2 - f_2g_1^2p_1^2}\left(\frac{q_1}{g_1p_1^2} - \frac{q_2}{g_2p_2^2}\right) \qquad \text{--- 7}$$

which, on multiplying into the bracket by the factor $g_1 g_2 p_1^2 p_2^2$ and taking out the factor $q_1 q_2$

$$= \frac{-v g_1 g_2 q_1 q_2}{f_1 g_2^2 p_2^2 - f_2 g_1^2 p_1^2} \left(\frac{g_1 p_2^2}{q_2} - \frac{g_1 p_1^2}{q_1} \right) \qquad \text{------ 76}$$

which, on rearranging the order so that plasma 1 appears first and taking out the factor $1/f_1 f_2$

$$= \frac{-v}{f_1 f_2} \quad \frac{g_1 g_2 q_1 q_2}{\frac{g_1^2 p_1^2}{f_1} - \frac{g_2^2 p_2^2}{f_2}} \left(g_1 p_1 \cdot \frac{p_1}{q_1} - g_2 p_2 \cdot \frac{p_2}{q_2} \right) \qquad \text{----- 77}$$

This gives the value of a_1 at which the curves cross and just as before (Section 5.2.1) leads to a necessary condition for the better plasma to give the better D.L. This condition is once again unusable, for the same reason, namely ignorance of the value of v. As before a sufficient condition, more restrictive than necessary, is obtainable by examining under what circumstances the value of a_1 at the crossing point takes a negative value. It is apparent from equation 77 that if plasma 1 is the better, so that $p_1/q_1 > p_2/q_2$, such a condition is that $g_1^2 p_1^2/f_1 > g_2^2 p_2^2/f_2$, and these quantities are now examined.

$$\frac{g^2 p^2}{f} = g^2 p^2 \frac{(1 + Qg)}{Pg+R} \qquad \text{from equation 17}$$

$$\therefore \frac{g_1^2 p_1^2}{f_1} - \frac{g_2^2 p_2^2}{f_2} = \frac{g_1^2 p_1^2 (1 + Qg_1)}{Pg_1 + R} - \frac{g_2^2 p_2^2 (1 + Qg_2)}{Pg_2 + R} \qquad \text{-- 78}$$

$$= \frac{1}{(Pg_1+R)(Pg_2+R)} \left[(g_1^2 p_1^2 + Qg_1^3 p_1^2)(Pg_2+R) - (g_2^2 p_2^2 + Qg_2^3 p_2^2)(Pg_1+R) \right]$$

$$\text{--- 79}$$

$$= \frac{1}{(Pg_1+R)(Pg_2+R)} \left[g_1^2 g_2 P p_1^2 + g_1^3 g_2 PQ p_1^2 + g_1^2 p_1^2 R + g_1^3 p_1^2 RQ \right.$$
$$\left. - g_1 g_2^2 P p_2^2 - g_1 g_2^3 PQ p_2^2 - g_2^2 p_2^2 R - g_2^3 p_2^2 RQ \right] \quad --- 80$$

$$= \frac{1}{(Pg_1+R)(Pg_2+R)} \left[Pg_1 g_2 (g_1 p_1^2 - g_2 p_2^2) + R(g_1^2 p_1^2 - g_2^2 p_2^2) \right.$$
$$\left. + PQ g_1 g_2 (g_1^2 p_1^2 - g_2^2 p_2^2) + RQ(g_1^3 p_1^2 - g_2^3 p_2^2) \right] \quad --- 81$$

$$= \frac{Pg_1 g_2 (g_1 p_1^2 - g_2 p_2^2) + (PQ g_1 g_2 + R)(g_1^2 p_1^2 - g_2^2 p_2^2) + RQ(g_1^3 p_1^2 - g_2^3 p_2^2)}{(Pg_1+R)(Pg_2+R)} \quad --- 82$$

P, Q and R are all positive, so that this expression will certainly be positive if

$$g_1 p_1^2 > g_2 p_2^2$$

and $g_1^2 p_1^2 > g_2^2 p_2^2$ (or $g_1 p_1 > g_2 p_2$ since g and p are positive by definition)

and $g_1^3 p_1^2 > g_2^3 p_2^2$

Under these conditions, if $p_1/q_1 > p_2/q_2$, equation 77 shows that the critical value of a_1 is always negative.

5.2.14 (Linear Cases)

As before, the conditions are less restrictive if the dependence of dark current on gain is linear, so that $Q = 0$ in the expression for f (equation 17). Then the conditions are, from equation 82

$$g_1 p_1^2 > g_2 p_2^2$$

and $g_1^2 p_1^2 > g_2 p_2^2$

These conditions are included in the simpler but more restrictive subset

$$p_1 > p_2 \text{ and } g_1 p_1 > g_2 p_2 .$$

These two conditions also apply for the special case $a = ga_1$, i.e. $f = g$, since the term inside the bracket in equation 77 has to be positive as well as the factor outside.

However, for the special case $a = a_1$ the single criterion $g_1^2 p_1^2 > g_2^2 p_2^2$ or $g_1 p_1 > g_2 p_2$ applies.

5.2.15 General Case (Same Gain)

If the same gain is used for the two plasmas, the single condition $p_1 > p_2$ is adequate.

5.2.16 Criteria When Maximum Gain is Used.

As in the case of the noise being proportional to the background, the effect of working at the maximum gain (i.e. the gain at which the amplified gross signal gives full scale on the measuring instrument) is now examined for the case of the noise depending on the square root of the background. This is because as was shown earlier (Section 5.2.7), in most cases the D.L. improves as the gain is increased.

As before, the expression for the maximum gain in the general case has been found to be too complicated to be useful. Here, for brevity, only the two special cases, namely, $a = ga_1$ and $a = a_1$ will be considered. These are where the dark current behaves like an analytical signal so that $a = ga_1$, and where the dark current is constant so that $a = a_1$.

5.2.17 Special Case 1. Dark Current Versus Gain is Straight Line Through The Origin.

In this case the dark current is amplified like a signal so that $f_1 = g_1$ and $f_2 = g_2$.

From equation 58 the maximum gain, that is the gain for which the gross signal fills the scale, is $A/(up + vq + a_1)$.

Then from equation 72,

$$\frac{b_1}{(x_1-b_1)^2} - \frac{b_2}{(x_2-b_2)^2} = \frac{g_1(vq_1+a_1)}{g_1^2u^2p_1^2} - \frac{g_2(vq_2+a_1)}{g_2^2u^2p_2^2}$$

and by cancelling g's

$$= \frac{vq_1+a_1}{g_1u^2p_1^2} - \frac{vq_2+a_1}{g_2u^2p_2^2} \qquad \text{---} 83$$

and by substitution for g

$$= \frac{vq_1+a_1}{u^2p_1^2A}(up_1+vq_1+a_1) - \frac{vq_2+a_1}{u^2p_2^2A}(up_2+vq_2+a_1) \qquad \text{---} 84$$

$$= \frac{1}{u^2A}\left(\frac{uvp_1q_1 + v^2q_1^2 + a_1vq_1 + up_1a_1 + vq_1a_1 + a_1^2}{p_1^2}\right. \qquad \text{---} 85$$

$$\left. - \frac{uvp_2q_2 + v^2q_2^2 + a_1vq_2 + up_2a_1 + vq_2a_1 + a_1^2}{p_2^2}\right)$$

$$= \frac{1}{u^2A}\left(\frac{uvq_1}{p_1} + \frac{v^2q_1^2}{p_1^2} + \frac{2a_1vq_1}{p_1^2} + \frac{ua_1}{p_1} + \frac{a_1^2}{p_1^2}\right. \qquad \text{---} 86$$

$$\left. - \frac{uvq_2}{p_2} - \frac{v^2q_2^2}{p_2^2} - \frac{2a_1vq_2}{p_2^2} - \frac{ua_1}{p_2} - \frac{a_1^2}{p_2^2}\right)$$

$$= \frac{1}{u^2A}\left[uv\left(\frac{q_1}{p_1} - \frac{q_2}{p_2}\right) + v^2\left(\frac{q_1^2}{p_1^2} - \frac{q_2^2}{p_2^2}\right) + 2a_1v\left(\frac{q_1}{p_1^2} - \frac{q_2}{p_2^2}\right)\right. \qquad \text{---} 87$$

$$\left. + ua_1\left(\frac{1}{p_1} - \frac{1}{p_2}\right) + a_1^2\left(\frac{1}{p_1^2} - \frac{1}{p_2^2}\right)\right]$$

For DL_1 to be better than DL_2, this quantity must be negative. It will certainly be so if $\frac{p_1}{q_1} > \frac{p_2}{q_2}$ and $p_1 > p_2$, so that if the better plasma has also the greater radiancy for the spectral line in question, it must give the better D.L.

These conditions are more restrictive than is necessary, because they require each of the five terms individually to be negative, whereas the requirement of interest is only in the sum being negative. Thus it is possible that the better D.L. may be obtained from the better plasma even if the radiances are not related $p_1 > p_2$.

The circumstances under which this is so can be deduced by finding critical values of a_1 where the curves of $\frac{b_1}{(x_1-b_1)^2}$ and $\frac{b_2}{(x_2-b_2)^2}$ cross. Since these quantities now depend quadratically on a_1, there are now two crossing points.

From equation 87, the curves cross when

$$a_1^2\left(\frac{1}{p_1^2}-\frac{1}{p_2^2}\right)+\ a_1\ \left[\ u\left(\frac{1}{p_1}\ -\frac{1}{p_2}\ \right)+\ 2v\ \left(\frac{q_1}{p_1^2}\ -\ \frac{q_2}{p_2^2}\right)\right]$$

$$+\ uv\ \left(\frac{q_1}{p_1}-\frac{q_2}{p_2}\ \right)+\ v^2\ \left(\frac{q_1^2}{p_1^2}\ -\ \frac{q_2^2}{p_2^2}\right)=\ 0 \qquad ---\ 88$$

that is

$$\frac{a_1^2(p_2^2-p_1^2)}{p_1^2p_2^2}\ +\ a_1\left[\frac{u(p_2-p_1)}{p_1p_2}\ +\ \frac{2v(p_2^2q_1-p_1^2q_2)}{p_1^2p_2^2}\right]$$

$$+\ \frac{uv(p_2q_1\ -\ p_1q_2)}{p_1p_2}\ +\ \frac{v^2(p_2^2q_1^2\ -\ p_1^2q_2^2)}{p_1^2p_2^2}\ =\ 0 \qquad ---\ 89$$

that is

$$a_1^2(p_2^2-p_1^2)\ +\ a_1\ \ [u(p_2-p_1)p_1p_2\ +\ 2v(p_2^2q_1-p_1^2q_2)]$$

$$+\ uv(p_2q_1\ -\ p_1q_2)\ +\ v^2(p_2^2q_1^2-p_1^2q_2^2)\ \ =\ \ 0 \qquad ---\ 90$$

To solve the quadratic equation $A_oa_1^2\ +\ B_oa_1\ +\ C_o\ =\ 0$, we require the value of $\sqrt{B_o^2-4A_oC_o}$

Here

$$B_o^2-4A_oC_o\ =\ u^2(p_2-p_1)^2p_1^2p_2^2\ +\ 4v^2(p_2^2q_1-p_1^2q_2)^2$$

$$+\ 4uvp_1p_2(p_2-p_1)(p_2^2q_1-p_1^2q_2)$$

$$-\ 4uvp_1p_2(p_2q_1-p_1q_2)(p_2^2-p_1^2)$$

$$-\ 4v^2(p_2^2-p_1^2)(p_2^2q_1^2-p_1^2q_2^2) \qquad ---\ 91$$

$$=\ u^2(p_2-p_1)^2p_1^2p_2^2$$

$$+\ 4v^2(p_2^4q_1^2+p_1^4q_2^2-2p_1^2p_2^2q_1q_2-p_2^4q_1^2+p_1^2p_2^2q_1^2+p_1^2p_2^2q_2^2-p_1^4q_2^2)$$

$$+\ 4uvp_1p_2(p_2-p_1)(p_2^2q_1-p_1^2q_2-p_2^2q_1-p_1p_2q_1\ +\ p_1p_2q_2\ +\ p_1^2q_2)$$

$$---\ 92$$

$$= u^2(p_2-p_1)^2 p_1^2 p_2^2$$

$$+ 4v^2 p_1^2 p_2^2 (q_1^2 + q_2^2 - 2q_1 q_2)$$

$$+ 4uvp_1^2 p_2^2 (p_2-p_1)(q_2-q_1) \quad ---93$$

$$= p_1^2 p_2^2 [u^2(p_2-p_1)^2 + 4uv(p_2-p_1)(q_2-q_1) + 4v^2(q_2-q_1)^2] \quad ---94$$

$$= p_1^2 p_2^2 [u(p_2-p_1) + 2v(q_2-q_1)]^2 \quad ---95$$

so that $\sqrt{B_o^2-4A_oC_o} = p_1 p_2 [u(p_2-p_1)+2v(q_2-q_1)]$ ---96

Then. using the standard solution of a quadratic equation,

$$a_1 = \frac{-B_o \pm \sqrt{B_o^2-4A_oC_o}}{2A_o} \quad ---97$$

i.e. $$a_1 = \frac{-u(p_2-p_1)p_1p_2 - 2v(p_2^2q_1 - p_1^2q_2) \pm p_1p_2\,[u(p_2-p_1)+2v(q_2-q_1)]}{2(p_2^2-p_1^2)} \quad --98$$

Consider first the root with the negative sign

$$a_1 = \frac{-2u(p_2-p_1)p_1p_2 - 2v[p_2^2q_1 - p_1^2q_2 + p_1p_2(q_2-q_1)]}{2(p_2^2-p_1^2)} \quad ---99$$

$$= \frac{-u(p_2-p_1)p_1p_2 - v(p_2^2q_1 - p_1^2q_2 + p_1p_2q_2 - p_1p_2q_1)}{p_2^2-p_1^2} \quad ---100$$

$$= \frac{-u(p_2-p_1)p_1p_2 - v[q_1p_2(p_2-p_1) + q_2p_1(p_2-p_1)]}{p_2^2-p_1^2} \quad ---101$$

$$= \frac{-up_1p_2 - v(q_1p_2 + q_2p_1)}{p_2 + p_1} \quad ---102$$

This is always negative since all the variables are necessarily positive , and hence of no interest.

Consider now the root with the positive sign.

$$a_1 = \frac{-2v(p_2^2q_1 - p_1^2q_2) + 2vp_1p_2(q_2-q_1)}{2(p_2^2-p_1^2)} \quad ---103$$

$$= \frac{-v}{p_2^2-p_1^2}(p_2^2q_1 - p_1^2q_2 - p_1p_2q_2 + p_1p_2q_1) \quad ---104$$

$$= \frac{-vq_1q_2}{p_2^2-p_1^2} \cdot \left(\frac{p_2^2}{q_2} - \frac{p_1^2}{q_1} - \frac{p_1p_2}{q_1} + \frac{p_1p_2}{q_2}\right) \quad ---105$$

$$= \frac{-vq_1 q_2}{p_2^2 - p_1^2} \left(\frac{p_2}{q_2} (p_2 + p_1) - \frac{p_1}{q_1} (p_2 + p_1) \right) \quad --- 106$$

$$= \frac{-vq_1 q_2}{p_2 - p_1} \left(\frac{p_2}{q_2} - \frac{p_1}{q_1} \right) = \frac{- vq_1 q_2}{p_1 - p_2} \left(\frac{p_1}{q_1} - \frac{p_2}{q_2} \right) \quad --- 107$$

This is the root of interest. This value for the crossing point of the curves of $b/(x-b)^2$ when the maximum gain is applied is in fact identical to that previously obtained (equation 59) for the crossing point of the curves x/b for the same kind of linear dependence of dark current on gain. The identity of the results seems surprising, but is probably of little fundamental significance.

5.2.18 Special Case 2. Dark Current Versus Gain is a Horizontal Straight Line.

In this case $a = a_1$ so that $f = 1$. It follows that $R = 1$ (Section 5.1.5) and hence from equation 31 that the maximum useful gain is given by

$$g = C = \frac{A - a_1}{up + vq} \quad --- 108$$

Then from equation 71

$$\frac{b}{(x-b)^2} = \frac{\frac{A - a_1}{up + vq} \cdot vq + a_1}{\frac{(A - a_1)^2 u^2 p^2}{(up + vq)^2}} \quad --- 109$$

$$= \frac{(A - a_1) vq(up + vq) + a_1 (up + vq)^2}{(A - a_1)^2 u^2 p^2} \quad --- 110$$

$$= \frac{1}{(A - a_1)} \cdot \frac{vq}{up} \cdot \left(1 + \frac{vq}{up} \right) + \frac{a_1}{(A - a_1)^2} \left(1 + \frac{vq}{up} \right)^2 \quad --- 111$$

This is an increasing function of q/p or a decreasing function of p/q. Hence the larger p/q is, the smaller $b/(x-b)^2$ and hence the D.L. Thus under maximum amplification and in conditions of constant dark current, the best DLs are obtained from the best plasma.

5.2.19 Noise Proportional to Any Power of the Background.

It has just been shown that with maximum amplification and for dark current independent of gain, the best D.L. is obtained from the best plasma both for linear and square root dependence of noise. It is of interest to examine whether a similar result is true for an n^{th} power dependence regardless of the value of n. This is done by expressing $b/(x-b)^n$ as a function of p/q.

Equation 71 may be generalised to read

$$\frac{b}{(x-b)^n} \qquad \frac{gvq + a_1}{g^n u^n p^n} \qquad \text{--- 112}$$

so that at maximum gain, using equation 60

$$\frac{b}{(x-b)^n} = \frac{\dfrac{A - a_1}{up+vq} \cdot vq + a_1}{\dfrac{(A-a_1)^n u^n p^n}{(up+vq)^n}} \qquad \text{--- 113}$$

$$= \frac{(A-a_1)vq(up+vq)^{n-1} + a_1(up+vq)^n}{(A-a_1)^n u^n p^n} \qquad \text{--- 114}$$

$$= \frac{1}{(A-a_1)^{n-1}} \cdot \frac{vq}{up}\left(1 + \frac{vq}{up}\right)^{n-1} + \frac{a_1}{(A-a_1)^n}\left(1 + \frac{vq}{up}\right)^n \qquad \text{-- 11}$$

which always increases with q/p, or decreases withp/q provided n is positive. The result is thus general for $\sigma^{-}(b) = kb^n$ for any positive value of n.

5.3 Summary of Deductions.

The important arguments and deductions contained in this chapter may be summarised thus.

a) The measured net ratio of signal to background is not independent of the spectrometer, but the plasma with the highest radiance ratio will give the highest measured net ratio on any spectrometer, irrespective of the gain on the P.M. tube and whether the dark current is constant or amplified along with the signal.

b) It is desirable that the better plasma should yield the better detection limits on any spectrometer and the conditions under which this result may be obtained are summarised in Table 10 for the three types of dark current that have been observed in this laboratory, for two ways in which the noise in the background depends on the background, and for three relations between the gains used. Plasma 1 is taken to be the better, so that $p_1/q_1 > p_2/q_2$.

c) The necessary conditions, i.e. those which determine rigorously whether the better plasma does or does not give the better D.L., are not tabulated, since the criteria cannot be reliably evaluated because the factor v is unknown. Sufficient conditions are given: if the conditions are satisfied then the desired result is obtained while if they are not the desired result may or may not be obtained. The quantities involved in these criteria, which are more restrictive than the necessary conditions, are expressible in terms of g and p, or equally in terms of g and up, since $p_1 > p_2$ can be replaced by $up_1 > up_2$. It has been shown (equation 70) that $x-b = gup$ so that up can be evaluated from $(x-b)/g$, physically measurable quantities. The criteria are tabulated in Table 11 in terms of the measurable quantities : gross signal, gross background and gain (x, b, g and x^1, b^1, g^1 for the two plasmas). (See footnote on page 119).

TABLE 10.

Sufficient Conditions under which the better plasma gives the better D.L. on a given spectrometer.

		$a = \frac{Pg + R}{1 + Qg} \cdot a_1$	$a = ga_1$	$a = a_1$
$\sigma(a) = kb$	Any gains g_1, g_2	$p_1 > p_2$ and $g_1 p_1 > g_2 p_2$ and $g_1^2 p_1 > g_2^2 p_2$	$p_1 > p_2$	$g_1 p_1 > g_2 p_2$
	Same gain	$p_1 > p_2$	$p_1 > p_2$	$p_1 > p_2$
	Max. g_1* Max. g_2*	Too complicated to use.	$p_1 > p_2$	No restriction
$\sigma(a) = k\sqrt{b}$	Any gains g_1, g_2	$g_1 p_1^2 > g_2 p_2^2$ and $g_1^2 p_1^2 > g_2^2 p_2^2$ and $g_1^3 p_1^2 > g_2^3 p_2^2$	$g_1 p_1^2 > g_2 p_2^2$ and $g_1^2 p_1^2 > g_2^2 p_2^2$	$g_1^2 p_1^2 > g_2^2 p_2^2$
	Same gain	$p_1 > p_2$	$p_1 > p_2$	$p_1 > p_2$
	Max. g_1* Max. g_2*	Too complicated to use.	$p_1 > p_2$	No restriction.

* to fill the scale.

TABLE 11.

Sufficient conditions under which the better plasma gives the better D.L. on a given spectrometer.

		$a = \frac{Pg + R}{1 + Qg} \cdot a_1$	$a = ga_1$	$a = a_1$
$(b) = kb$	Any gains g_1 , g_2	$\frac{x-b}{g} > \frac{x^1-b^1}{g^1}$ and $x-b > x^1-b^1$ and $g(x-b) > g(x^1-b^1)$	$\frac{x-b}{g} > \frac{x^1-b^1}{g^1}$	$x-b > x^1-b^1$
	Same gain	$x-b > x^1-b^1$	$x-b > x^1-b^1$	$x-b > x^1-b^1$
	Max. g_1* Max. g_2*	Too complicated to use.	$x(x-b) > x^1(x^1-b^1)$	No restriction.
$(b) = k\sqrt{b}$	Any gains g_1 , g_2	$\frac{x-b}{\sqrt{g}} > \frac{x^1-b^1}{\sqrt{g^1}}$ and $x-b > x^1-b^1$ and $\sqrt{g}(x-b) > \sqrt{g^1}(x^1-b^1)$	$\frac{x-b}{\sqrt{g}} > \frac{x^1-b^1}{\sqrt{g^1}}$ and $x-b > x^1-b^1$	$x-b > x^1-b^1$
	Same gain	$x-b > x^1-b^1$	$x-b > x^1-b^1$	$x-b > x^1-b^1$
	Max.g_1* Max.g_2*	Too complicated to use.	$\sqrt{x}(x-b) > \sqrt{x^1}(x^1-b^1)$	No restriction.

* to fill the scale.

x, b, g and x^1 , b^1 , g^1 represent the measured quantities from two different plasmas and should not be confused with the symbols x_1 , b_1 , which are the quantities measured at unit gain.

5.4 Conclusions.

It follows from the deductions made in this chapter that the intrinsic merit of two or more plasmas can be compared on a spectrometer by comparing their net signal to background ratios. The plasma with the highest net signal to background ratio will be the best plasma on any spectrometer. A given plasma may give different values for this ratio on different spectrometers but the order of two plasmas will remain unchanged.

If two plasmas are examined at the same gain on any spectrometer, the better one will give the better D.L. if it also gives the greater net signal. If different gains are used, simple criteria involving the gains can be used similarly. If these criteria are not satisfied, the better plasma may or may not give the best D.L. at the gains used.

CHAPTER 6.

FURTHER EXPERIMENTS FOLLOWING IMPROVEMENTS TO THE MEASURING SYSTEM.

It was decided to repeat the previous experiments (section 3.1) with sodium at 5890Å using a 10 p.p.m. solution and the full gain (X1024) of the polychromator in order to produce a readable background. Improvements were also made to the measuring system as follows:

Section 6.1 Use of D.V.M. and a 1M ohm resistor.

The profile meter was replaced with a digital voltmeter and the potential drop across the 1M ohm resistor R701 (Fig. 32) was measured.

Section 6.1.1 Sodium Results.

The values obtained with the above modification are tabulated in Table 12. The nomenclature of Fig. 36 is used, and will be here on. (Note: The SC 15 generator had been serviced and was able to provide higher powers).

Table 12. Height/Power/Emission Relationships.
Sodium 5890Å line. Digital Voltmeter Readings.
1 megohm resistor.

(i)

Plasma gas flow 4.5 ℓ/min. Ar.
Nebuliser gas flow 2.0 ℓ/min. Ar.
Coolant gas flow 20.0 ℓ/min. N_2

SC 15 generator.
Concentration of the element as the chloride, 10 p.p.m.

(a) = 0.077 volts.

Power kW	Height cms.	b volts	x volts	x - b volts	x/b	(x - b)/(b - a)
0.67	2.74	.077	0.350	0.273	4.5	*
	3.24	.077	0.318	0.241	4.1	*
	4.24	.077	0.250	0.173	3.2	*
	5.24	.077	0.207	0.130	2.7	*
	6.24	.077	0.162	0.085	2.1	*

Power kW	Height cms.	b volts	x volts	x - b volts.	x/b	$\frac{x-b}{b-a}$	
	7.24	.077	0.120	0.043	1.6	*	
0.81	2.74	.079	0.415	0.336	5.4	*	(168)
	3.24	.077	0.407	0.330	5.3	*	
	4.24	.077	0.342	0.265	4.4	*	
	5.24	.077	0.301	0.224	3.9	*	
	6.24	.077	0.264	0.187	3.4	*	
	7.24	.077	0.221	0.144	2.9	*	
1.04	2.74	0.079	0.449	0.370	5.7	*	(185)
	3.24	0.078	0.447	0.369	5.7	*	(369)
	4.24	0.078	0.461	0.383	5.9	*	(383)
	5.24	0.078	0.457	0.379	5.9	*	(379)
	6.24	0.078	0.436	0.358	5.6	*	(358)
	7.24	0.077	0.354	0.277	4.6	*	
1.22	2.74	0.081	0.508	0.427	6.3	*	(107)
	3.24	0.080	0.517	0.437	6.5	*	(146)
	4.24	0.080	0.537	0.457	6.7	*,	(152)
	5.24	0.078	0.534	0.456	6.9	*	(456)
	6.24	0.078	0.444	0.366	5.7	*	(366)
	7.24	0.078	0.318	0.240	4.1	*	(240)
1.44	2.74	0.082	0.555	0.473	6.8	*	(95)
	3.24	0.081	0.542	0.461	6.7	*	(115)
	4.24	0.080	0.550	0.470	6.9	*	(156)
	5.24	0.079	0.534	0.455	6.8	*	(227)
	6.24	0.078	0.356	0.278	4.6	*	(278)
	7.24	0.078	0.272	0.194	3.5	*	(194)

(ii)

Plasma gas flow 15.0 ℓ/min. Ar. RD 150 generator.

Nebuliser gas flow 5.0 ℓ/min. Ar. Concentration of the element as

Coolant gas flow 34.0 ℓ/min. N_2 the chloride, 10 p.p.m.

Power kW	Height cms.	b volts	x volts.	x - b volts.	x/b	$\frac{x-b}{b-a}$
1.84	2.28	0.465	2.048	1.583	4.4	4
	2.58	0.135	1.425	1.290	10.6	22
	3.08	0.109	1.308	1.199	12.0	37
	3.58	0.099	0.996	0.897	10.1	41
	4.08	0.090	0.619	0.529	6.9	41
	4.58	0.090	0.396	0.306	4.4	24
2.57	2.28	1.148	2.877	1.729	2.5	1.6
	2.58	0.235	1.446	1.211	6.2	7.7
	3.08	0.144	1.349	1.205	9.4	18
	3.58	0.119	0.991	0.872	8.3	21
	4.08	0.110	0.344	0.234	3.1	7.1
	4.58	0.077	0.300	0.197	2.9	*
3.35	2.28	2.287	3.067	0.780	1.3	0.4
	2.58	0.395	1.792	1.397	4.5	4.4
	3.08	0.207	1.529	1.322	7.4	10.2
	3.58	0.160	0.471	0.311	2.9	3.8
	4.08	0.145	0.419	0.274	2.9	4
	4.58	0.141	0.351	0.210	2.5	3.3
4.33	2.28	2.711	4.357	1.646	1.6	0.6
	2.58	0.979	2.205	1.227	2.3	1.4
	3.08	0.347	0.696	0.349	2.0	1.3
	3.58	0.257	0.594	0.337	2.3	1.9
	4.08	0.233	0.521	0.288	2.3	1.9
	4.58	0.220	0.414	0.194	1.9	1.4

Power kW.	Height cms.	b volts.	x volts.	x - b volts.	x/b	(x - b)/(b - a)
5.44	2.28	4.554	6.917	2.363	1.5	0.53
	2.58	1.753	2.870	1.117	1.6	0.67
	3.08	0.636	1.046	0.410	1.6	0.73
	3.58	0.448	0.972	0.524	2.1	1.41
	4.08	0.382	0.732	0.350	1.9	1.15
	4.58	0.368	0.578	0.210	1.6	0.72
6.54	2.28	7.170	9.261	2.091	1.3	0.29
	2.58	3.402	3.665	0.263	1.1	0.08
	3.08	1.386	1.900	0.514	1.4	0.39
	3.58	0.911	1.519	0.608	1.7	0.73
	4.08	0.709	1.086	0.377	1.5	0.60
	4.58	0.660	0.906	0.246	1.4	0.42

[ ] Maximum values.

* Since the dark current was 0.077 ± 0.001 millivolts the t test of significance showed that the b - a results were unreliable for 95% confidence.

In these last experiments, Table 12 (ii), the gross signal still increased with power but the net signal, at a given height, passed through a maximum (which could be the norm temperature). It was felt that the higher values obtained for the net ratio $(\frac{x-b}{b-a})$ were valueless since the D.V.M. could not be read with an accuracy that would make the readings meaningful.

Section 6.2 Use of D.V.M. and 10M.ohm resistor.

The D.V.M. was made to read across a 10M.ohm resistor, which is the largest resistor which could be used without incurring excessive noise and leakage effects, replacing R701 (Fig.32) in order to read the dark current more accurately and the experiment repeated for higher powers only.

Section 6.2.1 Sodium Results.

The results obtained are tabulated in Table 13. Again the gross signal increases with power and the maximum values of net and gross ratio appear at almost the same power and heights as before and these values would give the lowest detection limit. This time the net signal does not go through a maximum. However, there were indications that the photomultiplier tubes may have been exposed to too much light at too high a gain, so that not too much reliance can be placed on these results.

Table 13. Height/Power/Emission Relationships.

Sodium 5890Å line. Digital Voltmeter Readings.

10 meg. ohm. Resistor.

Plasma gas flow 15.0 ℓ/min. Ar. RD 150 generator.

Nebuliser gas flow 5.0 ℓ/min. Ar. Concentration of the element as

Coolant gas flow 34.0 ℓ/min. N_2. the chloride, 10 p.p.m.

a = 0.00456 volts.

Power kW.	Height cms.	b volts.	x volts.	x - b volts.	x/b.	(x - b)/(b - a)
2.11	2.11	1.952	3.286	1.334	1.68	0.69
	2.26	.498	1.696	1.197	3.41	2.42
	2.76	.058	1.240	1.182	21.38	22.30
	3.26	.032	1.147	1.114	35.84	39.79
	3.76	.023	.871	0.8479	37.87	45.59
	4.26	.018	.531	0.5127	29.50	37.42
2.57	2.11	2.949	4.472	1.523	1.52	0.52
	2.26	.866	2.436	1.569	2.81	1.82
	2.76	.107	1.508	1.401	14.09	13.72
	3.26	.056	1.275	1.218	22.77	23.42
	3.76	.040	0.726	0.6902	18.15	19.50

Power kW.	Height cms.	b volts.	x volts.	x - b volts.	x/b.	$\frac{x-b}{b-a}$
3.08	2.11	4.247	6.079	1.837	1.43	0.43
	2.26	1.453	3.213	1.76	2.21	1.22
	2.76	.194	1.808	1.613	9.32	8.49
	3.26	.086	1.286	1.199	14.95	16.62
	3.76	.063	0.638	0.575	10.13	9.76
4.45	2.11	8.150	10.312	2.162	1.27	0.27
	2.26	3.224	5.398	2.174	1.67	0.68
	2.76	.618	2.588	1.969	4.19	3.21
	3.26	.209	.848	0.6385	4.06	3.12
	3.76	.179	.784	0.6057	4.38	3.48
	4.26	.135	.630	0.4949	4.67	3.78
	4.76	.115	.448	0.3337	3.90	3.03
5.5	2.11	10.145	12.545	2.40	1.24	0.24
	2.26	5.115	7.608	2.493	1.49	0.49
	2.76	1.222	2.784	1.129	2.28	1.28
	3.26	.423	1.158	0.735	2.74	1.76
	3.76	.289	1.134	0.844	3.92	2.96
	4.26	.237	.816	0.5796	3.44	2.50
	4.76	.198	.547	0.3498	2.76	1.81
6.47	2.11	12.225	14.745	2.52	1.21	0.21
	2.26	7.465	10.186	2.72	1.36	0.36
	2.76	2.050	2.698	0.648	1.32	0.32
	3.26	0.779	1.922	1.142	2.47	1.47
	3.76	0.504	1.502	0.998	2.98	2.00
	4.26	0.372	1.020	0.647	2.74	1.76
	4.76	0.296	0.669	0.373	2.26	1.28

[ ] maximum values

Section 6.3 F.E.T. Measuring System.

In view of the results obtained in sections 6.1.1 and 6.2.1 major changes were now made to the measuring set. The profiling valve (Fig. 32) was replaced with the circuit shown in Fig. 46.

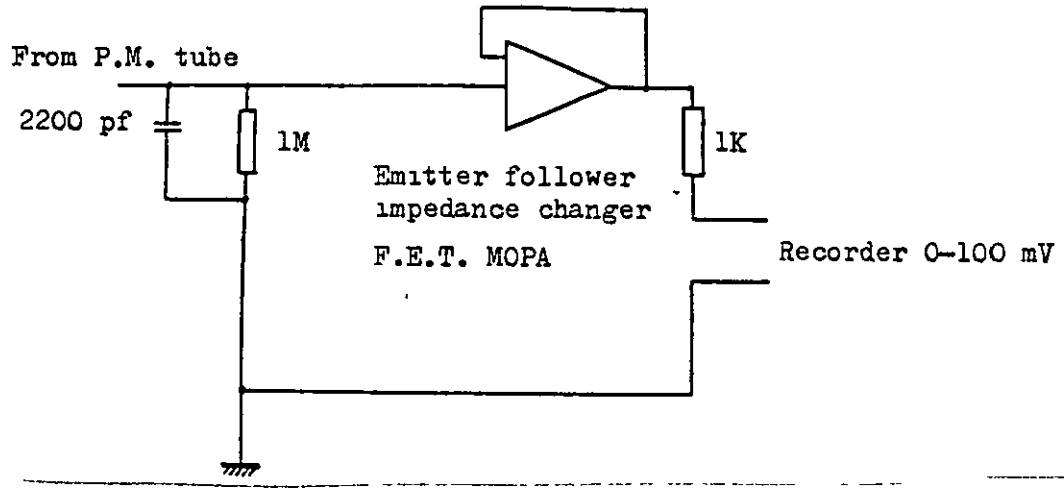

Fig. 46. F.E.T. Measuring system.

Section 6.3.1 Sodium Results.

Using the equipment detailed in Fig. 46 the experiments were repeated and the data obtained for sodium is tabulated in Tables 14 to 20.

Table 14. Height/Power/Emission Relationships.

Sodium 5890Å line. F.E.T. Recorder Readings.

SC 15 generator. Na 10 p.p.m., as the chloride.

Power in plasma 0.67 kW. Gas flows as in Table 12.

Top of cell (cm.) 2.44

Top of plasma (cm.) 1.1 (unreliable because of difficulty in locating the top of the plasma).

Height cm.	Gain.	a mv.	b mv.	x mv.	b - a mv.	x - b mv.	x/b.	x - b / b - a
2.46	4	27.1	27.7	57.0	* (.6)	29.3	2.1	*
2.60	4	27.1	27.3	58.0	* (.2)	30.7	2.1	*
3.10	4	27.1	27.3	57.0	* (.2)	29.7	2.1	*
3.60	4	27.1	27.4	56.7	* (.3)	29.3	2.1	*

Height cm.	Gain.	a mv.	b mv.	x mv.	b - a mv.	x - b mv.	x/b.	x - b / b - a
4.10	4	27.1	27.3	55.0	* (.2)	27.7	2.0	*
4.60	4	27.1	27.2	53.4	* (.1)	26.2	2.0	*
5.10	4	27.1	27.2	51.1	* (.1)	23.9	1.9	*
6.10	4	27.1	27.1	46.0	*	18.9	1.7	*
7.10	4	27.1	27.1	39.0	*	11.9	1.4	*

* Since the dark current was 27.1 ± .5 millivolts the t test of significance showed that the b - a results were unreliable for 95% confidence.

Table 15. Height/Power/Emission Relationships.

Sodium 5890Å line. F.E.T. Recorder Readings.

SC 15 generator. Na 10 p.p.m., as the chloride.

Power in plasma 1.19 kW. Gas flows as in Table 12.

Top of cell (cm.) 2.52

Top of plasma (cm.) 0.66

Height cm.	Gain.	a mv.	b mv.	x mv.	b - a mv.	x - b mv.	x/b.	x - b / b - a
2.52	4	26.9	27.9	94.3	1.0	66.4	3.4	66 ± 33
2.66	4	26.9	27.3	76.0	* (.4)	48.7	2.8	*
3.16	4	26.9	27.2	75.5	* (.3)	48.3	2.8	*
3.66	4	26.9	27.1	69.9	* (.2)	42.8	2.6	*
4.16	4	26.9	27.1	65.1	* (.2)	38.0	2.4	*
4.66	4	26.9	27.1	61.0	* (.2)	33.9	2.3	*
5.16	4	26.9	27.1	53.5	* (.2)	26.4	2.0	*
6.16	4	26.9	27.1	51.8	* (.2)	24.7	1.9	*
7.16	4	26.9	27.1	46.0	* (.2)	18.9	1.7	*
8.16	4	26.9	27.0	39.9	* (.1)	12.9	1.5	*

* Unreliable for reasons stated earlier.

Table 16. Height/Power/Emission Relationships.

Sodium 5890Å line. F.E.T. Recorder Readings

RD 150 generator. Na 10 p.p.m., as the chloride.

Power in plasma 1.28 KW. Gas flows as in Table 12.

Top of cell (cm.) 2.20

Top of plasma (cm.) 2.18

Height cm.	Gain.	a mv.	b mv.	x mv.	b - a mv.	x - b mv.	x/b.	(x - b)/(b - a)
2.43	2	24.2	26.1	48.3	1.9	22.2	1.9	12
2.68	2	24.2	25.9	53.4	1.7	27.5	2.1	16
2.93	2	24.2	26.0	52.4	1.8	26.4	2.0	15
3.18	2	24.2	26.0	53.1	1.8	27.1	2.0	15
3.43	2	24.2	26.0	55.8	1.8	29.8	2.1	17
3.68	2	24.2	26.1	56.0	1.9	29.9	2.1	16
3.93	2	24.2	26.0	51.8	1.8	25.8	2.0	14
4.18	2	24.0	26.0	47.8	1.8	21.8	1.8	12
4.68	2	24.2	26.3	47.4	2.1	21.1	1.8	10
5.18	2	24.2	26.1	45.0	1.9	18.9	1.7	10

Table 17. Height/Power/Emission Relationships.

Sodium 5890Å line. F.E.T. Recorder Readings

SC 15 generator. Na 10 p.p.m., as the chloride.

Power in plasma 1.42 KW. Gas flows as in Table 12.

Top of cell (cm.) 2.46

Top of plasma (cm.) 1.10

Height cm.	Gain.	a mv.	b mv.	x mv.	b - a mv.	x - b mv.	x/b.	$\frac{x-b}{b-a}$
2.46	4	27.0	28.2	94.5	1.2	66.3	3.4	55 ± 22
2.60	4	27.0	27.6	97.3	* (.6)	69.7	3.5	*
3.10	4	27.0	27.2	80.2	* (.2)	53.0	2.9	*
3.60	4	27.0	27.1	83.2	* (.1)	56.1	3.1	*
4.10	4	27.0	27.1	85.8	* (.1)	58.7	3.2	*
4.60	4	27.0	27.1	73.0	* (.1)	45.9	2.7	*
5.10	4	27.0	27.2	61.0	* (.2)	33.8	2.2	*
6.10	4	27.0	27.1	49.0	* (.1)	21.9	1.8	*
7.10	4	27.0	27.1	42.0	* (.1)	14.9	1.5	*
8.10	4	27.0	27.1	37.2	* (.1)	10.1	1.4	*

* Unreliable for reasons stated earlier.

Table 18. Height/Power/Emission Relationships.

Sodium 5890Å line. F.E.T. Recorder Readings

RD 150 generator. Na 10 p.p.m., as the chloride.

Power in plasma 2.03 KW. Gas flows as in Table 12.

Top of cell (cm.) 2.22

Top of plasma (cm.) 2.34

Height cm.	Gain.	a mv.	b mv.	x mv.	b - a mv.	x - b mv.	x/b.	(x - b)/(b - a)
2.45	2	24.1	27.2	75.1	3.1	47.9	2.8	15
2.70	2	24.1	26.6	77.2	2.5	50.6	2.9	20
2.95	2	24.1	26.1	79.6	2.0	53.5	3.0	27
3.20	2	24.1	26.4	76.6	2.3	50.2	2.9	22
3.45	2	24.1	26.3	67.0	2.2	40.7	2.5	19
3.70	2	24.1	26.2	62.7	2.1	36.5	2.4	17
3.95	2	24.1	26.1	55.0	2.0	28.9	2.1	14
4.20	2	24.1	26.1	49.6	2.0	23.5	1.9	12
4.70	2	24.1	26.2	39.9	2.1	13.7	1.5	7
5.20	2	24.1	26.0	36.0	1.9	10.0	1.4	5

Table 19. Height/Power/Emission Relationships.

Sodium 5890Å line. F.E.T.Recorder Readings.

RD 150 generator. Na 10 p.p.m., as the chloride.

Power in plasma 3.57 KW. Gas flows as in Table 12.

Top of cell (cm.) 2.25

Top of plasma (cm.) 2.65

Height cm.	Gain.	a mv.	b mv.	x mv.	b - a mv.	x - b mv.	x/b.	x - b / b - a
2.50	2	24.1	39.5	90.4	15.4	50.9	2.3	3
2.75	2	24.1	30.0	60.0	5.9	30.0	2.0	5
3.00	2	24.1	28.2	61.0	4.1	32.8	2.2	8
3.25	2	24.1	27.6	52.3	3.5	24.7	1.9	7
3.50	2	24.1	27.0	41.2	2.9	14.2	1.5	5
3.75	2	24.1	26.9	36.0	2.8	9.1	1.3	3
4.00	2	24.1	27.0	36.0	2.9	9.0	1.3	3
4.25	2	24.1	26.8	33.9	2.7	7.1	1.3	3

Table 20. Height/Power/Emission Relationships.

Sodium 5890Å line. F.E.T. Recorder Readings

RD 150 generator. Na 10 p.p.m., as the chloride.

Power in plasma 5.60 KW Gas flows as in Table 12.

Top of cell (cm.) 2.20

Top of plasma (cm.) 3.10

Height cm.	Gain.	a mv.	b mv.	x mv.	b - a mv.	x - b mv.	x/b.	x - b / b - a
2.45	1	24.0	35.0	55.5	11.0	20.5	1.6	2
2.70	1	24.0	32.0	40.5	8.0	8.5	1.3	1
2.95	1	24.0	28.0	33.7	4.0	5.7	1.2	1
3.20	2	24.2	30.9	45.0	6.7	14.1	1.5	2
3.45	2	24.2	29.4	44.6	5.2	15.2	1.5	3
3.70	2	24.2	28.9	43.8	4.7	14.9	1.5	3
3.95	2	24.2	28.4	41.0	4.2	12.6	1.4	3
4.20	2	24.2	28.4	39.5	4.2	11.1	1.4	3
4.70	2	24.2	28.5	35.1	4.3	6.6	1.2	2
5.20	2	24.2	28.0	33.8	3.8	5.8	1.2	2

Again it can be seen that the maximum net and gross ratios occur at places where the values of x and b would give similar D.L. and that the lowest D.L. occurs at low powers.

Fig. 47 is a plot of net signal, normalised to a constant gain of eleven, against height above the base of the plasma for each power.

It can be seen that in most cases there is an optimum height in the tail-flame, for each power, where the intensity is at a maximum, as is indicated by the open circles in Fig. 48, which also indicates that this position is nearer to the plasma the higher the power. The filled circles indicate highest recorded readings rather than true maxima.

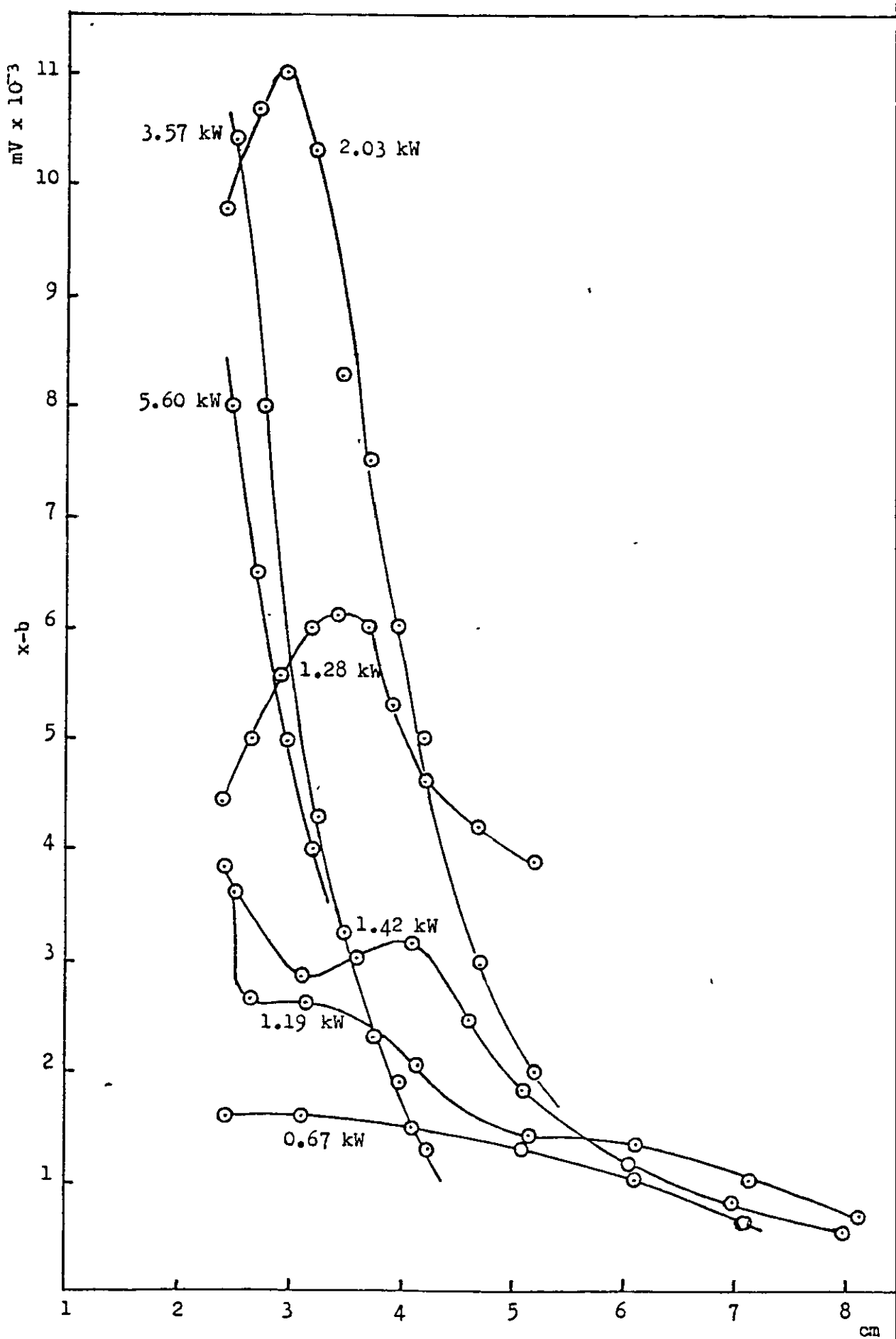

Fig. 47. Height/power/emission relationships. Na 5890A° 10 ppm. Plot of net signal, normalised to gain 11, versus height above the base of the plasma, at various powers.

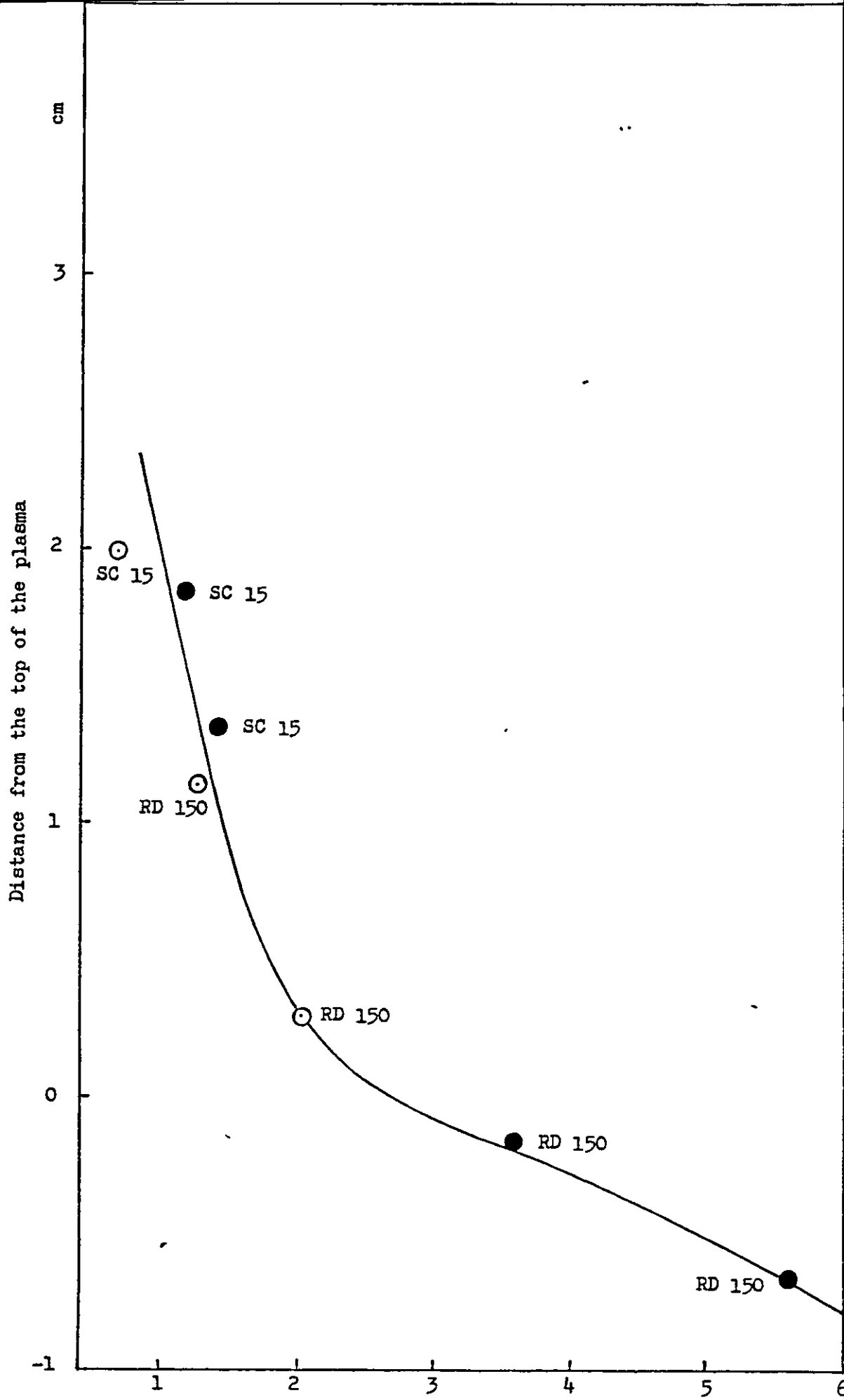

Fig.48. Height/power/emission relationship. Na 5890A° 10 ppm. Showing how the optimum viewing position changes with power, i.e. maximum x-b at each power ⊙, or highest recorded reading ●.

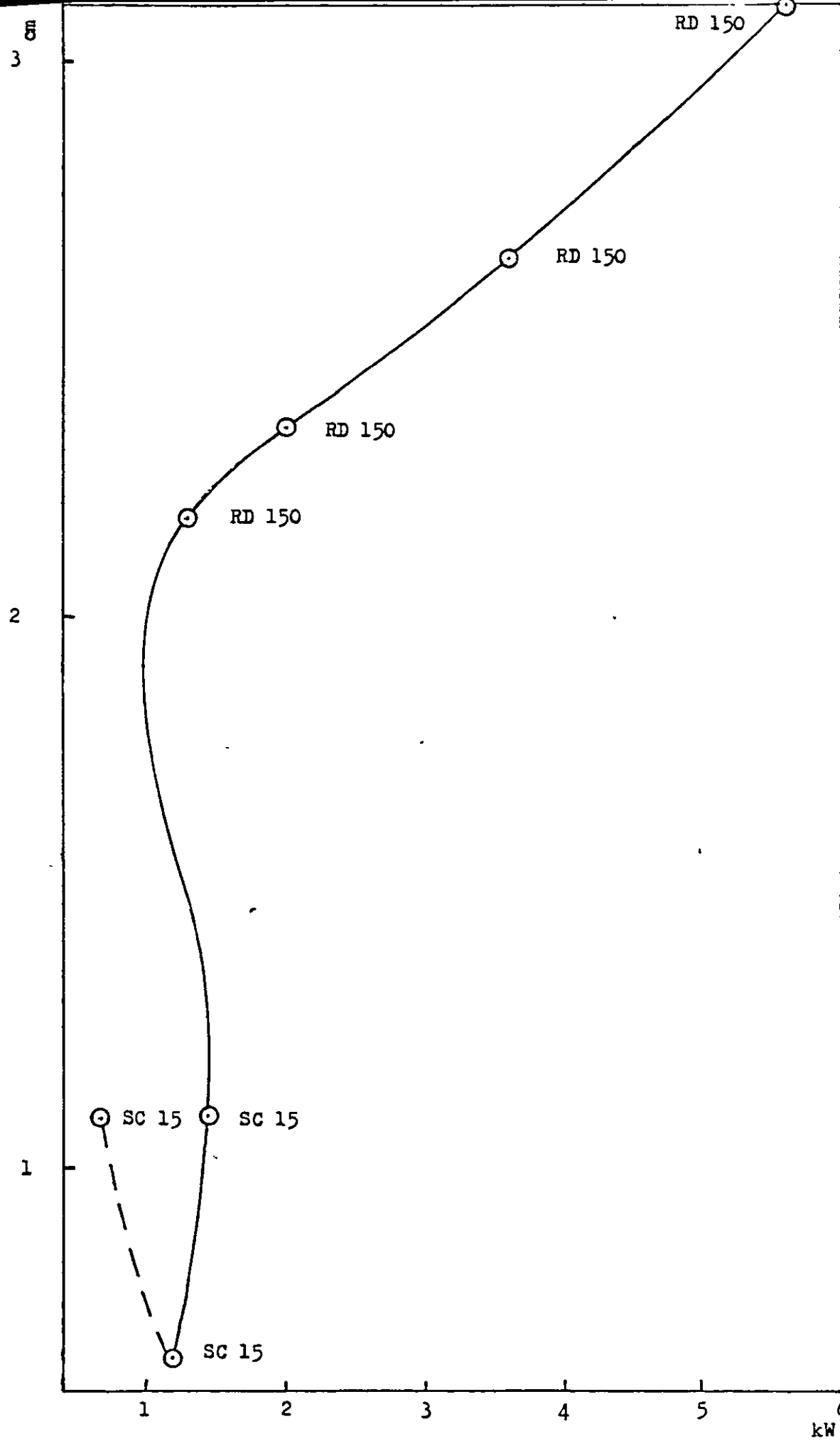

Fig. 49. Height/power/emission relationship. Na 5890A° 10 ppm. Showing how the plasma increases in length with power.

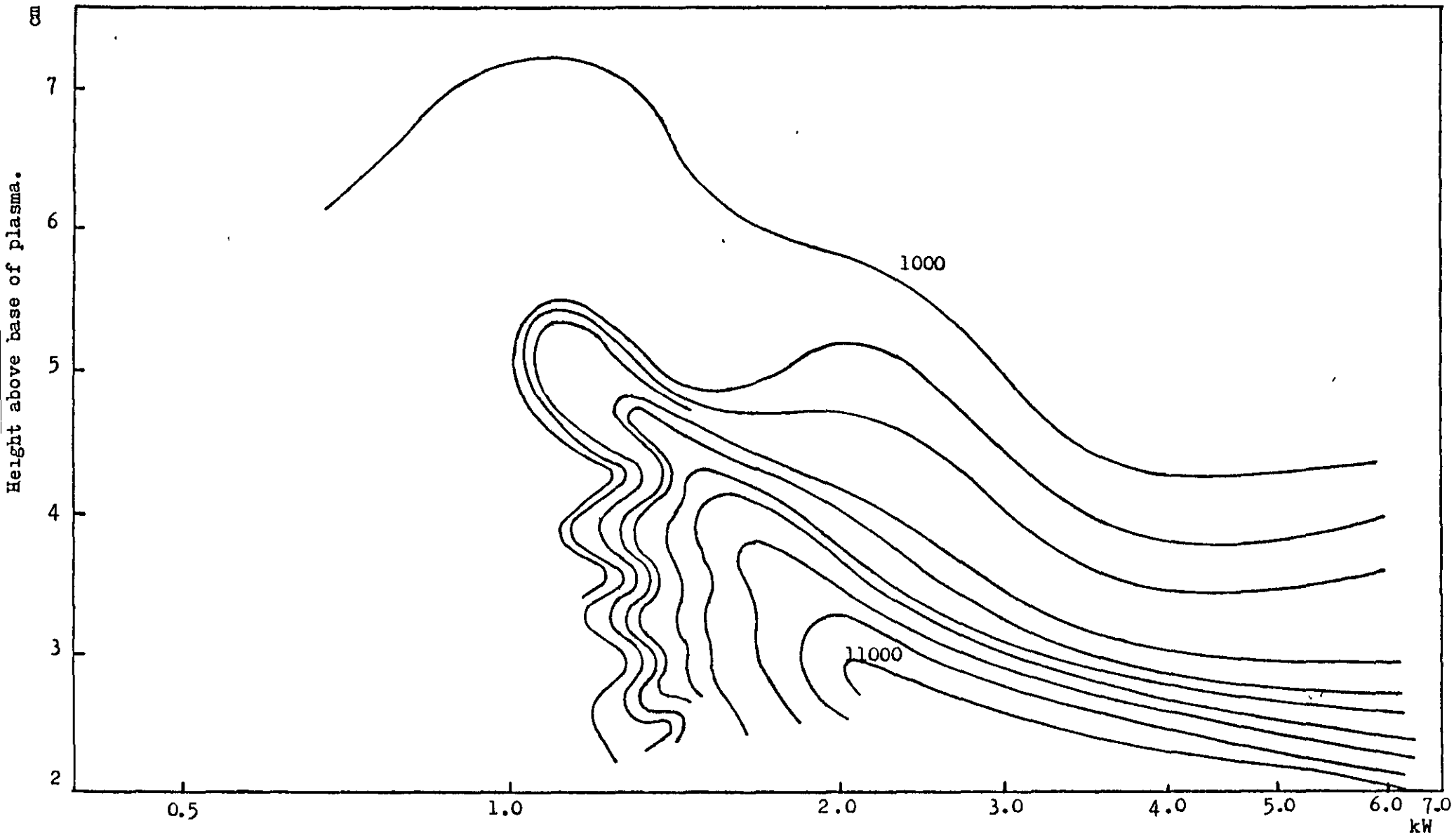

Fig. 50. Height/power/emission relationships. Na 5890A° 10 ppm. Contours of emission at intervals of 1000 m.v.

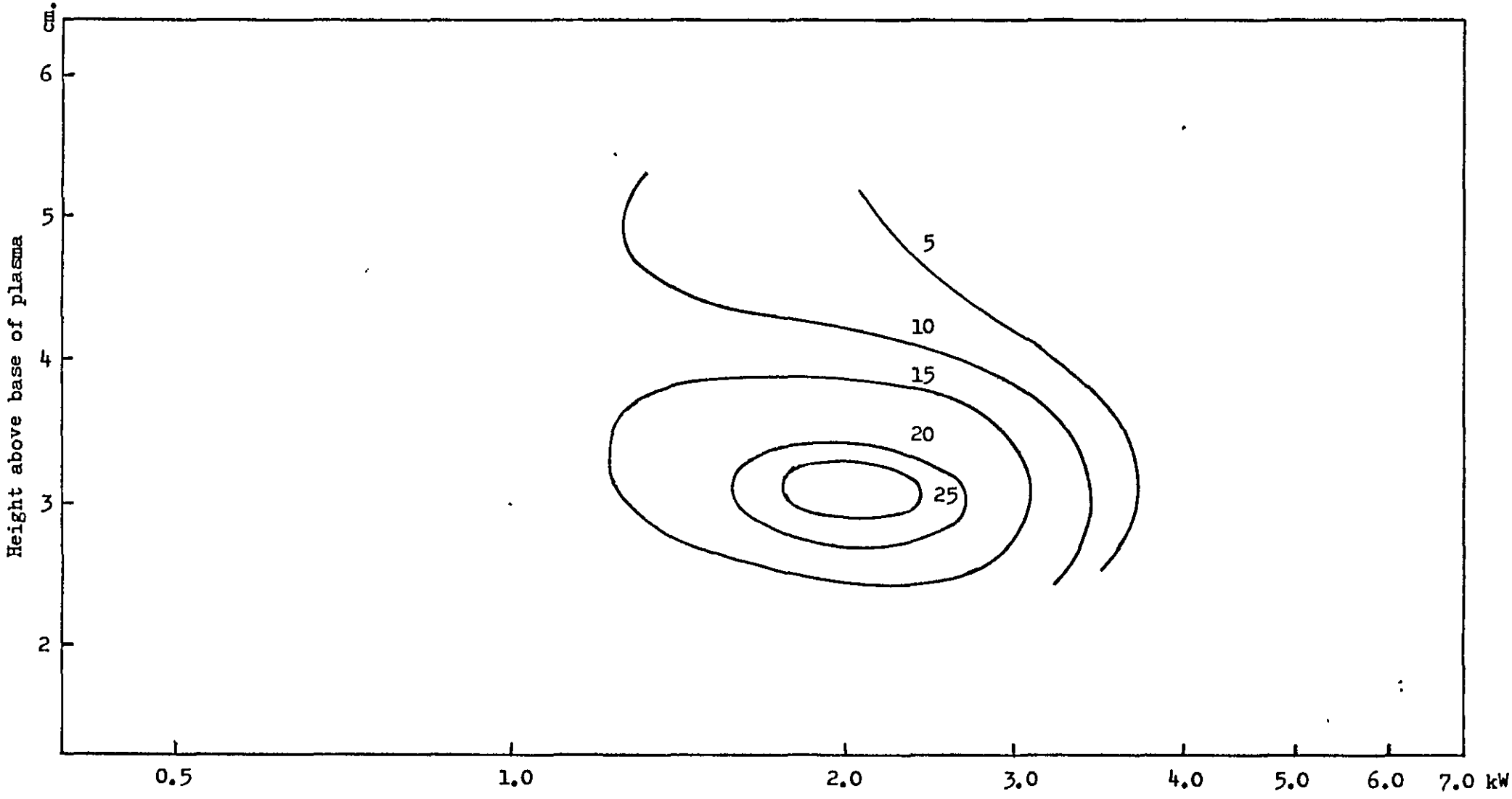

Fig. 51. Height/power/emission relationships. Na 5890A° 10 ppm. Contours of $\frac{x-b}{b-a}$ at intervals of 5 units.

(It should be noted that the maximum for the two highest powers appears to be in the plasma). The net signal, at a given height, increases with power and passes through a maximum, which could be the norm temperature, at about 2.5 kW in the plasma. The dip in signal at the changeover point between the two generators is explained by the change in frequency between the two generators. The 36 MHz generator being more efficient than the 7 MHz generator. Fig. 49 shows from the data in Tables 14 to 20 how the length of the visibly brilliant plasma increases with power.

Fig. 50 is a contour map of net signal versus height and power. It does indicate the possibility of a peak for maximum net signal at heights of < 2.8 cm. above the base of the plasma, and powers > 2.03 kW. Fig. 51 is a contour map of the net ratio $\frac{x - b}{b - a}$ versus height and power, which clearly shows a peak.

Section 6.3.2 Zinc Results.

Using the equipment detailed in Fig. 46 the information obtained is tabulated in Tables 21 to 27 for the 3072Å line of zinc and in Tables 28 to 34 for the 3076Å line. These two lines of the same element differ in respect of their excitation potentials and of their norm temperatures. Both lines come from the neutral atom but the 3072Å line has an excitation potential of 8.01 ev with a norm temperature of 11,000K (ignoring the effect of partial pressure) whereas the 3076Å line has an excitation potential of 4.01 ev and a norm temperature of 9,000K (again ignoring partial pressures).

With both lines the net signal. x-b, normalised to constant gain, increases with increasing power at all heights unlike the x-b signal from the sodium 5890Å line which passes through a maximum. This is consistent with thermal excitation and implies that the temperature reached by the analyte is below the norm temperature of the two zinc lines but is above that of the sodium line.

Table 21. Height/Power/Emission Relationships.

Zinc 3072Å line. F.E.T. Recorder Readings

SC 15 generator. Zn 13000 p.p.m., as the nitrate.

Power in plasma 0.79 kW Gas flows as in Table 12.

Top of cell (cm.) 2.32

Top of plasma (cm.) 0.70

Height cm.	Gain.	a mv.	b mv.	x mv.	b - a mv	x - b mv	x/b.	x - b / b - a
2.36	6	26.3	27.5	28.2	1.2	* (.7)	1	*
2.50	6	26.3	26.8	27.0	* (.5)	* (.2)	1	*

* Unreliable for reasons stated earlier.

Table 22. Height/Power/Emission Relationships.

Zinc 3072Å line. F.E.T. Recorder Readings

SC 15 generator. Zn 13000 p.p.m., as the nitrate.

Power in plasma 1.25 kW Gas flows as in Table 12.

Top of cell (cm.) 2.38

Top of plasma (cm.) 0.56

Height cm.	Gain.	a mv.	b mv.	x mv.	b - a mv	x - b mv	x/b.	x - b / b - a
2.42	5	26.7	27.9	29.7	1.2	1.8	1.1	1.5
2.56	5	26.7	27.2	28.0	* (.5)	* (0.8)	1.0	*
3.06	5	26.7	26.9	27.1	* (.2)	* (0.2)	1.0	*

* Unreliable for reasons stated earlier.

Table 23. Height/Power/Emission Relationships.

Zinc 3072Å line. F.E.T. Recorder Readings

SC 15 generator. Zn 13000 p.p.m., as the nitrate.

Power in plasma 1.67 kW Gas flows as in Table 12.

Top of cell (cm.) 2.42

Top of plasma (cm.) 1.02

Height cm.	Gain.	a mv.	b mv.	x mv.	b - a mv	x - b mv	x/b.	x - b / b - a
2.46	4	25.9	28.0	33.2	2.1	5.2	1.2	2.5
2.60	4	25.9	27.0	31.2	1.1	4.2	1.2	3.8
3.10	4	25.9	26.2	28.4	* (0.3)	2.2	1.1	*
3.60	4	25.9	26.0	27.0	* (0.1)	1.0	1.0	*
4.10	4	25.9	25.9	26.4	*	* (.5)	1.0	*

* Unreliable for reasons stated earlier.

Table 24. Height/Power/Emission Relationships.

Zinc 3072Å line. F.E.T. Recorder Readings

RD 150 generator. Zn 13000 p.p.m., as the nitrate.

Power in plasma 2.03 kW Gas flows as in Table 12.

Top of cell (cm.) 2.22

Top of plasma (cm.) 2.38

Height cm.	Gain.	a mv.	b mv.	x mv.	b - a mv.	x - b mv.	x/b.	x - b / b - a
2.45	1	31.8	33.2	36.6	1.4	3.4	1.1	2.4
2.70	1	31.8	33.2	35.6	1.4	2.4	1.1	1.7
2.95	1	31.8	32.8	35.0	1.0	2.2	1.1	2.2
3.20	1	31.8	32.8	35.0	1.0	2.2	1.1	2.2
3.70	1	31.8	32.6	34.5	*(0.8)	1.9	1.1	*
4.20	1	31.8	32.5	33.9	*(0.7)	1.4	1.0	*
4.70	1	31.8	32.5	33.4	*(0.7)	* (.9)	1.0	*
5.20	1	31.8	32.3	33.0	*(0.5)	* (.7)	1.0	*

* Unreliable for reasons stated earlier.

Table 25. Height/Power/Emission Relationships.

Zinc 3072Å line. F.E.T. Recorder Readings

RD 150 generator. Zn 13000 p.p.m., as the nitrate.

Power in plasma 3.57 kW Gas flows as in Table 12.

Top of cell (cm.) 2.24

Top of plasma (cm.) 2.67

Height cm.	Gain.	a mv.	b mv.	x mv.	b - a mv	x - b mv	x/b	x - b / b - a
2.48	1	28.4	30.6	37.0	2.2	6.4	1.2	2.9
2.73	1	28.4	30.0	35.8	1.6	5.8	1.2	3.6
2.98	1	28.4	30.0	35.1	1.6	5.1	1.2	3.2
3.23	1	28.4	29.9	35.0	1.5	5.1	1.2	3.4
3.48	1	28.4	29.8	34.2	1.4	4.4	1.1	3.1
3.73	1	28.4	29.8	34.7	1.4	4.9	1.2	3.5
4.23	1	28.4	29.8	34.0	1.4	4.2	1.1	3.0
4.73	1	28.4	29.8	33.1	1.4	3.3	1.1	2.4
5.23	1	28.4	29.5	32.0	1.1	2.5	1.1	2.3

Table 26. Height/Power/Emission Relationships.

Zinc 3072Å line. F.E.T. Recorder Readings

RD 150 generator. Zn 13000 p.p.m., as the nitrate.

Power in plasma 5.56 kW Gas flows as in Table 12.

Top of cell (cm.) 2.20

Top of plasma (cm.) 3.03

Height cm.	Gain.	a mv.	b mv.	x mv.	b - a mv	x - b mv	x/b.	(x - b)/(b - a)
2.43	1	30.1	38.5	48.8	8.4	10.3	1.3	1.2
2.68	1	30.1	35.5	47.4	5.4	11.9	1.3	2.2
2.93	1	30.1	34.4	48.4	4.3	14.0	1.4	3.3
3.18	1	30.1	33.5	50.0	3.4	16.5	1.5	4.9
3.43	1	30.1	33.1	51.1	3.0	18.0	1.5	6.0
3.68	1	30.1	33.2	51.0	3.1	17.8	1.5	5.7
3.93	1	30.1	32.6	48.0	2.5	15.4	1.5	6.2
4.18	1	30.1	32.4	45.5	2.3	13.1	1.4	5.7
4.68	1	30.1	32.5	41.1	2.4	8.6	1.3	3.6
5.18	1	30.1	32.3	38.7	2.2	6.4	1.2	2.9

Table 27. Height/Power/Emission Relationships.

Zinc 3072Å line. F.E.T. Recorder Readings

RD 150 generator. Zn 13000 p.p.m., as the nitrate.

Power in plasma 6.73 kW. Gas flows as in Table 12.

Top of cell (cm.) 2.22

Top of plasma (cm.) 3.57

Height cm.	Gain.	a m.v.	b m.v.	x m.v.	b - a m.v.	x - b m.v.	x/b.	$\frac{x-b}{b-a}$
2.45	1	32.8	45.0	63.0	12.2	18.0	1.4	1.5
2.70	1	32.8	39.2	60.5	6.4	21.3	1.5	3.3
2.95	1	32.8	37.5	63.8	4.7	26.3	1.7	5.6
3.20	1	32.8	35.9	66.9	3.1	31.0	1.9	10.0
3.45	1	32.8	35.4	70.5	2.6	35.1	2.0	13.5
3.70	1	32.8	35.0	70.1	2.2	35.1	2.0	16.0
3.95	1	32.8	34.8	62.0	2.0	27.2	1.8	13.6
4.20	1	32.8	35.1	54.5	2.3	19.4	1.6	8.4
4.70	1	32.8	34.5	47.5	1.7	13.0	1.4	7.6
5.20	1	32.8	33.7	43.4	* (.9) 9.7		1.3	*

* Unreliable for reasons stated earlier.

☐ Maximum value of $\frac{x-b}{b-a}$. Tables 21 to 27 and Tables 24 to 27 for b - a, x - b and $^{x}/_{b}$ (i.e. same gain).

Table 28. Height/Power/Emission Relationships.

Zinc 3076Å line. F.E.T. Recorder Readings

SC 15 generator. Zn 13000 p.p.m., as the nitrate.

Power in plasma 0.79 kW. Gas flows as in Table 12.

Top of cell (cm.) 2.32

Top of plasma (cm.) 0.70

Height cm.	Gain.	a m.v.	b m.v.	x m.v.	b - a m.v.	x - b m.v.	x/b.	x - b / b - a
2.36	6	26.3	27.3	45.5	1.0	18.2	1.7	18.2
2.50	6	26.3	27.0	39.4	* (.7)	12.4	1.5	*
3.00	6	26.3	26.5	29.3	* (.2)	2.8	1.1	*

* Unreliable for reasons stated earlier.

Table 29. Height/Power/Emission Relationships.

Zinc 3076Å line. F.E.T. Recorder Readings

SC 15 generator. Zn 13000 p.p.m., ss the nitrate.

Power in plasma 1.25 kW. Gas flows as in Table 12.

Top of cell (cm.) 2.38

Top of plasma (cm.) 0.56

Height cm.	Gain.	a m.v.	b m.v.	x m.v.	b - a m.v.	x - b m.v.	x/b.	x - b / b - a
2.42	5	26.8	28.0	70.5	1.2	42.5	2.5	35
2.56	5	26.8	27.3	56.6	* (.5)	29.3	2.1	*
3.06	5	26.8	27.0	44.0	* (.2)	17.0	1.6	*
3.56	5	26.8	26.8	29.0	* (0)	2.2	1.1	*

* Unreliable for reasons stated earlier.

[ ] Maximum values. Tables 28 to 34.

Table 30. Height/Power/Emission Relationships.

Zinc 3076Å line. F.E.T. Recorder Readings

SC 15 generator. Zn 13000 p.p.m., as the nitrate.

Power in plasma 1.67 kW Gas flows as in Table 12.

Top of cell (cm.) 2.42

Top of plasma (cm.) 1.02

Height cm.	Gain.	a m.v.	b m.v.	x m.v.	b - a m.v.	x - b m.v.	x/b.	x - b / b - a
2.46	4	25.9	28.4	93.0	2.5	64.6	3.3	25.8
2.60	4	25.9	27.9	89.0	2.0	61.1	3.2	30.8
3.10	4	25.9	26.7	72.5	* (.8)	45.8	2.7	*
3.60	4	25.9	26.3	57.8	* (.4)	31.5	2.2	*
4.10	4	25.9	26.1	50.0	* (.2)	23.9	1.9	*
4.60	4	25.9	26.0	45.5	* (.1)	19.5	1.8	*
5.10	4	25.9	26.0	41.5	* (.1)	15.5	1.6	*
6.10	4	25.9	26.0	35.5	* (.1)	9.5	1.4	*

* Unreliable for reasons stated earlier.

[ ] Maximum values. Tables 28 to 34.

Table 31. Height/Power/Emission Relationships.

Zinc 3076Å line. F.E.T. Recorder Readings

RD 150 generator. Zn 13000 p.p.m., as the nitrate.

Power in plasma 2.03 kW Gas flows as in Table 12.

Top of cell (cm.) 2.22

Top of plasma (cm.) 2.38

Height cm.	Gain.	a m.v.	b m.v.	x m.v.	b - a m.v.	x - b m.v.	x/b.	x - b / b - a
2.45	1	31.8	33.4	59.9	1.6	26.5	1.8	16.6
2.70	1	31.8	33.1	54.2	1.3	21.1	1.6	16.2
2.95	1	31.8	33.0	53.3	1.2	20.3	1.6	16.9
3.20	1	31.8	33.2	53.0	1.4	19.8	1.6	14.0
3.70	1	31.8	32.5	51.1	* (.7)	18.6	1.6	*
4.20	1	31.8	32.5	52.5	* (.7)	20.0	1.6	*
4.70	1	31.8	32.6	52.5	* (.8)	19.9	1.6	*
5.20	1	31.8	32.0	50.1	* (.2)	18.1	1.6	*

* Unreliable for reasons stated earlier.

Table 32. Height/Power/Emission Relationships.

Zinc 3076Å line. F.E.T Recorder Readings

RD 150 generator. Zn 13000 p.p.m., as the nitrate.

Power in plasma 3.57 kW. Gas flows as in Table 12.

Top of cell (cm.) 2.24

Top of plasma (cm.) 2.67

Height cm.	Gain.	a m.v.	b m.v.	x m.v.	b - a m.v.	x - b m.v.	x/b.	$\frac{x-b}{b-a}$
2.48	1	28.4	30.3	58.0	1.9	27.7	1.9	14.6
2.73	1	28.4	30.2	56.0	1.8	25.8	1.9	14.3
2.98	1	28.4	29.8	52.2	1.4	22.4	1.8	16.0
3.23	1	28.4	29.6	50.0	1.2	20.4	1.7	17.0
3.48	1	28.4	29.6	50.8	1.2	21.2	1.7	17.7
3.73	1	28.4	29.7	50.3	1.3	20.6	1.7	15.8
4.23	1	28.4	29.5	50.5	1.1	21.0	1.7	19.0
4.73	1	28.4	30.0	49.1	1.6	19.1	1.6	11.9
5.23	1	28.4	29.5	46.2	1.1	16.7	1.6	15.2

Table 33. Height/Power/Emission Relationships.

Zinc 3076Å line. F.E.T. Recorder Readings

RD 150 generator. Zn 13000 p.p.m., as the nitrate.

Power in plasma 5.56 kW. Gas flows as in Table 12.

Top of cell (cm.) 2.20

Top of plasma (cm.) 3.03

Height cm.	Gain.	a m.v.	b m.v.	x m.v.	b - a m.v.	x - b m.v.	x/b.	$\frac{x-b}{b-a}$
2.43	1	30.1	38.6	73.7	8.5	35.1	1.9	4.1
2.68	1	30.1	35.6	72.0	5.5	36.4	2.0	6.6
2.93	1	30.1	34.8	73.6	4.7	38.8	2.1	8.3
3.18	1	30.1	33.6	75.6	3.5	42.0	2.3	12.0
3.43	1	30.1	33.3	75.6	3.2	42.3	2.3	13.2
3.68	1	30.1	32.9	74.3	2.8	41.4	2.3	14.8
3.93	1	30.1	32.6	68.8	2.5	36.2	2.1	14.5
4.18	1	30.1	32.6	66.9	2.5	34.3	2.1	13.7
4.68	1	30.1	32.6	60.1	2.5	27.5	1.8	11.0
5.18	1	30.1	33.0	56.0	2.9	23.0	1.7	7.9

Table 34. Height/Power/Emission Relationships

Zinc 3076Å line. F.E.T. Recorder Readings

RD 150 generator.

Power in plasma 6.73 kW

Top of cell (cm.) 2.22

Top of plasma (cm.) 3.57

Zn 13000 p.p.m., as the nitrate.

Gas flows as in Table 12.

Height cm.	Gain.	a m.v.	b m.v.	x m.v.	b - a m.v.	x - b m.v.	x/b.	$\frac{x-b}{b-a}$
2.45	1	32.8	47.0	79.5	14.2	32.5	1.7	2.3
2.70	1	32.8	37.8	91.1	5.0	53.3	2.4	10.7
2.95	1	32.8	36.9	94.2	4.1	57.3	2.6	14.0
3.20	1	32.8	36.0	94.1	3.2	58.1	2.6	18.2
3.45	1	32.8	35.0	90.8	2.2	55.8	2.6	25.4
3.70	1	32.8	35.3	85.8	2.5	50.5	2.4	20.2
3.95	1	32.8	35.5	73.8	2.7	38.3	2.1	14.2
4.20	1	32.8	34.4	71.0	1.6	36.6	2.1	22.9
4.70	1	32.8	34.3	63.9	1.5	29.6	1.9	19.7
5.20	1	32.8	34.2	62.3	1.4	28.1	1.8	20.1

The behaviour of the ratio $\frac{x - b}{b - a}$ is different in the case of the 3072Å line from its behaviour in the case of the 3076Å line. With the 3072Å line this ratio shows a tendency to pass through a maximum with increasing power at positions near the plasma whilst at positions further out from the plasma it increases with power. In contrast the ratio $\frac{x - b}{b - a}$ for the 3076Å line, whilst showing a similar maximum at low powers near the plasma exhibits, at positions further out from the plasma, a fall in value followed by a rise in value with increasing power. The behaviour of the net signals, x - b and the ratio $\frac{x - b}{b - a}$ is shown in Figs. 52 - 57. The contour map of $\frac{x - b}{b - a}$ for the 3072Å line, Fig. 54, shows the ratio increasing with power at height between 3.0 and 4.0 cm. above the base of the plasma in contrast with the contour map of the 3076Å line, Fig. 57. where the ratio appears to be at a maximum at heights of $>$ 3.0 cm. above the base of the plasma and at powers between 1 to 2 kW. The inaccuracies involved in reading the differences between the dark current and the background signal preclude a more accurate fixing of the maximum. Fig. 57 suggests the possibility of two temperatures maxima or possibly two different modes of excitation although with the evidence available this can only be conjecture.

The maximum value of the gross ratio $^{x}/_{b}$, which is inversely proportional to the D.L., appears near to the maximum value of the ratio $\frac{x - b}{b - a}$ and the influence of the net signal, x - b is clearly seen, i.e. for a constant $\frac{x - b}{b - a}$ the ratio with the largest x - b will give the largest value of $^{x}/_{b}$.

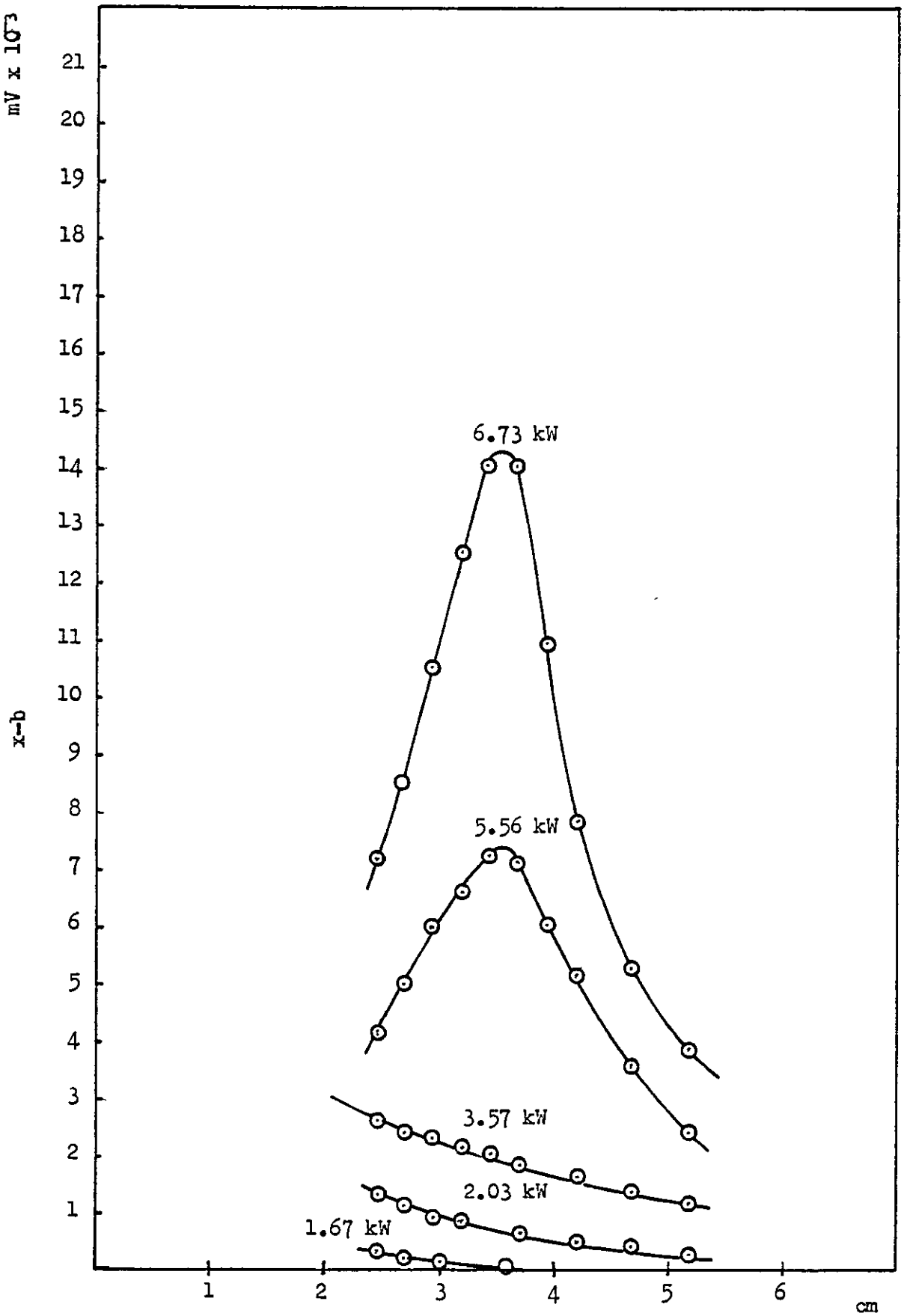

Fig. 52 Height/power/emission relationships. Zn 3072A° 13,000 ppm. Plot of net signal, normalised to gain 11, versus height above base of the plasma, at various powers.

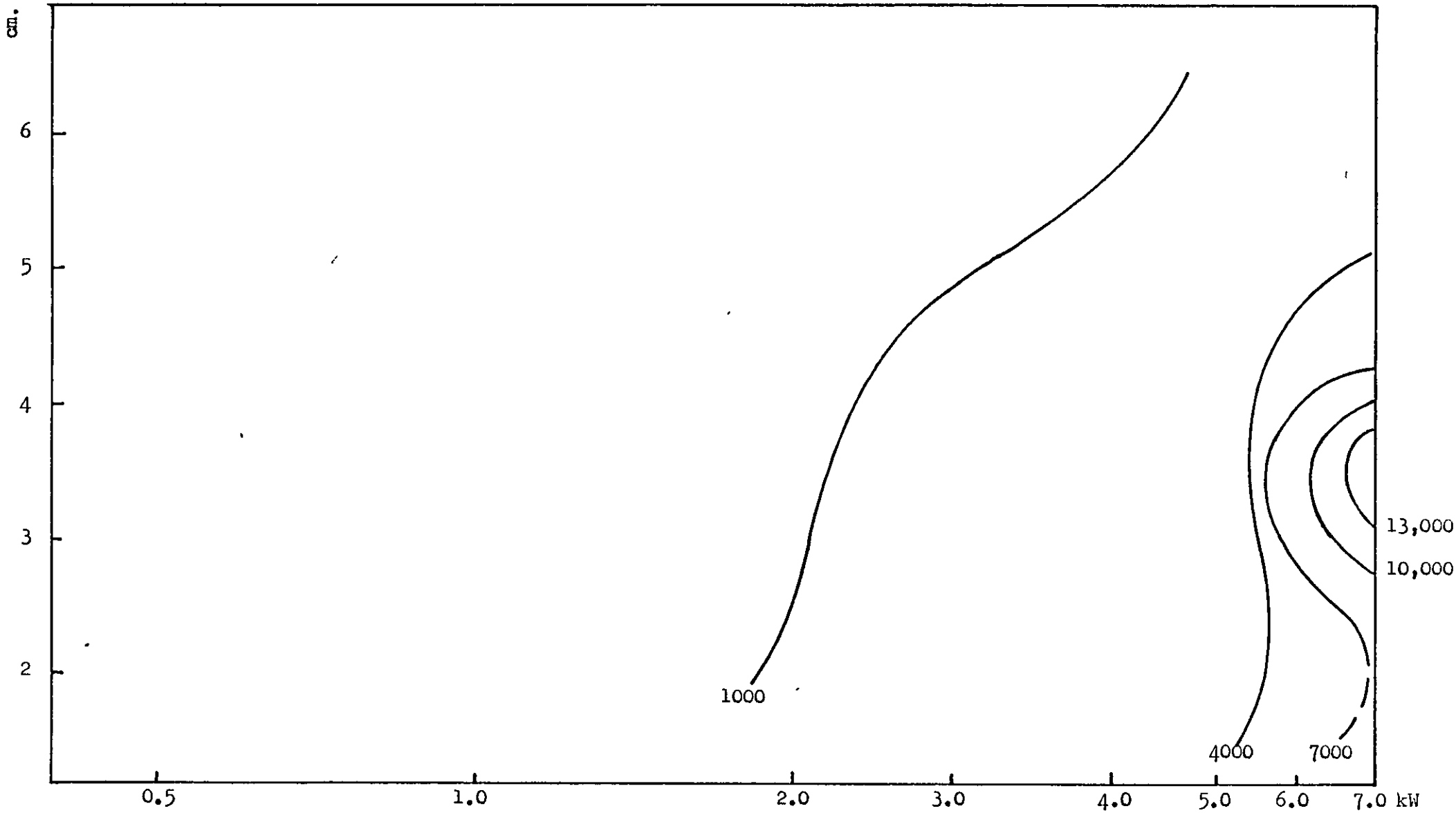

Fig. 53 Height/power/emission relationships. Zn 3072A° 13,000 ppm. Contours of emission at intervals of 3000 mV.

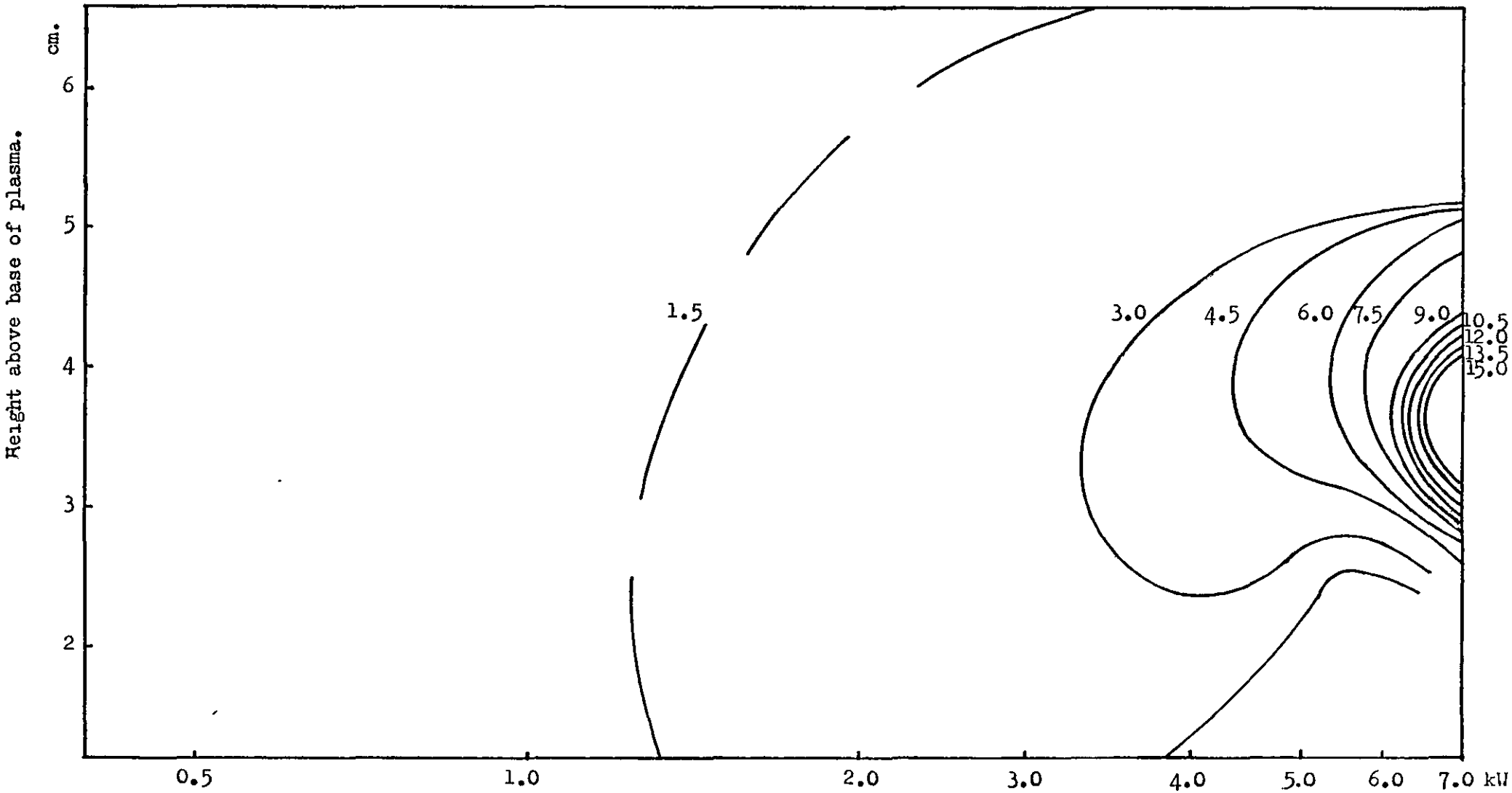

Fig. 54 Height/power/emission relationships. Zn 3072A° 13,000 ppm. Contours of $\frac{x-b}{b-a}$ at intervals of 1.5 units.

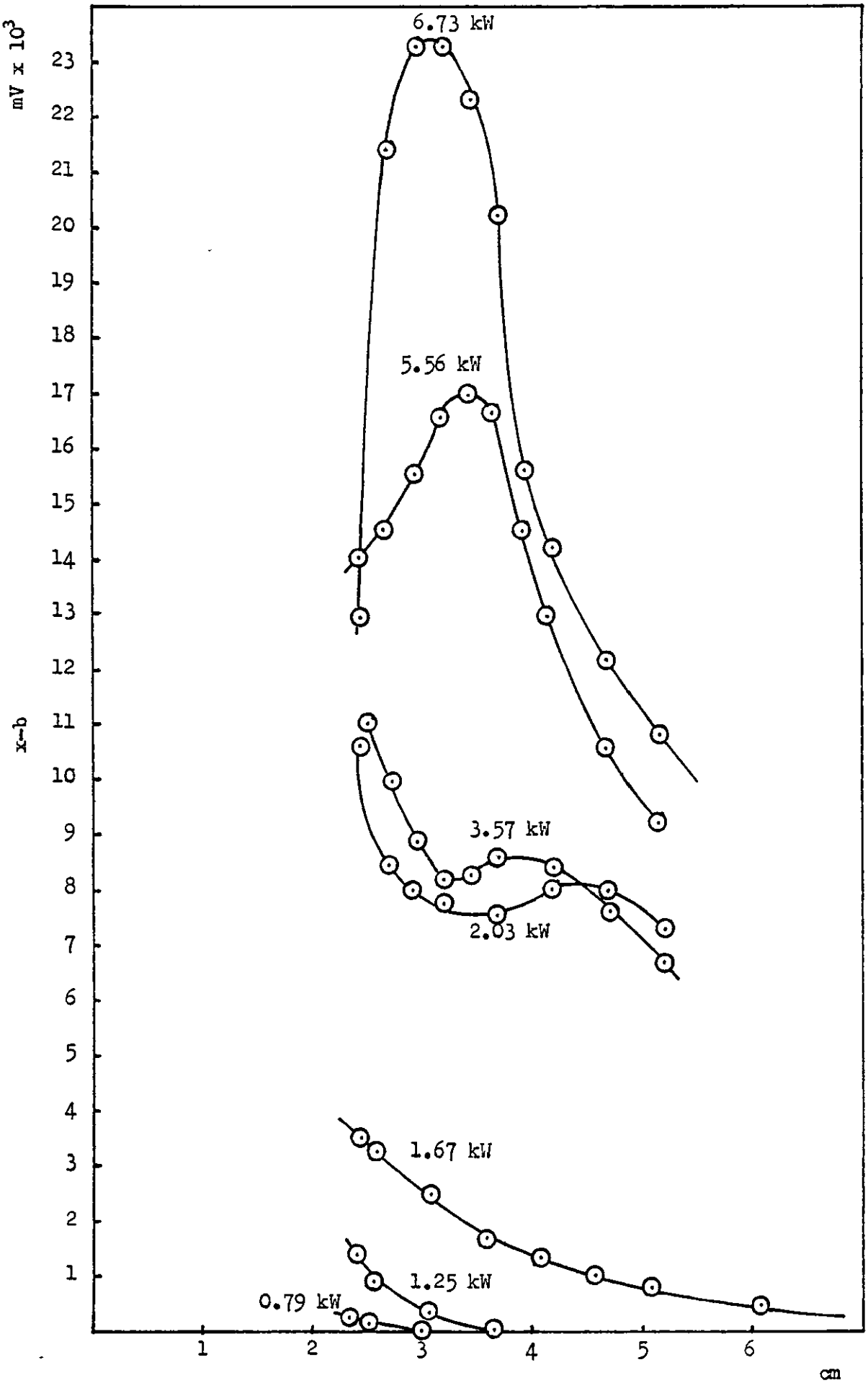

Fig. 55 Height/power/emission relationships. Zn 3076A° 13,000 ppm. Plot of net signal, normalised to gain 11, versus height above base of the plasma, at various powers.

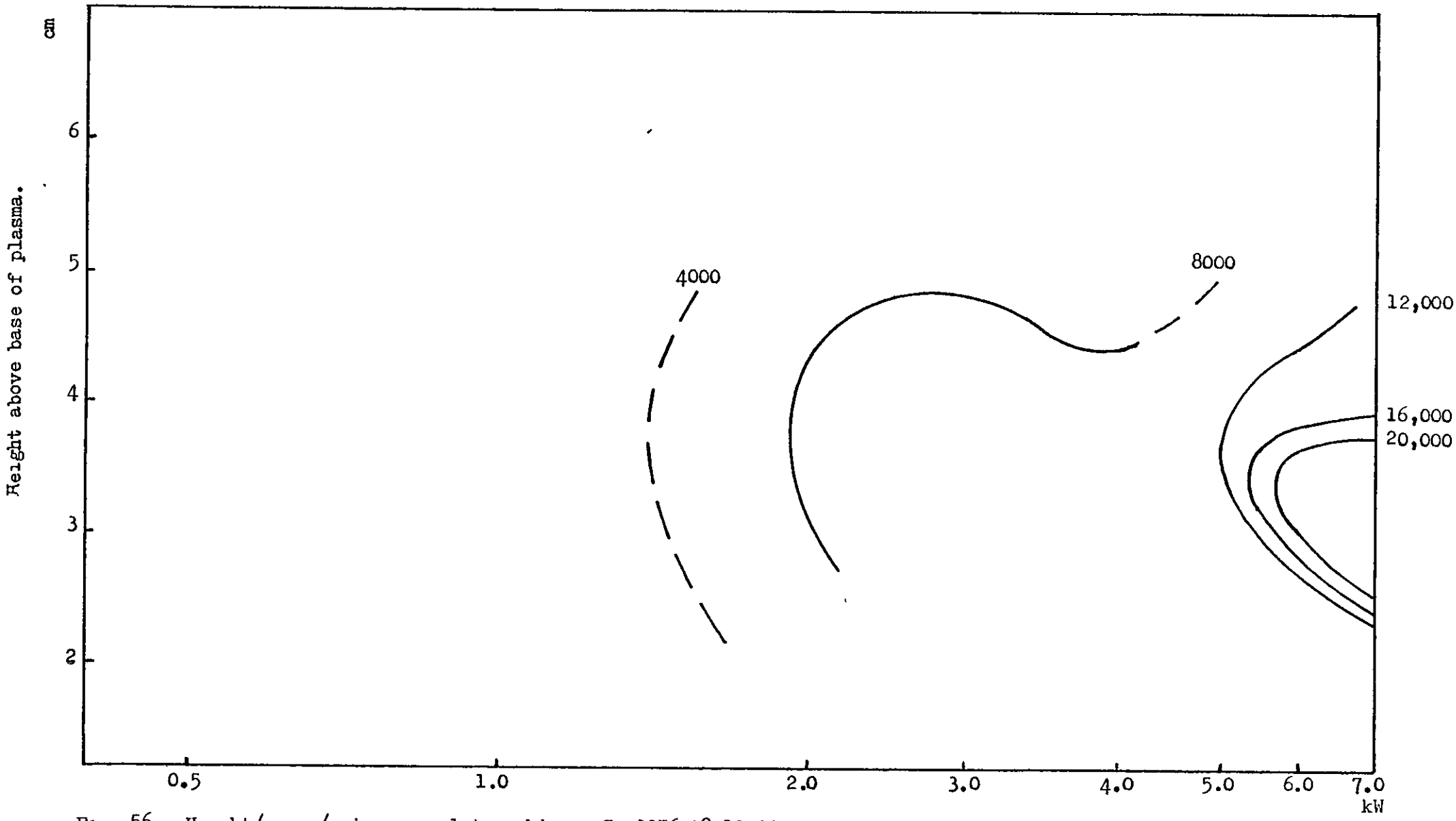

Fig. 56 Height/power/emission relationships. Zn 3076 A° 13,000 ppm. Contours of emission at intervals of 4000 mV.

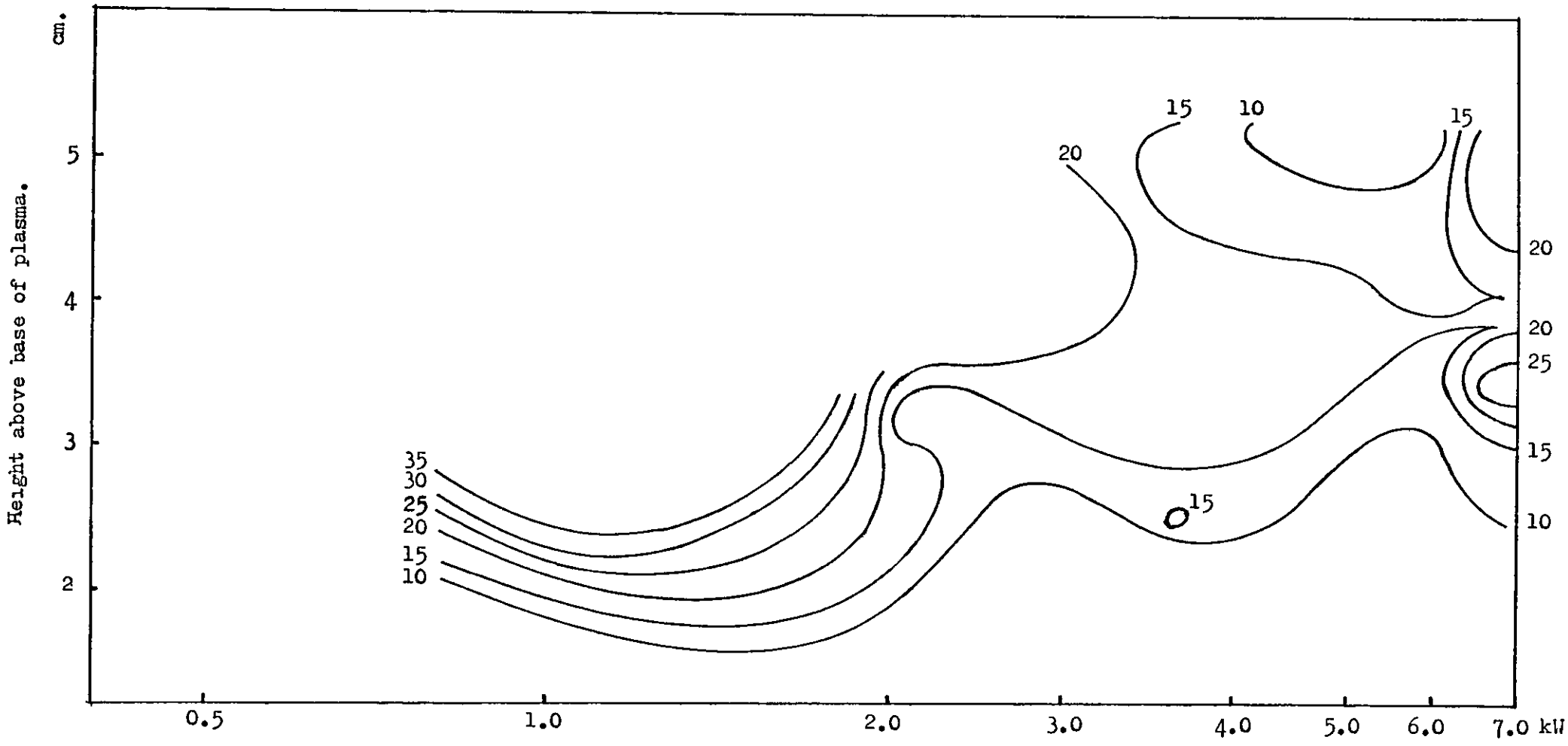

Fig. 57 Height/power/emission relationships. Zn 3076A° 13,000 ppm. Contours of $\frac{x-b}{b-a}$ at intervals of 5 units.

Section 6.3.3 Boron Results.

Using the equipment detailed in Fig. 46 the information obtained is tabulated in Tables 58-64 for the 2497Å line of boron.

Table 58. Height/Power/Emission Relationships.

Boron 2497Å line. F.E.T. Recorder Readings

SC 15 generator. Boron 1000 p.p.m. as boric acid.

Power in plasma 0.75 kW Gas flows as in Table 12.

Top of cell (cm.) 2.48

Top of plasma (cm.) 0.88

Height cm.	Gain.	a m.v.	b m.v.	x m.v.	b - a m.v.	x - b m.v.	x/b.	x - b / b - a
2.44	11	33.0	33.1	33.9	* (.1)	6.8	1.2	*
2.48	11	33.0	33.1	39.0	* (.1)	5.9	1.2	*
3.08	11	33.0	33.1	33.3	* (.1)	* (.2)	1.0	*

* Unreliable for reasons stated earlier.

Table 59. Height/Power/Emission Relationships.

Boron 2497Å line. F.E.T. Recorder Readings

SC 15 generator. Boron 1000 p.p.m. as boric acid.

Power in plasma 1.06 kW Gas flows as in Table 12.

Top of cell (cm.) 2.50

Top of plasma (cm.) 1.04

Height cm.	Gain.	a m.v.	b m.v.	x m.v.	b - a m.v.	x - b m.v.	x/b.	x - b / b - a
2.50	10	31.0	31.4	59.9	* (.4)	28.5	1.9	*
2.64	10	31.0	31.3	54.0	* (.3)	22.7	1.7	*
3.14	10	31.0	31.1	38.3	* (.1)	7.2	1.2	*
3.64	10	31.0	31.1	33.3	* (.1)	2.2	1.1	*

* Unreliable for reasons stated earlier.

Table 60. Height/Power/Emission Relationships.

Boron 2497Å line. F.E.T. Recorder Readings

SC 15 generator. Boron 1000 p.p.m. as boric acid.

Power in plasma 1.56 kW Gas flows as in Table 12.

Top of cell (cm.) 2.40

Top of plasma (cm.) 1.00

Height cm.	Gain.	a m.v.	b m.v.	x m.v.	b - a m.v.	x - b m.v.	x/b.	x - b / b - a
2.36	8	28.8	30.1	67.2	1.3	37.1	2.2	28.5
2.50	8	28.8	30.1	75.0	1.3	44.9	2.5	34.5
3.00	8	28.8	29.8	56.1	1.0	26.3	1.9	26.3
3.50	8	28.8	29.8	47.4	1.0	17.6	1.6	17.6
4.00	8	28.8	29.8	42.0	1.0	12.2	1.4	12.2
4.50	8	28.8	29.6	37.0	* (.8)	7.4	1.3	*
5.00	8	28.8	29.7	34.0	* (.9)	4.3	1.1	*

* Unreliable for reasons stated earlier.

Table 61. Height/Power/Emission Relationships.

Boron 2497Å line. F.E.T. Recorder Readings

RD 150 generator. Boron 1000 p.p.m. as boric acid.

Power in plasma 2.05 kW Gas flows as in Table 12.

Top of cell (cm.) 2.22

Top of plasma (cm.) 2.45

Height cm.	Gain.	a m.v.	b m.v.	x m.v.	b - a m.v.	x - b m.v.	x/b.	x - b / b - a
2.45	4	27.0	28.4	65.9	1.4	37.5	2.3	26.8
2.70	4	27.0	29.6	57.0	2.6	27.4	1.9	10.5
2.95	4	27.0	27.9	49.8	* (.9)	21.9	1.8	* (24
3.20	4	27.0	27.8	46.9	* (.8)	19.1	1.7	* (24
3.45	4	27.0	27.4	45.1	* (.4)	17.7	1.6	* (44
3.70	4	27.0	27.6	45.0	* (.6)	17.4	1.6	* (29
3.95	4	27.0	27.6	44.0	* (.6)	16.4	1.6	* (27
4.20	4	27.0	27.8	43.1	* (.8)	15.3	1.6	* (19
4.70	4	27.0	28.1	42.8	1.0	14.7	1.5	14.7
5.20	4	27.0	27.7	39.8	* (.7)	12.1	1.4	* (17

* Unreliable for reasons stated earlier.

[ ] Maximum value.

Table 62. Height/Power/Emission Relationships.

Boron 2497Å line. F.E.T. Recorder Readings

RD 150 generator. Boron 1000 p.p.m. as boric acid.

Power in plasma 3.64 kW Gas flows as in Table 12.

Top of cell (cm.) 2.22

Top of plasma (cm.) 2.70

Height cm.	Gain.	a m.v.	b m.v.	x m.v.	b - a m.v.	x - b m.v.	x/b.	x - b / b - a
2.45	2	25.2	25.4	46.4	* (.2)	21.0	1.9	* (105)
2.70	2	25.2	25.6	43.0	* (.4)	17.4	1.7	* (44)
2.95	2	25.2	26.0	41.0	* (.8)	15.0	1.6	* (19)
3.20	2	25.4	25.8	40.0	* (.4)	14.2	1.6	* (36)
3.45	2	25.4	25.8	40.0	* (.4)	14.2	1.6	* (36)
3.70	2	25.4	26.0	41.3	* (.6)	15.3	1.6	* (26)
3.95	2	25.4	26.0	42.1	* (.6)	16.1	1.6	* (27)
4.20	2	25.4	26.1	42.6	* (.7)	16.5	1.6	* (24)
4.70	2	25.4	25.9	39.0	* (.5)	13.1	1.5	* (26)
5.20	2	25.4	26.4	37.7	1.0	11.3	1.4	11.3

* Unreliable for reasons stated earlier.

Table 63. Height/Power/Emission Relationships.

Boron 2497Å line. F.E.T. Recorder Readings

RD 150 generator. Boron 1000 p.p.m. as boric acid.

Power in plasma 5.60 kW Gas flows as in Table 12.

Top of cell (cm.) 2.17

Top of plasma (cm.) 2.88

Height cm.	Gain.	a m.v.	b m.v.	x m.v.	b - a m.v.	x - b m.v.	x/b.	x - b / b - a
2.40	2	24.5	26.5	65.6	2.0	39.1	2.5	19.6
2.65	2	24.5	26.4	66.5	1.9	40.1	2.5	21.1
2.90	2	24.5	26.3	69.7	1.8	43.4	2.7	24.1
3.15	2	24.5	26.1	77.1	1.6	51.0	3.0	31.9
3.40	2	26.5	26.8	74.4	* (.3)	47.6	2.8	* (158)
3.65	2	26.5	26.8	78.5	* (.3)	51.7	2.9	* (172)
3.90	2	26.5	26.7	69.5	* (.2)	42.8	2.6	* (214)
4.15	2	26.5	26.8	62.0	* (.3)	35.2	2.3	* (117)
4.65	2	26.5	27.2	51.8	* (.7)	24.6	1.9	* (35)
5.15	2	26.5	26.9	45.9	* (.4)	19.0	1.7	* (48)

* Unreliable for reasons stated earlier.

☐ Maximum value.

Table 64. Height/Power/Emission Relationships.

Boron 2497Å line. F.E.T. Recorder Readings

RD 150 generator. Boron 1000 p.p.m. as boric acid.

Power in plasma 6.62 kW Gas flows as in Table 12.

Top of cell (cm.) 2.27

Top of plasma (cm.) 3.67

Height cm.	Gain.	a m.v.	b m.v.	x m.v.	b - a m.v.	x - b m.v.	x/b.	x - b / b - a
2.50	1	26.2	26.6	52.5	* (.4)	25.9	2.0	* (65)
2.75	1	26.2	27.0	57.0	* (.8)	30.0	2.1	* (38)
3.00	1	26.2	27.3	65.0	1.1	37.7	2.4	34.3
3.25	1	26.2	27.3	69.8	1.1	42.5	2.6	38.6
3.50	1	26.2	27.3	70.0	1.1	42.7	2.6	38.8
3.75	1	26.2	27.1	64.2	* (.9)	37.1	2.4	* (41)
4.00	1	26.2	26.6	55.0	* (.4)	28.4	2.1	* (71)
4.25	1	26.2	26.5	50.0	* (.3)	23.5	1.9	* (78)
4.75	1	26.2	27.2	44.0	1.0	16.8	1.6	16.8
5.25	1	26.2	27.1	39.0	* (.9)	11.9	1.4	* (13)

* Unreliable for reasons stated earlier.

[ ] Maximum value.

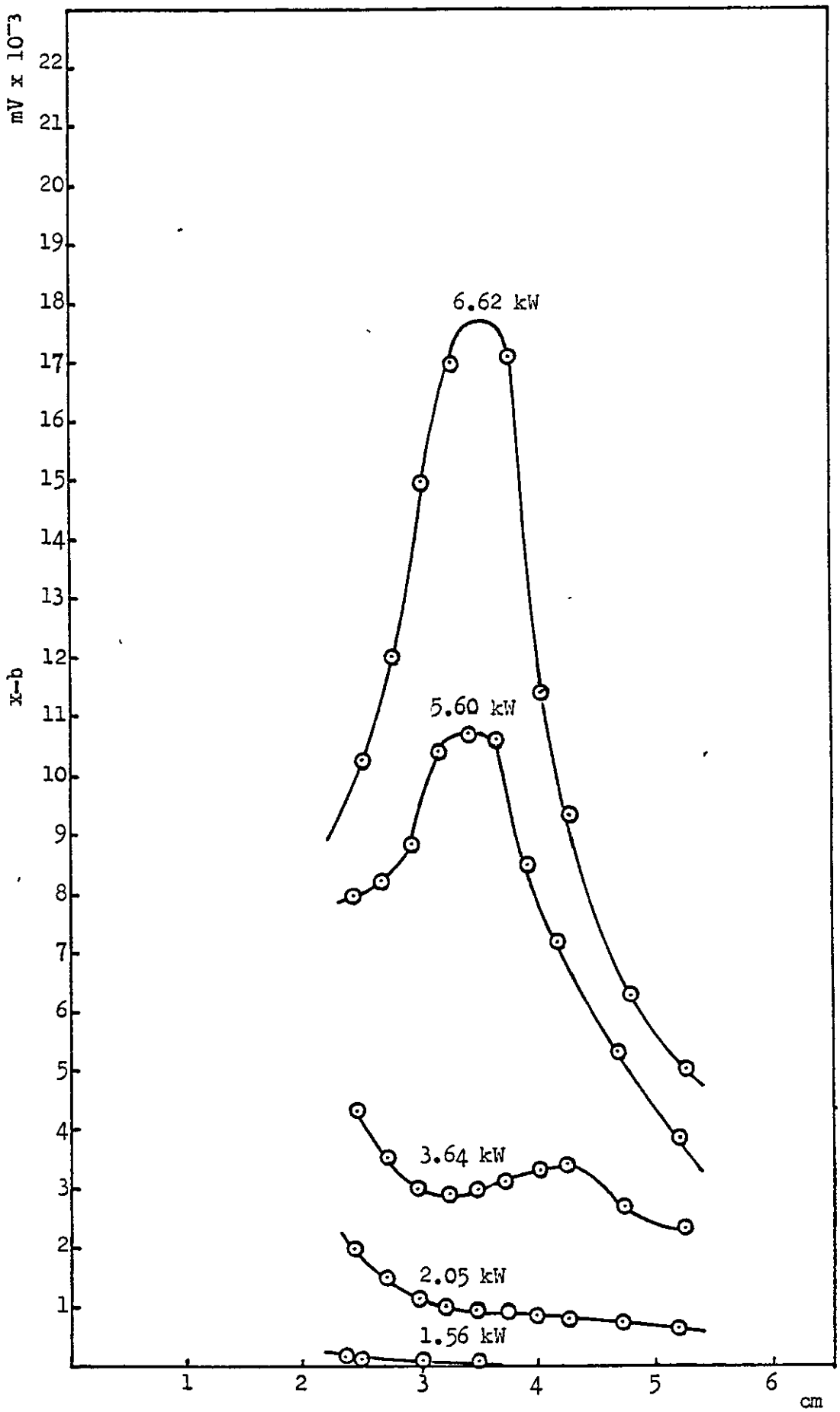

Fig. 58 Height/power/emission relationships. B 2497A° 1000 ppm. Plot of net signal, normalised to gain 11, versus height above the base of the plasma, at various powers.

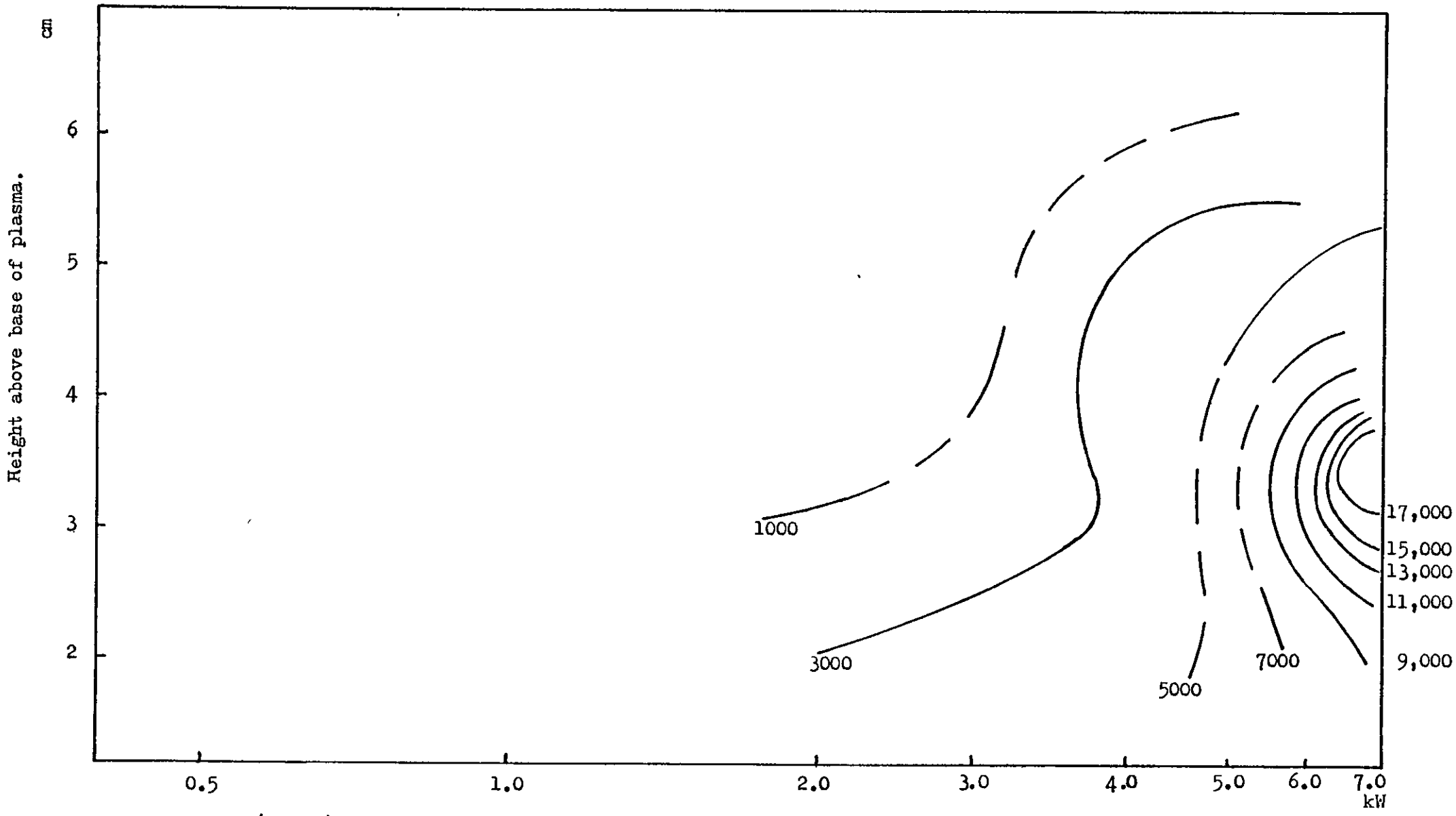

Fig. 59 Height/power/emission relationships. B 2497A° 1000 ppm. Contours of emission at intervals of 2000 mV.

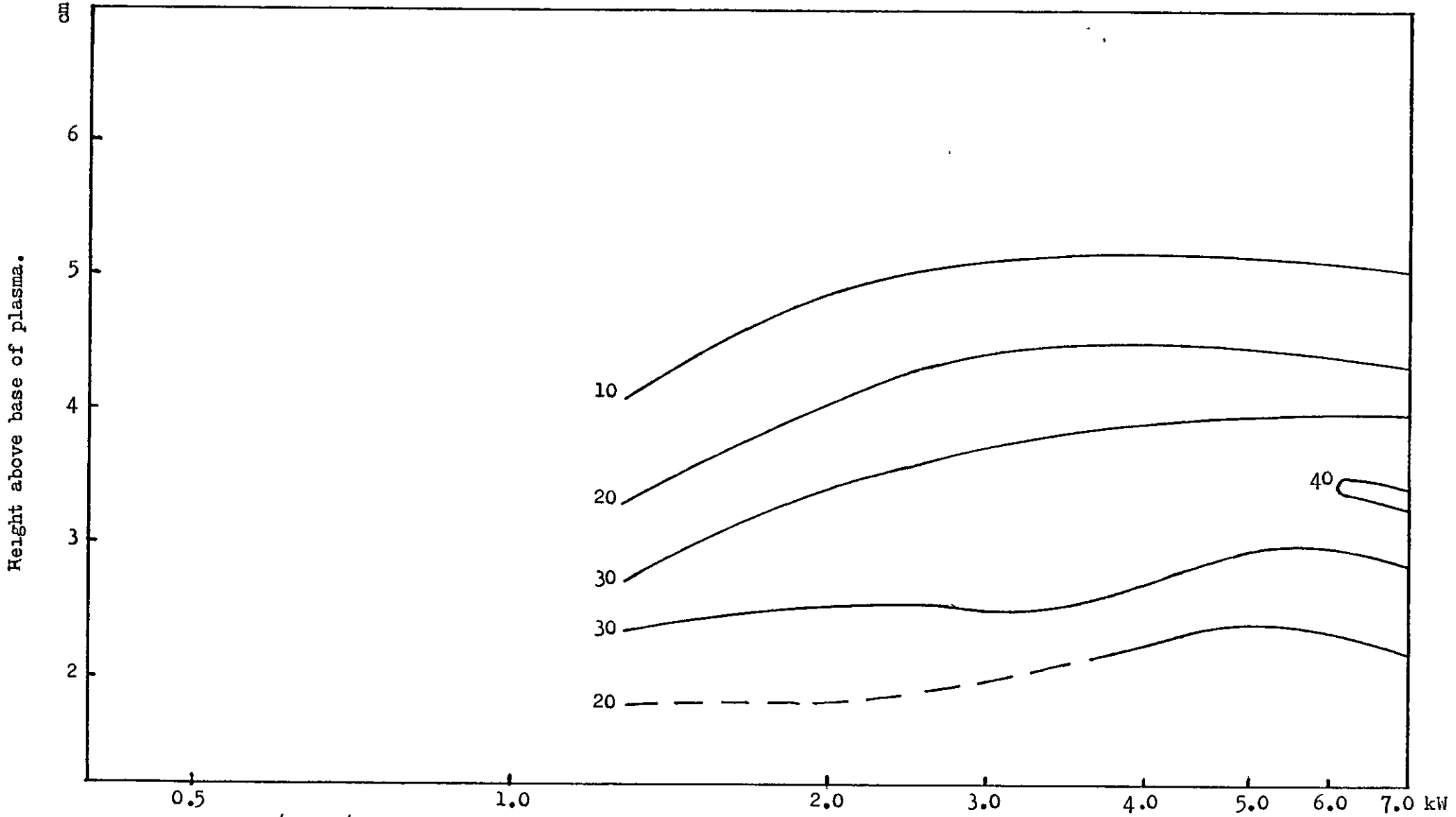

Fig. 60 Height/power/emission relationship, B 2497A° 1000 ppm. Contours of $\frac{x-b}{b-a}$ at intervals of 10 units.

The boron line examined has an excitation potential of 4.9 ev and is a neutral atom line with a norm temperature, uncorrected for partial pressure, of 10,500K. This might be expected to behave in a similar fashion to the zinc 3076Å line.

As with the zinc lines, the net signal, x - b for boron, increases with increasing power, normalised to constant gain, at all heights. It is difficult to make any comment about the ratio $\frac{x - b}{b - a}$, there are so many gaps in the readings, due to the inaccuracy involved, as to make any judgment unreliable. Nevertheless, Figs. 58-60 show the behaviour of the signals and the ratio $\frac{x - b}{b - a}$. The contour map of $\frac{x - b}{b - a}$ (Fig. 60) with height of observation and power as variables does indicate the possibility of a maximum at high powers.

Section 6.4. Integration Following Changes to the Measuring Set.

It was decided to repeat the boron experiment using integration to obtain more reliable figures for the differences between the dark current and background readings. Changes were first made to the Measuring Set (Section 2.8) to remove inaccuracies in timing exposures along with other faults.

The pre-exposure and exposure clock timers were replaced by a digital time system driven by a 1 MHz crystal oscillator giving a precision to the timing of 1 part in 10^5 or better. The valve system (see Fig.31) was replaced by a F.E.T. follower amplifer constructed as an impedance changer between the integrating capacitors of the Polychromator and the read-out unit. This is protected, as shown in Fig. 61, so that if a voltage in excess of approximately 20 volts is generated on the capacitors no damage

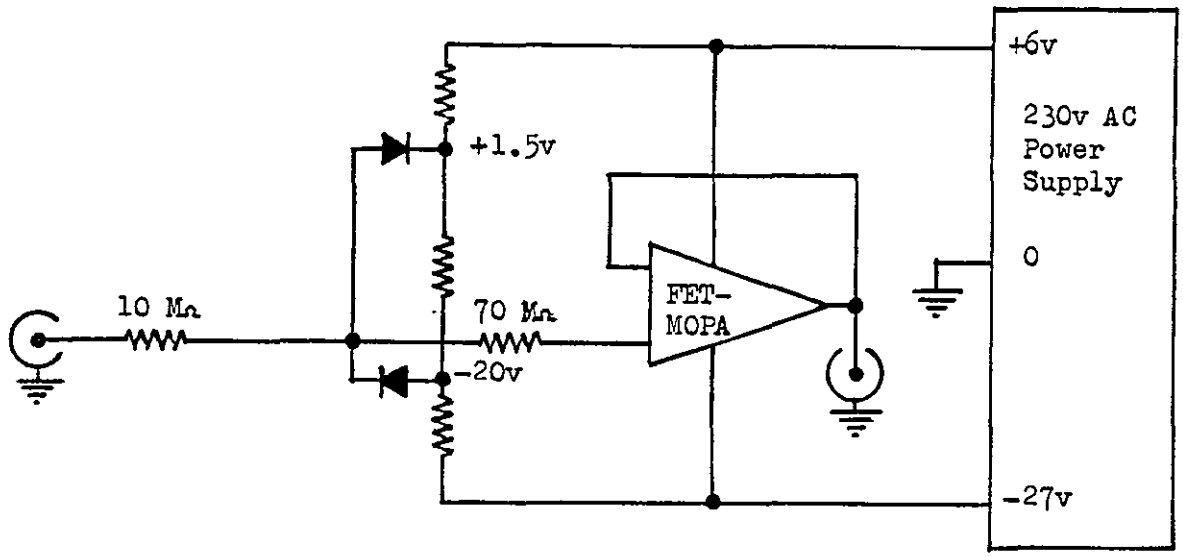

Low reverse current leakage type diodes
Input resistance ≏ 10^{10} ohms

Fig. 61. Solid state measuring set.

would ensue and as this is approximately the limit of linear charge any readings at this limit are arranged to give an "overload" condition.

The output from this unit is read by a digital panel meter. This meter is of the dual ramp integrating type with a B.C.D. output. Basically the meter is driven by a 2 MHz oscillator and charges an integrating capacitor from the unknown for a count of 40,000 cycles. This corresponds to 20 milliseconds so any 50 cycle pickup is averaged out. This capacitor is then discharged at a constant rate. A counter is started when the discharge is initiated and stops when the capacitor is discharged to zero. It is this figure which appears on the display. The input is attenuated to give a reading of 3.9999 just below the overload condition at approximately 20 volts. In the Profile position

(Section 2.9) the same amplifier is used but the D.P.M. is continuously monitoring the chosen channel. A moving coil voltmeter may be plugged into the amplifier output. As before the voltage is generated across a 1M ohm resistor by the P.M. anode current (Fig. 32. R701).

Section 6.4.1 Boron Results.

Using the equipment detailed in Section 6.4, the information obtained is tabulated in Tables 65-71 and in Figs. 62-64.

Whilst the results are similar to those obtained without integration (Section 6.3.3) there are important differences. The possibility of a high reading for x - b close to the base of the plasma is indicated and there are indications of two maxima. This is also suggested by the contour map of emission Fig. 63. The contour map of $\frac{x - b}{b - a}$, Fig. 64 demonstrates the existence of two peaks, the higher of the two occurring at powers of approximately 1.55 kW.

Table 65. Height/Power/Emission Relationships.

Boron 2497Å line. Integration with solid state Measuring Set.

SC 15 generator. Boron 1000 p.p.m. as

Power in plasma 0.75 kW. boric acid.

Top of cell (cm.) 2.24

Top of plasma (cm.) 0.96

Plasma gas flow (ℓ/min.) 5 Ar. Gain 6.

Nebuliser gas flow (ℓ/min.) 3.75 Ar. Pre-exposure 25 secs.

Coolant gas flow (ℓ/min.) 20.0 N_2. Exposure 80 secs.

Height cm.	a cts.	b cts.	x cts.	b - a cts.	x - b cts.	x/b.	$\frac{x-b}{b-a}$
1.54	24	64	2383	40	2319	37	58
1.80	24	85	3184	61	3099	37	51
2.30	24	76	2880	52	2804	38	53
2.80	24	43	1272	18	1229	30	65
3.30	24	32	447	8	415	14	52

Table 66. Height/Power/Emission Relationships.

Boron 2497Å line. Integration with solid state Measuring Set.

SC 15 generator.

Power in plasma 1.24 kW.

Top of cell (cm.) 2.34

Top of plasma (cm.) 1.14

All other conditions as in Table 65.

Height cm.	a cts.	b cts.	x cts.	b - a cts.	x - b cts.	x/b.	$\frac{x-b}{b-a}$
1.90	23	140	6082	117	5942	43	51
2.40	23	125	6533	102	6408	52	63
2.90	23	112	6059	89	5947	54	67
3.40	23	100	4830	77	4730	48	61
3.90	23	90	3276	67	3186	36	48

Table 67. Height/Power/Emission Relationships.

Boron 2497Å line. Integration with solid state Measuring Set.

SC 15 generator.

Power in plasma 1.55 kW.

Top of cell (cm.) 2.3

Top of plasma (cm.) 1.0

All other conditions as in Table 65.

Height cm.	a cts.	b cts.	x cts.	b - a cts.	x - b cts.	x/b.	$\frac{x-b}{b-a}$
1.85	25	214	6939	189	6725	32	36
2.36	25	190	7579	169	7389	40	45
2.86	25	168	7691	143	7523	46	53
3.36	25	146	7781	121	7635	53	63
3.86	25	125	7566	100	7441	61	74
4.36	25	106	6130	81	6024	58	74
4.86	25	87	3764	52	3677	43	71
5.36	25	69	2699	44	2630	39	60

☐ Maximum values.

Table 68. Height/Power/Emission Relationships.

Boron 2497Å line. Integration with solid state Measuring Set.

RD 150 generator. Boron 1000 p.p.m. as

Power in plasma 1.62 kW. boric acid.

Top of cell (cm.) 2.27

Top of plasma (cm.) 1.24

Plasma gas flow (ℓ/min.) 12 Ar. Gain 6.

Nebuliser gas flow (ℓ/min.) 4.85 Ar. Pre-exposure 25 secs.

Coolant gas flow (ℓ/min.) 21.0 N_2 Exposure 80 secs.

Height cm.	a cts.	b cts.	x cts.	b - a cts.	x - b cts.	x/b.	$\frac{x-b}{b-a}$
2.39	15	552	18002	537	17450	33	32
2.89	15	284	11351	269	11067	40	41
3.39	15	160	6227	145	6067	39	42
3.89	15	104	2349	89	2245	23	25
4.39	15	52	676	37	624	13	17

Table 69. Height/Power/Emission Relationships.

Boron 2497Å line. Integration with solid state Measuring Set.

RD 150 generator.

Power in plasma 2.23 kW.

Top of cell (cm.) 2.27

Top of plasma (cm.) 1.28

All other conditions as in Table 68.

Height cm.	a cts.	b cts.	x cts.	b - a cts.	x - b cts.	x/b.	$\frac{x-b}{b-a}$
2.39	15	3385	48400	3385	45000	14	13
2.89	15	2810	39655	2810	36830	14	13
3.39	15	1990	31005	1990	29000	16	15
3.89	15	1390	23665	1390	22260	17	16
4.39	15	950	16095	950	15130	17	16
4.89	15	490	9655	490	9150	20	19
5.39	15	250	4975	250	4710	20	19
5.89	15	132	2347	132	2200	18	17
6.39	15	59	864	59	790	15	13

Table 70. Height/Power/Emission Relationships.

Boron 2497Å line. Integration with solid state Measuring Set.

RD 150 generator.

Power in plasma 3.02 kW.

Top of cell (cm.) 2.3

Top of plasma (cm.) 1.34 Exposure 20 secs.

All other conditions as in Table 68.

Smoothed graphically and normalised to 80 seconds exposure.

Height cm.	a cts.	b cts.	x cts.	b - a cts.	x - b cts.	x/b.	$\frac{x-b}{b-a}$
2.42	15	4847	120787	4832	115940	25	24
2.92	15	2575	82670	2560	80095	32	31
3.42	15	2207	72679	2192	70472	33	32
3.92	15	1991	65591	1976	63600	33	32
4.42	15	1791	58987	1776	57196	33	32
4.92	15	1615	53455	1600	51840	33	32
5.42	15	1475	47635	1460	46160	32	32
5.92	15	1355	39895	1340	38540	29	29

Table 71. Height/Power/Emission Relationships.

Boron 2497Å line. Integration with solid state Measuring Set.

RD 150 generator.

Power in plasma 4.13 kW.

Top of cell (cm.) 2.27

Top of plasma (cm.) 1.92 Exposure 10 secs.

All other conditions as in Table 68.

Smoothed graphically and normalised to 80 seconds exposure.

Height cm.	a cts.	b cts.	x cts.	b - a cts.	x - b cts.	x/b.	$\frac{x-b}{b-a}$
2.39	15	13007	216047	12992	203040	17	16
2.89	15	8079	155279	8064	147200	19	18
3.39	15	5607	124007	5992	118400	22	20
3.89	15	5055	112655	5040	107600	22	21
4.39	15	4935	108535	4920	103600	22	21
4.89	15	4975	107775	4960	102800	22	21
5.39	15	5095	111495	5080	106400	22	21
5.89	15	5295	116495	5280	111200	22	21
6.39	15	5455	117455	5440	112000	22	21
6.89	15	5535	117535	5520	112000	21	20
7.19	15	5495	116295	5480	110800	21	20

☐ Maximum value.

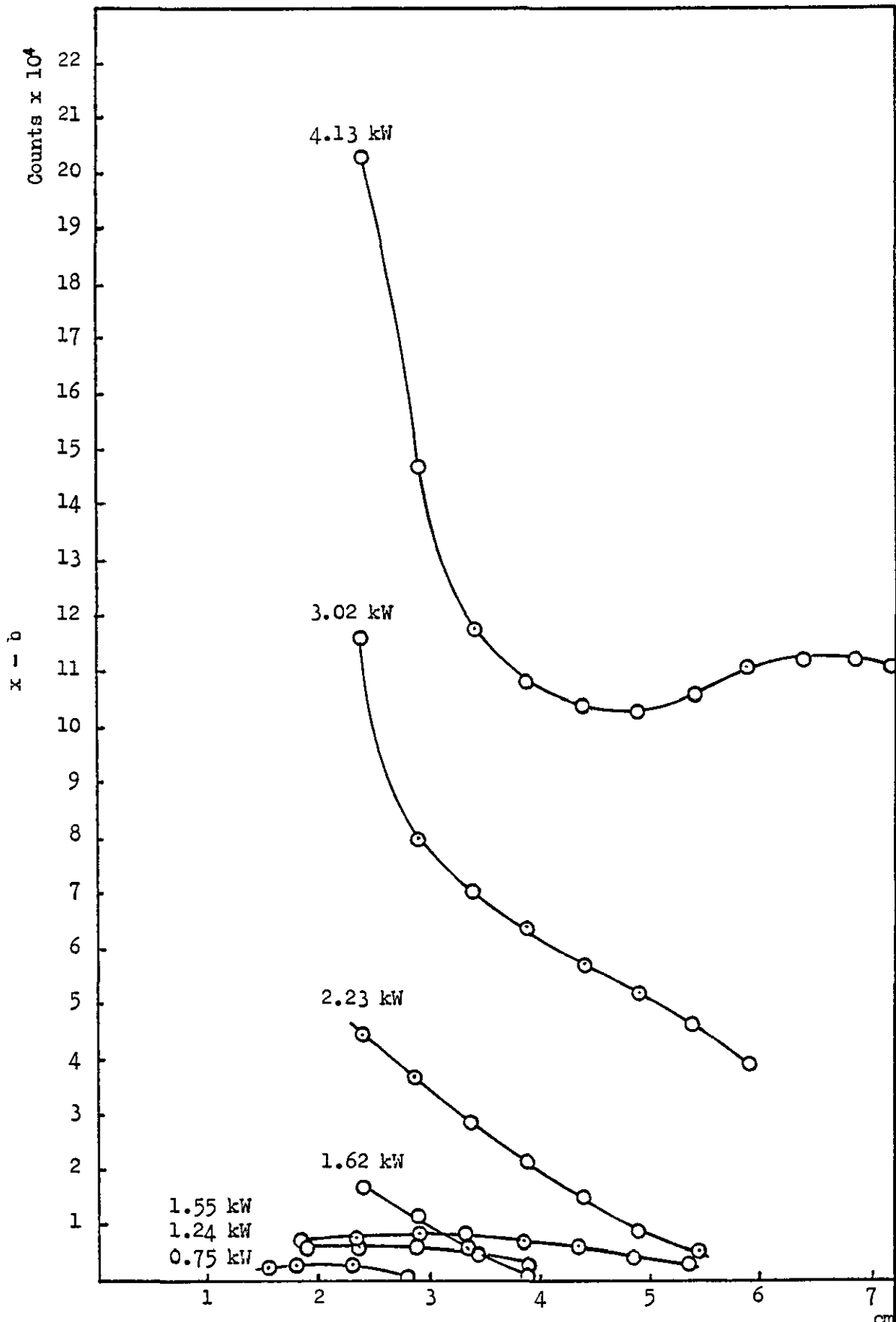

Fig. 62. Height/power/emission relationships. B 2497 A° 1000 ppm. Plot of net signal, normalised to an exposure of 80 secs. at constant gain, versus height above the base of the plasma, at various powers.

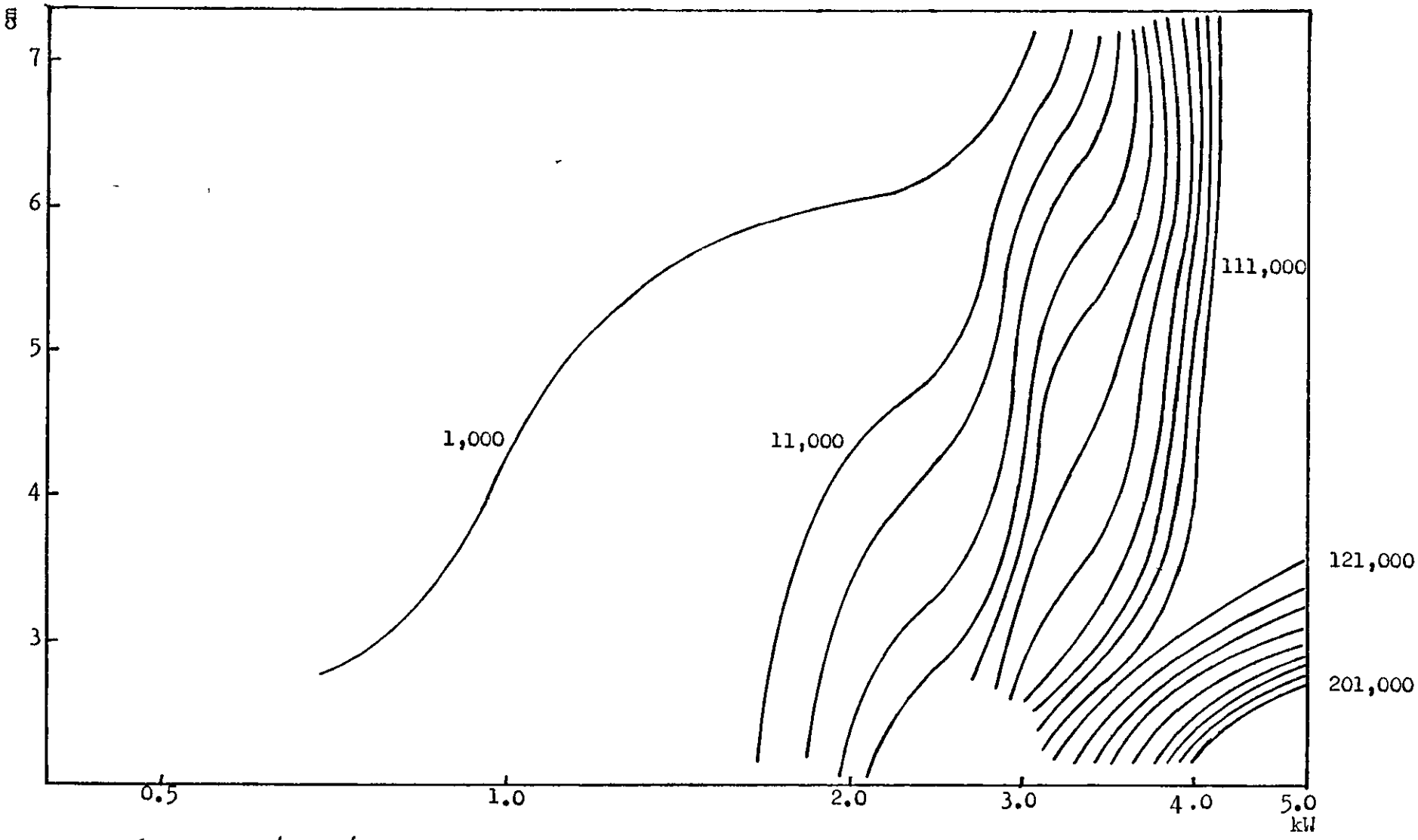

Fig. 63. Height/power/emission relationships. B 2497A° 1000 ppm. Contours of emission at intervals of 10,000 counts.

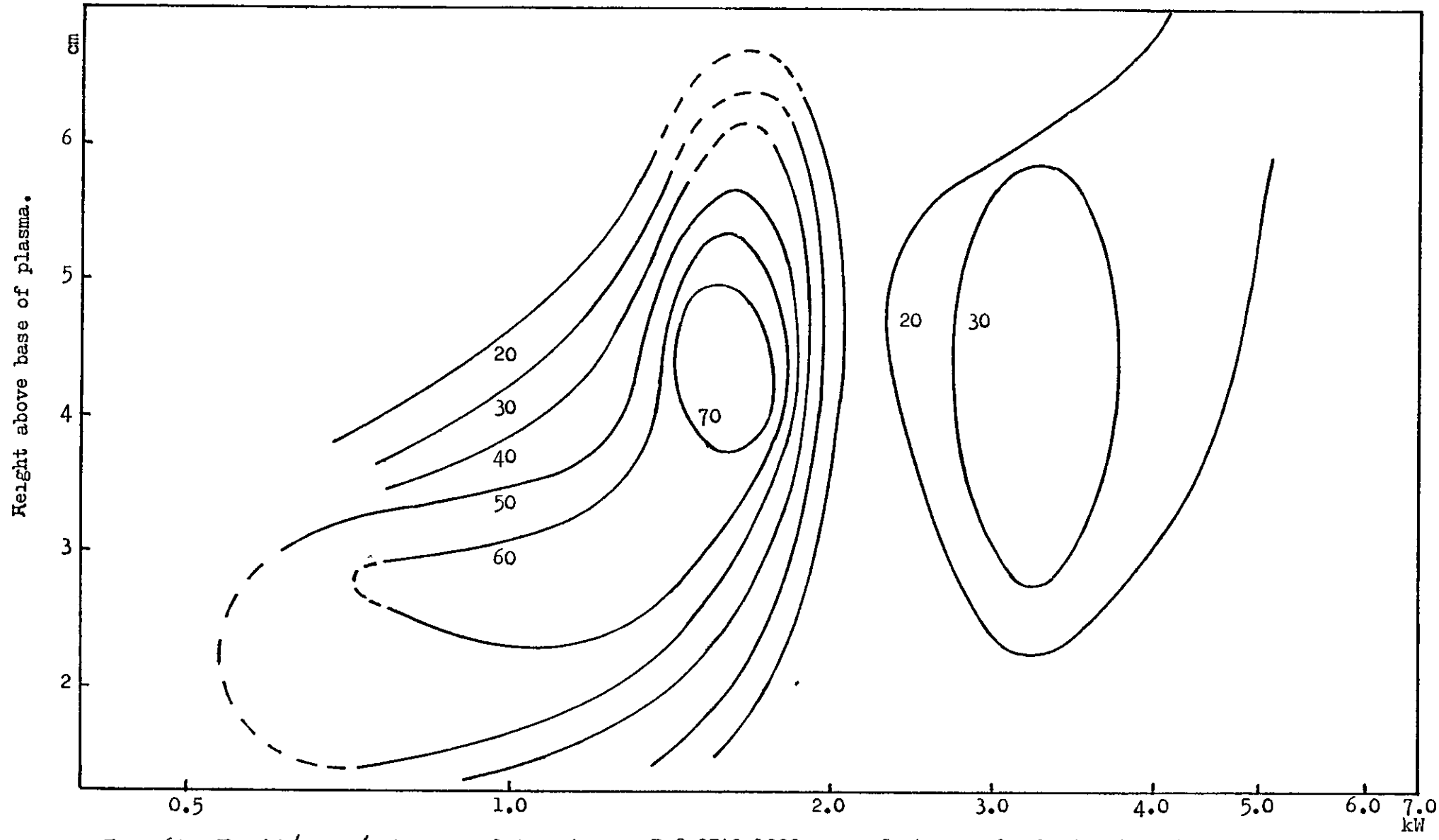

Fig. 64. Height/power/emission relationships. B 2497A° 1000 ppm. Contours of $\frac{x-b}{b-a}$ at intervals of 10 units.

Section 6.5 Observations.

Improvements to the measuring system have not resulted in an ability to measure. with sufficient accuracy. the small differences between the dark current and the background signals. Integration, whilst giving the required accuracy, is time consuming (an estimated 5 hours of continuous measurement time to complete the work reported in Section 6.4.1), which means that drifts in optical alignment could have occurred and thus have affected the overall picture of what was happening. For this and other reasons, which will be discussed in Chapter 8, it was felt that a different approach to the problem was necessary. Nevertheless, certain observations can be made and conclusions drawn. on the work so far completed with the elements sodium, zinc and boron, or more specifically the lines Na 5890Å, Zn 3072Å, Zn 3076Å and B 2497Å.

a) At constant power and at heights between 2 to 6.5 cm. above the base of the plasma, maxima occur for the net signal x - b with every suggestion that maxima might occur much closer to the base of the plasma. There is also evidence for the existence of two sets of maxima, one closer to the base of the plasma than the other.

b) The length of the plasma increases with power and it appears that the height where the maxima for x - b occurs may move nearer to the tip of the plasma and may actually move into the plasma.

c) There is some suggestion that the norm temperature has been reached in the case of sodium since at constant height above the base of the plasma x - b goes through a maximum as power is increased. What is difficult to understand is that if the norm temperature has been reached it might be expected that these maxima would have the same value which they did not.
The explanation may lie in different quantities of analyte in the tail-flame through turbulence, gas-flow or whatever, causing changes in partial pressure.

d) There is evidence that more than one maximum for $\frac{x - b}{b - a}$ may occur in any system which may explain the reason for some of the conflicting reports of the role of power which appeared in the literature.

CHAPTER 7.

HEAT TRANSFER FROM THE PLASMA TO THE ANALYTE.

One curious feature of the work described in the preceding chapter was the movement of the optimum viewing height, for maximum net signal, nearer to the plasma as the power in the plasma was increased (Section 6.5.a). It might be thought that raising the power in the plasma i.e. raising its temperature, would cause this optimum position to move further away from the plasma. The following model, an extension of earlier work [68] is suggested as an explanation of this phenomenon.

Section 7.1 A Model of the Plasma.

In the annular configuration of the plasma, the gas stream carrying the sample atoms flows through a central cooler tunnel that is surrounded by the very hot fireball region where the applied power is dissipated. When this gas flow emerges from the tunnel, it forms a well defined and narrow tail flame. Because of its small radius, the emission of the analyte atoms per unit surface is high, and this effect contributes to the sensitivity.

The sample atoms in the central tunnel are heated by radiation and by conduction from the fireball and the system is analogous to a tube furnace but without reactivity at the wall. Consider a very simple model (Fig. 65) in which the walls of the tunnel are at a constant temperature, T_o, for the length of the fireball and that beyond this length the temperature decreases exponentially with height. Assume that the sample atoms at a given height are all at the same temperature, T, which is the result of heating at a rate proportional to the difference between this temperature and the temperature of the

68) S.Greenfield, Proc. Analyt. Div. Chem. Soc., 1976, 13, 280.

surrounding tunnel. This results in an exponential increase in temperature with distance along the tunnel. Beyond the end of the tunnel, the plasma gases will cool exponentially while the temperature of the sample atoms continues to increase at a reduced rate, since the temperature difference is decreasing sharply. When the temperature of the sample atoms reaches that of the plasma gases, it too will decrease exponentially. Then, the greater the length of the plasma the greater is the maximum temperature of the sample atoms and the closer to the plasma is the position of the temperature maximum. Variation of the plasma temperature, T_o, at least on this model, simply makes a proportional variation in the sample temperature at all heights. It does not alter the position of the maximum temperature, only its value.

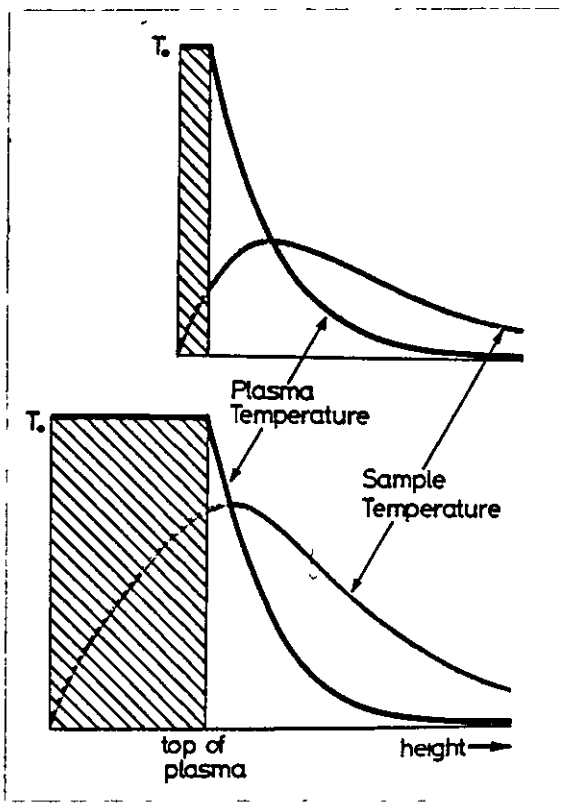

Fig. 65. Model for Sample Heating. The longer the plasma, the higher is the temperature attained by the sample and the closer to the top of the plasma does the maximum atom temperature occur.

An increase in power that causes an increase in the temperature and size of the plasma will result in an increase in the temperature of the sample atoms owing to both effects and a movement of the position of maximum temperature nearer the fireball.

This model is consistent with the experimental observations of Chapter 6, and as will be seen, is supported by calculated temperatures for the analyte stream at various heights being in agreement with measured temperatures in the tail-flame.

Section 7.2. Temperature Measurements.

The plane mirror which is used to reflect the radiation from the source onto the grating of the F.A.19 Polychromator (Section 2.5) can be rotated via a micrometer screw allowing a scan of some 30 angstroms either side of the normal wavelength of a channel line. By connecting this screw to a small driver motor it was possible to scan over several lines near to a chosen channel line. Thus it was possible to scan over the two zinc lines of wavelengths 3072.06Å and 3075.90Å using a common photomultiplier. These two lines are an almost ideal line pair for temperature determination by measurement of the ratio of the line intensities [69]. The excitation potentials for these lines of 8.08 and 4.01 e.v. respectively, differ widely, whereas the difference in wavelength is very small. Zinc has an ionisation potential of 9.39 e.v. Using the equation [69]

$$\frac{dT}{T} = \frac{T}{5040(V_a - V_b)} \cdot 0.434 \frac{dI}{I} \qquad \text{------ 116}$$

where V_a, V_b = excitation potentials and I = ratio of intensities, an estimate of the R.S.D. for T is in the range 0.5 - 1.5% for a corresponding R.S.D. intensity ratio of 5 - 10% and a temperature range

69) P.W.J.M.Boumans, "Theory of Spectrochemical Excitation", Hilger & Watts, 1966, 106-110.

of 5000-7000 K. Values of gA (the statistical weight times the transition probability) are well established and agreement is good. The temperature is given by the equation [69]

$$T = \frac{20510}{2.580 + \log_{10} \frac{(I\ 3076)}{(I\ 3072)}} \qquad \text{------- 117}$$

Section 7.2.1 Values of Temperature Obtained.

Using a zinc nitrate solution of 1.5% wt./vol. concentration, height/power/temperature relationships were obtained. These are tabulated in Tables 72-78 and shown graphically in Figs. 66 and 67. Where the OH background made a significant contribution it was subtracted.

It can be seen by reference to these figures that there is a maximum temperature in the tail-flame which tends to be closer to the end of the plasma the higher the power. Furthermore, as suggested, after reaching this maximum temperature the temperature of the analyte decreases exponentially, as shown by the fit of the data to the curve $y = ae^{bx}$ which has been used to extrapolate the line by substituting the measured values in the equation. Fig. 68 is a contour map of temperature versus power and height.

So far the experimental facts seem to fit the model fairly well, if only qualitatively. However, on the same graphs of temperature (Figs. 66-67) are given calculated values for the temperatures in the tunnel itself. How these were derived is explained in Section 7.3.

Table 72. Height/Power/Temperature Relationships.

S.C.15 generator.
Power in plasma 0.80 kW.
Top of cell (cm.) 2.32
Top of plasma (cm.) 0.70
Plasma gas flow (ℓ/min.) 6.0
Injector gas flow (ℓ/min.) 2.6
Coolant gas flow (ℓ/min.) 20
a = 26.3

Height cm.	Gain.	I^{x}_{3076} m.v.	I^{b}_{3076} m.v.	I^{x}_{3072} m.v.	I^{b}_{3072} m.v.	$\frac{I^{x-b}_{3076}}{I^{x-b}_{3072}}$	T°K
2.42	6	45.5	27.3	28.2	27.5	36.4	4952
2.56	6	39.4	27.0	27.0	26.8	62	4690

Table 73. Height/Power/Temperature Relationships.

S.C.15 generator.
Power in plasma 1.25 kW.
Top of cell (cm.) 2.38
Top of plasma (cm.) 0.60
Plasma gas flow (ℓ/min.) 6.0
Injector gas flow (ℓ/min.) 2.6
Coolant gas flow (ℓ/min.) 20
a = 26.7

Height cm.	Gain.	I^{x}_{3076} m.v.	I^{b}_{3076} m.v.	I^{x}_{3072} m.v.	I^{b}_{3072} m.v.	$\frac{I^{x-b}_{3076}}{I^{x-b}_{3072}}$	T°K
2.420	5	70.5	28.0	29.7	27.9	23.611	5188
2.560	5	56.6	27.3	28.0	27.2	36.625	4950

Table 74. Height/Power/Temperature Relationships.

S.C.15 generator.

Power in plasma 1.67 kW.

Top of cell (cm.) 2.42

Top of plasma (cm.) 1.02

Plasma gas flow (ℓ/min.) 6.0

Injector gas flow (ℓ/min.) 2.6

Coolant gas flow (ℓ/min.) 20

a = 25.9

Height cm.	Gain.	I^{x}_{3076} m.v.	I^{b}_{3076} m.v.	I^{x}_{3072} m.v.	I^{b}_{3072} m.v.	$\frac{I^{x-b}_{3076}}{I^{x-b}_{3072}}$	T°K
2.420	4	93.0	28.4	33.2	28.0	12.423	5582
2.56	4	89.0	27.9	31.2	27.0	14.548	5480
3.06	4	72.5	26.7	28.4	26.2	20.818	5261
3.56	4	57.8	26.3	27.0	26.0	31.50	5029
4.06	4	50.0	26.1	26.4	25.9	52.20	4772

Table 75. Height/Power/Temperature Relationships.

R.D. 150 generator.

Power in plasma 2.03 kW.

Top of cell (cm.) 2.22

Top of plasma (cm.) 2.38

Plasma gas flow (ℓ/min.) 13.0

Injector gas flow (ℓ/min.) 4.8

Coolant gas flow (ℓ/min.) 35.0

a = 31.8

Height cm.	Gain.	I^{x}_{3076} m.v.	I^{b}_{3076} m.v.	I^{x}_{3072} m.v.	I^{b}_{3072} m.v.	$\frac{I^{x-b}_{3076}}{I^{x-b}_{3072}}$	T°K
2.45	1	59.9	33.4	36.6	33.2	7.794	5908
2.70	1	54.2	33.1	35.6	33.2	8.792	5820
2.95	1	53.3	33.0	35.0	32.8	9.227	5786
3.20	1	53.0	33.2	35.0	32.8	9.00	5803
3.70	1	51.1	32.5	34.5	32.6	9.789	5743
4.20	1	52.5	32.5	33.9	32.5	14.286	5491
4.70	1	52.5	32.6	33.4	32.5	22.111	5226
5.20	1	50.1	32.0	33.0	32.3	25.86	5137

Table 76. Height/Power/Temperature Relationships.

R.D.150 generator.

Power in plasma 3.57 kW.

Top of cell (cm.) 2.24

Top of plasma (cm.) 2.67

Plasma gas flow (ℓ/min.) 13

Injector gas flow (ℓ/min.) 4.8

Coolant gas flow (ℓ/min.) 35

a = 28.4

Height cm.	Gain.	I^{x}_{3076} m.v.	I^{b}_{3076} m.v.	I^{x}_{3072} m.v.	I^{b}_{3072} m.v.	$\frac{I^{x-b}_{3076}}{I^{x-b}_{3072}}$	T°K
2.45	1	58.0	30.3	37.0	30.6	4.328	6377
2.70	1	56.0	30.2	35.8	30.0	4.448	6353
2.95	1	52.2	29.8	35.1	30.0	4.392	6394
3.20	1	50.0	29.6	35.0	29.9	4.000	6446
3.70	1	50.3	29.7	34.7	29.8	4.204	6402
3.95	1	50.5	29.5	34.0	29.8	5.000	6255
4.20	1	49.1	30.0	33.1	29.8	5.788	6136
4.75	1	46.2	29.5	32.0	29.5	6.680	6024

Table 77. Height/Power/Temperature Relationships.

R.D.150 generator.

Power in plasma 5.56 kW.

Top of cell (cm.) 2.20

Top of plasma (cm.) 3.03

Plasma gas flow (ℓ/min.) 13

Injector gas flow (ℓ/min.) 4.8

Coolant gas flow (ℓ/min.) 35

a = 30.1

Height cm.	Gain.	I^{x}_{3076} m.v.	I^{b}_{3076} m.v.	I^{x}_{3072} m.v.	I^{b}_{3072} m.v.	$\frac{I^{x-b}_{3076}}{I^{x-b}_{3072}}$	T°K
2.45	1	73.7	38.6	48.8	38.5	3.408	6590
2.70	1	72.0	35.6	47.4	35.5	3.059	6690
2.95	1	73.6	34.8	48.4	34.4	2.771	6785
3.20	1	75.6	33.6	50.0	33.5	2.545	6869
3.45	1	75.6	33.3	51.1	33.1	2.35	6950
3.70	1	74.3	32.9	51.0	33.2	2.326	6961
3.95	1	68.8	32.6	48.0	32.6	2.350	6950
4.20	1	66.9	32.6	45.5	32.4	2.618	6841
4.75	1	60.1	32.6	41.1	32.5	3.198	6649
5.20	1	56.0	33.0	38.7	32.3	3.594	6541

Table 78. Height/Power/Temperature Relationships.

R.D.150 generator.

Power in plasma 6.73 kW.

Top of cell (cm.) 2.22

Top of plasma (cm.) 3.57

Plasma gas flow (ℓ/min.) 13

Injector gas flow (ℓ/min.) 4.8

Coolant gas flow (ℓ/min.) 35

a = 32.8

Height cm.	I^{x}_{3076} m.v.	I^{b}_{3076} m.v.	I^{x}_{3072} m.v.	I^{b}_{3072} m.v.	$\frac{I^{x-b}_{3076}}{I^{x-b}_{3072}}$	T°K
2.45	79.5	47.0	63.0	45.0	1.806	7230
2.70	91.1	37.8	60.5	39.2	2.502	6887
2.95	94.2	36.9	63.8	37.5	2.179	7028
3.20	94.1	36.0	66.9	35.9	1.874	7190
3.45	90.8	35.0	70.5	35.4	1.590	7374
3.70	85.8	35.3	70.1	35.0	1.439	7491
3.95	73.8	35.5	62.0	34.8	1.408	7517
4.20	71.0	34.4	54.5	35.1	1.887	7182
4.75	63.9	34.3	47.5	34.5	2.277	6982
5.20	62.3	34.2	43.4	33.7	2.897	6742

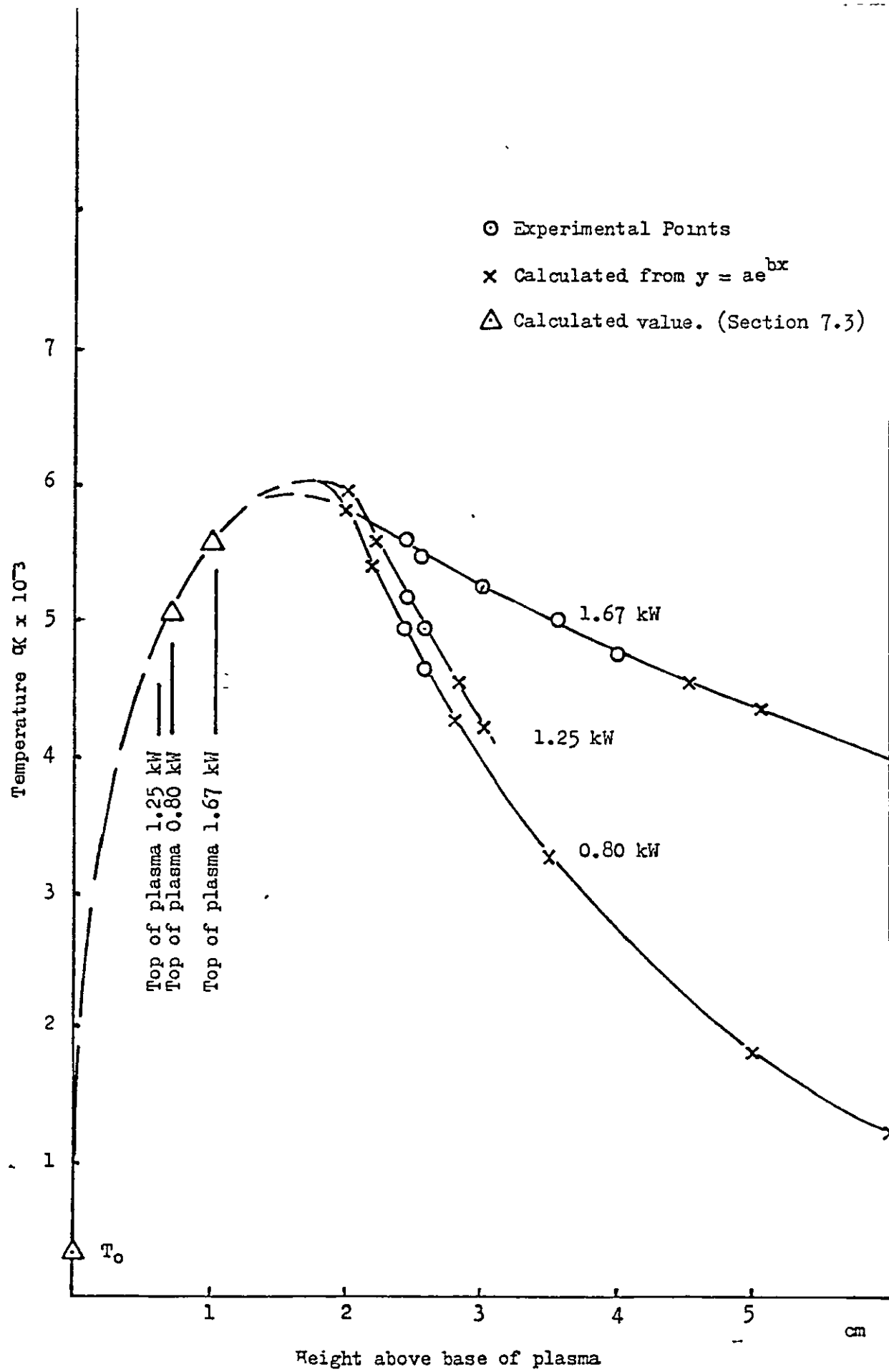

Fig. 66. Height/power/temperature relationships. Plot of measured and calculated temperatures versus height above the base of the plasma, at various powers. S.C. 15 Generator.

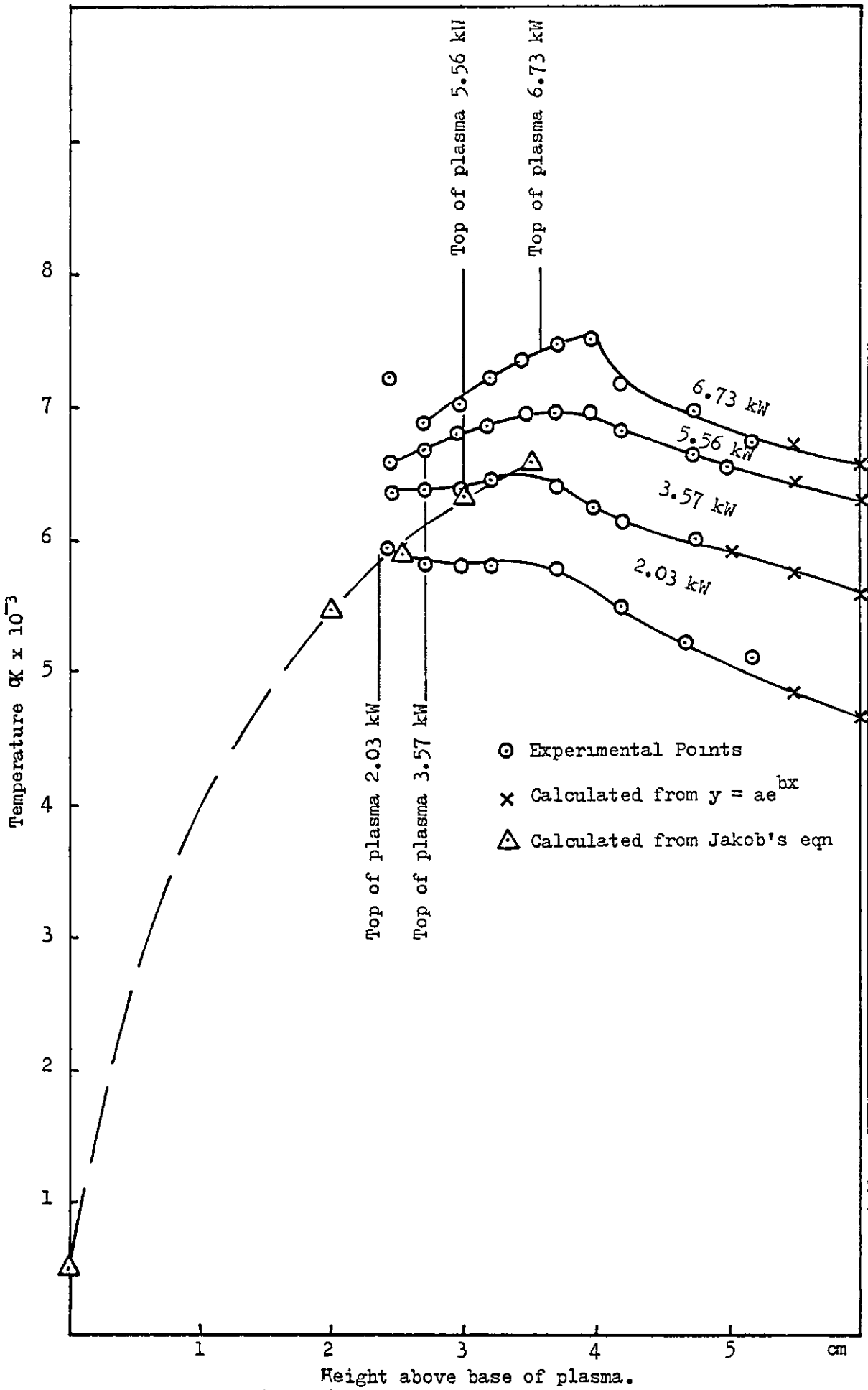

Fig. 67. Height/power/temperature relationships. Plot of measured and calculated temperatures versus height above the base of the plasma at various powers. RD 150 Generator.

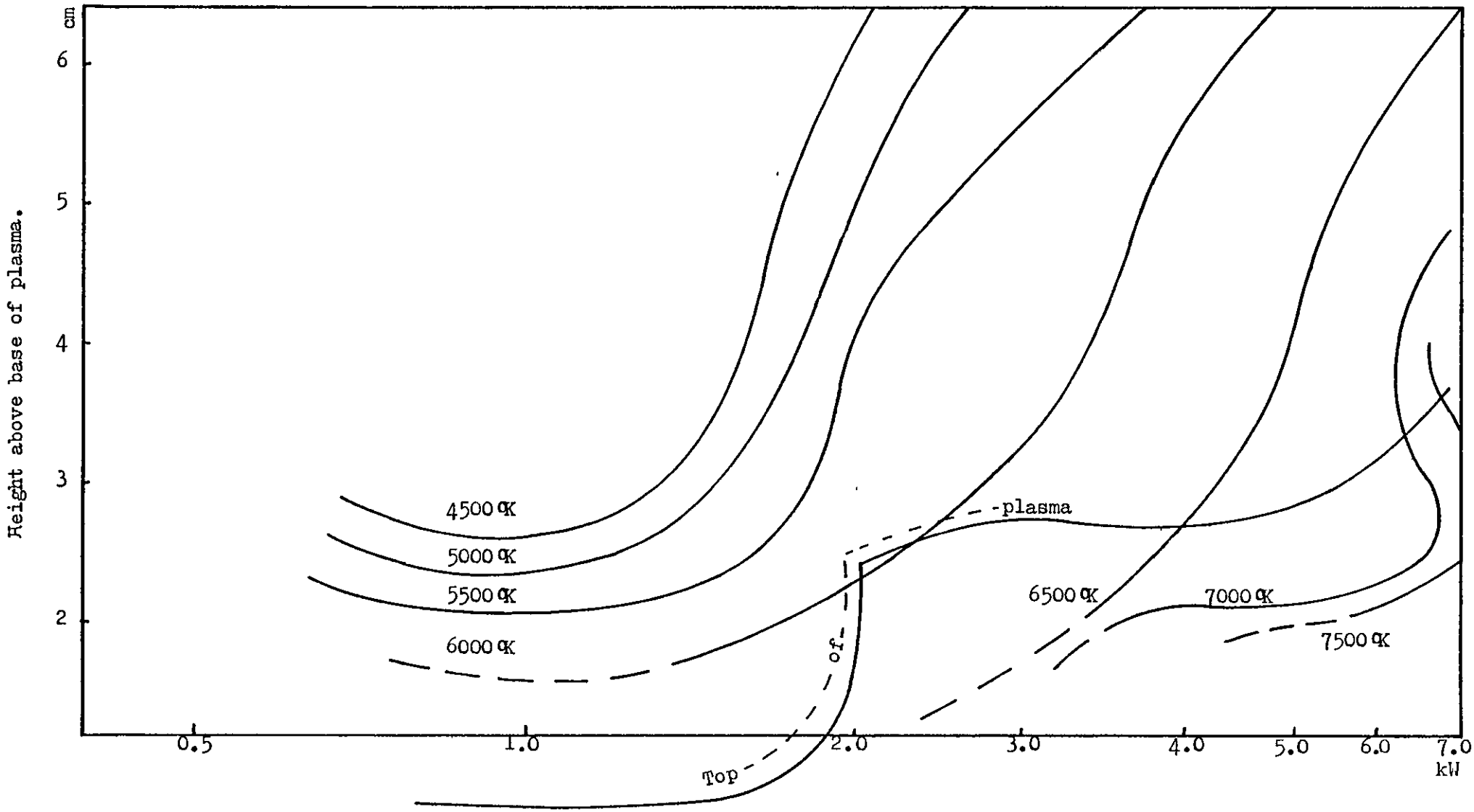

Fig. 68. Height/power/temperature relationships. Contours of temperature at intervals of 500 °K.

Section 7.3 Heat Transfer.

The problem of heat transfer by convection, to a gas flowing through a tube was first considered by Graetz[70] and a convenient exposition has been given by Jakob[71]. The problem has been solved, by Graetz, only by neglecting the variations of the thermal properties of the fluid, through using mean values.

The quantities which are relevant to the emission of spectral lines are the temperature distribution and the straightforward mean temperature as a function of distance along the tunnel. A frequently quoted empirical approximation applies to what is known as the "cup mixing temperature" [72]. This is the temperature which would be obtained if the fluid flowing through the tube were collected in a cup and mixed. Because the velocity of the fluid is not constant over the cross-section of the tube, the cup-mixing temperature has to take this into account; there is a greater contribution from the centre of the tube, where the velocity is high, than from near the wall, where the velocity is low. For problems of heat transfer, the cup-mixing temperature is the appropriate mean to use; for the purposes of the present work, however, where the emission is related to temperature and the heat transferred from the plasma by the injector flow is of little importance, the ordinary arithmetic mean temperature is the quantity of interest. The simpler empirical relation is thus not relevant here but has been discussed because it misled this author for a time.

70) L. Graetz, Ann. Phys., 1885, 25, 337.

71) M. Jakob, "Heat Transfer", Vol.1, Wiley, New York, 1949., 451-464.

72) A. J. Ede "An Introduction to Heat Transfer" Pergamon Press 1967.

The appropriate solution is Jakob's [71] equation 22-45.

$$\theta/\theta_o = 1.477e^{-m_o x}R_o - 0.810e^{-m_1 x}R_1 + 0.385e^{-m_2 x}R_2 \quad ------ \quad 118$$

Jakob [71] has tabulated values of R_o, R_1 and R_2 as functions of the fractional radial coordinate r/s (s being the radius of the tube) and these are given in Table 79. x is the distance along the tube.

Table 79. Values of R_o, R_1 and R_2 for Various Values of $^r/_s$.

$^r/_s$	R_o	R_1	R_2
0	1	1	1
0.2	0.929	0.607	0.206
0.4	0.738	-0.106	-0.407
0.6	0.483	-0.432	0.104
0.8	0.224	-0.305	0.278
1.0	0	0	0

m_o, m_1 and m_2 are given by :-

$$m_o = 11.5 \text{ k/cw.}$$

$$m_1 = 69.7 \text{ k/cw.}$$

$$m_2 = 166.6 \text{ k/cw.}$$

where k is the thermal conductivity of the fluid (watt. cm^{-1}. deg^{-1}), c its specific heat (J.g^{-1}. deg^{-1}) at constant pressure, and w the mass flow (g. sec^{-1}) of the fluid.

θ is the difference between the temperature T_s of the tunnel wall (assumed constant) and the temperature T at radius r and distance x along the tunnel. θ_o is the value at x = o.

Thus if the variable is changed to temperature rather than temperature difference, and we define M = kx/cw we have

$$\frac{T - T_s}{T_o - T_s} = 1.477\, R_o e^{-11.5M} - 0.81\, R_1 e^{-69.7M} + 0.385 R_2 e^{-166.6M} \quad ---- \quad 119$$

Note that M, involving thermal conductivity and specific heat is a function of temperature, so that the straightforward approach of solving for T cannot be adopted.

To avoid this problem the following procedure was used. The expression on the right hand side of equation 119, is plotted (Fig. 69) as a function of M for a series of values of $^{r}/_{s}$, which determine the factors R_o, R_1 and R_2.

Values are chosen for the tunnel temperature T_s, the inlet gas temperature T_o and the desired temperature T, so that the left hand side of equation 119 can be determined.

For the given values of $^{r}/_{s}$, the values of M satisfying equation 119 can be obtained from the intersections of the curves of Fig. 69 with the appropriate horizontal straight line. From such values of M, x/w can be evaluated if values of k/c are known. Such values depend on temperature and here the mean temperature $\frac{1}{2}(T_o + T)$ is used.

Values of k/c are obtained by consideration of the Prandtl number, defined as $\mu c/k$ where μ is the viscosity. The Prandtl number [73], for a perfect monatomic gas, is independent of temperature and has the value $^{2}/_{3}$. This has been confirmed for argon over a moderate range of temperatures [73]. Thus k/c can be evaluated from $3\mu/2$.

The dependance of viscosity on temperature has been well approximated [74] by

$$\mu = \mu_o \left(\frac{T}{273}\right)^{0.82}$$

73) R.C.Reid and T.K.Sherwood "The Properties of Gases and Liquids", 2nd Ed., McGraw-Hill, 1966.

74) J.Jeans, "Kinetic Theory of Gases", Cambridge, 1940.

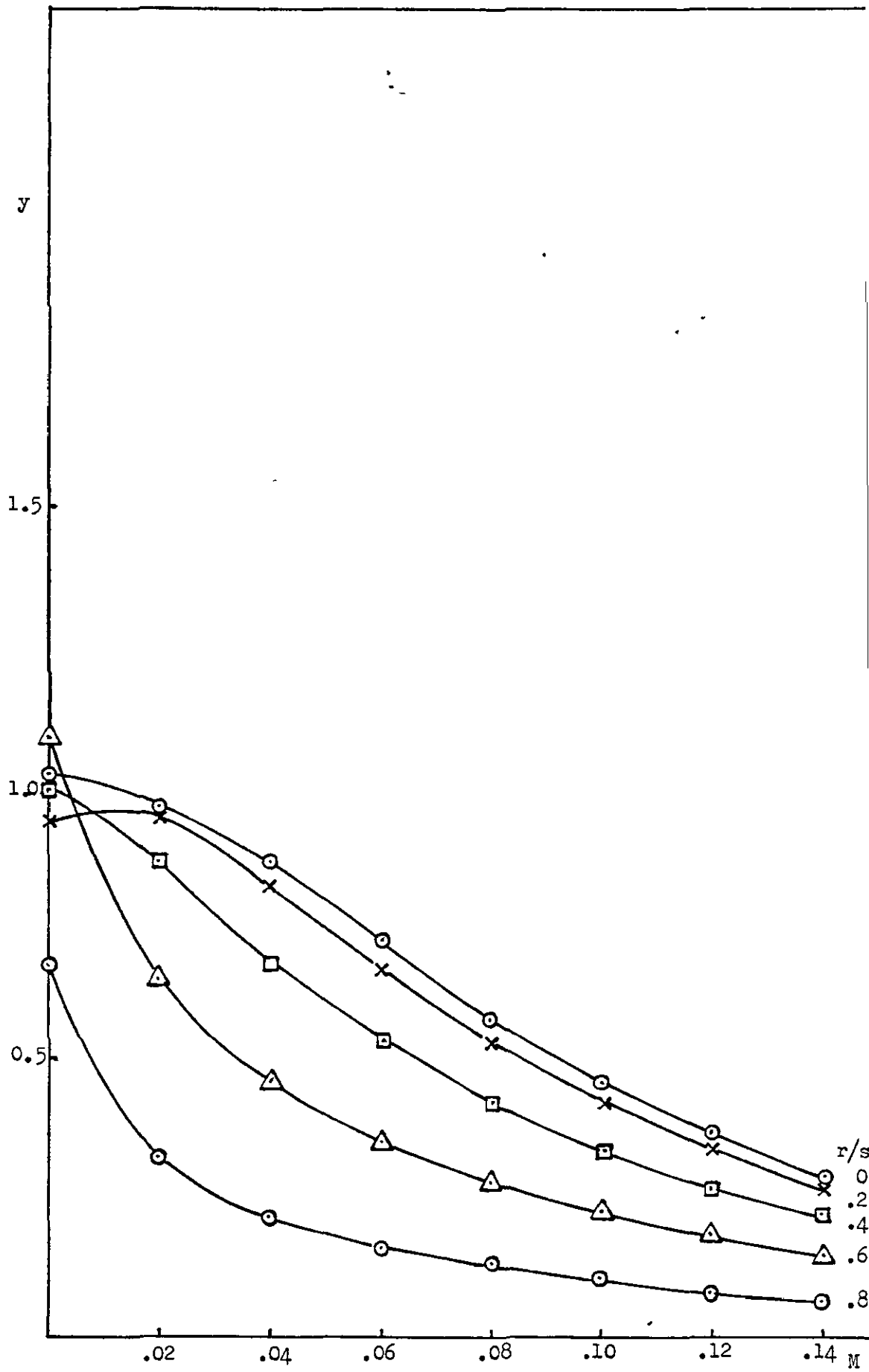

Fig. 69. Plot of $y = 1.447R_o e^{-11.5M} - 0.81R_1 e^{-69.7M} + 0.385R_2 e^{-1.66M}$ for various values of r/s (Jakobs p.455).

For argon [75], when μ is expressed in poises, $\mu_o = 0.00021$

Then $k/c = 3.17 \times 10^{-6} T^{0.82}$

With these values of k/c, values of x/w can be evaluated from the values of M obtained graphically.

Thus given the tunnel temperature T_s, the inlet gas temperature T_o and the mass flow of the fluid w, the values of x and r/s where a given temperature T is reached are obtained, so that a contour map with isotherms as contours can be plotted as they are for the low and high powered plasmas in Figs. 70-71. From these, by interpolation, a radial temperature profile at any height can be obtained as in Figs. 72-73 and by dividing the cross-section of the tunnel into annuli a mean temperature can be deduced, by weighting the calculated temperature of an annulus by its fractional cross-sectional area and summing the contributions.

An example (for T_s = 10,000 K, T_o = 500 K and w = 4.8 ℓ/min. is shown in Table 80. The tunnel was divided into five annuli of inner radius a and outer radius b. It was found that such a calculation was stable with respect to the number of annuli used.

The annuli have the fractional areas shown in column 2, their sum being unity. The mean temperature T_m of each annulus, obtained from the plotted profiles, is multiplied by its fractional area to give its contribution to the mean temperature and the sum of these contributions gives an overall mean temperature.

75) G.W.C.Kaye and T.H.Laby "Tables of Physical and Chemical Constants", 14th Ed., Longmans, 1973.

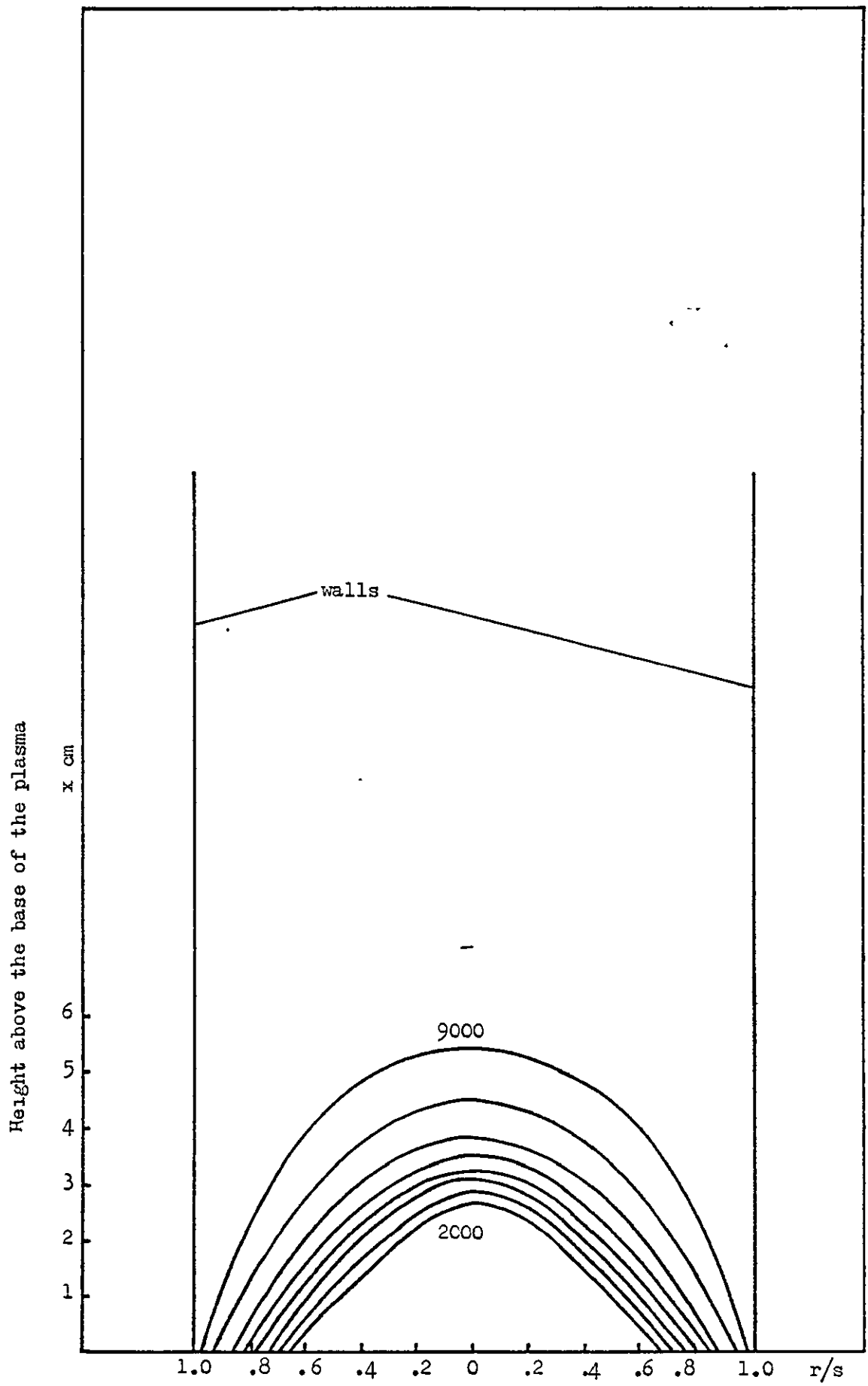

Fig. 70. Calculated temperature profile, for the analyte, as a function of height x and radius r/s. S.C. 15 Generator. Tunnel temperature 10,000°K, inlet gas 350°K, flow 2.6ℓ/min. argon.

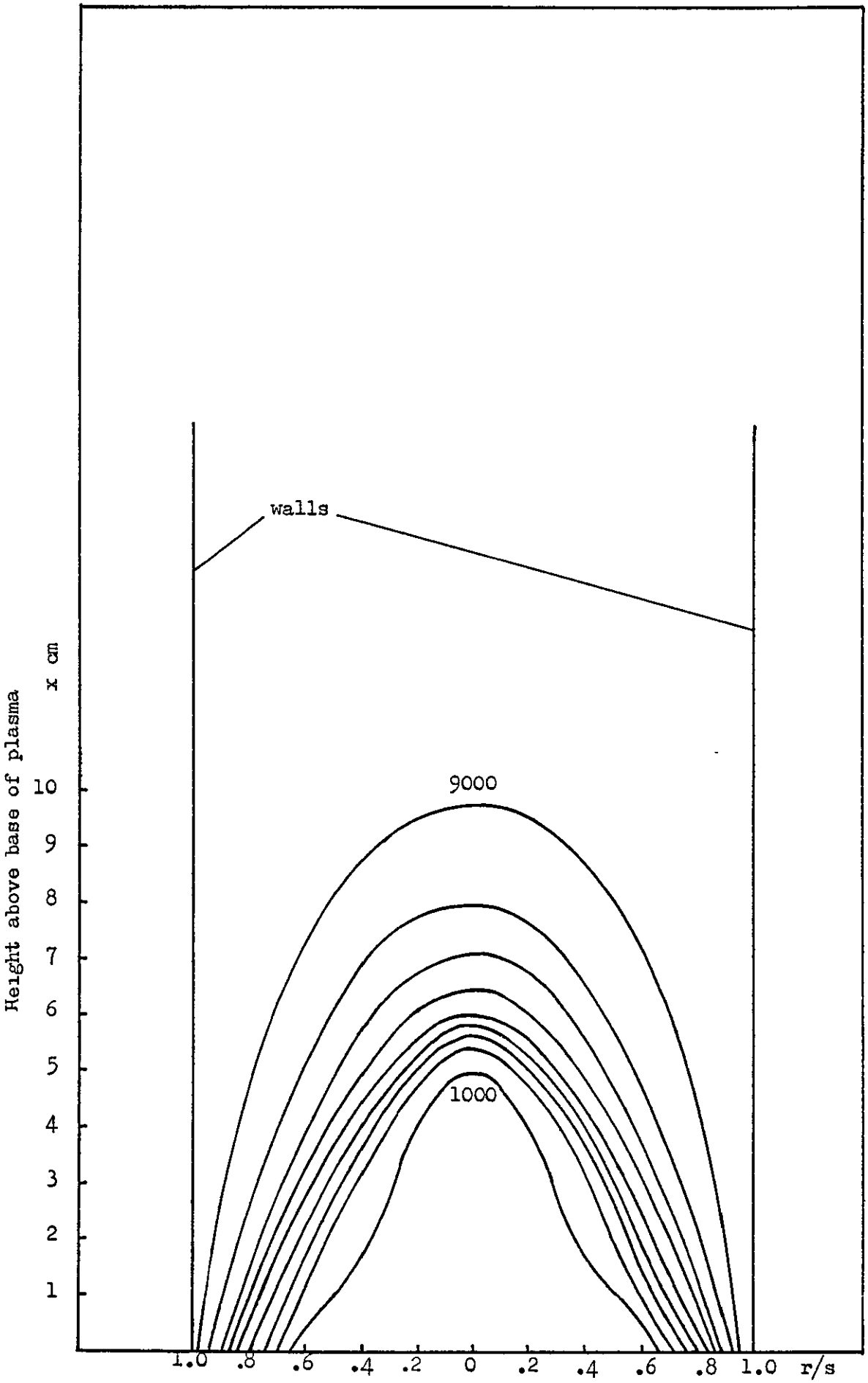

Fig. 71. Calculated temperature profile, for the analyte, as a function of height x and radius r/s. RD 150 Generator. Tunnel temperature 10,000°K. Inlet gas 500°K. Flow 4.8ℓ/min. argon.

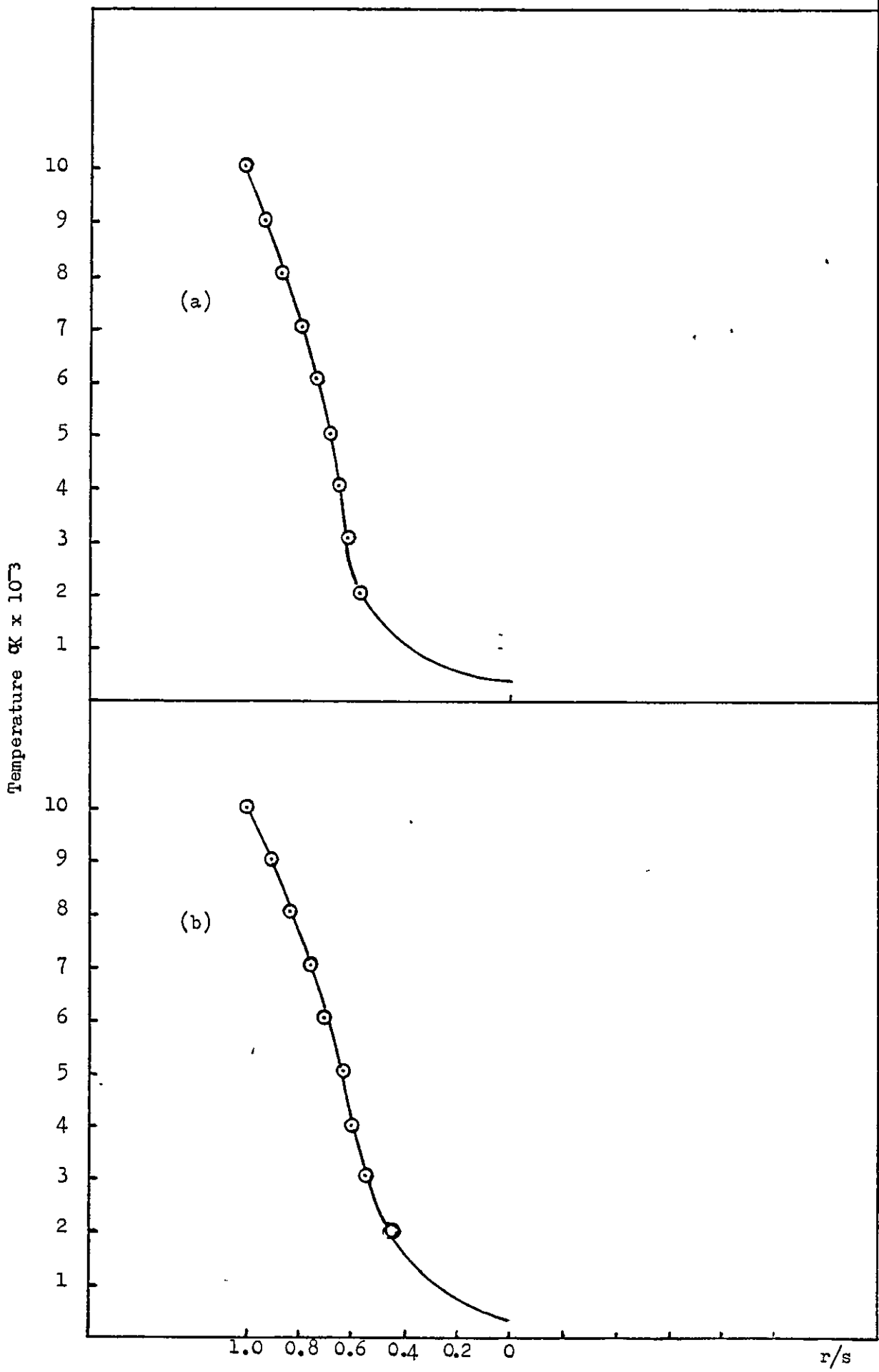

Fig. 72. Radial temperature profile at heights of 0.7 cm (a) and 1.0 cm (b). S.C. 15 Generator.

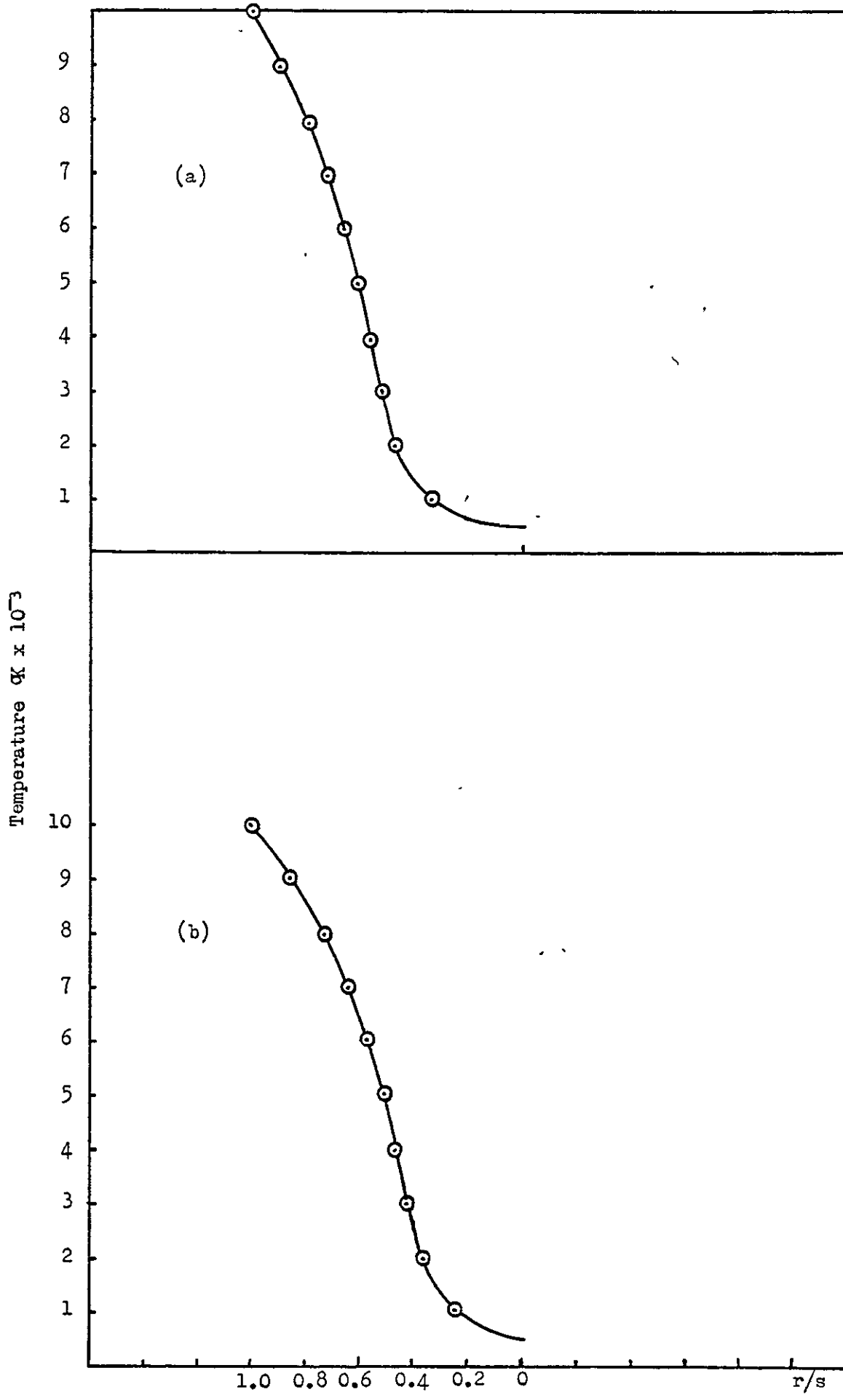

Fig. 73. Radial temperature profile at heights of 2.5 cm (a) and 3.5 cm (b). RD 150 Generator.

Table 80. Example of Calculation of Mean Temperatures from Profiles Obtained from Map of Isotherms.

Height (cm.) →			2.0		2.5		3.0		3.5	
Fractional Radii of Annulas. a.	b.	Fractional Area b^2-a^2	Mean Temp. Tm	$Tm(b^2-a^2)$	Tm	$Tm(b^2-a^2)$	Tm	$Tm(b^2-a^2)$	Tm	$Tm(b^2-a^2)$
0	0.2	0.04	700	28	700	28	700	28	700	28
0.2	0.4	0.12	900	108	1100	132	1500	180	1700	204
0.4	0.6	0.20	2500	500	3250	650	4000	800	4500	900
0.6	0.8	0.28	6000	1680	6500	1820	7200	2016	7500	2100
0.8	1.0	0.36	8700	3132	9000	3240	9200	3312	9300	3348
Mean Temperature				5448		5870		6336		6580

Another example (for T_s = 10,000 K, T_o = 350 K and w = 2.6 ℓ/min.) is shown in Table 81.

Table 81. Example of Calculation of Mean Temperature from Profiles Obtained from Map of Isotherms.

Height (cm)			0.7		1.0	
Fractional Radii of Annulas. a.	b.	Fractional Area. $b^2 - a^2$	Mean Temp. T_m	$T_m(b^2-a^2)$	T_m	$T_m(b^2-a^2)$
0	0.2	0.04	500	20	500	20
0.2	0.4	0.12	1100	108	900	132
0.4	0.6	0.20	2500	320	1600	500
0.6	0.8	0.28	6000	1540	5500	1680
0.8	1.0	0.36	9000	3060	8500	3240
Mean Temperature				5048		5572

These mean temperatures are plotted in Figs. 66 and 67. The line produced can be made to fit the measured line reasonably well in the case of the low powered plasma. The mean temperature of 5572 K was calculated for a height of 1 cm. (which is the top of the plasma for 1.67 kW) where there is no measurement for temperature. All temperatures measured were made outside the cell because of cell staining. The lowest measured temperature is at 2.42 cm. (the top of the cell) where the temperature is 5574, a remarkable coincidence. After emerging from the plasma tunnel it might be expected that the injector flow would continue to be heated until it reached the temperature of the sheath, and then to cool, so the calculated value seems quite sensible.

The other mean temperature of 5048 K, calculated for the low powered plasma is for a tunnel length of 0.7 cm, which corresponds to the top of a plasma of power 0.8 kW. In this case the temperature at the top of the cell (1.7 cm. above the top of the plasma) is 4952 K. Again very good agreement is obtained.

The fit of the lines for the high powered plasma is not as good as for the low-powered. There is a discrepancy of approximately 800 K for a plasma 3.5 cm. long. Nevertheless, there is nothing to suggest that the model put forward in Section 7.1 does not fit the experimental facts reasonably well and there is nothing inconsistent with the view that excitation is thermally controlled.

CHAPTER 8

OPTIMISATION OF PLASMA CONDITIONS.

In the preceding chapters it has been shown beyond doubt that the measured emission from a plasma source is dependant in value upon the parameters height of viewing and the power (temperature) of the plasma. Furthermore, these parameters are inter-active. It was also known that the emission was dependant upon the nebuliser gas flow as is demonstrated by reference to the data in Fig. 74 which shows clearly that there is an optimum nebuliser gas flow to give maximum emission. A similar dependance occurs with the plasma gas flow; this is shown in Fig. 75. The question arises, are all these parameters inter-active one on the other? If they are, then clearly before any comparisons can be made between plasma torches it is necessary to ensure that each torch is operating under its optimum conditions. It was decided that in future experiments such an optimisation would be carried out.

Section 8.1 Factorial Optimisation of Plasmas.

Experiments based on factorial designs are widely used and have been extensively described[76]. Such experiments are planned so that the different independent variables, in this case, power, position of observation and the three gas flows, can be varied from a high level to a low level according to a pattern and from the 2^n experiments (32 in this case) the effects of the independent variable and their inter-actions one with another can be extracted. The response to be maximised is the ratio $\frac{x - b}{b - a}$.

76. D.L.Davies "The Design and Analysis of Experiments" 2nd Ed., Oliver and Boyd, 1956.

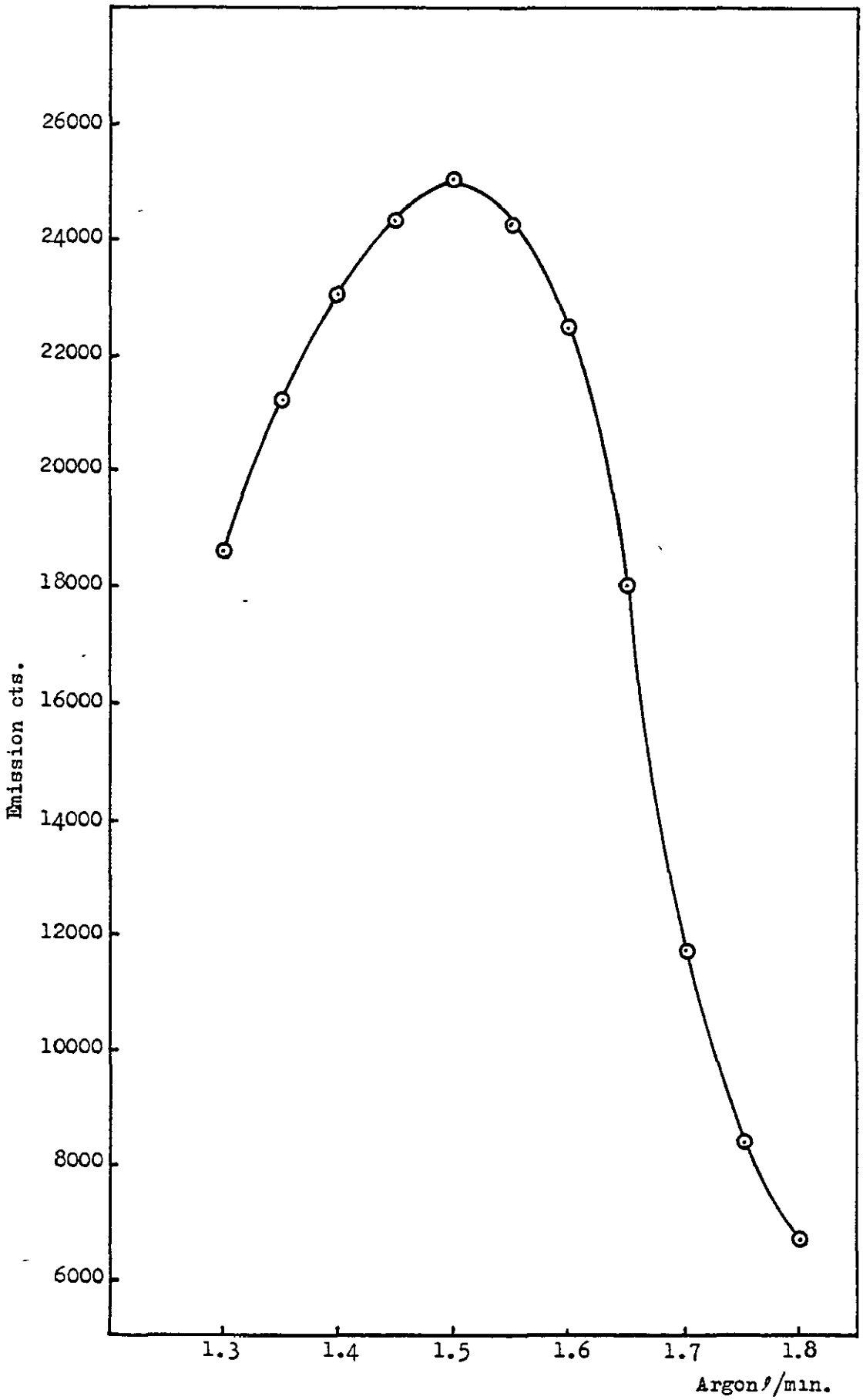

Fig. 74. Effect of nebuliser gas flowrate on the emission from 100 ppm of Calcium at 3968 A°.

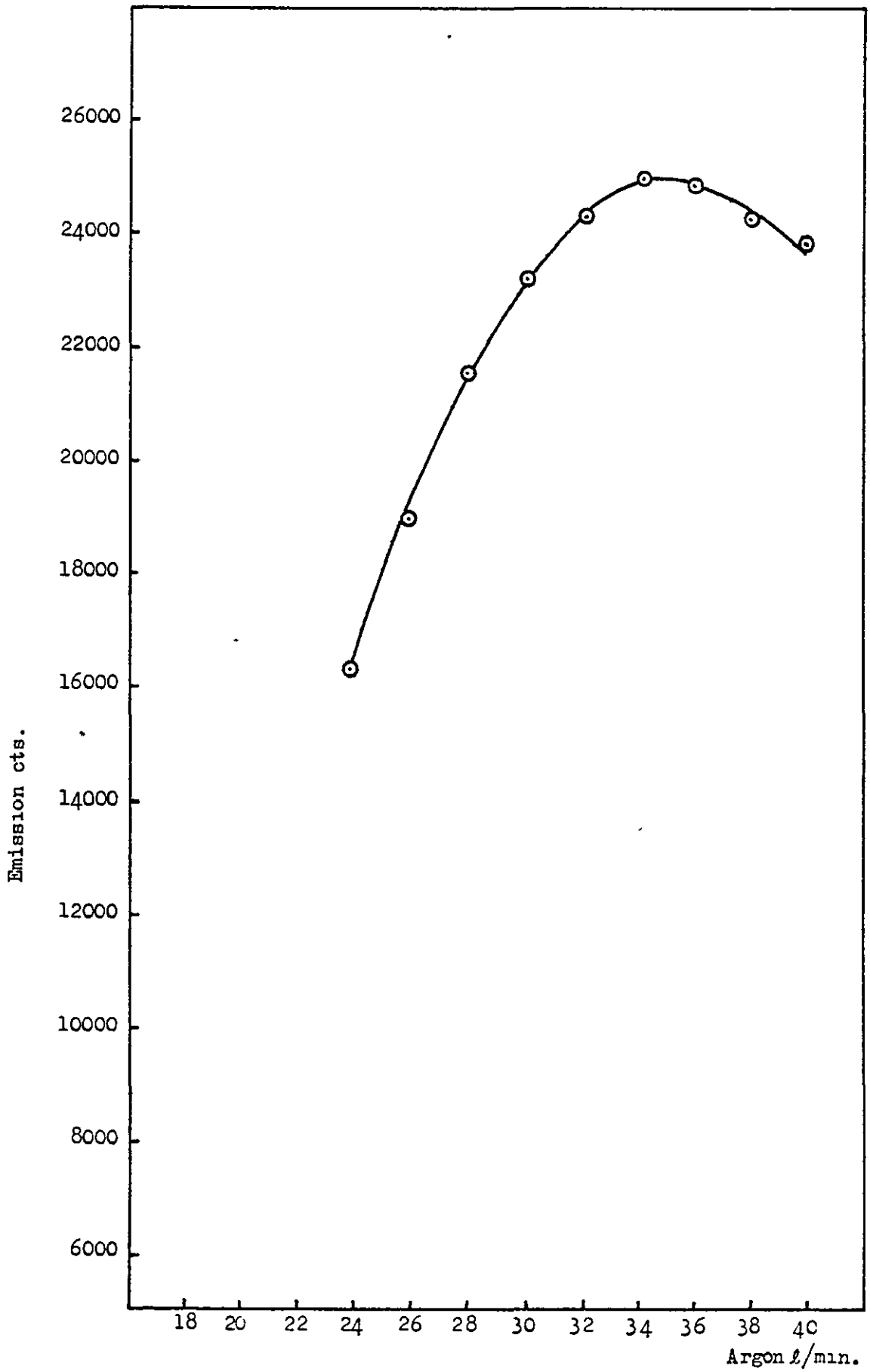

Fig. 75. Effect of plasma gas flowrate on the emission from 100 ppm of Calcium at 3968A°.

Many experiments, each requiring approximately four hours to complete, were carried out and data from a typical example is shown in Table 82. The two levels of the five variables are specified in the top left hand corner and the numbers -1 and 1 in the five columns indicate low and high levels used for the particular readings. Corresponding to these conditions are shown the measurements of x and b, from which are derived the values of $\frac{x - b}{b - a}$. The next four columns are part of the simple systematic calculation (Ref. 76, p.263): the top half of the first column consists of sums of successive pairs of responses and the second half of differences between successive pairs. This process is repeated in the next four columns, the last of which gives the values of 16 times the effects. In general for n variables there are n such columns and the effects are obtained from the final column by dividing by 2^{n-1}. The variables to which the effects in the last column refer are those which have + signs in the first five columns for the given line. The top line is simply the total of all the readings: the next line shows that an effect of $\frac{74}{16}$ is due to height, the only variable which has a +1 in the first column, the line after gives an effect of $\frac{-5.8}{16}$ to the coolant flow, and the next $\frac{16}{16}$ to the interaction between height and coolant. The ten largest effects are listed in Table 83.

TABLE 82. FACTORIAL OPTIMISATION OF PLASMA VARIABLES.

Height*	Coolant*	Plasma*	Nebuliser*	Power*	80 second exposure.										
Low 950	12	3	8	4.3	x	b	a	x-b	b-a	x-b					Estimate of
High 1250	21	10	16	5.0	Counts	Counts	Counts	Counts	Counts	b-a					16 Effects.
-1	-1	-1	-1	-1	749	51	13	698	38	18	67	119	199	408	692
1	-1	-1	-1	-1	15782	326	13	15456	313	49	52	80	209	284	74
-1	1	-1	-1	-1	507	37	13	470	24	20	43	58	152	70	-58
1	1	-1	-1	-1	22624	688	13	21936	675	32	37	151	132	4	16
-1	-1	1	-1	-1	53598	2188	13	51410	2175	24	27	95	37	-34	26
1	-1	1	-1	-1	176440	9040	13	167400	9027	19	31	57	33	-24	-124
-1	1	1	-1	-1	50128	2520	13	47608	2507	19	84	61	6	4	-4
1	1	1	-1	-1	155968	8392	13	147576	8379	18	67	71	-2	12	34
-1	-1	-1	1	-1	29	16	13	13	3	4	50	43	-21	54	-10
1	-1	-1	1	-1	4428	199	13	4229	186	23	45	-6	-13	-28	-12
-1	1	-1	1	-1	33	16	13	17	3	6	31	38	-10	-92	4
1	1	-1	1	-1	6207	247	13	5960	234	25	26	-5	-14	-32	46

TABLE 82 contd.

Height*	Coolant*	Plasma*	Nebuliser*	Power*	80 second exposure.										
Low 950	12	3	8	4.3	x	b	a	x-b	b-a	x-b					
High 1250	21	10	16	5.0	Counts	Counts	Counts	Counts	Counts	b-a					Estimate of 16 Effects.
-1	-1	1	1	-1	34704	728	13	33976	715	48	36	11	-15	-12	180
1	-1	1	1	-1	177184	4776	13	172408	4763	36	25	-5	19	8	6
-1	1	1	1	-1	29752	960	13	28792	947	30	37	7	0	42	-22
1	1	1	1	-1	159872	4240	13	155632	4227	37	34	-9	12	-8	-16
-1	-1	-1	-1	1	33336	1456	13	31880	1443	22	31	-15	-39	10	-124
1	-1	-1	-1	1	55088	1904	13	53184	1891	28	12	-6	93	-20	-66
-1	1	-1	-1	1	28928	1376	13	27552	1363	20	-5	4	-38	-4	10
1	1	-1	-1	1	71240	2736	13	68504	2723	25	-1	-17	10	-8	8
-1	-1	1	-1	1	86648	4800	13	81848	4787	17	19	-5	-49	8	-82
1	-1	1	-1	1	248032	16728	13	231304	16715	14	19	-5	-43	-4	60
-1	1	1	-1	1	81152	5392	13	75760	5379	14	-12	-11	-16	34	20
1	1	1	-1	1	254344	20072	13	234272	20059	12	7	-3	-16	12	-50

TABLE 82 contd.

Height*	Coolant*	Plasma*	Nebuliser*	Power*	80 second exposure										
Low 950	12	3	8	4.3	x	b	a	x-b	b-a	x-b					
High 1250	21	10	16	5.0	Counts	Counts	Counts	Counts	Counts	b-a					Estimate of 16 Effects.
-1	-1	-1	1	1	2576	144	13	2432	131	19	6	-19	9	132	-30
1	-1	-1	1	1	42304	2392	13	39912	2379	17	5	4	-21	48	-4
-1	1	-1	1	1	1072	136	13	936	123	8	-3	0	0	6	-12
1	1	-1	1	1	59032	3384	13	55648	3371	17	-2	19	8	0	-22
-1	-1	1	1	1	78608	3520	13	75088	3507	21	-2	-1	23	-30	-84
1	-1	1	1	1	279280	16432	13	262848	16419	16	9	1	19	8	-6
-1	1	1	1	1	70872	3576	13	67296	3563	19	-5	11	2	-4	38
1	1	1	1	1	280840	17712	13	263128	17699	15	-4	1	-10	-12	-8

* These figures refer to instrument readings and could be converted to more familiar units by reference to calibration curves. This was not necessary and was not done.

TABLE 83. VARIABLES WITH THE LARGEST EFFECTS.

Variable.	Effect.
Plasma x Nebuliser	180
Height x Plasma	-124
Power	-124
Plasma x Nebuliser x Power	-84
Plasma x Power	-82
Height	74
Height x Power	-66
Height x Plasma x Power	60
Coolant	-58
Height x Coolant x Plasma x Power	-50

The expressions Plasma, Nebuliser and Coolant refer to the flows of gas.

If the effects due to one variable, which are known as the main effects regardless of their magnitude, are much bigger than the interactions involving two or more variables, the response surface will approximate to a hyperplane in the five dimensions under discussion and a direction can be chosen so that moving along this direction will result in rapid maximisation of the response. In this case, however, the two largest effects are interactions (plasma gas - nebuliser gas and plasma gas - height) so that the response surface is far from planar. In these circumstances it is not possible to predict the best search direction for anything more than an infinitesimal shift and the only reasonable procedure is to try to fit the response surface to a surface involving higher power terms corresponding to the interactions.

The values of $\frac{x-b}{b-a}$ were fitted by an in-house multiple regression program to several hyper surfaces : the best fit was :-

$$y = 40.9x_3 + 0.000256x_1^2 - 0.000335x_1x_2 - 0.0883x_1x_3 - 0.106x_1x_5 - 0.245x_2x_3 + 2.862x_3x_4 - 7.133x_3x_5 - 0.646x_4^2 + 2.759x_4x_5 + 9.355x_5^2 - 0.529x_3x_4x_5 + 0.000952x_1x_3x_5 + 0.0000468x_1x_2x_3x_5 \quad ---- \quad 122$$

Then, using this "best" equation for the surface, numerical methods can be used to trace a path from any starting point to a maximum value.

When this was tried, the fit of the surface to the experimental points was poor, and when maxima were sought from five different starting positions, without exception they led to predicted conditions which were not physically realisable.

In a number of cases, the main effects were predominant, so that a search directive could be predicted. However, when experimental searches were made in these directions, very little improvement could be obtained. Changes in signal to background ratio seemed to be quite small compared with uncertainties of measurement, and probably the only conclusion that could safely be drawn from this work was that long and fairly level ridges existed in directions involving all the five variables (i.e. directions in five dimensions analogous to diagonals in two dimensions).

Section 8.2. Optimisation by The Simplex Method.

In the Simplex method the response is measured with conditions defined by the vertices of the simplex, which is a regular figure with n + 1 vertices in an n-dimensional space. In two dimensions the simplex is a triangle, in 3 dimensions a tetrahedon, with analogues in spaces of higher dimensions. The vertex with the poorest response is to be replaced by its reflection in the centroid of the remaining vertices, so that experimental conditions corresponding to this reflected position are chosen and a new measurement made. Certain extra rules are sometimes required[77], but these need not concern us here.

Table 84 shows data for an example.

77. M.J.Box., D.Davies., and W.H.Swann., "Non-Linear Optimization Techniques", Oliver and Boyd, 1969.

TABLE 84. OPTIMISATION BY THE SIMPLEX METHOD.

Height*	Coolant*	Plasma*	Nebuliser*	Power*	x	b	a	x-b	b-a	$\frac{x-b}{b-a}$	Vertex.
1250	12	3	8	4.3	31318	826	15	30492	811	38	1
950	12	10	16	4.3	70242	1760	15	68482	1745	39	2
1250	21	10	16	4.3	263688	9960	15	253728	9945	26	3
1250	12	10	16	4.3	267440	10392	15	257048	10377	25	4
1250	12	3	8	4.3	33672	1752	15	31920	1737	18	5
950	21	10	16	4.3	57560	1728	15	55832	1713	33	6
1130	15.6	8.6	14.4	4.3		Centroid					
1010	19.2	14.2	20.8	4.3	40008	1256	15	38752	1241	31	7
1010	19.2	14.2	20.8	4.75	78376	2192	15	76184	2177	35	8
1034	16.7	10.3	16.3	4.39		Centroid					
818	12.4	10.6	16.6	4.5	49328	1136	15	48192	1121	43	9
996	15.3	9.6	15.5	4.43		Centroid					
982	11.4	5.0	10.2	4.56	74784	2040	15	72744	2025	36	10
1002	13.4	8.56	14.3	4.48		Centroid					
1054	5.8	7.12	12.6	4.66	147816	3760	15	144056	3745	38	11
1011	10.7	7.1	12.7	4.46		Centroid					
1012	2.2	0.0	4.6	4.17	Plasma gas value predicted not possible, therefore following values were used.						
1012	2.2	3.1	4.6	4.18	4016	520	15	3496	505	7	12

Of the initial vertices, number 5 was the worst. Then the centroid of the other five was calculated for each variable and a new vertex defined by taking, for each variable $x^1 = 2X - x$, where X is the centroid, x the old value and x^1 the new. Not very much improvement was found compared with the uncertainties of measurement, and after several experiments of this kind, little confidence was felt that a significant optimisation was being achieved.

One possible reason for the failure both of the factorial design and the simplex approaches is that they are both dependent on choosing discrete values for the operating conditions and then making measurements at these conditions. The question of scale is important: if two sets of conditions are too close to each other, the difference in measured response will depend on noise and so apparently irrational and unrepeatable shifts may be chosen. If they are too far apart they may straddle the desired peak and the shifts obtained can be capriciously dependant on minor variations in slope among the "foothills". For this reason, there is much to be said for an experimental method where the response can be measured continuously. Much of the literature[76] is concerned with optimisation of mathematical functions and with batch yields from a plant and both these necessarily involve discrete experimentation or computation. However, in the present experiments, where the result can be seen instantly, continuous measurement can be made. It is possible to sweep the variables throughout their physically realisable range and so to get rid of the problem of scale.

Section 8.3 Optimisation by The Alternating Variable Search Method.

In this method each independent variable is considered in turn and altered until a maximum of the function is located, the remaining (n - 1) variables remaining fixed. The current best point therefore moves parallel to each axis in turn, changing direction when a maximum in the current direction of search is reached.

If the countours of the objective function are hyperspherical then, in this case, five linear searches should find the maximum. If, however, the contours are elongated in some direction, as is shown in Fig. 76 for two variables, only small steps can be taken and the method is inefficient. However, wide sweeps can be made and the problem of scale is avoided.

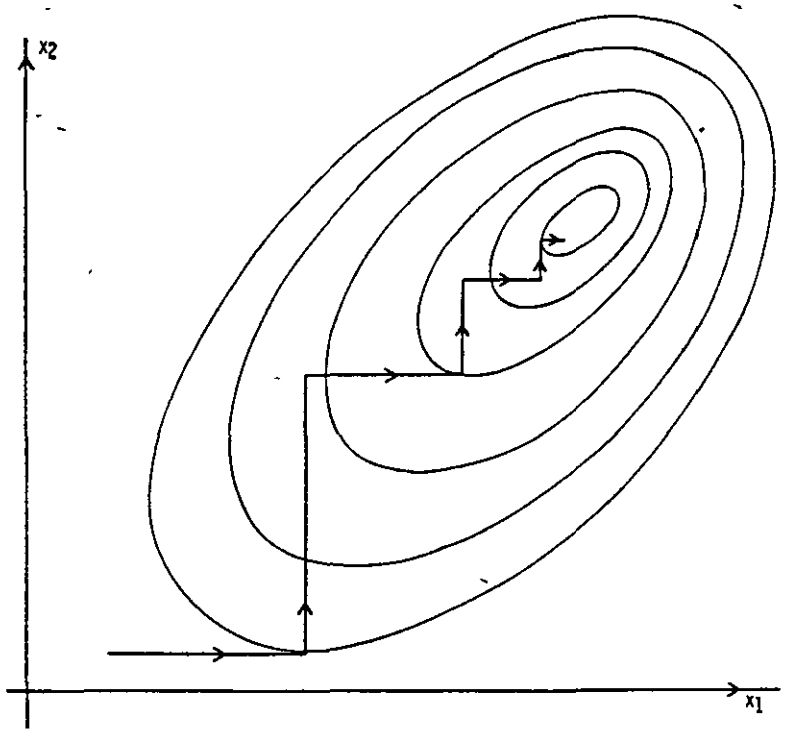

Fig. 76. Alternating Variable Search Method, with Two Variables, Applied to Elongated Contours.

The technique adopted was to use two channels of the polychromator, one for the signal as usual and the other to represent the background. It was of course necessary to ensure that the second channel gave a reading that was proportional to that of the first over a large range of conditions when water was nebulised, but no difficulty was found in choosing a channel which satisfied this condition. The two channels were then connected via operational amplifiers, much the same as in Fig. 46., to an X-Y recorder so that X represented the signal and Y the background. One variable at a time was altered and from the resulting trace a value was chosen corresponding to the point which when connected to the origin gave the line of least slope. It is at this point that the ratio $\frac{x - b}{b - a}$ has its maximum value.

Section 8.3.1 Algebraic Justification of Section 8.3.

Referring to Fig. 77 it can be seen that what is actually maximised is $\frac{x - a}{b_1 - a_1}$.

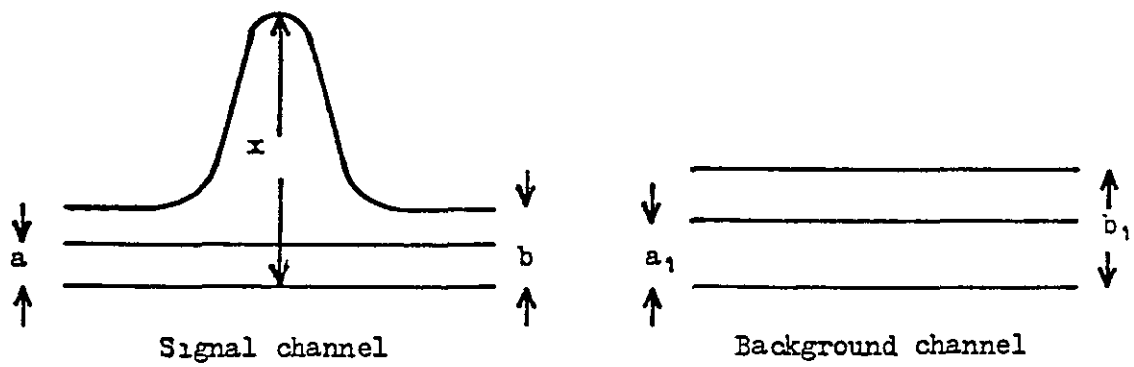

Fig. 77. Representations of the signals to the X - Y recorder.

However, from the straight line through the origin on the recorder chart when water is nebulised it can be said :-

$$b_1 - a_1 = k\,(b - a) \qquad \text{-------123}$$

where k is some constant.

So that what is maximised is :-

$$\frac{x - a}{k(b-a)} = \frac{1}{k}\,\frac{x - b}{b - a} + 1 \qquad \text{-------124}$$

Section 8.3.2. The Alternating Variable Search Method in Operation.

The next five figures show the plots obtained from the X - Y recorder in one complete cycle of a search for the optimum values for the boron line 2498Å. The first variable to be altered was power. The data obtained is shown in Fig. 78.

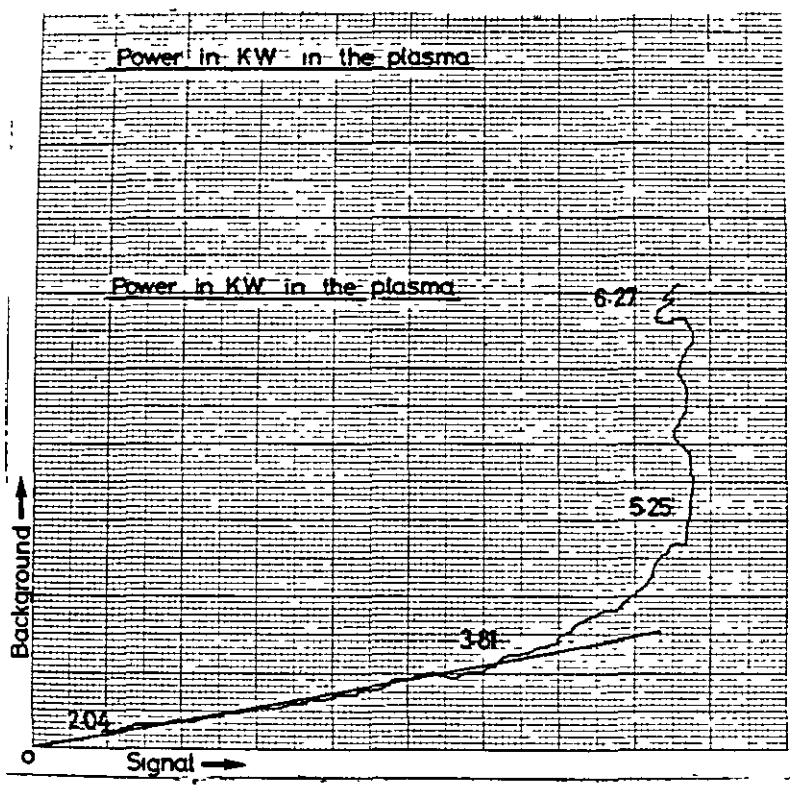

Fig. 78. Variation of Signal and Background, Corrected for Dark Current, With Power. Boron 2498Å.

The horizontal coordinate is the signal from the boron channel at 2497.7Å and the vertical coordinate the estimate of the background at 2542.4Å. The ratio of $\frac{x - b}{b - a}$ has its maximum value when the slope of the vector from the origin has its smallest value. It can be seen that this ratio is almost constant between 2 and 3.8 kW: this illustrates the presence of long ridges of which more will be said later. At a power somewhat above 3.8 kW it deteriorated, very dramatically. The power was, therefore, set to 3.8 kW and the next variable altered. Note that this value of 3.8 is not necessarily the final value. It represents the optimum value of power for the settings used for the other variables, but in the next cycle of optimisation, when all the other variables may have new values, it may be replaced by a higher or lower value.

The next variable to be altered was the height of observation, measured from the top of the plasma. The data obtained is shown in Fig. 79.

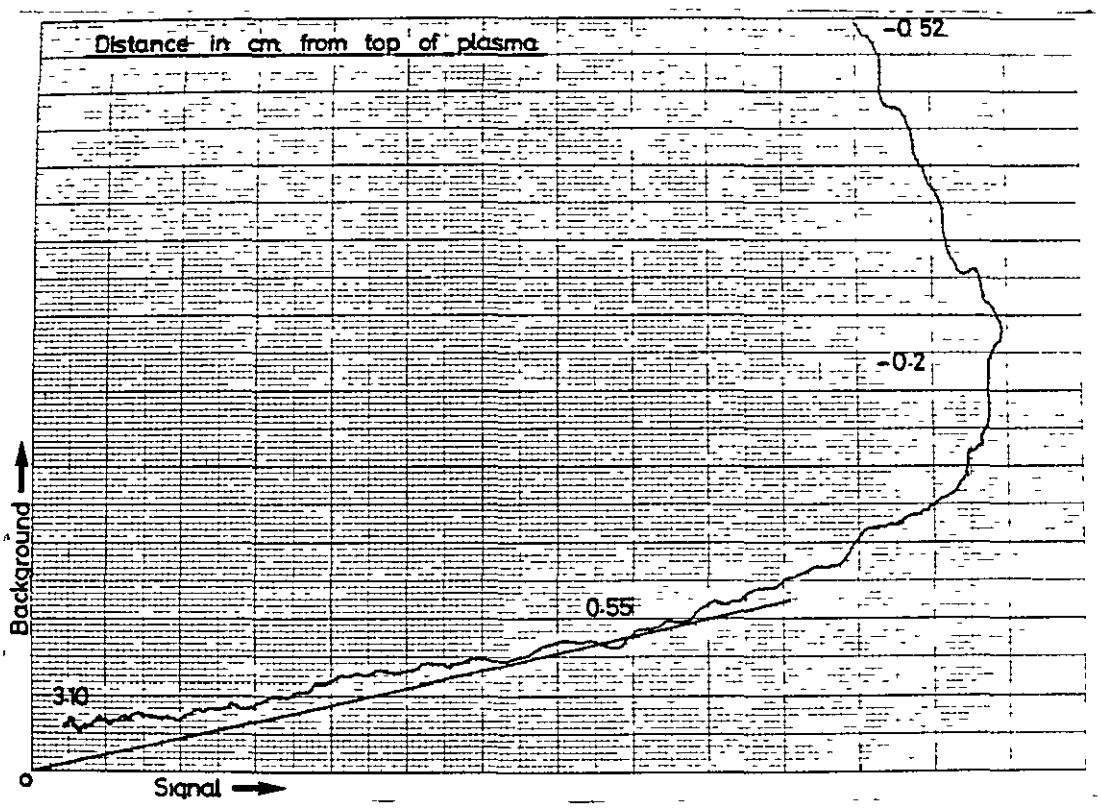

Fig. 79. Variation of Signal and Background, Corrected for Dark Current, With Height of Observation. Boron 2498Å.

The ratio improved modestly as the plasma was approached until the distance was 5-6 mm. Thereafter it worsened until, when the plasma was entered another dramatic deterioration was seen.

Data showing the effect of varying the nebuliser gas flow is given in Fig. 80.

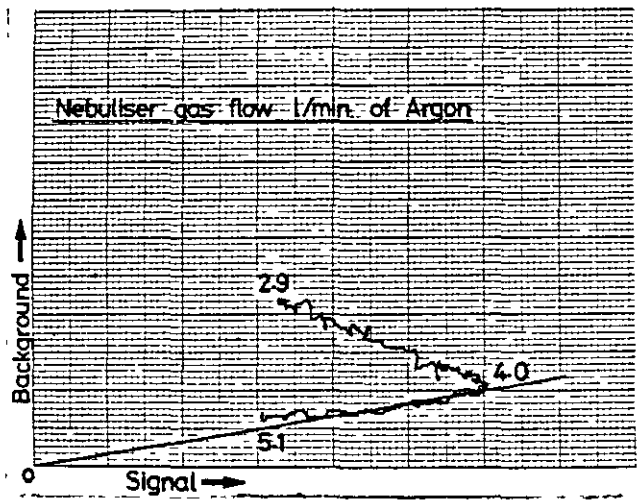

Fig. 80. Variation of Signal and Background, Corrected for Dark Current, With Nebuliser Gas Flow. Boron 2498Å.

Here again there existed a ridge with a constant ratio of $\frac{x - b}{b - a}$ between 5.1 and 4.0 ℓ/min. The ratio and the signal both decreased for lower values.

The effect of varying the plasma gas flow is shown in Fig. 81.

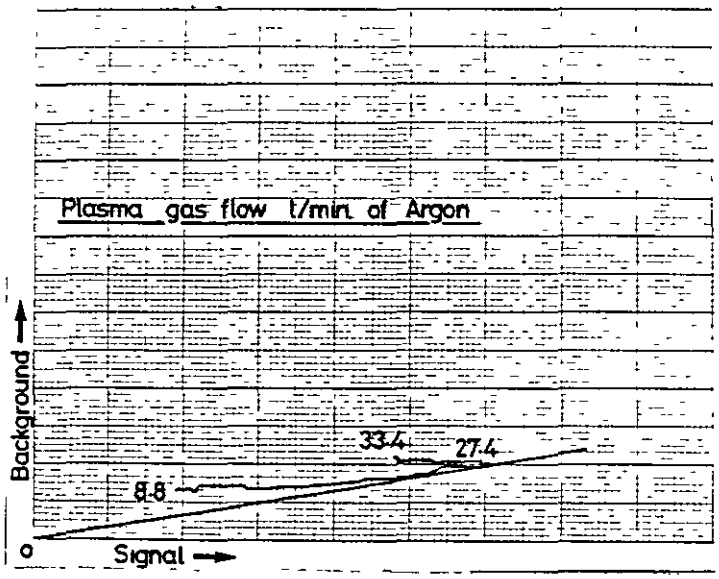

Fig. 81. Variation of Signal and Background, Corrected for Dark Current, With Plasma Gas Flow. Boron 2498Å.

In this experiment there were large variations in the signal and only quite small ones in the background.

Data showing the effect of varying the coolant gas flow are given in Fig. 82. It shows that, for boron, the ratio does not depend very strongly on the coolant gas flow, but that, nevertheless the range 20-30 ℓ/min. is preferred.

These Figs. 78 - 82, illustrates one cycle of the optimisation process and this was repeated until no further improvement was achieved.

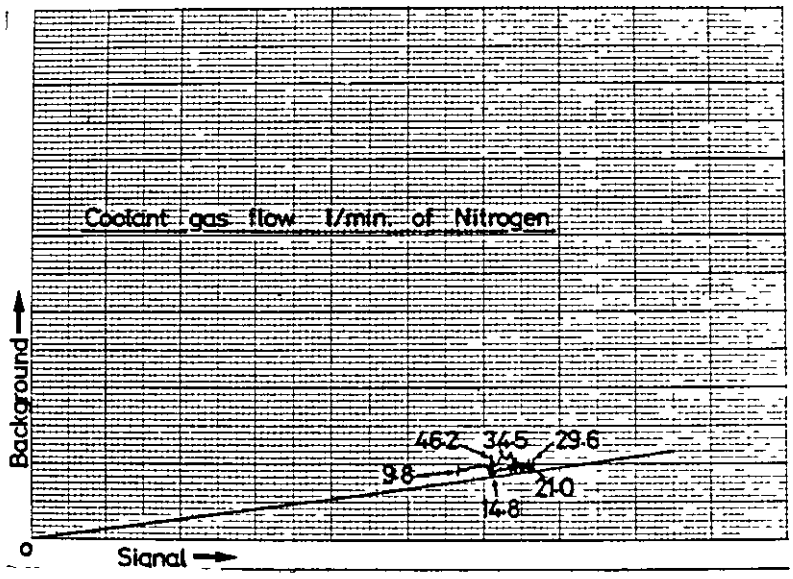

Fig. 82. Variation of Signal and Background, Corrected for Dark Current, With Coolant Gas Flow. Boron 2498Å.

It is possible, when long diagonal ridges occur that this procedure will not lead to the true maximum but to a position on the ridge which is a maximum with respect to x and y separately but not when varied together. Accordingly it was checked that altering the variables in pairs did not lead to any improvement. In these experiments, there was further evidence of long ridges. These showed up on the X - Y recorder as straight lines which, if projected backwards, passed through the origin. When these occurred the ratio $\frac{x - b}{b - a}$ was constant over a range of the variable and the value was chosen furthest away from the origin since this point has the bonus of higher sensitivity.

In another experiment using a manganese sulphate solution and the line at 2576Å, four different searches by different routes converged to the same values, these routes are tabulated in Table 85. One of these was very slow indeed, requiring 17 cycles. An interesting feature is that from one set of initial conditions the path split into two different branches, as is shown by the data in Table 85 and diagramatically in Fig. 83, in the sense that it was possible to obtain the same value of the ratio $\frac{x - b}{b - a}$ with two very different values of plasma gas flow, while for intermediate values the ratio deteriorated. In Fig. 83 the values of the gas flow in litres per minute are marked against the points where the recorder pen came to rest; the parts between show how the pen moved when the flow was in process of being altered. The line through the origin indicates where the optimum values occurred. It was a great relief when the two branches eventually came together at the true optimum.

Once the position of maximum signal to background ratio had been established the signal and the background were measured separately using the integrator. The background was estimated by plotting the signal obtained when the plane mirror was rotated (Section 7.2) so that measurements could be taken either side of the atomic line. (The reason for this approach was to avoid the possibility of interference due to the presence of impurities in the deionised water).

Referring to the data in Table 85 it is interesting to note that the value of the ratio $\frac{x - b}{b - a}$, for the initial conditions at the head of the table, was 1173. After optimisation this value rose to 5740, a five-fold increase.

Table 85. Optimisation by Alternating Variable Search Method. Mn 2576.1Å Line.

1000 p.p.m. concentration as manganese sulphate.
Background channel Fe 2599Å RD 150 Generator.

Cycle No.	Height cm.	Power kW	Plasma ℓ/min.	Nebuliser ℓ/min.	Coolant ℓ/min.	Comment.
1	3.46	3.71	20	3.4	37.5	Top of
2	5.40	6.16	35	3.1	37.5	plasma 3.8 cm.
3	5.40	6.90	33	2.9	37.5	
4	5.40	6.90	33	2.9	37.5	
1	3.46	3.75	20	3.4	38	Repeat from
2	6.10	6.00	40	3.1	38	similar
3	5.40	6.00	40	2.9	38	starting point.
4	5.20	5.75	38	2.8	38	
5	5.10	5.75	36	2.8	38	
6	5.10	5.89	35	2.7	38	
7	5.10	5.89	35	2.7	38	
1	2.40	5.78	40	4.0	38	Repeat from a
2	5.90	5.94	34	3.2	38	different
3	5.30	6.42	36	3.2	38	starting point.
4	5.40	6.90	35	3.0	38	
5	5.10	6.36	34	2.9	38	
6	5.10	6.02	35	2.9	38	
7	5.10	5.89	35	2.9	38	
8	5.10	5.89	35	2.9	38	

Cycle No.	Height cm.	Power kW.	Plasma ℓ/min.	Nebuliser ℓ/min.	Coolant ℓ/min.	Comment.
1*	6.40	1.20	10	2.5	38	Repeat from
2	3.80	4.26	14	2.6	38	a different
3	3.90	4.99	14	2.6	38	starting point.
4	3.90	5.61	18	3.1	38	
5	4.70	6.16	23	3.1	38	
6	5.10	6.24	39	3.1	38	
7	5.30	6.06	38	3.1	38	
8	5.30	6.06	38	3.1	38	
1*	3.80	4.26	42	2.6	38	Repeat from
2	4.40	3.61	42	2.6	38	a different
3	4.60	3.83	40	2.6	38	starting point.
4	4.40	4.14	40	2.6	38	
5	4.60	4.14	38	2.6	38	
6	4.70	4.17	38	2.6	38	
7	4.70	4.87	38	2.7	38	
8	4.80	5.37	38	2.7	38	
9	4.80	5.17	37	2.7	38	
10	4.80	5.09	39	2.7	38	
11	4.80	4.95	34	2.7	38	
12	5.0	5.17	36	2.8	38	
13	5.10	5.59	34	2.8	38	
14	5.0	5.81	36	2.9	38	
15	5.2	6.12	35	3.0	38	
16	5.1	6.12	35	3.0	38	
17	5.1	6.12	35	3.0	38	

* Branch points of Fig. 83.

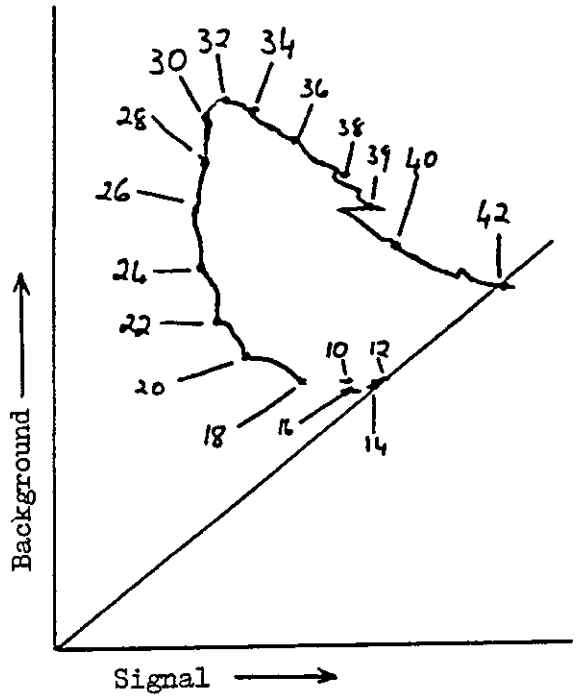

Fig. 83. Variation of Signal and Background, Corrected for Dark Current, With Plasma Gas Flow. Mn 2576Å Showing branching.

Although it appeared that the method was achieving the desired result it was felt that further confirmation should be sought by determining the signal to background ratio after each cycle. This promised to be a very time consuming business, if the integrator was used, as a number of replicates would have to be taken in order to establish statistical accuracy. It was also felt that a graphic representation of the ratio $\frac{x - b}{b - a}$ would engender confidence in the procedure (although the author would not care to stretch this particular argument too far). Accordingly, after each cycle of yet another Mn 2576.1Å line part optimisation, the zero, dark current, background and element signals were recorded by using the F.E.T. recorder system detailed in Section 6.3, Fig. 46. The cycle details are tabulated in Table 86 and the recorder traces are shown in Figs. 84 - 89.

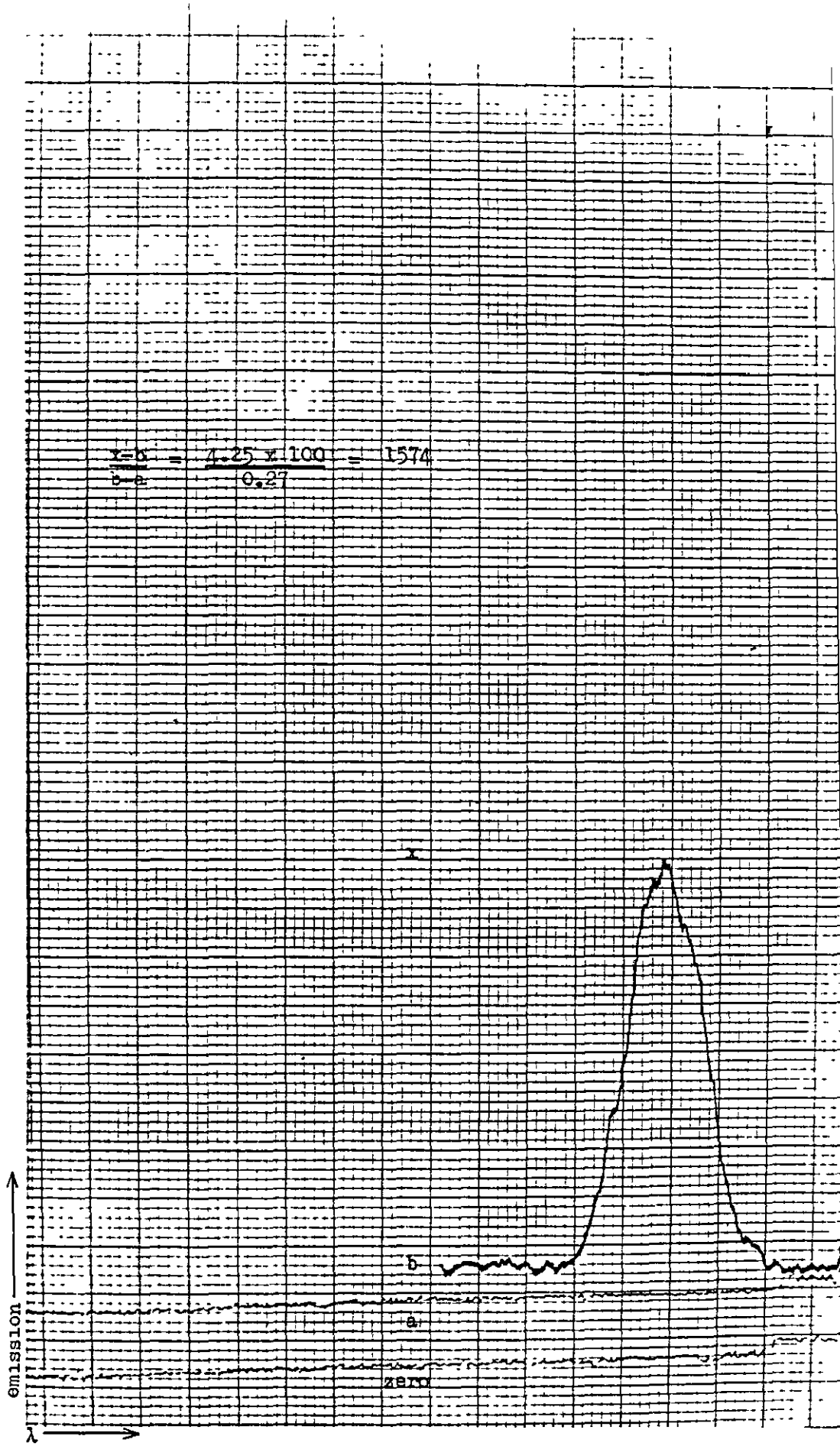

Fig. 84. Part optimisation by the alternating variable search metho Mn 2576 A° line 10 ppm concentration. Scan of signals after 1 cycle.

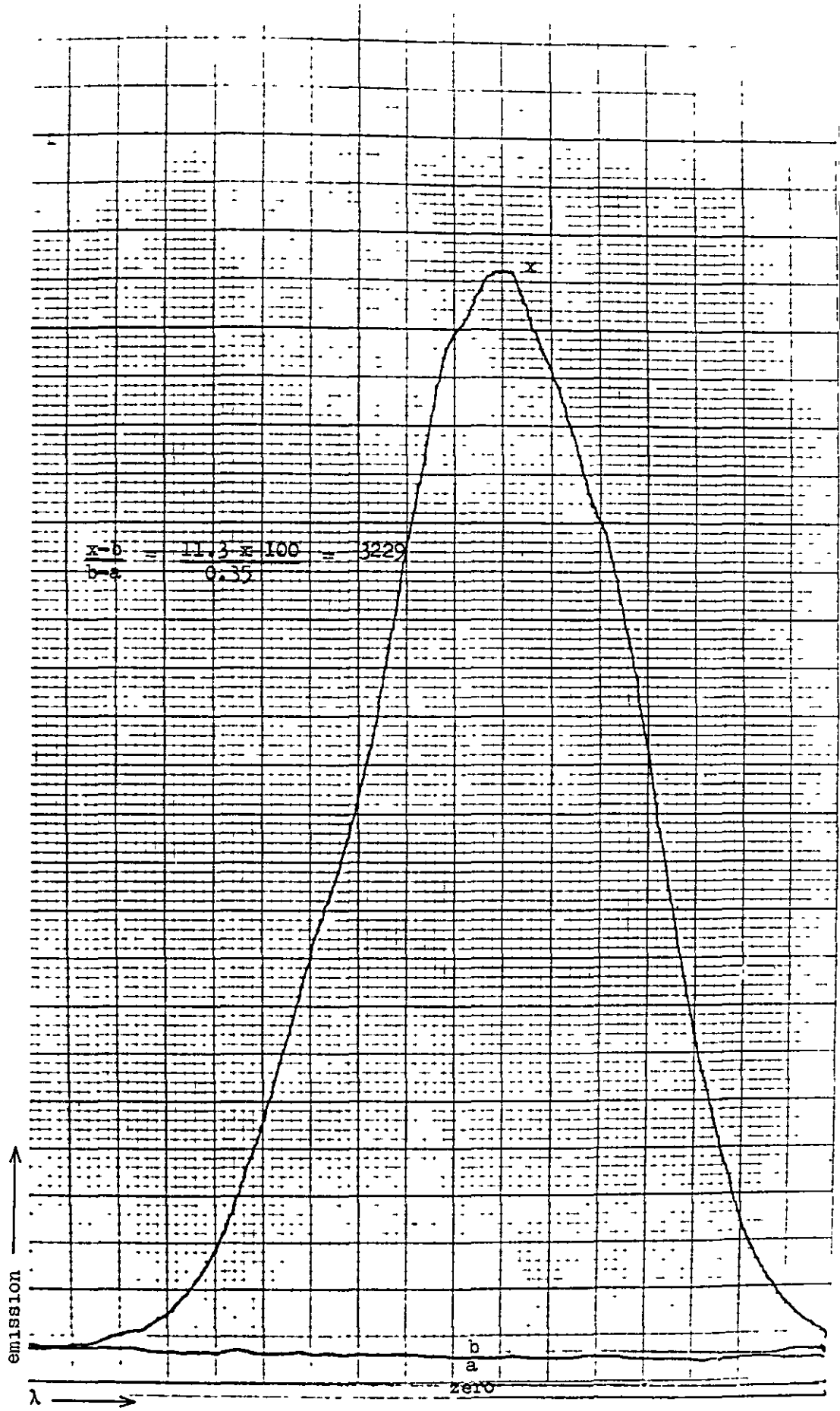

Fig. 85. Part optimisation by the alternating variable search method. Mn 2576 A° line 10 ppm concentration. Scan of signals after 2 cycles.

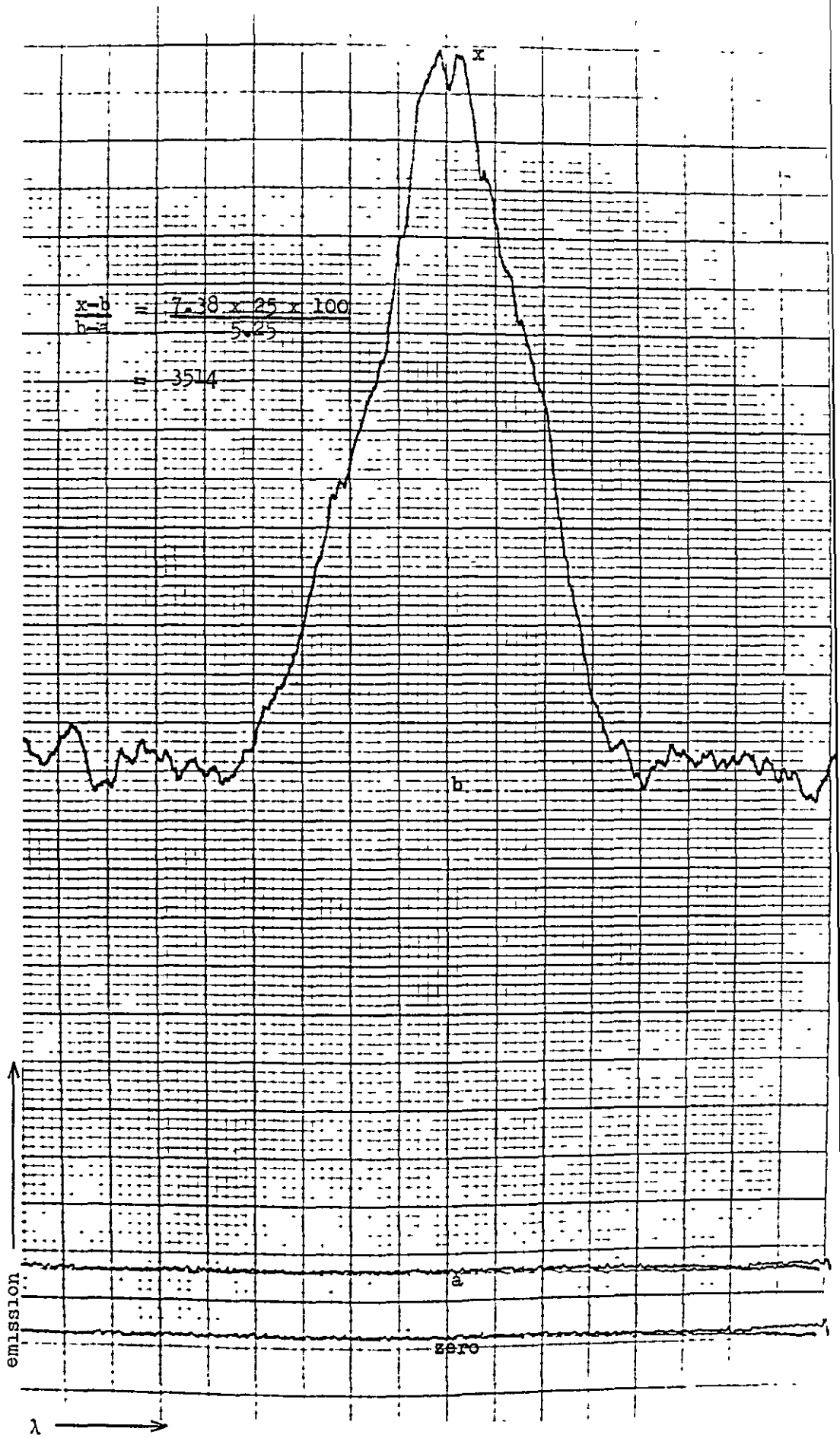

Fig. 86. Part optimisation by the alternating variable search metho
Mn 2576 A° line 0.4 ppm concentration. Scan of signals
after 3 cycles.

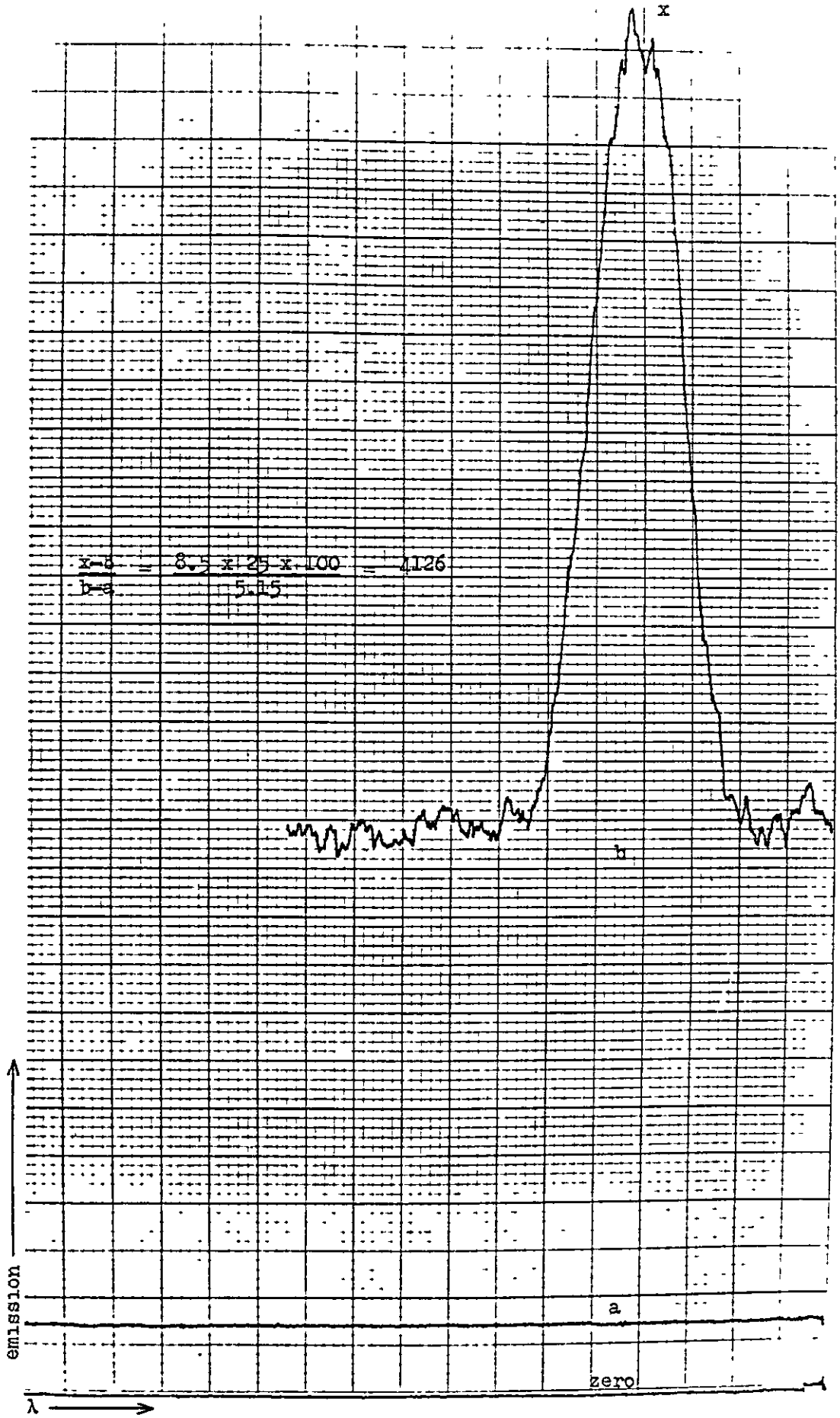

Fig. 87. Part optimisation by the alternating variable search method. Mn 2576 A° line 0.4 ppm concentration. Scan of signals after 4 cycles.

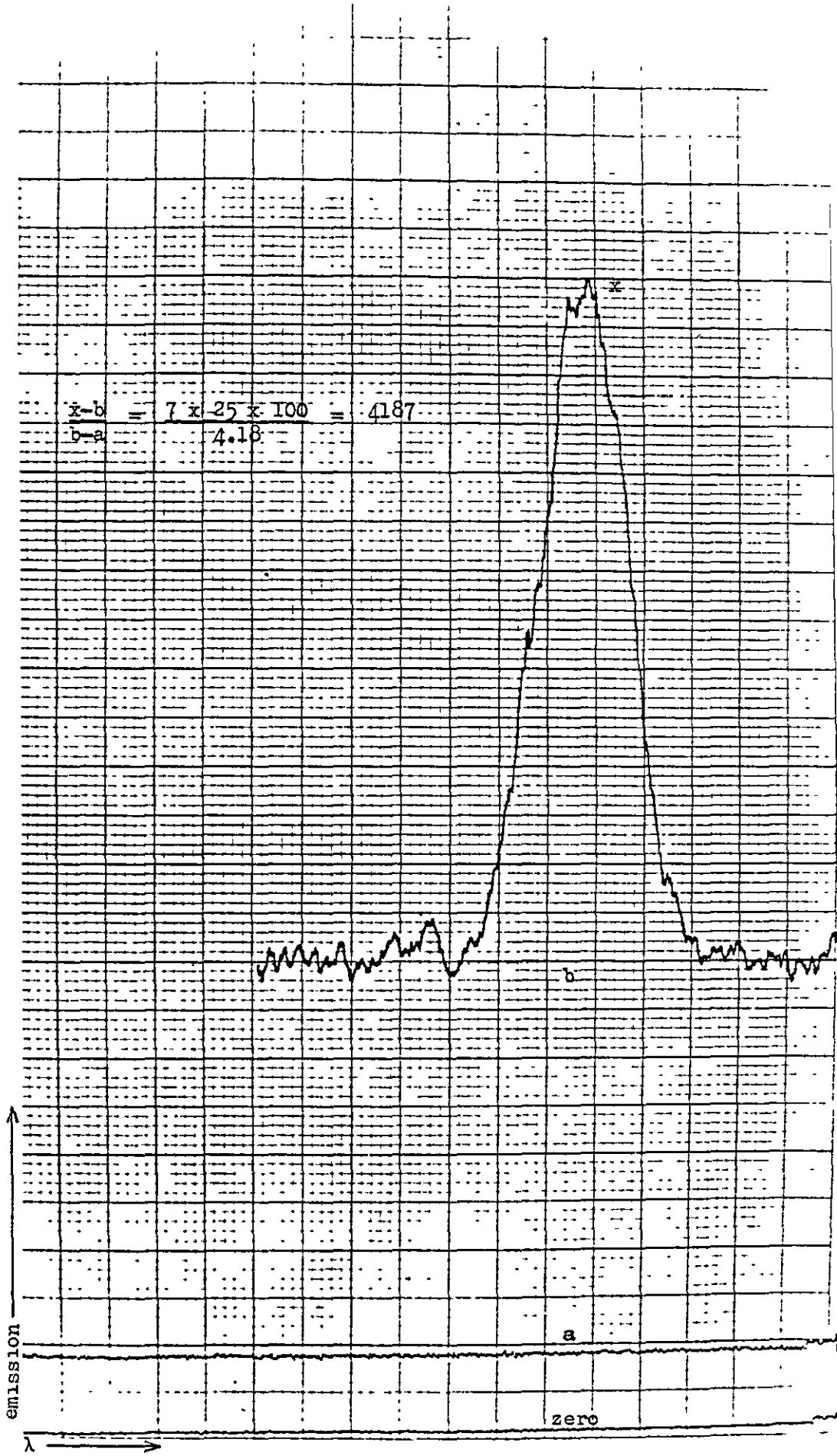

Fig. 88. Part optimisation by the alternating variable search metho Mn 2576 A° line 0.4 ppm concentration. Scan of signals after 5 cycles.

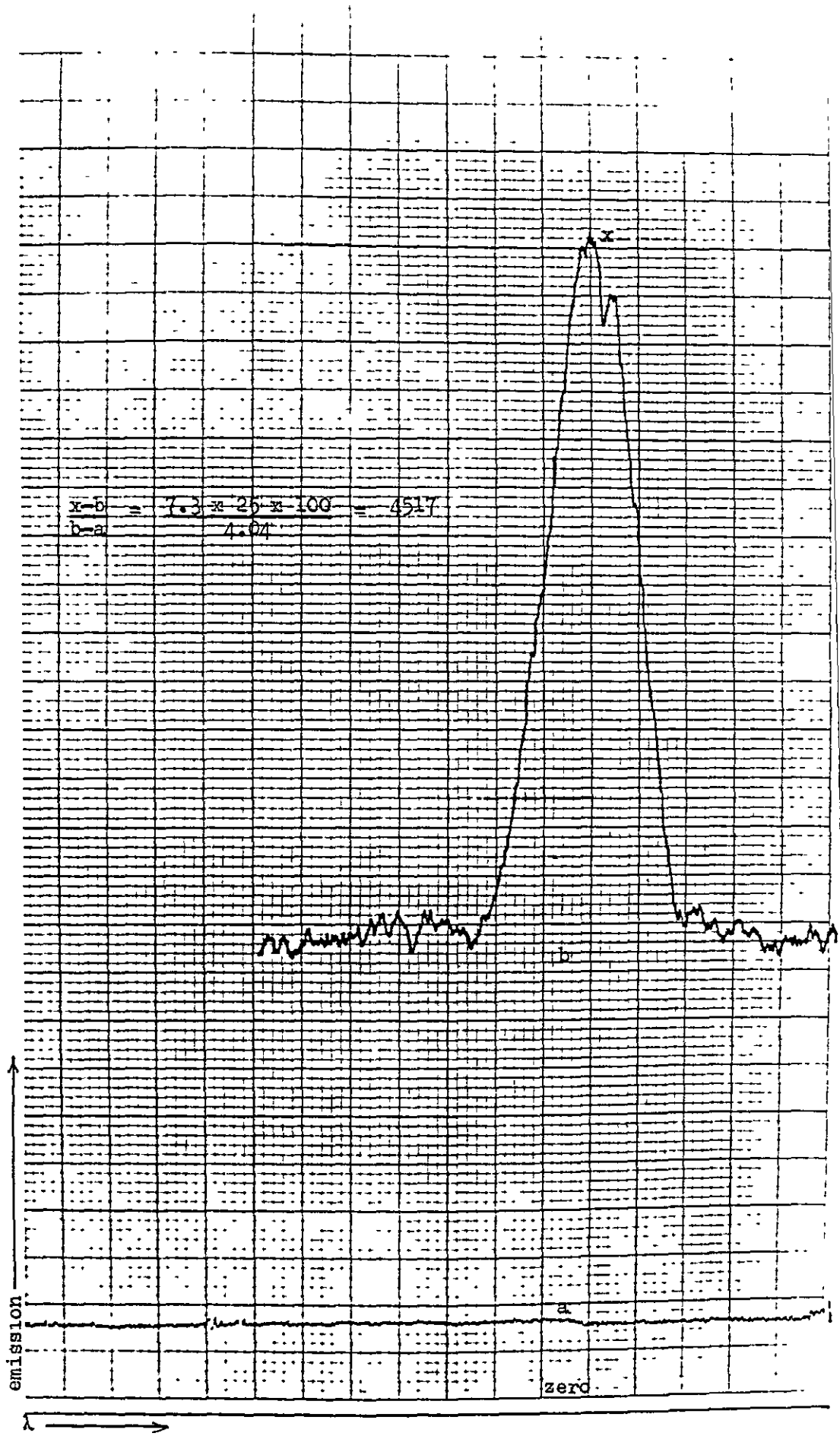

Fig. 89. Part optimisation by the alternating variable search method Mn 2576 A° line 0.4 ppm concentration. Scan of signals after 6 cycles.

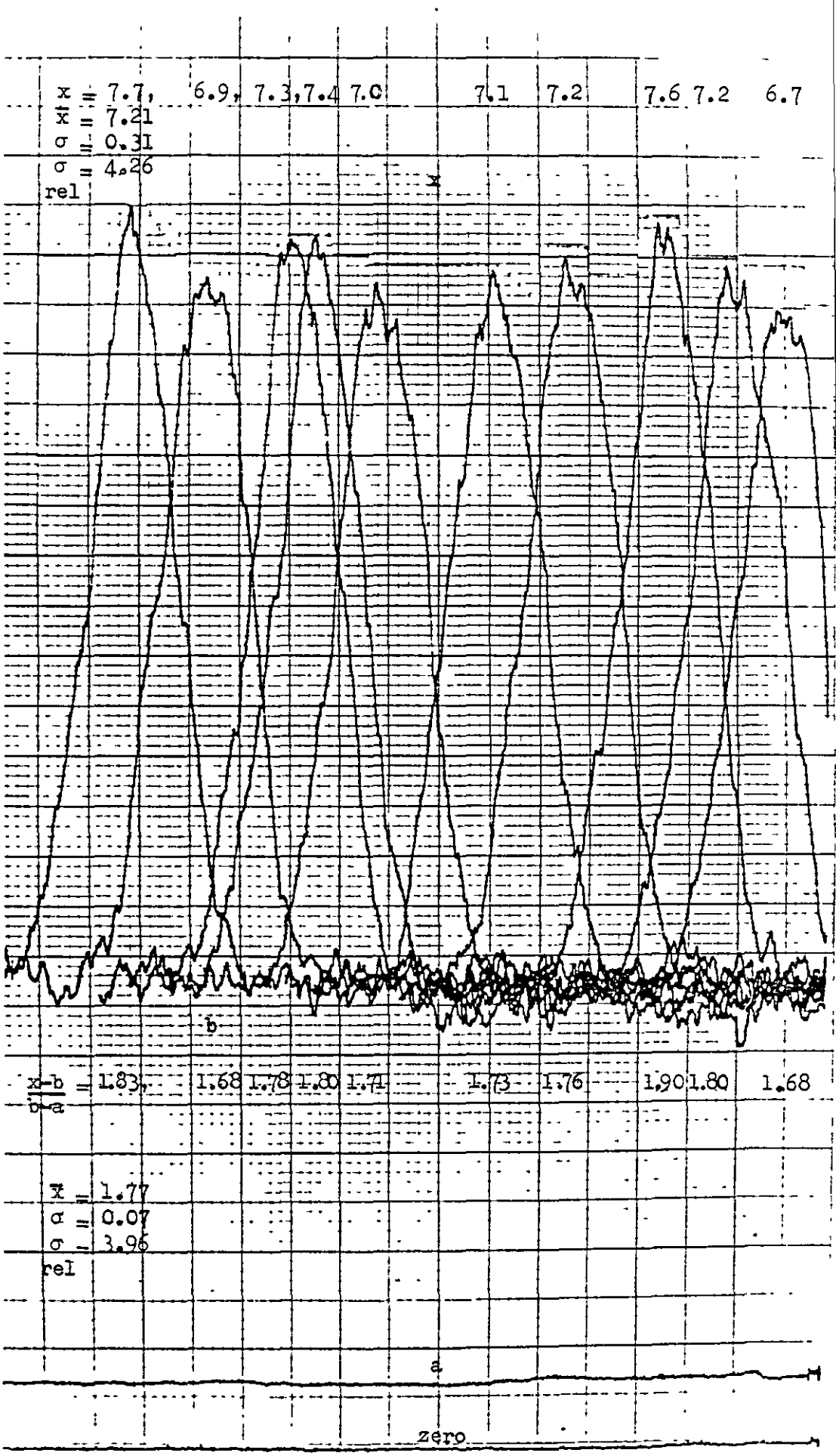

Fig. 90. Showing repeated scans of background and element signals using the F.E.T. measuring system with a 100 mv recorder.

Table 86. Part Optimisation by Alternating Variable Search Method. Mn 2576.1Å line.

10 p.p.m. concentration as manganese sulphate.

Background channel V 3093Å. R.D.150 Generator.

Cycle No.	Height*	Power*	Plasma*	Nebuliser*	Coolant*	$\frac{x-b}{b-a}$ normalised to 1000 p.p.m.
1	1050	4.2	5	7	12	1574
2	1200	4.2	9	7	16	3229
3	1200	4.7	10	7	12	3514
4	1180	4.8	11.5	7	20	4126
5	1180	4.6	12.5	7	19	4187
6	1170	4.65	13.5	7	20	4517

* As this was only a part optimisation the instrument readings were not converted to appropriate units.

Fig. 90 shows repeated scans of one set of signals and gives an indication of the precision of the scanning procedure, which although not high, is probably sufficiently high to give confidence that there is genuine improvement in the $\frac{x - b}{b - a}$ ratio as the optimisation proceeds.

Although the alternating variable search method appeared to work it was felt that the use of an X - Y recorder was too cumbersome and a more easily used system was required.

Section 8.4 The Signal Divider.

The basis of this instrument is the Analog Devices Integrated Circuit AD 530L operated in the divide mode. The integrated circuit contains a transconductance multiplying element (⊗), stable reference and output amplifier on a monolithic silicon chip. The only external components required (apart from a ± 15v power supply) were trim potentiometers for adjusting feedthrough, output zero and gain.

The AD 530L divides in two quadrants (± Z, -X) with a 10 Z/X transfer function and a maximum error of 1.5% in the temperature range 0 to +70°C. Fig. 91 is a functional diagram of the device in block form.

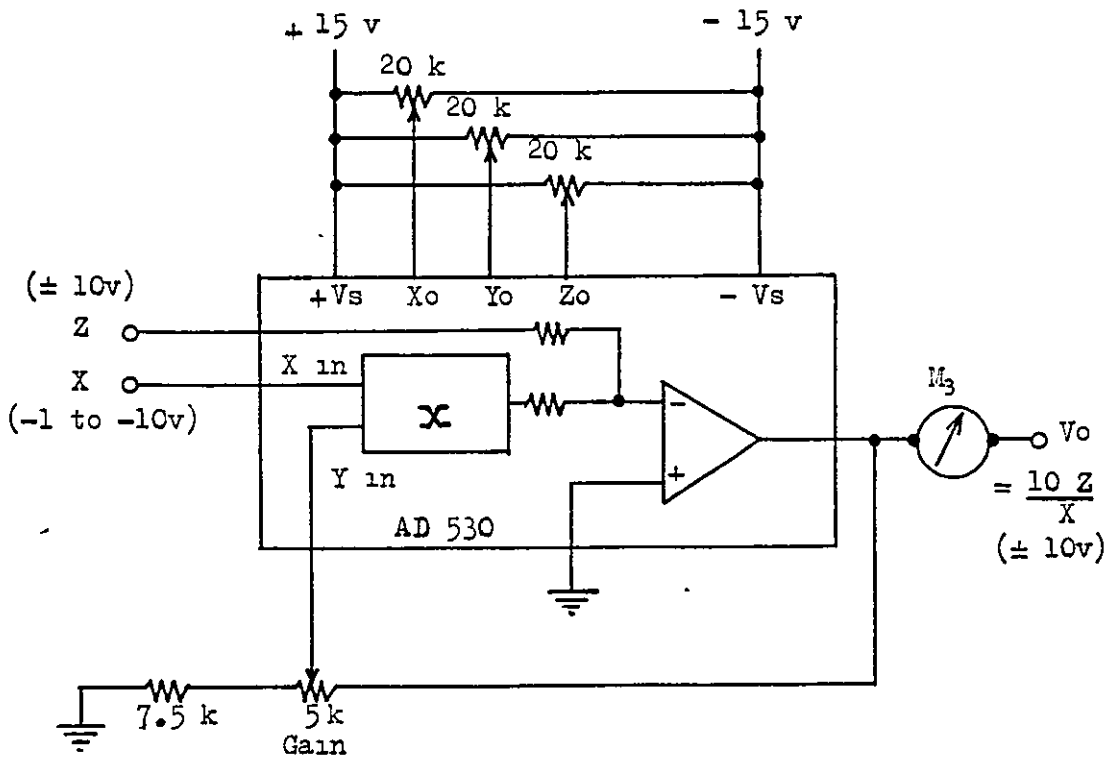

Fig. 91. The Signal Divider.

Section 8.4.1 The Trim Procedure.

Although the trim procedure had been carefully done by the workshop personnel of Albright & Wilson Ltd., and no external controls had been provided, the trim procedure used is given here for completeness.

1) All potentiometers were set to mid-scale.

2) With Z = 0v, Z_o was trimmed to hold V_o constant, as X was varied from - 10 v.D.C., to - 1 v.D.C.

3) With Z = 0v, X = - 10 v.D.C., Y_o was trimmed for 0 v.D.C. out.

4) With Z = X and/or Z = -X, X_o was trimmed for the minimum worst case variation as X varied from - 10 v.D.C. to - 1 v.D.C.

5) Steps 2 and 3 were repeated if step 4 required a large initial adjustment.

6) With Z = X and/or Z = - X, the gain was trimmed for the closest average approach to ± 10 v.D.C. as X was varied from - 10 v.D.C. to - 3 v.D.C.

At + 25°C, X = - 10 v.D.C., Z = ± 10 v.D.C., $Error_{max.}$ = ± 0.2%.

X = - 1 v.D.C., Z = ± 1 v.D.C., $Error_{max.}$ = ± 1.5%.

Section 8.4.2. The Operation of the Signal Divider.

The multiplier ⅀, in the divide mode is used in a feed-back configuration where the Y input controls the feed-back factor. With X at full scale (- 10 v.D.C.) the gain (V_o/Z) becomes unity after trimming. Reducing the X input reduces the feed-back around the operational amplifier by a similar amount and this increases the gain. As X approaches zero, the circuit gain approaches the open loop gain of the operational amplifier producing a proportional degradation in accuracy, noise and frequency response and so limiting the usable dynamic range.

The divide mode error (e_d) is related to the basic multiplier error (e_m) by

$$e_d \cong \frac{10e_m}{X}$$

So that as X approaches zero the divide error, when trimmed as a multiplier, can become very large. However, the divider is limited to operate in two quadrants and the trim procedure given minimizes this error over a 10/1 range in X to give the specification shown above.

The error is acceptable over the range X = -1 to -10 v.D.C. but it is recommended that the range be limited to - 3 to -10 v.D.C. if possible.

Section 8.4.3 Signal Preamplification.

From the previous section it will be appreciated that the signal input X level should ideally be - 3 to -10 v.D.C. and that the signal input Z can vary $\pm$ 10 v.D.C. but must always be less than X.

The signals obtained from the photomultiplier were negative and required amplification to meet the input requirements of the AD 530.

To this end the instrument was provided with two additional operational amplifiers with switched gains of 1, 10, 30, 100 and 300 operating in the non-inverting mode. As shown in Fig. 92 in block form, switched time constants of 1, 2.2 and 4.7 secs. or any combination of these were provided on the inputs to minimise variation in P.M. signal.

In the normal case it was assumed that the background signal would be less than the total signal and the P.M. signal would be fed to the Z input after amplification. However, so long as $Z \leq X$ at the divider input this condition could be reversed by use of the gain available on the P.M. detectors.

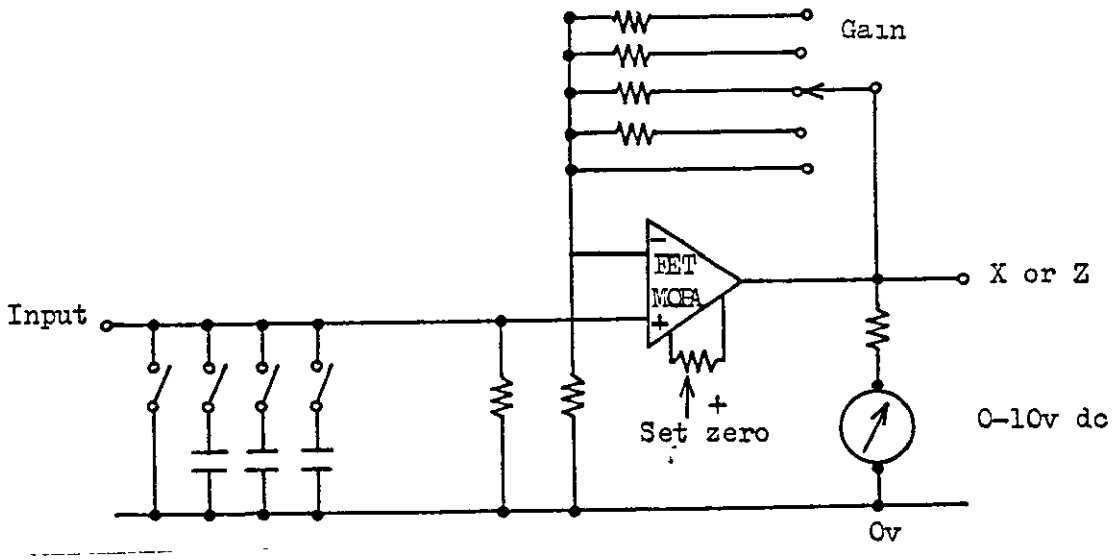

Fig. 92. Preamplifiers.

The output meter (M_3) scaled 0-10 v.D.C. shows the output voltage resulting from the transfer function $\frac{10Z}{X}$ and thus gives a signal proportional to $\frac{10 \times \text{Background}}{\text{Signal} + \text{Background}}$ if the preamplifications employed for X and Z are equal.

This system was used to optimise the operating conditions for the plasmas formed during the comparison of torches which will be described in Chapter 10. It was first decided to investigate the effect of slit orientation on the signal to background ratio.

CHAPTER 9.

ORIENTATION OF THE SPECTROMETER ENTRANCE SLIT WITH REFERENCE TO THE SIGNAL TO BACKGROUND RATIO.

Since the entrance slit of the Polychromator is horizontal it was suspected that this might have a detrimental effect on the signal to background ratio $(\frac{x - b}{b - a})$ obtained when viewing a vertical tail-flame. It might also be expected that the signal peak obtained at optimum viewing position would tend to be sharper than if the plasma was viewed with a vertical slit. All this follows quite naturally since the plasma is, in effect, being traversed by a horizontal aperture 8.3μ x .48 cm which, on the one hand, would admit extraneous background radiation and on the other would result in less averaging. The possible effects of slit orientation were investigated in the following manner.

Section 9.1 Profiling with Quartz Optical Fibres.

A vertical "cribbage" board was constructed with an array of 11 x 37 (407) holes into which a 3 mm bundle of quartz fibres could be fitted. The other end of the fibre optic was placed close to the slits of the Polychromator. This whole arrangement was placed on the optical bar of the Polychromator, as shown in Fig. 93, and on to it was projected an image of the tail-flame, magnified 4.2 times. The profile of this image was obtained by inserting the optical fibre bundle into each hole in turn and obtaining an integrated measure of the radiation, first with a water aerosol injected through the plasma, and then with an aerosol of an element. In this way it was possible to obtain a profile of the ratio $\frac{x - b}{b - a}$.

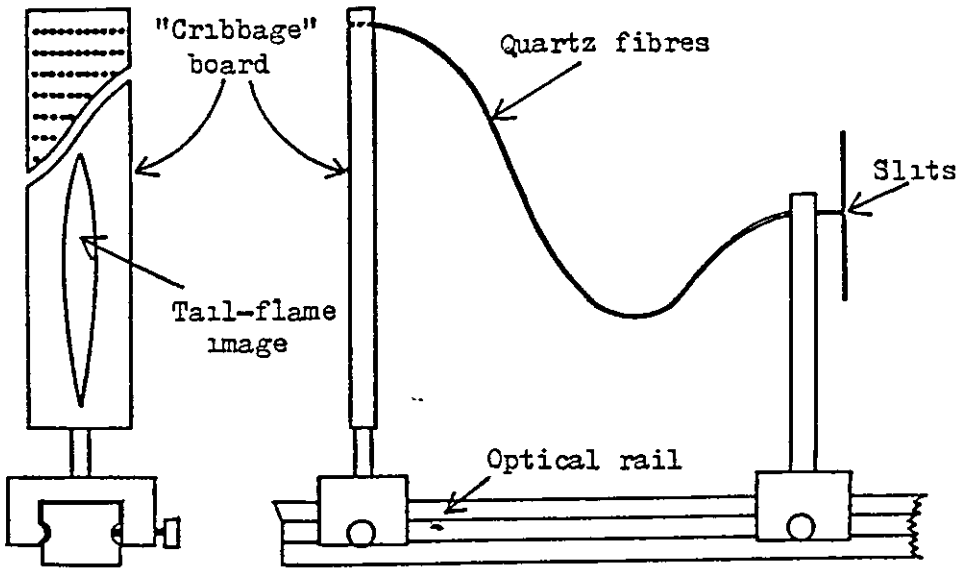

Fig. 93. Profiling of the tail-flame with optical fibres.

Section 9.1.1 Profile of $\frac{x - b}{b - a}$ for the Zinc 3072Å line.

Using a 13,000 ppm solution of zinc nitrate, partially optimised conditions and the quartz fibre arrangement, the profile shown in Table 87 was obtained.

It can readily be seen that if the co-ordinates 6, 24 are taken as the centre a better value of $\frac{x - b}{b - a}$ is obtained for a vertical strip than for a horizontal one. From Fig. 94, which is a plot of $\frac{x - b}{b - a}$ versus the height of the magnified image of the tail-flame, it can be seen that a vertical strip of 7 mm would give the best $\frac{x - b}{b - a}$ ratio. This strip would be not greater than one hole wide which is equivalent to 0.7 mm in the tail-flame.

Table 87. Section of the Profile of $\frac{x - b}{b - a}$ for the Zinc 3072Å line. (Inverted Image).

Row.									
12.		3	4	5	6	7	8	9	10
13.				.74	0.99	0.74	0.44		
14.			5	1.03	1.83	1.03	0.45	0.16	
15.			0.64	1.52	2.57	1.52	0.64	0.20	0.1
16.		.19	1.14	2.21	4.14	2.21	1.14	0.19	0.16
17.		0.36	1.83	3.04	5.43	3.04	1.83	0.36	0.22
18.	35	0.51	2.50	3.89	6.76	3.89	2.50	0.51	0.35
19.	71	0.75	3.35	5.00	8.24	5.00	3.35	0.75	0.71
20.	83	0.87	4.22	5.87	9.76	5.87	4.22	0.87	0.83
21.	0	1.15	4.88	6.39	10.46	6.39	4.88	1.15	0.90
22.	3	1.33	5.27	7.09	11.14	7.09	5.27	1.33	0.9
23.	5	1.67	5.44	7.52	11.36	7.52	5.44	1.67	0.
24.	06	1.75	5.05	7.76	11.37	7.76	5.05	1.75	
25.	.06	1.94	4.85	8.13	11.35	8.13	4.85	1.94	1
26.	1.00	2.19	4.89	7.81	11.16	7.81	4.89	2.19	
27.	.20	2.27	4.84	8.23	10.92	8.23	4.84	2.27	
28.	3	2.69	5.06	8.58	10.61	8.58	5.06	2.69	
29.		2.83	5.18	8.10	10.41	8.10	5.18	2.83	
30.		33	5.53	7.95	10.24	7.95	5.53	2.83	1
31.		7	5.41	7.97	9.85	7.97	5.41	2.67	1
32.			5.29	8.36	9.58	8.12	5.29	2.58	
33.			.00	8.65	9.33	8.35	5.00	2.5	
34.				8.57	8.88	8.57	4.93	2	
35.					.75	8.62	4.85		
36.						.92	4.		

Top of plasma 3.10 cm from base.

4.57 cm. from base of plasma.

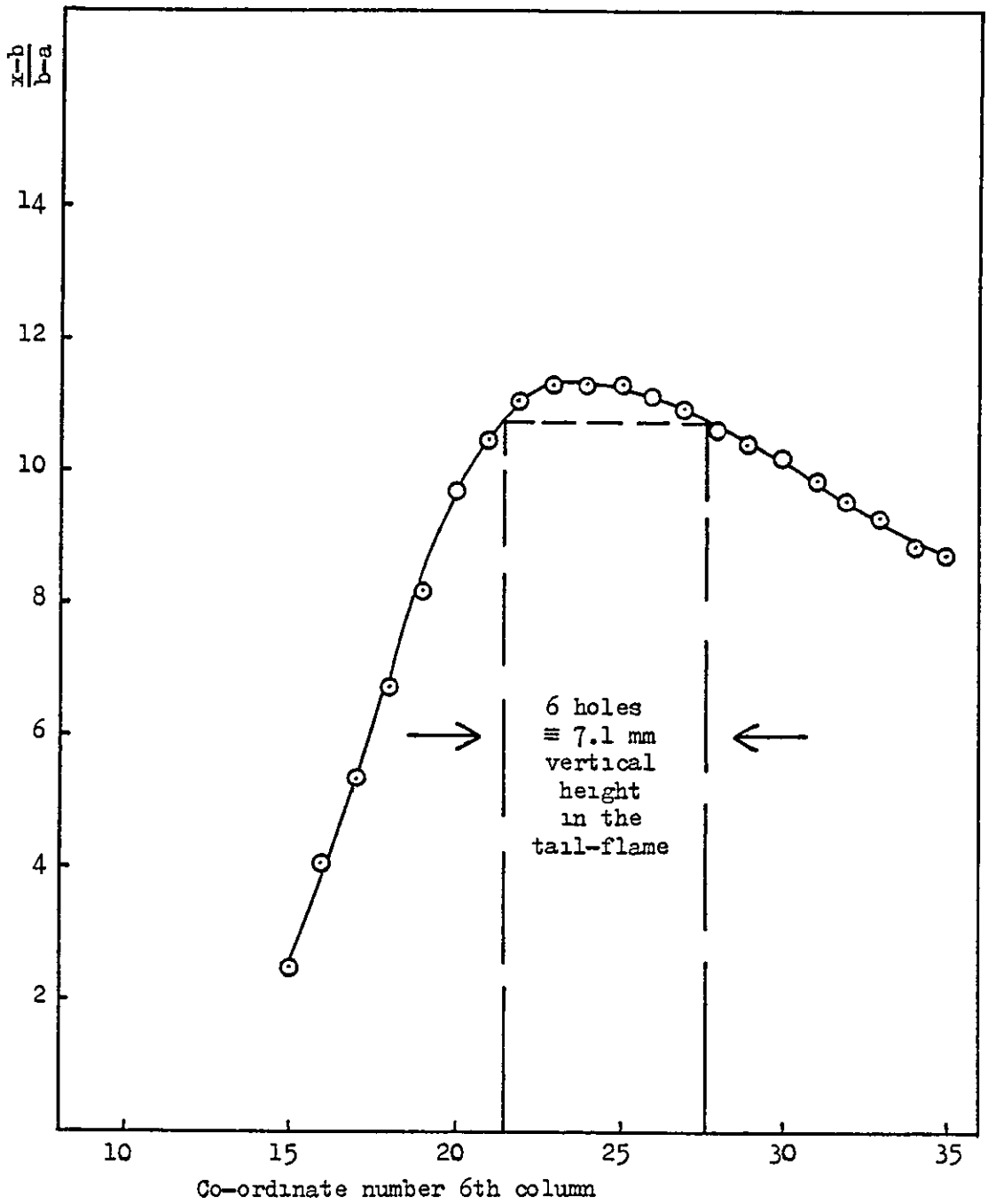

Fig. 94. Plot of $\frac{x-b}{b-a}$ against the vertical height of the magnified image of the tail-flame.

Section 9.2 Use of the Mechanical Wedge to Increase $\frac{x - b}{b - a}$ Ratio.

As confirmation of the previous experiments it was decided to progressively reduce the length of the horizontal slit of the Polychromator using the mechanical wedge (Section 2.7). Again the 13,000 ppm zinc nitrate was used and the 3072Å line. The normal lens was used throwing a 4.7 times magnified image on to the slit. After partial optimisation the optimum height of viewing was found to be 4.53 cm from the base of the plasma (the previous experiment predicted 4.57 cm).

Section 9.2.1 Effect of Reducing the Slit Length on the Ratio $\frac{x - b}{b - a}$ for the Zinc 3072Å line.

When the length of the horizontal slit was progressively reduced, the $\frac{x - b}{b - a}$ ratio increased as is shown in Table 88 and Fig. 95.

Table 88. Increase of the $\frac{x - b}{b - a}$ Ratio With Decreasing Slit Length.

Slit Length mm.	$\frac{x - b}{b - a}$
20.0	7.4
17.5	7.9
15.0	8.1
12.5	9.3
10.0	10.5
7.5	12.4
5.0	13.9
4.0	14.1
3.0	14.5
2.0	14.7
1.0	14.2

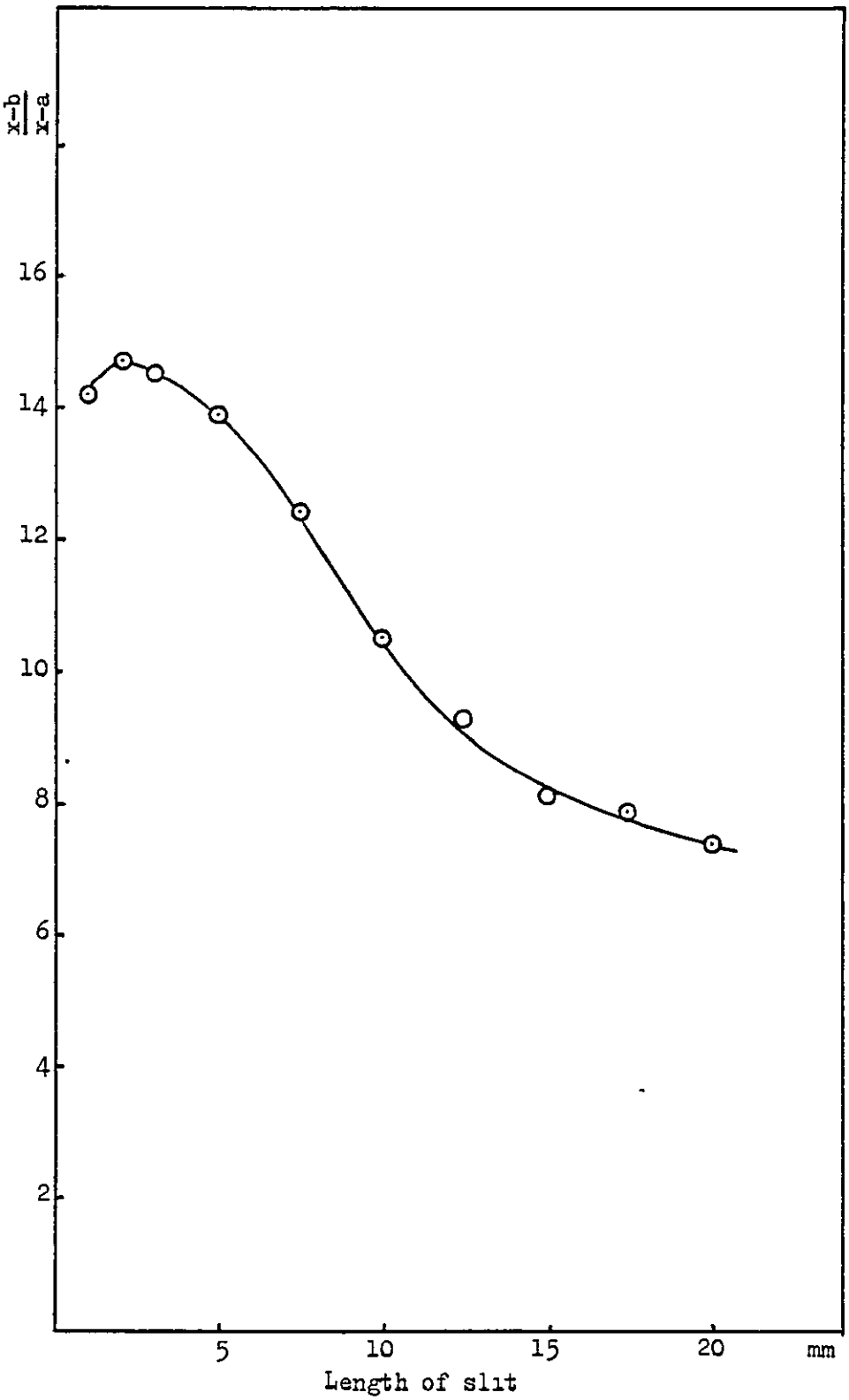

Fig. 95. Plot of $\frac{x-b}{x-a}$ against slit length.

It can be seen from Fig. 95 that a slit length of under 3.25 mm, corresponding to 0.69 mm in the plasma, would give the highest average ratio for $\frac{x - b}{b - a}$.

Section 9.3 Rotation of the Tail-flame Image.

The previous experiments have shown that a better value of the ratio of $\frac{x - b}{b - a}$ should be obtained by viewing the tail-flame of the plasma with a vertical slit. An alternative would be to rotate the image of the tail-flame through 90°, with a Dove prism, and view with a horizontal slit. In the case of the Polychromator this was the only practicable thing to do and a glass Dove prism was obtained.

Section 9.3.1 Results Obtained with the Dove Prism for a Number of Visible Lines.

In Chapter 10 there will be reported the results of optimisation experiments carried out with the equipment described in Section 8.4. However, most of the visible lines examined and described in Chapter 10 were of vertical and horizontal images of the tail-flame viewed with a horizontal slit and it seems convenient to list some of these here as a demonstration of the effectiveness of using, in effect, a vertical slit for plasma spectroscopy. The results obtained are given in Table 89. Plasma operating conditions are not given as they have no relevance here.

Table 89. The Effect of Slit Orientation on the Ratio $\frac{x - b}{b - a}$. Use of Dove Prism.

Element.	Conc. p.p.m.	Line Å	Type of Plasma.	Vertical Image.	Horizontal Image.
Cs	1000	4555	S/Ar/Ar	53.0 ± 2	380 ± 34
Cs	1000	4555	G/Ar/Ar	16.7 ± 0.5	47.7 ± 1.7
Cs	1000	4555	G/Ar/Ar	170 ± 11	842 ± 360
Ba	1	4554	S/Ar/Ar	59.1 ± 0.5	110 ± 1
Ba	1	4554	G/Ar/Ar	97 ± 1.5	209 ± 6
Ba	1	4554	G/Ar/Ar	418 ± 11	716 ± 38
Al	1000	3961	S/Ar/Ar	16,842 ± 400	35,151 ± 1389
Na	1	5896	S/Ar/Ar	142 ± 15	221 ± 25
Na	1000	5896	S/Ar/Ar	21,751 ± 2400	27,245 ± 3000
Na	1	5896	G/Ar/Ar	70 ± 5	67 ± 3
Na	1	5896	G/Ar/N_2	350 ± 55	480 ± 92
Na	1	5896	S/Ar/Ar	174 ± 38	205 ± 12

It can be seen from Table 89 that there is in most cases a significant improvement in the ratio of $\frac{x - b}{b - a}$ when the tail-flame is viewed longtitudinally. Sodium is an exception in that the difference is probably not significant. However, it will be shown later that the prism used absorbs a proportion of 5896Å radiation.

CHAPTER 10.

A COMPARISON OF PLASMAS VARIOUSLY PRODUCED.

Having arrived at what appeared to be a suitable system for optimisation and the equipment to achieve it (Chapter 8) the stage seemed set to make the comparison of high and low power systems which is the prime object of this research project. Since the usual torch used in low power systems is that of Scott, (Fig. 21, Ref. 49) one was procured. It had an additional plasma gas entry in order to check the optimum plasma gas flow, although it is claimed that the torch operates effectively with only one gas flow apart from the aerosol. It was decided to operate this on argon only, since this is the normal way of running the torch, (subsequent work showed that it could be run with a nitrogen coolant, but with nitrogen it was very temperamental and demanded a skilled operator to function at all). The other torch used was that of Greenfield (Fig. 25, Ref. 2., and Figs. 27, 28) which had been used for the work to date. This torch is normally used at high power with a nitrogen coolant but could be operated at low power (and high power) with either argon or nitrogen as coolant. In the work that follows both coolants were used.

Since the Scott torch was reputed[49] to require a low aerosol flow with a high liquid uptake the normal Unicam nebuliser (Section 2.4) was replaced with a Meinhard T-230-A3 nebuliser which is a concentric type uptaking 3.5 ml/min. at an argon flow of 1 litre/min. at 30 lbs/sq.in.

It was, however, operated at 150 lbs/sq.in. in order that higher gas flows could be obtained for the Greenfield torch. The nebuliser is illustrated in Fig. 96.

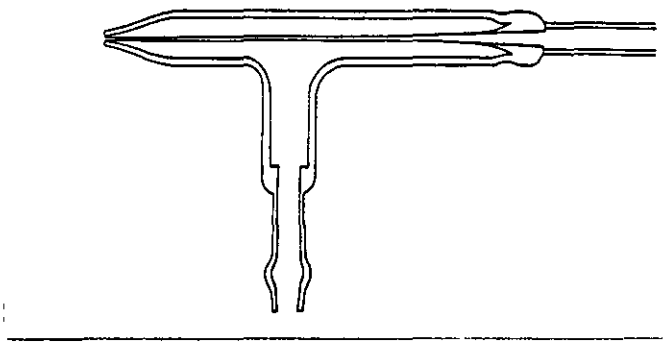

Fig. 96. Meinhard Nebuliser.

Since the Scott torch is normally used with the Scott spray chamber (Fig. 21, Ref. 49) and the Greenfield torch is used with the cyclone spray chamber, shown in Fig. 97, tests were carried out to

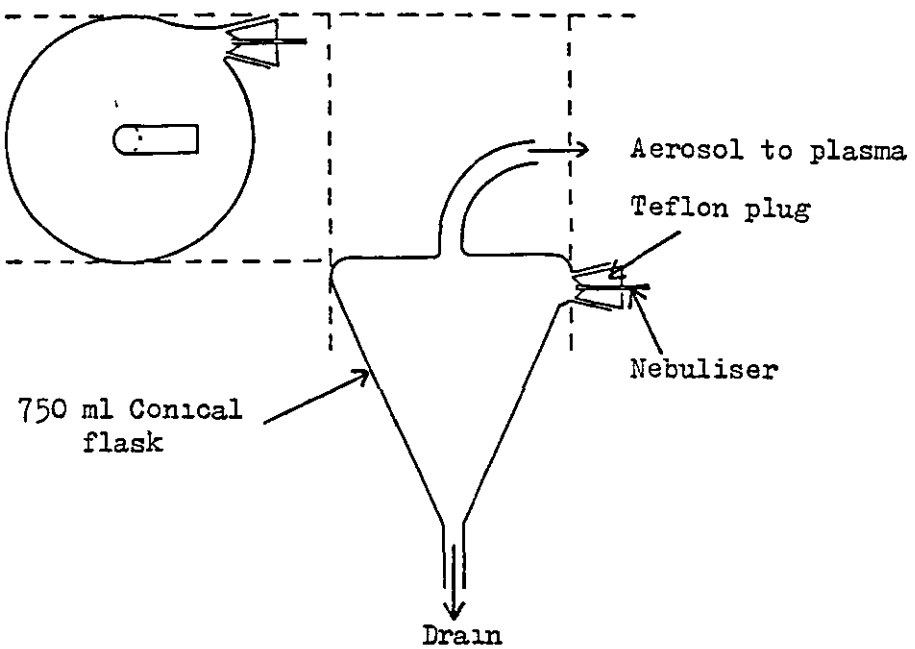

Fig. 97. Cyclone Spray Chamber.

see which, if either, was more effective. The author was pleasantly surprised to find the cyclone chamber, if anything, gave a higher $\frac{x - b}{b - a}$ ratio, notwithstanding the fact that the Scott chamber was mounted in the usual manner directly under the torch and the cyclone chamber was connected to the torch by 35 cm of 1.2 cm bore plastic tubing. Typical figures obtained are shown in Table 90.

Table 90. A Comparison of the $\frac{x - b}{b - a}$ Ratios Achieved with Different Spray Chambers. Na 5896Å line. 1 ppm NaCl Optimised Operating Conditions.

	$\frac{x - b}{b - a}$
Scott Torch Mounted Directly to Scott Spray Chamber.	100 ± 12
Scott Torch Joined by 35 cm of 1.2 cm (I.D.) Plastic Tubing to Scott Spray Chamber.	130 ± 18
Scott Torch Joined by 35 cm of 1.2 cm (I.D.) Plastic Tubing to Cyclone Spray Chamber.	205 ± 12

Since the externally connected cyclone chamber is more convenient to use, and no discernable delay was experienced during sample changing, it was decided to use the Meinhard nebuliser with the cyclone spray chamber throughout the experiments.

The Dove prism was used for all the visible lines since it served the dual purpose of rotating the image and filtering out the second order U.V. background thus enhancing the $\frac{x - b}{b - a}$ ratio. It was known that it also attenuated some of the higher wavelength signals but the overall effect was still to improve the $\frac{x - b}{b - a}$ ratio and it was judged permissible to use it since it was common to all comparisons.

Section 10.1 Optimisation Using the Signal Divider.

Time would only permit a limited number of elements being investigated and these were chosen so as to cover a wide range of concentrations and physical properties. Table 91 is thought to represent a reasonable choice. It was not possible to examine shorter wavelengths on the Polychromator.

Table 91. Physical Data of Elements Examined.

Element.	State.	Wavelength Å	Transition Prob. 10^8/sec.	Ex.Pot. e.v.	Ion Pot. e.v.	Conc. ppm.	Norm. Temp. * °K
Na	U_1	5896	1.8	2.10	5.14	1000	3,700
Na	U_1	5896	1.8	2.10	5.14	1	2,700
Cs	U_3	4555	1.4	2.70	3.90	1000	2,600
Ba	V_1	4554	0.9	2.71	5.20	1	11,000
Al	U_1	3961	1.3	3.10	6.00	1	3,100
Al	U_1	3961	1.3	3.10	6.00	1000	4,400
V	V_1	3093	4.3	4.38	6.74	1000	14,000
Zn	U	3076	.013	4.01	9.40	1000	10,100
Zn	U	3072	2.0	8.01	9.40	1000	13,000
Al	V_2	2816	1.2	11.71	5.99	1000	18,500

* corrected for partial pressure, using an in-house computer program.

Section 10.1.1 Sodium Results with the Scott Torch.

The optimisation cycles, conditions and $\frac{x - b}{b - a}$ ratios for sodium are shown in Table 92. In this and all subsequent examples the final signals are obtained by integration; the intermediate values are analogue signals from the signal divider meter readings scaled to the final integration value. x represents the gross signal, b the gross background and a the dark current, as before.

Table 92. Optimisation Cycles. Signal Divider
1 p.p.m. Sodium as the Chloride 5896Å line.
Vertical Image. Scott Torch. S.C.15 Generator.

Number of Cycle.	1	2	3
Power kW	1.08	0.56	0.63
Plasma Gas Flow ℓ/min.	0.0	1.6	2.1
Nebuliser Gas Flow ℓ/min.	1.0	2.2	2.7
Coolant Gas Flow ℓ/min.	15.0	19	20.0
Viewing Height above Base cm.	2.8	4	4.2
Length of Plasma cm.	n.d.	n.d.	3.0
x	965	1007	1256.5 (mean of 2) *
b	422	17	17.7 (σ = 2.3. 10 det.) *
a	9	9	9.0 (σ = 1.3. 10 det.) *
$\frac{x - b}{b - a}$	1.3	124	142 $\pm$ 15

* Gain 10. 10 sec. exposure.

Cycle number three conditions were used as the starting point for an optimisation with the image rotated at 1 ppm concentration, and for 1000 ppm with the image vertical and horizontal. No change in optimum conditions was found, so that the conditions of cycle three were optimum for all cases investigated. The results are shown in Table 93.

Table 93. Optimised Values of x, b and a for vertical and horizontal Images of 1 ppm and 1000 ppm. Sodium 5896Å line Radiation.

	1 ppm Na Vertical Image.	1 ppm Na Horizontal Image.	1000 ppm Na Vertical Image.	1000 ppm Horizontal Image.
x	1256.5 *	1566 *	228,400 **	258,840 **
b	17.7	16	17.0	16.0
a	9.0	9	6.5	6.5
$\frac{x-b}{b-a}$	142	221	21,751	27,245
σ	$\pm$ 15	$\pm$ 51	$\pm$ 2,400	$\pm$ 3,000

* Gain 10. 10 sec.exp. ** Gain 4. 100 sec. exp.

Section 10.1.2 Sodium Results with the Greenfield Torch.

The experiment with 1 ppm concentration was then repeated using the Greenfield torch running first with an argon coolant and then with a nitrogen coolant with vertical and horizontal images and also without any filter or prism. The results of these experiments are shown in Tables 94 to 97.

It is interesting to note that with both the Scott and Greenfield torches there is no significant difference between the vertical and horizontal images, but if these results are compared with the results from the vertical unfiltered image one can deduce that most of the background is second order ultra-violet which the glass has filtered out. Unfortunately the glass prism also absorbs a significant proportion of the sodium radiation.

Table 94. Optimisation Cycles. Signal Divider.
1 ppm Sodium as the Chloride. 5896Å line.
Vertical Image. Greenfield Torch. Argon Coolant.
SC 15 Generator.

Number of Cycle.	1	2	3	
Power kW.	1.23†	1.52†	1.51†	
Plasma Gas Flow ℓ/min.	1.5	1.3	0.5	
Nebuliser Gas Flow ℓ/min.	3.4	3.4	3.3	
Coolant Gas Flow ℓ/min.	24.0	20.0	20.0	
Viewing Height above Base cm.	4.1	5.5	5.7	
Length of Plasma cm.	n.d.	n.d.	3.6	
x	370	778	778	(mean of 2)*
b	24.9	21.5	20.4	(σ = 1.8. 10 det.)*
a	9.6	9.6	9.6	(σ = 1.0. 10 det.)*
$\frac{x-b}{b-a}$	23	64	70 ± 5	

† The power was the lowest obtainable throughout and therefore in a formal sense this is not a true optimisation. This minimum power is strongly dependent on the gas flows.

* Gain 10. 10 sec. exp.

Table 95. Optimised Values† of x, b and a for Vertical and Horizontal Images of 1 ppm Sodium 5896Å line Radiation.

	Vertical Image.	Horizontal Image.	Without Filter.
x	778*	852*	1057*
b	20.4	22.0	109
a	9.6	9.6	9.6
$\frac{x-b}{b-a}$	70	67	9.5
σ	± 5	± 3	± 0.5

* Gain 10. 10 sec. exp.

† Table 94. Cycle 3.

Table 96. Optimisation Cycles. Signal Divider.
1 ppm Sodium as the Chloride. 5896Å line.
Vertical Image. Greenfield Torch. Nitrogen Coolant.
SC 15 Generator.

Number of Cycle.	1	2	3	
Power kW	0.91	0.82†	0.81†	
Plasma Gas Flow ℓ/min.	6.5	5.2	5.2	
Nebuliser Gas Flow ℓ/min.	3.5	3.5	3.4	
Coolant Gas Flow ℓ/min.	7.0	7.0	7.0	
Viewing Height above Base cm.	4.0	4.0	4.0	
Length of Plasma cm.	n.d.	n.d.	1.2	
x	1462	1220	1342	(mean of 2)*
b	13.3	12.4	12.3	(σ=1.06. 10 det.)*
a	8.5	8.5	8.5	(σ = 1.6. 10 det.)*
$\frac{x-b}{b-a}$	300	310	350 ± 55	

† The power was the lowest obtainable throughout and therefore in a formal sense this is not a true optimisation.

* Gain 10. 10 sec. exp.

Table 97. Optimised Values† of x, b and a for Vertical and Horizontal Images of 1 ppm Sodium 5896Å line Radiation.

	Vertical Image.	Horizontal Image.	Without Filter.
x	1342	1598	1839
b	12.3	11.8	46.1
a	8.5	8.5	8.5
$\frac{x-b}{b-a}$	350	480	48
σ	55	92	1.5

† Table 96. Cycle 3.

Section 10.1.3 Sodium Results with the Scott Torch and a New Meinhard Nebuliser.

It had been noticed that the optimised operating conditions for the Scott torch were different from those stated in many papers, e.g. Ref. 4 particularly the nebuliser gas flow. However, it was found that at the time of the torch comparison the particular Meinhard nebuliser in use had abraded to such an extent that it was passing 1.7 ℓ/min of gas at 30 lbs/sq.in. with a liquid uptake of only 1.2 ml/min. This did not invalidate the comparison but it could account for the differing flow-rate. Accordingly a new Meinhard nebuliser, properly standardised and certificated, was obtained and a new optimisation was done on the Scott torch. The results obtained are shown in Tables 98 and 99.

Table 98. Optimisation Cycles. Signal Divider. 1 ppm Sodium as the Chloride. 5896Å line. Horizontal Image. Scott Torch. New Meinhard Nebuliser. Argon Coolant. SC 15 Generator.

Number of Cycle.	1	2	3	4	5	6	7	
Power kW	1.08	0.79	0.84	0.89	0.95	1.0	1.0	
Plasma Gas Flow ℓ/min.	0.0	2.0	2.0	1.4	1.1	0.9	0.2	
Nebuliser Gas Flow ℓ/min.	1.0	1.0	1.8	2.1	2.2	2.4	2.2	
Coolant Gas Flow ℓ/min.	15.0	16.0	20.0	21.5	21.5	23.0	22.0	
Viewing Height above Base cm.	3.1	5.0	5.0	5.4	5.5	5.7	5.6	
Length of Plasma cm.	n.d.	n.d.	n.d.	n.d.	n.d.	n.d.	3.4	
x	531	175	819	887	1065	1326	1614	(σ=11. 10 det.)
b	138	17.3	17.3	15.8	15.9	17.3	17.4	(σ=0.43. 10 det.
a	9.6	9.6	9.6	9.6	9.6	9.6	9.6	(σ=0.16. 10 det.
$\frac{x-b}{b-a}$		3±0.2	20±4	104±25	140±40	166±40	170±40	205±12

Table 99. Optimised Values of x, b and a for Vertical and Horizontal Images of 1 ppm Sodium 5896Å line Radiation. New and Old Meinhard Nebulisers

	New Nebuliser.		Old Nebuliser.	
	Vertical Image.	Horizontal Image.	Vertical Image.	Horizontal Image.
x	1129	1614.0	1256.5	1566
b	16	17.4	17.7	16
a	9.6	9.6	9.0	9.0
$\frac{x - b}{b - a}$	174	205	142	221
σ	38	12	15	51

In all probability there are no significant differences between the values of $\frac{x - b}{b - a}$ for the last four cycles of Table 98 and the second column of Table 93. (There are, however, differences between the net signals of the last four cycles of Table 98). The nebuliser gas flow is inclined to be lower with the new nebuliser but was still higher than reported in the literature.

Section 10.1.4 Sodium Results with the Greenfield Torch and a New Meinhard Nebuliser.

A new optimisation, starting with the conditions of cycle number 3, Table 94, was then carried out using the new nebuliser on the Greenfield torch with argon as the coolant. The results are shown in Table 100.

Table 100. Optimisation Cycles. Signal Divider. 1 ppm Sodium as the Chloride. 5896Å line. Horizontal Image. Greenfield Torch. New Meinhard Nebuliser. Argon Coolant. S.C.15 Generator.

Number of Cycle.	1	2	3	4
Power kW	1.44†	1.39†	1.39†	1.39†
Plasma Gas Flow ℓ/min.	0.25	0.00	0.00	0.50
Nebuliser Gas Flow ℓ/min.	3.2	3.2	2.3	2.2
Coolant Gas Flow ℓ/min.	26.0	24	24	24
Viewing Height above Base cm.	7.7	5.7	5.3	5.1
Length of Plasma cm.	n.d.	n.d.	n.d.	4.1
x	94	224	378	499.6 (σ = 2.8. 10 det.)*
b	16	19	22	22.0 (σ = 1.0. 10 det.)*
a	12.5	12.5	12.5	12.5 (σ = 0.5. 10 det.)*
$\frac{x - b}{b - a}$	22	32	37	50±6

† The power was the lowest obtainable throughout and therefore in a formal sense this is not a true optimisation.

* Gain 10. 10 sec. exp.

Again there are probably no significant differences between the values of $\frac{x - b}{b - a}$ for the last three cycles of optimisation in Table 100 and the last two cycles in Table 94. There are, however, some differences between the net signals (x - b) shown in the second column of Table 95 and the last three cycles shown in Table 100. The new nebuliser might appear to give less sensitivity than the old but the higher dark current could mean a falling off in performance of the P.M. tube. It must be emphasised that in neither case are the conditions truly optimised.

The optimisation was then repeated using nitrogen as the coolant with the conditions of cycle number 3, Table 96 as the starting condition. The experiment had to be abandoned after the first cycle as the indicated reduction in plasma gas flow repeatedly extinguished the plasma. The results obtained for the first cycle are shown in Table 101.

Table 101. Optimisation Cycles. Signal Divider. 1 ppm Sodium as the Chloride. 5896Å line. Horizontal Image. Greenfield Torch. New Meinhard Nebuliser. Nitrogen Coolant. S.C.15 Generator.

Number of Cycle.	1	2	
Power kW.	0.8		
Plasma Gas Flow ℓ/min.	7.0		
Nebuliser Gas Flow ℓ/min.	2.2		
Coolant Gas Flow ℓ/min.	7.0		Experiments abandoned as the indicated reduction in plasma gas flow would not permit the running of the torch.
Viewing Height above Base cm.	3.8		
Length of Plasma cm.	0.6		
x	538		
b	17.7		
a	12.3		
$\frac{x - b}{b - a}$	96		

Section 10.1.5 Summary of the Results Obtained on Both Torches and Nebulisers for the Sodium 5896Å line.

The experimental results for sodium of Section 10 are summarised in Table 102 for the two nebulisers now designated No. 1 (old) and No. 2 (new).

Table 102. Optimised Operating Conditions and Values of x, b and a. 1 ppm Sodium as the Chloride. 5896Å line. Horizontal Image.

	Nebuliser No. 1.			Nebuliser No. 2.		
Torch	Greenfield	Scott	Greenfield	Greenfield	Scott	Greenfield
Coolant	N_2	Ar	Ar	N_2	Ar	Ar
Power kW	0.81†	0.62	1.51†	0.80	1.00	1.39†
Plasma Gas Flow ℓ/min.	5.2	2.1	0.5	7.0††	0.2	0.5
Nebuliser Gas Flow ℓ/min.	3.4	2.7	3.3	2.2	2.2	2.2
Coolant Gas Flow ℓ/min.	7.0	20.0	20.0	7.0	22.0	24.0
Viewing Height above Base cm.	4.0	4.2	5.7	3.8	5.6	5.1
Length of Plasma cm.	1.2	3.0	3.6	0.6	3.4	4.1
x	1598	1566	852	538	1614	499.6
b	11.8	16	22	17.7	17.4	22
a	8.5	9	9.6	12.3	9.6	12.5
$\frac{x - b'}{b - a}$	480±92	221±51	67±3	96±	205±12	50±6

† The power was the lowest power obtainable with the indicated gas flows and therefore, in a formal sense, this is not a true optimisation.

†† The plasma gas flow was the lowest possible and therefore, in a formal sense, this is not a true optimisation.

Section 10.1.6 Caesium Results with the Scott Torch and Nebuliser No. 1.

The next element to be investigated was caesium. It was first investigated using nebuliser No. 1. Table 103 gives the results obtained on the Scott torch.

Table 103. Optimisation Cycles. Signal Divider 1000 ppm Caesium as the Nitrate. 4555Å line. Vertical Image. Scott Torch. Nebuliser No. 1. S.C.15 Generator.

Number of Cycle.	1	2	3	4	
Power kW.	1.08	0.66	0.58	0.57	
Plasma Gas Flow ℓ/min.	0.0	1.0	1.4	1.9	
Nebuliser Gas Flow ℓ/min.	3.2	2.5	2.5	2.6	
Coolant Gas Flow ℓ/min.	15.0	16.0	19.0	20.0	
Viewing Height above Base cm.	2.8	3.4	3.6	3.8	
Length of Plasma cm.	n.d.	n.d.	n.d.	2.4	
x	1194	1072	1108	1132	(mean of 2)*
b	500	44	32	28.1	(σ = 0.5. 10 det.)*
a	7.3	7.3	7.3	7.3	(σ = 0.3. 3 det.)*
$\frac{x - b}{b - a}$	1.4±0.1	28±7	43±10	53±2	

* Gain 11. 10 sec. exp.

The last set of conditions was used as the start of an optimisation with the image rotated. No shifts were found and both results are shown in Table 104.

Table 104. Optimised Values† of x, b and a for Vertical and Horizontal Images of 1 p.p.m. Caesium 4555Å line Radiation.

	Vertical Image.	Horizontal Image.
x	1132	1532
b	28.1	11
a	7.3	7
$\frac{x-b}{b-a}$	53	380
σ	2	34

† Table 103. Cycle No. 4.

Section 10.1.7 Caesium Results with the Greenfield Torch and Nebuliser No. 1.

The experiments of Section 10.1.4 were then repeated with the Greenfield torch running first with an argon and then with a nitrogen coolant. The results obtained are shown in Tables 105 to 108.

Table 105. Optimisation Cycles. Signal Divider 1000 p.p.m. Caesium as the Nitrate 4555Å line. Vertical Image. Greenfield Torch Nebuliser No. 1. Argon Coolant. S.C.15 Generator.

Number of Cycle	1	2	3	4	5	
Power kW	1.42	1.5	1.5†	1.5†	1.5†	
Plasma Gas Flow ℓ/min.	6.5	6.3	5.3	2.2	1.5	
Nebuliser Gas Flow ℓ/min.	3.1	3.3	3.5	3.5	>3.6	
Coolant Gas Flow ℓ/min.	19.0	19.0	21.0	21.0	21.0	
Viewing Height above base cm.	6.5	6.1	6.3	6.3	6.3	
Length of Plasma cm.	n.d.	n.d.	n.d.	n.d.	3.7	
x	143	242	239	301	301	(mean of 2)*
b	38.4	38.4	27.3	27.3	23.6	(σ=0.37. 10 det.)
a	7.0	7.0	7.0	7.0	7.0	(σ=0.3. 4 det.)
$\frac{x-b}{b-a}$	3.3±0.4	6.5±0.8	10.4±1.2	13.5±1.5	16.7±0.5	

† Minimum power obtainable with these gas flows. Therefore, strictly not a true optimisation.

* Gain 11. 10 sec.exp.

The final readings obtained with the unrotated image were used for an optimisation with the image rotated. Surprisingly a new and genuine (i.e. power was not the least obtainable) optimisation was found as is shown in Table 106. It must be said that, although the operating conditions are definitely different, there is no significant differences between the ratio of $\frac{x - b}{b - a}$ which are obtained for each cycle. However, there is a difference between the values of x and between the values of $\frac{x - b}{b - a}$ for the two images.

Table 106. Optimisation Cycles. Signal Divider 1000 p.p.m. Caesium as the Nitrate 4555Å line. Horizontal Image. Greenfield Torch. Nebuliser No.1. Argon Coolant. S.C.15 Generator.

Number of Cycle.	1	2	3	
Power kW	1.5†	1.57	1.57	
Plasma Gas Flow ℓ/min.	1.5	0.1	0.1	
Nebuliser Gas Flow ℓ/min.	>3.6	3.5	3.4	
Coolant Gas Flow ℓ/min.	21.0	17.0	17.0	
Viewing Height above base cm.	6.3	5.7	5.5	
Length of Plasma cm.	n.d.	n.d.	3.9	
x	307.5	605	703	(σ=8. 4 det.)*
b	14.5	19.6	21.3	(σ=0.42. 3 det.)*
a	7.0	7.0	7.0	(σ=0.3. 4 det.)*
$\frac{x - b}{b - a}$	39.1±4	46.5±4	47.7±1.7	

* Gain 11. 10 sec. exp. † Minimum power.

No changes in optimisation conditions were found for the vertical and horizontal images when using the nitrogen cooled torch. These are shown in Tables 107 and 108.

Table 107. Optimisation Cycles. Signal Divider. 1000 p.p.m. Caesium as the Nitrate 4555Å line. Vertical Image. Greenfield Torch. No.1 Nebuliser. Nitrogen Coolant. S.C.15 Generator.

Number of Cycle.	1	2	3	4	5	
Power kW	1.69	0.9†	0.81†	0.79†	0.79†	
Plasma Gas Flow ℓ/min.	8.4	6.5	4.7	4.7	4.7	
Nebuliser Gas Flow ℓ/min.	3.2	3.2	3.1	3.2	3.2	
Coolant Gas Flow ℓ/min.	7.0	17.0	18.0	18.5	18.5	
Viewing Height above base cm.	4.3	5.3	4.7	4.7	4.7	
Length of Plasma cm.	n.d.	n.d.	n.d.	n.d.	0.7	
x	465	326	645	609	657.5	(mean of 2)*
b	63	13	11.7	10.5	10.9	(σ = 0.23. 10 det.)*
a	7.1	7.1	7.1	7.1	7.1	(σ = 0.09. 10 det.)*
$\frac{x-b}{b-a}$	7.2±0.7	53±9	138±27	176±44	170±11	

† Minimum Power obtainable.

* Gain 11. 10 sec. exp.

Table 108. Optimised Values† of x, b and a for Vertical and Horizontal Images of 1 p.p.m. Caesium 4555Å line Radiation.

	Vertical Image.	Horizontal Image.
x	657.5	766
b	10.9	8
a	7.1	7.1
$\frac{x-b}{b-a}$	170	842
σ	11	360*

* High value due to small value of b - a and rather inadequate statistics.

† Table 107. Cycle No.5.

Section 10.1.8 Caesium Results with the Scott Torch and Nebuliser No. 2.

The experiments of Section 10.1.6 were repeated using No.2 nebuliser and the results are shown in Table 109.

Table 109. Optimisation Cycles. Signal Divider. 1000 p.p.m. Caesium as the Nitrate. 4555Å line. Horizontal Image. Scott Torch. Nebuliser No. 2. S.C.15 Generator.

Number of Cycle.	1	2	
Power kW	0.55	0.66	
Plasma Gas Flow ℓ/min.	1.90	0.0	
Nebuliser Gas Flow ℓ/min.	2.60	1.7	
Coolant Gas Flow ℓ/min.	20.0	20.0	
Viewing Height above Base cm.	3.5	3.7	
Length of Plasma cm.	n.d.	2.7	
x	337	998	(σ = 19.6. 5 det.)*
b	11.4	14.9	(σ = 0.3. 10 det.)*
a	7.3	7.3	(σ = 0.15. 10 det.)*
$\frac{x - b}{b - a}$	79	129±6	

* Gain 11. 10 sec. exp.

Section 10.1.9 Caesium Results with the Greenfield Torch and Nebuliser No. 2.

The experiments of Section 10.1.7 were repeated using No. 2 nebuliser and the results are shown in Tables 110 and 111.

Table 110. Optimisation Cycles. Signal Divider.
1000 p.p.m. Caesium as the Nitrate. 4555Å line.
Horizontal Image. Greenfield Torch. Nebuliser No.2.
Argon Coolant. S.C.15 Generator.

Number of Cycle.	1	2	
Power kW.	1.58	1.42†	
Plasma Gas Flow ℓ/min.	0.10	0.0	
Nebuliser Gas Flow ℓ/min.	3.40	2.7	
Coolant Gas Flow ℓ/min.	22.00	22.00	
Viewing Height above Base cm.	6.2	6.2	
Length of Plasma cm.	n.d.	4.1	
x	583	698	(σ = 2.5. 2 det.)*
b	17	17.1	(σ = 0.2. 10 det.)*
a	9.9	9.9	(σ = 0.1. 10 det.)*
$\frac{x-b}{b-a}$	79	95±3	

† Minimum power obtainable.

* Gain 11. 10 sec. exp.

Table 111. Optimisation Cycles. Signal Divider.
1000 p.p.m. Caesium as the Nitrate. 4555Å line.
Horizontal Image. Greenfield Torch. Nebuliser No.2.
Nitrogen Coolant. S.C.15 Generator.

Number of Cycle.	1	2	3	
Power kW.	1.26	1.09	0.91†	
Plasma Gas Flow ℓ/min.	6.0	5.00	4.50†	
Nebuliser Gas Flow ℓ/min.	3.2	2.8	2.80††	
Coolant Gas Flow ℓ/min.	10.0	8.0	8.0	
Viewing Height above Base cm.	4.4	4.4	4.4	
Length of Plasma cm.	n.d.	n.d.	0.8	
x	721	853	974	(σ = 10. 2 det.)*
b	17	15	12.7	(σ = 0.2. 10 det.)*
a	9.9	9.9	9.9	(σ = 0.1. 10 det.)*
$\frac{x-b}{b-a}$	99	164	343±27	

† Lowest value which would permit running for more than one minute.

†† Highest value practicable. A higher value was indicated.

* Gain 11. 10 sec. exp.

Section 10.1.10 Summary of the Results Obtained on Both Torches and Nebulisers for the Caesium 4555Å Line.

The experimental results for caesium of Section 10 are summarised in Table 112.

Table 112. Optimised Operating Conditions and Values of x, b and a. 1000 p.p.m. Caesium as the Nitrate. 4555Å Line. Horizontal Image.

	Nebuliser No. 1.			Nebuliser No. 2.		
Torch.	Greenfield	Scott	Greenfield	Greenfield	Scott	Greenfield
Coolant	N_2	Ar	Ar	N_2	Ar	Ar
Power kW	0.79†	0.57	1.57	0.91†	0.66	1.42†
Plasma Gas Flow ℓ/min.	4.7	1.9	0.1	4.5†	0.0	0.0
Nebuliser Gas Flow ℓ/min.	3.2	2.6	3.4	2.8††	1.7	2.7
Coolant Gas Flow ℓ/min.	18.5	20.0	17.0	8.0	20.0	22.0
Viewing Height above Base cm.	4.7	3.8	5.5	4.4	3.7	6.2
Length of Plasma cm.	0.7	2.4	3.9	0.8	2.7	4.1
x	766	1532	703	974	998	698
b	8	11	21.3	12.7	14.9	17.1
a	7.1	7.0	7.0	9.9	7.3	9.9
$\frac{x-b}{b-a}$	842±360 (170±11)*	380±34 (53±2)*	47.7±1.7 (16.7±0.5)*	343±27	129±6	95±3

† Lowest value practicable.

†† Highest value practicable.

* Vertical image values - given because of the poor statistics on the horizontal image results.

Section 10.1.11 Barium Results with the Scott Torch and Nebuliser No.1.

Barium was the next element to be investigated using the two torches and nebulisers. The results obtained with the Scott torch are shown in Tables 113-114.

Table 113. Optimisation Cycles. Signal Divider 1 p.p.m. Barium as the Nitrate. 4554Å line. Vertical Image. Scott Torch. Nebuliser No. 1. Argon Coolant. S.C.15 Generator.

Number of Cycle.	1	2	3	
Power kW.	1.06	0.78	0.80	
Plasma Gas Flow ℓ/min.	0.0	1.3	1.3	
Nebuliser Gas Flow ℓ/min.	1.0	1.7	1.7	
Coolant Gas Flow ℓ/min.	15.0	19.0	22.0	
Viewing Height above Base cm.	2.8	3.4	3.2	
Length of Plasma cm.	n.d.	n.d.	3.2	
x	18413	16846	21940	(mean of 2)*
b	5022	558	372	(σ = 2.9. 10 det.)*
a	7	7	7	(σ = 0.3. 10 det.)*
$\frac{x-b}{b-a}$	2.6±0.3	29±7	59.1±0.5	

* Gain 11. 10 sec. exp.

The last set of conditions was used as the start of an optimisation with the image horizontal. No shifts were found the corresponding ratio was 110 as shown in Table 114.

Table 114. Optimised Values† of x, b and a for Vertical and Horizontal Images of 1 p.p.m. Barium 4554Å line Radiation.

	1 p.p.m. Ba Vertical Image.	1 p.p.m. Ba Horizontal Image.
x	21940	30994
b	372	289
a	7	7
$\frac{x-b}{b-a}$	59.1	110
σ	±0.5	±1

† Table 113, Cycle 3.

Section 10.1.12 Barium Results with the Greenfield Torch and Nebuliser No. 1.

The results obtained using the Greenfield torch are shown in Tables 115-118.

Table 115. Optimisation Cycles. Signal Divider. 1 p.p.m. Barium as the Nitrate. 4554Å line. Vertical Image. Greenfield Torch. Nebuliser No.1. Argon Coolant. S.C.15 Generator.

Number of Cycle.	1	2	3	4	
Power kW.	1.50†	1.47†	1.49†	1.48†	
Plasma Gas Flow ℓ/min.	5.8	0.0	0.0	0.2	
Nebuliser Gas Flow ℓ/min.	2.9	2.3	2.5	2.5	
Coolant Gas Flow ℓ/min.	22.0	16.5	15.0	15.0	
Viewing Height above Base cm.	6.8	4.8	4.8	4.8	
Length of Plasma cm.	n.d.	n.d.	n.d.	3.8	
x	1406	6821	7064	6821	(mean of 2)*
b	163	85	82	76.3	(σ = 0.95. 10 det.)*
a	7	7	7	7	(σ = 0.4. 4 det.)*
$\frac{x-b}{b-a}$	8±2	86±9	93±9	97±1.5	

* Gain 10. 10 sec. exp.

† Lowest power obtainable.

It was checked that the horizontal image did not require a change in conditions. The results obtained on the two images are shown in Table 116.

Table 116. Optimised Values† of x, b and a for Vertical and Horizontal Images of 1 p.p.m. Barium 4554Å line Radiation.

	1 p.p.m. Ba Vertical Image.	1 p.p.m. Ba Horizontal Image.	1 p.p.m. Ba No Filter.
x	6821	8627	9514
b	76.3	48	99
a	7	7	7
$\frac{x-b}{b-a}$	97	209	102
σ	±1.5	±6	±1

† Table 105. Cycle 4.

Table 117. Optimisation Cycles. Signal Divider.
1 p.p.m. Barium as the Nitrate. 4554Å line.
Vertical Image. Greenfield Torch. Nebuliser No.1.
Nitrogen Coolant. S.C.15 Generator.

Number of Cycle.	1	2	3	4	5	
Power kW.	1.52	1.65	1.13	1.05	0.99	
Plasma Gas Flow ℓ/min.	5.2	8.6	6.7	5.2	4.2	
Nebuliser Gas Flow ℓ/min.	1.3	2.0	2.7	2.7	2.6	
Coolant Gas Flow ℓ/min.	6.0	14.0	14.5	14.0	14.5	
Viewing Height above Base cm.	3.0	3.0	3.8	3.8	3.8	
Length of Plasma cm.	n.d.	n.d.	n.d.	n.d.	0.7	
x	10377	42257	12297	8073	6921	(mean of 2)*
b	3910	1958	59.4	30.2	23.9	(σ=0.38.10 det.)*
a	7.4	7.4	7.4	7.4	7.4	(σ=0.22.10 det.)*
$\frac{x-b}{b-a}$	1.7±0.2	21±2	238±12	353±35	418±11	

* Gain 11. 10 sec. exp.

Table 118. Optimised Values† of x, b and a for
Vertical and Horizontal Images of 1 p.p.m. Barium
4554Å line Radiation.

	1 p.p.m. Ba Vertical Image.	1 p.p.m. Ba Horizontal Image.	1 p.p.m. Ba No Filter.
x	6921	7822	9523
b	23.9	18.3	30.3
a	7.4	7.4	7.4
$\frac{x-b}{b-a}$	418	716	415
σ	11	38	16

† Table 107. Cycle No. 5.

Section 10.1.12 Barium Results with the Scott Torch and Nebuliser No. 2.

The results obtained with the No. 2 nebuliser and the Scott Torch are shown in Table 119.

Table 119. Optimisation Cycles. Signal Divider. 1 p.p.m. Barium as the Nitrate. 4554Å line. Horizontal Image. Scott Torch. Nebuliser No. 2. Argon Coolant. S.C.15 Generator.

Number of Cycle.	1	2	
Power kW.	0.81	0.66	
Plasma Gas Flow ℓ/min.	1.3	0.0	
Nebuliser Gas Flow ℓ/min.	1.7	0.95	
Coolant Gas Flow ℓ/min.	22.0	20.0	
Viewing Height above Base cm.	2.9	3.3	
Length of Plasma cm.	n.d.	2.6	
x	152	4452	(mean of 2)*
b	38	26.1	(σ = 0.41. 10 Det.)*
a	7	7	(σ = 0.15. 10 Det.)*
$\frac{x - b}{b - a}$	4	232 ± 12	

* Gain 11. 10 sec. exp.

Section 10.1.13 Barium Results with the Greenfield Torch and Nebuliser No. 2.

The results obtained with the Greenfield torch and nebuliser No. 2 are shown in Tables 120-121.

Table 120. Optimisation Cycles. Signal Divider.
1 p.p.m. Barium as the Nitrate. 4554Å line.
Horizontal Image. Greenfield Torch. Nebuliser No.2.
Argon Coolant. S.C.15 Generator.

Number of Cycle.	1	2	3	4	
Power kW.	1.5†	1.42†	1.46	1.41†	
Plasma Gas Flow ℓ/min.	0.0	0.0	2.0	2.0	
Nebuliser Gas Flow ℓ/min.	1.4	1.0	1.2	1.2	
Coolant Gas Flow ℓ/min.	24.0	24.0	20.0	20.0	
Viewing Height above Base cm.	2.9	4.8	4.8	4.8	
Length of Plasma cm.	n.d.	n.d.	n.d.	3.6	
x	2627	2627	4358	4358	(σ = 25. 5 det.)*
b	553	43.5	38.9	38.9	(σ = 0.5. 10 det.)*
a	9.3	9.3	9.3	9.3	(σ = 0.2. 10 det.)*
$\frac{x-b}{b-a}$	4	76	146	146±3	

* Gain 11. 10 sec. exp.

† Lowest power obtainable.

Table 121. Optimisation Cycles. Signal Divider.
1 p.p.m. Barium as the Perchlorate. 4554Å line.
Horizontal Image. Greenfield Torch. Nebuliser No.2.
Nitrogen Coolant. S.C.15 Generator.

Number of Cycle.	1	2	3	4	
Power kW.	1.55†	0.95	0.95	0.95	
Plasma Gas Flow ℓ/min.	7.0	6.0	5.0	5.0	
Nebuliser Gas Flow ℓ/min.	1.7	1.8	1.6	1.7	
Coolant Gas Flow ℓ/min.	20.0	20.0	12.0	12.0	
Viewing Height above Base cm.	2.9	3.2	3.2	3.2	
Length of Plasma cm.	n.d.	n.d.	n.d.	0.7	
x	29395	4849	7270	6232	(σ = 39. 10 det.)*
b	774	27.3	31.7	27.3	(σ = 1.2. 10 det.)*
a	9	9	9	9	(σ = 0.2. 10 det.)*
$\frac{x-b}{b-a}$	36	263	319	339±23	

† Maximum Power.

* Gain 11. 10 secs. exp.

Section 10.1.14 Summary of the Results obtained on Both Torches and Nebulisers for the Barium 4554Å line.

The experimental results for barium of Section 10 are summarised in Table 122.

Table 122. Optimised Operating Conditions and Values of x, b and a. 1 p.p.m. Barium as the Nitrate. 4554Å line. Horizontal Image.

	Nebuliser No. 1.			Nebuliser No. 2.		
Torch.	Greenfield	Scott	Greenfield	Greenfield	Scott	Greenfield
Coolant.	N_2	Ar	Ar	N_2	Ar	Ar
Power kW	0.99	0.80	1.48†	0.95	0.66	1.41†
Plasma Gas Flow ℓ/min.	4.2	1.3	0.2	5.0	0.0	2.0
Nebuliser Gas Flow ℓ/min.	2.6	1.7	2.5	1.7	0.95	1.2
Coolant Gas Flow ℓ/min.	14.5	22.0	15.0	12.0	20.0	20.0
Viewing Height above Base cm.	3.8	3.2	4.8	3.2	3.3	4.8
Length of Plasma cm.	0.7	3.2	3.8	0.7	2.6	3.6
x	7822	30994	8627	6232	4452	4358
b	18.3	289	48	27.3	26.1	38.9
a	7.4	7	7	9	7	9.3
$\frac{x-b}{b-a}$	716±38	110±1	209±6	339±23	232±12	146±3

† Lowest power attainable.

Section 10.1.15 Aluminium Results with the Scott Torch and Nebuliser No. 1.

The results for the aluminium 3961Å line are shown in Tables 123-125.

Table 123. Optimisation Cycles. Signal Divider. 1000 p.p.m. Aluminium as the Perchlorate. 3961Å line. Vertical Image. Scott Torch. Nebuliser No.1. Argon Coolant. S.C.15 Generator.

Number of Cycle.	1	2	3	
Power kW.	1.06	1.21	1.11	
Plasma Gas Flow ℓ/min.	0.0	1.0	3.0	
Nebuliser Gas Flow ℓ/min.	1.0	1.8	2.5	
Coolant Gas Flow ℓ/min.	15.0	24.0	23.5	
Viewing Height above Base cm.	2.8	3.7	4.3	
Length of Plasma cm.	n.d.	n.d.	3.5	
x	69835	187690	232460	
b	976.5	167	33	(σ = 0.94. 10 det.)
a	19.2	19.2	19.2	(σ = 0.42. 10 det.)
$\frac{x-b}{b-a}$	72	1269	16842±400	

The experiment was repeated with the image rotated. Almost identical conditions were found as shown in Table 124.

Table 124. Optimisation Cycles. Signal Divider. 1000 p.p.m. Aluminium as the Perchlorate. 3961Å line. Horizontal Image. Scott Torch, Nebuliser No.1. Argon Coolant. S.C.15 Generator.

Number of Cycle.	1	2	3	4	
Power kW.	1.07	1.0	1.17	1.17	
Plasma Gas Flow ℓ/min.	0.0	1.3	2.0	2.0	
Nebuliser Gas Flow ℓ/min.	1.0	1.9	2.3	2.3	
Coolant Gas Flow ℓ/min.	15.0	21.5	22.0	24.0	
Viewing Height above Base cm.	2.8	4.4	4.0	4.0	
Length of Plasma cm.	n.d.	n.d.	n.d.	n.d.	
x	76566	92840	230288	239045*	
b	571.5	22.5	20.1	19.3	(σ = 0.67. 10 det.
a	12.5	12.5	12.5	12.5	(σ = 0.53. 10 det.
$\frac{x-b}{b-a}$	136	9282	30298	35151±1390	

* Gain 6. 1 sec. exp.

The above experiment was then repeated using 1 p.p.m. solution, the results obtained appear in Table 125.

Table 125. Optimisation Cycles. Signal Divider. 1 p.p.m. Aluminium as the Perchlorate. 3961Å line. Horizontal Image. Scott Torch. Nebuliser No. 1. Argon Coolant. S.C.15 Generator.

Number of Cycle.	1	2	3
Power kW	1.17	0.97	1.01
Plasma Gas Flow ℓ/min.	2.0	2.7	2.5
Nebuliser Gas Flow ℓ/min.	2.3	2.5	2.6
Coolant Gas Flow ℓ/min.	22.0	22.0	22.0
Viewing Height above Base cm.	4.0	4.6	4.6
Length of Plasma cm.	n.d.	n.d.	n.d.
x	403.0	346.5	381.0
b	41.6	39.3	39.3
a	33.7*	33.7*	33.7*
$\frac{x - b}{b - a}$	46	56	61

* Gain 8. 10 sec. exp.

The aluminium 2816Å line was then looked at using the Scott Torch and nebuliser No. 1. A 1% w/v aluminium perchlorate solution was used initially. The results are shown in Table 126.

Table 126. Optimisation Cycles. Signal Divider. 1% w/v. Aluminium as the Perchlorate. 2816Å line. Scott Torch. Nebuliser No.1. Argon Coolant. S.C.15 Generator.

Number of Cycle.	1	2	3	4	
Power kW.	1.07	1.13	1.19	1.21	
Plasma Gas Flow ℓ/min.	0.0	1.0	1.2	1.0	
Nebuliser Gas Flow ℓ/min.	1.0	1.7	1.7	1.8	
Coolant Gas Flow ℓ/min.	15.0	20.0	23.5	24.0	
Viewing Height above Base cm.	2.82	3.72	3.72	3.72	
Length of Plasma cm.	n.d.	n.d.	n.d.	4.4	
x	513	546	573	444.3	(mean of 3)
b	247	91	72	66.8	(σ = 0.47. 10 det.)
a	5	5	5	5	(σ = 0.3. 2 det.)
$\frac{x-b}{b-a}$	1.1±0.03	5.3±0.5	6.6±0.7	6.1±0.1	

Section 10.1.16 Aluminium Results with the Greenfield Torch and Nebuliser No. 1.

The 2816Å line was then examined with the Greenfield torch. The results were shown in Tables 127-128.

Table 127. Optimisation Cycles. Signal Divider. 1% w/v Aluminium as the Perchlorate. 2816Å line. Greenfield Torch. Nebuliser No.1. Argon Coolant. S.C.15 Generator.

Number of Cycle.	1	2	3
Power kW.	1.75†	1.88†	1.88†
Plasma Gas Flow ℓ/min.	3.5	1.3	2.5
Nebuliser Gas Flow ℓ/min.	3.5	3.3	3.1
Coolant Gas Flow ℓ/min.	23.5	21.0	22.5
Viewing Height above Base cm.	4.78	4.36	4.76
Length of Plasma cm.	n.d.	n.d.	3.12
x	n.d.	n.d.	428*
b	n.d.	n.d.	292*
a	n.d.	n.d.	9*
$\frac{x-b}{b-a}$	n.d.	n.d.	0.48±0.05

† Highest powers obtainable with these gas flows.
* Gain 8. 60 sec. exp.

Table 128. Optimisation Cycles. Signal Divider. 1% w/v Aluminium as the Perchlorate. 2816Å line. Greenfield Torch. Nebuliser No. 1. Nitrogen Coolant. S.C.15 Generator.

Number of Cycle.	1	2	3	4
Power kW.	1.43†	1.43†	1.46†	1.31†
Plasma Gas Flow ℓ/min.	8.3	5.6	5.0	5.0
Nebuliser Gas Flow ℓ/min.	3.3	3.4	3.4	3.4
Coolant Gas Flow ℓ/min.	6.0	5.5	3.0	5.0
Viewing Height above Base cm.	2.66	3.46	3.86	3.86
Length of Plasma cm.	n.d.	n.d.	n.d.	0.94
x	n.d.	n.d.	n.d.	542
b	n.d.	n.d.	n.d.	362
a	n.d.	n.d.	n.d.	9
$\frac{x-b}{b-a}$	n.d.	n.d.	n.d.	0.51±.05

† Highest powers obtainable.

* Gain 8. 60 sec. exp.

Section 10.1.17 Aluminium Results with the Scott Torch and Nebuliser No. 2.

The results obtained with the No. 2 nebuliser and the Scott Torch are shown in Tables 129-130.

Table 129. Optimisation Cycles. Signal Divider. 1 p.p.m. Aluminium as the Perchlorate. 3961Å line. Horizontal Image. Scott Torch. Nebuliser No. 2. Argon Coolant. S.C.15 Generator.

Number of Cycle.	1	2	3	4	5
Power kW.	1.11	1.34	1.12	1.12	1.12
Plasma Gas Flow ℓ/min.	3.0	2.0	2.0	0.5	0.0
Nebuliser Gas Flow ℓ/min.	2.5	2.7	1.7	1.75	1.75
Coolant Gas Flow ℓ/min.	24.0	24.5	26.0	26.0	26.0
Viewing Height above Base cm.	3.6	4.6	4.8	4.9	4.8
Length of Plasma cm.	n.d.	n.d.	n.d.	n.d.	3.6
x	179	333	658	750	768 (σ = 13. 3 det.)*
b	162	162	133	105	104 (σ = 0.84. 10 det.
a	65.1	65.1	65.1	65.1	65.1(σ = 0.41. 10 det.
$\frac{x-b}{b-a}$	0.2	1.8	8	16	17±0.5

* Gain 9. 10 sec. exp.

Table 130. Optimisation Cycles. Signal Divider. 1000 p.p.m. Aluminium as the Perchlorate. 2816Å line. Scott Torch. Nebuliser No.2. Argon Coolant. S.C. Generator.

Number of Cycle.	1	2	
Power kW.	1.16	1.16	
Plasma Gas Flow ℓ/min.	1.0	1.0	
Nebuliser Gas Flow. ℓ/min.	.85	1.0	
Coolant Gas Flow ℓ/min.	24.0	22.0	
Viewing Height above Base cm.	3.5	3.5	
Length of Plasma cm.	n.d.	3.8	
x	106	100.8	(σ = .63. 4 det.)
b	67	61.4	(σ = .6. 10 det.)
a	5.2	5.2	(σ = .13. 10 det.)
$\frac{x-b}{b-a}$	.63	.7 ± .02	

Section 10.1.18 Aluminium Results with the Greenfield Torch and Nebuliser No. 2.

The results obtained with the Greenfield torch and nebuliser No. 2 are shown in Tables 131 - 136.

Table 131. Optimisation Cycles. Signal Divider. 1 p.p.m. Aluminium as the Perchlorate. 3961Å line. Horizontal Image. Greenfield Torch. Nebuliser No.2. Argon Coolant. S.C.15 Generator.

Number of Cycle.	1	2	3	
Power kW.	1.39	1.34†	1.39†	
Plasma Gas Flow. ℓ/min.	1.5	3.0	2.0	
Nebuliser Gas Flow ℓ/min.	0.7	1.4	1.5	
Coolant Gas Flow ℓ/min.	16.0	16.0	16.0	
Viewing Height above Base cm.	3.5	4.3	4.3	
Length of Plasma cm.	n.d.	n.d.	4.0	
x	309	193	237.9	(σ = 1.4. 8 det.)*
b	159	35	34.9	(σ = 0.2. 10 det.)*
a	23.6	23.6	23.6	(σ = 0.2. 10 det.)*
$\frac{x-b}{b-a}$	1.1	14	18±0.4	

† Minimum power obtainable.
* Gain 7. 10 sec. exp.

Table 132. Optimisation Cycles. Signal Divider.
1 p.p.m. Aluminium as the Perchlorate. 3961Å line.
Horizontal Image. Greenfield Torch. Nebuliser No.2.
Nitrogen Coolant. S.C.15 Generator.

Number of Cycle.	1	2	3
Power kW.	1.47	1.14	1.15
Plasma Gas Flow ℓ/min.	6.5	6.0	6.0
Nebuliser Gas Flow ℓ/min.	2.8	3.0	2.7
Coolant Gas Flow ℓ/min.	10.0	12.0	15.0
Viewing Height above Base. cm.	4.8	4.4	4.4
Length of Plasma cm.	n.d.	n.d.	1.1
x	556	290	320 (σ = 2.6. 10 det.)*
b	42	28	27.1 (σ = 0.2. 10 det.)*
a	24.4	24.4	24.4 (σ = 0.2. 10 det.)*
$\frac{x-b}{b-a}$	29	73	108 ± 10

* Gain 7. 10 sec. exp.

Table 133. Optimisation Cycles. Signal Divider.
1000 p.p.m. Aluminium as the Perchlorate. 2816Å line.
Greenfield Torch. Nebuliser No.2. Argon Coolant.
S.C.15 Generator.

Number of Cycle.	1	2	
Power kW.	1.79	1.88†	
Plasma Gas Flow ℓ/min.	2.5	2.8	
Nebuliser Gas Flow ℓ/min.	3.1	3.0	
Coolant Gas Flow ℓ/min.	22.0	22.0	
Viewing Height above Base cm.	4.8	4.9	
Length of Plasma cm.	n.d.	4.1	
x	88	71.25	(σ = 1.0. 8 det.)*
b	85	65.2	(σ = 1.0. 5 det.)*
a	5.8	5.8	(σ = 0.3. 10 det.)*
$\frac{x-b}{b-a}$	.04	$.1 \pm .02$	

† Highest power available.

* Gain 8. 10 sec. exp.

Because of very small signals the above optimisation was carried out using one meter only, i.e. one channel, and was repeated using the high power R.D. 150 generator. The results are shown in Table 134.

Table 134. Optimisation Cycles. Signal Divider. 1000 p.p.m. Aluminium as the Perchlorate. 2816Å line. Greenfield Torch. Nebuliser No. 2. Argon Coolant. R.D. 150 Generator.

Number of Cycle.	1	2	
Power kW.	3.22	3.92	
Plasma Gas Flow ℓ/min.	10.0	3.0	
Nebuliser Gas Flow ℓ/min.	1.9	2.1	
Coolant Gas Flow ℓ/min.	40.0	40.0	
Viewing Height above Base cm.	3.4	3.4	
Length of Plasma cm.	n.d.	4.5	
x	4554	4793	(σ = 10.1. 5 det.)*
b	3030	3030	(σ = 4.5. 5 det.)*
a	5.4	5.4	(σ = 0.2. 5 det.)*
$\frac{x - b}{b - a}$	0.5	0.583±.004	

* Gain 8. 10 sec. exp.

Table 135. Optimisation Cycles. Signal Divider. 1000 p.p.m. Aluminium as the Perchlorate. 2816Å line. Greenfield Torch. Nebuliser No.2. Nitrogen Coolant. S.C.15 Generator.

Number of Cycle.	1.	2	
Power kW.	1.31	1.61†	
Plasma Gas Flow ℓ/min.	5.0	7.0	
Nebuliser Gas Flow ℓ/min.	3.4	2.0	
Coolant Gas Flow ℓ/min.	5.0	10.0	
Viewing Height above Base cm.	4.1	4.1	
Length of Plasma cm.	n.d.	1.2	
x	71.8	91.8	(σ = 1.0. 10 det.)*
b	69.8	87.4	(σ = 0.8. 10 det.)*
a	5.2	5.2	(σ = 0.2. 5 det.)*
$\frac{x - b}{b - a}$	.031	.054±.015	

* Gain 8. 10 sec. exp.

The signals obtained were so small and the response to variation of the parameters was very flat and it may be doubtful whether any genuine optimisation was achieved. The optimisation was carried out with one meter only. The experiment was repeated using the large generator.

Table 136. Optimisation Cycles. Signal Divider. 1000 p.p.m. Aluminium as the Perchlorate. 2816Å line. Greenfield Torch. Nebuliser No. 2. Nitrogen Coolant. R.D. 150 Generator.

Number of Cycle.	1	2	3	4	
Power kW.	5.1	3.1	2.5	2.6	
Plasma Gas Flow ℓ/min.	16.0	38.0	34.0	32.0	
Nebuliser Gas Flow ℓ/min.	2.5	1.8	1.8	1.8	
Coolant Gas Flow ℓ/min.	45.0	43.0	40.0	40.0	
Viewing Height above Base cm.	2.7	3.2	3.1	3.2	
Length of Plasma cm.	n.d.	n.d.	n.d.	3.7	
x	184	672	3380	2838	(σ = 7.6. 10 det.)*
b	142	380	1504	1249	(σ = 5.2. 10 det.)*
a	5.3	5.3	5.3	5.3	(σ = 0.3. 3 det.)*
$\frac{x - b}{b - a}$	0.31	0.78	1.25	$1.28^{\pm}.01$	

* Gain 8. 10 sec. exp.

Section 10.1.19 Summary of the Results Obtained on Both Torches and Nebulisers for the Aluminium 3961Å line.

The experimental results for aluminium of Section 10 are summarised in Table 137.

Table 137. Optimised Operating Conditions and Values of x, b and a. 1 p.p.m. and 1000 p.p.m. Aluminium as the Perchlorate. 3961Å line. Horizontal Image.

	Nebuliser No.1.		Nebuliser No.2.		
Torch.	Scott	Greenfield	Greenfield	Scott	Greenfield
Coolant.	Ar	Ar	N_2	Ar	Ar
Power kW.	1.01	1.17	1.15	1.12	1.39†
Plasma Gas Flow ℓ/min.	2.5	2.0	6.00	0.0	2.0
Nebuliser Gas Flow ℓ/min.	2.6	2.3	2.7	1.75	1.5
Coolant Gas Flow ℓ/min.	22.0	24.0	15.0	26.0	16.0
Viewing Height above Base cm.	4.6	4.0	4.4	4.8	4.3
Length of Plasma cm.	n.d.	n.d.	1.1	3.6	4.0
x	381	239045	320	768	237.9
b	39.3	19.3	27.1	104	34.9
a	33.7	12.5	24.4	65.1	23.6
$\frac{x-b}{b-a}$	61	35151	108±10	17±0.5	18±0.4
Conc. p.p.m.	1	1000	1	1	1

† Minimum power obtainable.

Section 10.1.20 Summary of the Results Obtained on Both Torches and Nebulisers for the Aluminium 2816Å line.

This summary is shown in Table 138.

Table 138. Optimised Operating Conditions and Values of x, b and a. 1% and 1000 p.p.m. Aluminium as the Perchlorate. 2816Å line.

	Nebuliser No.1.			Nebuliser No.2.		
Torch.	Greenfield	Scott	Greenfield	Greenfield	Scott	Greenfield
Coolant.	N_2	Ar	Ar	N_2	Ar	Ar
Power kW.	1.31†	1.21	1.88†	2.6	1.16	3.92
Plasma Gas Flow ℓ/min.	5.0	1.0	2.5	32.0	1.0	3.0
Nebuliser Gas Flow ℓ/min.	3.4	1.8	3.1	1.8	1.0	2.1
Coolant Gas Flow ℓ/min.	5.0	24.0	22.5	40.0	22.0	40.0
Viewing Height above Base cm.	3.86	3.72	4.76	3.2	3.5	3.4
Length of Plasma cm.	0.94	4.4	3.12	3.7	3.8	4.5
x	542	444.3	428	2838	100.8	4793
b	362	66.8	292	1249	61.4	3030
a	9	5	9	5.3	5.2	5.4
$\frac{x-b}{b-a}$	0.51±0.05	6.1±0.1	0.48±0.05	1.28±0.01	0.7±0.02	0.583±0.04
Conc. p.p.m.	(1%w.v.)	(1%w.v.)	(1%w.v.)	1000	1000	1000

† Highest power obtainable with these gas flows.

Section 10.1.21 Zinc Results with the Scott Torch and Nebuliser No.2.

The element zinc was investigated using the lines 3076Å and 3072Å the results obtained for the Scott Torch are shown in Tables 139 and 140.

Table 139. Optimisation Cycles. Signal Divider. 1000 p.p.m. Zinc as the Nitrate. 3076Å line. Scott Torch. Nebuliser No. 2. Argon Coolant. S.C.15 Generator.

Number of Cycle.	1	2	3	
Power kW.	1.05	0.95	0.89	
Plasma Gas Flow ℓ/min.	0.2	0.0	0.0	
Nebuliser Gas Flow ℓ/min.	2.0	1.0	1.0	
Coolant Gas Flow ℓ/min.	18.0	19.0	19.0	
Viewing Height above Base. cm.	3.1	3.5	3.3	
Length of Plasma cm.	n.d.	n.d.	2.7	
x	158	481	481	(σ = 4.1. 3 det.)*
b	68.9	54.1	52.2	(σ = 0.44. 10 det.)*
a	24.7	24.7	24.7	(σ = 0.33. 3 det.)*
$\frac{x-b}{b-a}$	2.0	14.5	15.6±.3	

* Gain 7. 10 sec. exp.

Table 140. Optimisation Cycles. Signal Divider. 1000 p.p.m. Zinc as the Nitrate. 3072Å line. Scott Torch. Nebuliser No.2. Argon Coolant. S.C.15 Generator.

Number of Cycle.	1	2	
Power kW	0.89	0.53†	
Plasma Gas Flow ℓ/min.	0.0	0.0	
Nebuliser Gas Flow ℓ/min.	1.0	0.5	
Coolant Gas Flow ℓ/min.	19.0	19.0	
Viewing Height above Base cm.	2.7	2.0	
Length of Plasma cm.	n.d.	3.4	
x	147	147	(σ = 1.7. 7 det.)*
b	101	83	(σ = 0.95. 10 det.)*
a	24.3	24.3	(σ = 0.33. 3 det.)*
$\frac{x-b}{b-a}$	0.6	1.09±.03	

† Minimum power obtainable.

* Gain 7. 10 sec. exp.

Section 10.1.22 Zinc Results with the Greenfield Torch and Nebuliser No.2.

The zinc results with the Greenfield Torch are shown in Tables 141 to 146.

Table 141. Optimisation Cycles. Signal Divider. 1000 p.p.m. Zinc as the Nitrate. 3076Å line. Greenfield Torch. Nebuliser No.2. Argon Coolant. S.C.15 Generator.

Number of Cycle.	1	2	
Power kW	1.51	1.44†	
Plasma Gas Flow ℓ/min.	2.5	0.0	
Nebuliser Gas Flow ℓ/min.	1.5	1.2	
Coolant Gas Flow ℓ/min.	27.0	26.0	
Viewing Height above Base cm.	3.8	3.5	
Length of Plasma cm.	n.d.	4.1	
x	1754	1950	(σ = 2.0. 3 det.)*
b	129	129.4	(σ = 1.3. 10 det.)*
a	26.8	26.8	(σ = 0.3. 10 det.)*
$\frac{x - b}{b - a}$	15.8	17.7±0.2	

† Minimum power.

* Gain 7. 10 sec. exp.

Table 142. Optimisation Cycles. Signal Divider. 1000 p.p.m. Zinc as the Nitrate. 3076Å line. Greenfield Torch. Nebuliser No. 2. N_2 Coolant. S.C.15 Generator.

Number of Cycle.	1	2	3	
Power kW	1.15	1.22	1.19	
Plasma Gas Flow ℓ/min.	6.5	8.0	9.0	
Nebuliser Gas Flow ℓ/min.	2.0	1.2	1.5	
Coolant Gas Flow ℓ/min.	10.5	14.0	14.0	
Viewing Height above Base cm.	2.9	2.9	2.9	
Length of Plasma cm.	n.d.	n.d.	0.8	
x	308	864	1011	(σ = 0.7. 3 det.)*
b	87	166	107	(σ = 3.5. 10 det.)*
a	28.1	28.1	28.1	(σ = 0.3. 10 det.)*
$\frac{x - b}{b - a}$	4.8	6.1	11.5±0.5	

* Gain 7. 10 sec. exp.

Table 143. Optimisation Cycles. Signal Divider. 1000 p.p.m. Zinc as the Nitrate. 3072Å line. Greenfield Torch. Nebuliser No. 2. Argon Coolant. S.C.15 Generator.

Number of Cycle.	1	2	
Power kW	1.88†	1.83†	
Plasma Gas Flow ℓ/min.	4.7	4.0	
Nebuliser Gas Flow ℓ/min.	3.1	0.7	
Coolant Gas Flow ℓ/min.	27.0	25.0	
Viewing Height above Base cm.	5.5	3.3	
Length of Plasma cm.	n.d.	4.2	
x	898	1061.6	(σ = 6.5. 5 det.)*
b	792	792	(σ = 3.8. 10 det.)*
a	30.1	30.1	(σ = 0.3. 10 det.)*
$\frac{x-b}{b-a}$	0.14	0.35±0.01	

† Maximum Power Available.

* Gain 7. 10 sec. exp.

Table 144. Optimisation Cycles. Signal Divider. 1000 p.p.m. Zinc as the Nitrate. 3072Å line. Greenfield Torch. Nebuliser No.2. Argon Coolant. R.D.150 Generator.

Number of Cycle.	1	2	
Power kW	2.18	1.88†	
Plasma Gas Flow ℓ/min.	10.0	13.0†	
Nebuliser Gas Flow ℓ/min.	2.0	1.9	
Coolant Gas Flow ℓ/min.	41.0	40.0	
Viewing Height above Base cm.	3.4	3.9	
Length of Plasma cm.	n.d.	3.6	
x	3219	2201	(σ = 6.3. 5 det.)*
b	1996	1152	(σ = 8.0. 5 det.)*
a	30.6	30.6	(σ = 0.6. 5 det.)*
$\frac{x-b}{b-a}$	0.62	0.94±0.01	

† Reductions in both plasma gas and power were indicated to give improved ratio, but when these were applied the plasma could not be kept alight.

Table 145. Optimisation Cycles. Signal Divider. 1000 p.p.m. Zinc as the Nitrate. 3072Å line. Greenfield Torch. Nebuliser No. 2. Nitrogen Coolant. S.C.15 Generator.

Number of Cycle.	1	2	
Power kW	1.43	1.65†	
Plasma Gas Flow ℓ/min.	8.0	8.0	
Nebuliser Gas Flow ℓ/min.	1.5	1.7	
Coolant Gas Flow ℓ/min.	9.0	9.0	
Viewing Height above Base. cm.	3.3	3.3	
Length of Plasma cm.	n.d.	1.3	
x	421	648.8	(σ = 6.5. 5 det.)*
b	307	483.3	(σ = 2.7. 10 det.)*
a	30.1	30.1	(σ = 0.3. 10 det.)*
$\frac{x-b}{b-a}$	0.41	0.36±.02	

† Maximum power.

* Gain 7. 10 sec.exp.

Table 146. Optimisation Cycles. Signal Divider. 1000 p.p.m. Zinc as the Nitrate. 3072Å line. Greenfield Torch. Nebuliser No. 2. Nitrogen Coolant. R.D.150 Generator.

Number of Cycle.	1	2	3	4	5	6
Power kW.	3.3	3.3	3.2	3.0	2.6	2.6
Plasma Gas Flow ℓ/min.	10.8	9.0	12.0	16.0	17.0	18.0
Nebuliser Gas Flow ℓ/min.	1.3	1.8	1.8	1.8	1.8	1.8
Coolant Gas Flow ℓ/min.	42.0	39.0	37.0	36.0	36.0	36.0
Viewing Height above Base cm.	2.7	2.3	2.5	2.5	2.7	2.8
Length of Plasma cm.	n.d.	n.d.	n.d.	n.d.	n.d.	1.9
x	4262	4448	5070	6998	4386	4449(σ=16. 5 det.)*
b	3978	3916	2664	3352	1912	1912(σ=3.2. 6 det.)
a	33.5	33.5	33.5	33.5	33.5	33.5(σ=0.3. 4 det.)
$\frac{x-b}{b-a}$	0.70	0.14	0.91	1.10	1.32	1.35±0.01

* Gain 7. 10 sec. exp.

Section 10.1.23. Summary of the Results Obtained on Both Torches and Nebuliser No.2 for the Zinc 3076Å line.

The experimental results for the 3076Å line of zinc are summarised in Table 147.

Table 147. Optimised Operating Conditions and Values of x, b and a. 1000 p.p.m. Zinc as the Nitrate. 3076Å line.

		Nebuliser No. 2.	
Torch.	Greenfield	Scott	Greenfield
Coolant	N_2	Ar	Ar
Power kW	1.19	0.89	1.44 †
Plasma Gas Flow ℓ/min.	9.0	0.0	0.0
Nebuliser Gas Flow ℓ/min.	1.5	1.0	1.2
Coolant Gas Flow ℓ/min.	14.0	19.0	26.0
Viewing Height above Base cm.	2.9	3.3	3.5
Length of Plasma cm.	0.8	2.7	4.1
x	1011	481	1950
b	107	52.2	129.4
a	28.1	24.7	26.8
$\frac{x-b}{b-a}$	11.5±0.5	15.6±0.3	17.7±0.2

† Minimum power.

Section 10.1.24 Summary of the Results Obtained on Both Torches and Nebuliser No.2 from the Zinc 3072Å line.

Table 148. Optimised Operating Conditions and Values of x, b and a. 1000 p.p.m. Zinc as the Nitrate. 3072Å line.

		Nebuliser No. 2.	
Torch.	Greenfield	Scott	Greenfield
Coolant	N_2	Ar	Ar
Power kW	2.6	0.53†	1.88†
Plasma Gas Flow ℓ/min.	18.0	0.0	13.0†
Nebuliser Gas Flow ℓ/min.	1.8	0.5	1.9
Coolant Gas Flow ℓ/min.	36.0	19.0	40.0
Viewing Height above Base cm.	2.8	2.0	3.9
Length of Plasma cm.	1.9	3.4	3.6
x	4449	147	2201
b	1912	83	1152
a	33.5	24.3	30.6
$\frac{x-b}{b-a}$	1.35±0.01	1.09±0.03	0.94±0.01

† Lower values indicated but not achievable on the generators used.

Section 10.1.25 Vanadium Results with the Scott Torch and Nebuliser No.1.

The results for the vanadium 3093Å line are shown in Table 149 using nebuliser No.1.

Table 149. Optimisation Cycles. Signal Divider. 1000 p.p.m. Vanadium as the Perchlorate. 3093Å line. Scott Torch. Nebuliser No.1. Argon Coolant. S.C.15 Generator.

Number of Cycle	1	2	3
Power kW	1.08	0.70	0.76
Plasma Gas Flow ℓ/min.	0.0	1.3	0.6
Nebuliser Gas Flow ℓ/min.	1.0	1.4	1.6
Coolant Gas Flow ℓ/min.	15.0	21.0	21.0
Viewing Height above Base cm.	2.8	3.0	2.8
Length of Plasma cm.	n.d.	n.d.	3.0
x	26605	15968	27934
b	113.3	33.3	32
a	12	12	12
$\frac{x - b}{b - a}$	262	748	1395±35

Section 10.1.26 Vanadium Results with the Scott Torch and Nebuliser No. 2.

The results using nebuliser No.2 are shown in Table 150.

Table 150. Optimisation Cycles. Signal Divider. 1000 p.p.m. Vanadium as the Perchlorate. 3093Å line. Scott Torch. Nebuliser No.2. Argon Coolant. S.C.15 Generator.

Number of Cycle.	1	2	
Power kW	0.76	0.65	
Plasma Gas Flow ℓ/min	0.6	0.25	
Nebuliser Gas Flow ℓ/min.	1.6	0.75	
Coolant Gas Flow ℓ/min.	21.0	19.00	
Viewing Height above Base cm.	2.3	2.3	
Length of Plasma cm.	n.d.	3.1	
$\bar{x}$	1082	27228	(σ = 214. 8 det.)*
b	88	32.5	(σ = 0.6. 10 det.)
a	12.2	12.2	(σ = 0.25. 4 det.)
$\frac{x - b}{b - a}$	13	1340±43	

* Gain 2. 10 sec. exp.

Section 10.1.27 Vanadium Results with the Greenfield Torch and Nebuliser No.2.

These are shown in Tables 151 to 153.

Table 151. Optimisation Cycles. Signal Divider. 1000 p.p.m. Vanadium as the Perchlorate. 3093Å line. Greenfield Torch. Nebuliser No.2. Argon Coolant. S.C.15 Generator.

Number of Cycle.	1	2
Power kW	1.51†	1.46†
Plasma Gas Flow ℓ/min.	0.0	0.0
Nebuliser Gas Flow ℓ/min.	1.5	1.0
Coolant Gas Flow ℓ/min.	21.0	24.0
Viewing Height above Base cm.	3.9	3.3
Length of Plasma cm.	n.d.	4.0
x	3692	23524
b	42	24.4
a	6	6
$\frac{x - b}{b - a}$	101	1277±11

† Minimum power.

Table 152. Optimisation Cycles. Signal Divider.
1000 p.p.m. Vanadium as the Perchlorate. 3093Å line.
Greenfield Torch. Nebuliser No.2. N_2 Coolant.
S.C.15 Generator.

Number of Cycle.	1	2	3
Power kW	1.31	1.39	1.60†
Plasma Gas Flow ℓ/min.	6.5	5.0	6.5
Nebuliser Gas Flow ℓ/min.	2.1	1.4	1.4
Coolant Gas Flow ℓ/min.	14.0	10.0	10.0
Viewing Height above Base cm.	3.5	3.2	3.0
Length of Plasma cm.	n.d.	n.d.	1.4
x	1842	15427	22036 (σ = 191. 5 det.)*
b	26	36	38 (σ = 0.26. 10 det.)*
a	6	6	6 (σ = 0.03. 10 det.)*
$\frac{x-b}{b-a}$	91	513	687±10

† Maximum power available.
* Gain 2. 10 sec. exp.

Table 153. Optimisation Cycles. Signal Divider.
1000 p.p.m. Vanadium as the Perchlorate. 3093Å line.
Greenfield Torch. Nebuliser No.2. N_2 Coolant.
R.D.150 Generator.

Number of Cycle.	1	2	3
Power kW	1.98	1.78	1.66
Plasma Gas Flow ℓ/min.	10.5	5.0	5.0
Nebuliser Gas Flow ℓ/min.	1.4	2.1	2.1
Coolant Gas Flow ℓ/min.	30.0	30.0	30.0
Viewing Height above Base cm.	3.8	3.7	3.5
Length of Plasma cm.	n.d.	n.d.	1.6
x	7333	11520	12800 (σ = 47. 4 det.)*
b	20.7	21.5	21.9 (σ = 0.6. 9 det.)*
a	5.2	5.2	5.2 (σ = 0.3. 10 det.)*
$\frac{x-b}{b-a}$	472	705	765±31

* Gain 1. 10 sec. exp.

Section 10.1.28 Summary of the Results Obtained on Both Torches and Nebulisers for the Vanadium 3093Å Line.

The vanadium results of Section 10 are summarised in Table 154.

Table 154. Optimised Operating Conditions and Values of x, b and a. 1000 p.p.m. Vanadium as the Perchlorate. 3093Å line.

	Nebuliser No.1.		Nebuliser No.2.	
Torch.	Scott	Greenfield	Scott	Greenfield
Coolant.	Ar	N_2	Ar	Ar
Power kW.	0.76	1.66	0.65	1.46†
Plasma Gas Flow ℓ/min.	0.6	5.0	0.25	0.0
Nebuliser Gas Flow ℓ/min.	1.6	2.1	0.75	1.0
Coolant Gas Flow ℓ/min.	21.0	30.0	19.0	24.0
Viewing Height above Base cm.	2.8	3.5	2.3	3.3
Length of Plasma cm.	3.0	1.6	3.1	4.0
x	27934	12800	27228	23524
b	32	21.9	32.5	24.4
a	12	5.3	12.2	6
$\frac{x-b}{b-a}$	1395±35	765±31	1340±43	1277±11

† Minimum power.

Section 10.2 A Critical Examination of the Results of Chapter 10.

During the early stages of the experiments it was found that the signal to background ratios obtained when using the cyclone spray chamber were better than those obtained when using the chamber of Scott. The detailed results are given in Tables 90 and 155.

Table 155. Optimised Operating Conditions and Values of x, b and a. Scott Torch with Different Spray Chambers Nebuliser No. 2. 1 p.p.m. Sodium as the Chloride. 5896 Å line. Horizontal Image.

Chamber.	Scott.	Scott with Tube.	Cyclone.
Power kW.	1.0	0.93	1.0
Plasma Gas Flow ℓ/min.	>0.0	1.0	>0.0
Nebuliser Gas Flow ℓ/min.	2.7	2.5	2.2
Coolant Gas Flow ℓ/min.	15 to 24*	22.0	22.0
Viewing Height above Base cm.	5.8	6.3	5.6
x	917.0	636.0	1614.0
b	17.7	14.0	17.4
a	8.7	9.2	9.6
$\frac{x-b}{b-a}$	100±12	130±18	205±12

* No change in ratio from 15 to 24.

It was difficult to understand exactly how the signal to background ratio was influenced by the shape of the cyclone chamber, so this effect was investigated further. Table 156 shows the uptake rate, transfer efficiency and the mls/min. of liquid arriving at the injector tip, for different flow rates for the two systems. It was known that the uptake rate is effected by temperature, so all measurements were taken at the same temperature, in a temperature-controlled room.

Table 156. An Examination of the Parameters Involved in the Comparison of the Two Nebulisation Systems.

	Scott Chamber + Scott Torch.	Cyclone Chamber + Scott Torch.
	1) Optimised Conditions.	3) Optimised Conditions.
Nebuliser flow-rate ℓ/min.	2.7	2.2
Liquid uptake. mls/min.	7.48	5.89
Transfer efficiency %.	1.6	2.0
Mls/min. at injector.	0.12	0.118
	2) Non-Optimised Conditions.	4) Non-Optimised Conditions.
Nebuliser flow-rate ℓ/min.	2.2	2.7
Liquid uptake. mls/min.	6.71	7.06
Transfer efficiency %.	1.3	2.0
Mls/min. at injector.	0.087	0.141

Comparative Flow-rates.

Nebulisation into Free Air Without any Chamber

Nebuliser flow-rate ℓ/min.	2.2	2.7
Liquid uptake. mls/min.	5.8	7.31

It can clearly be seen from this table that although the uptake rate is less when the cyclone chamber is used the transfer efficiency is greater and the same or a larger amount of material is carried at the same or slower rate and therefore the residence time in the plasma is longer. No reason can be given why the uptake rates, when nebulising into free air and into the chambers, should be different, or why they should be different for different chambers. Back-pressure may be a reason but this does not completely explain all the variations. The different transfer efficiencies are probably explained by the greatly different surface to volume ratios of the

chambers. The cyclone chamber has the smaller ratio and it might be expected that less material would be deposited on its surface than is the case for the Scott chamber.

2.4% w/v anhydrous magnesium sulphate was the material sprayed through the nebuliser in these tests and the droplets were collected on microscope slides and examined under the microscope; no difference in particle size or distribution could be detected. However, the collection of the particles was by no means complete, and in particular it was noticed that much of the fine mist was carried round the slide without impinging on it. Little, therefore, can be said about the distributions of the finest particles.

The number of comparisons which could be made of the effect of the two nebulisers on the optimum conditions and on the signal to background ratios was limited to those that could be made using the Scott torch. This was due in the first instance to a failure to achieve formal optimisation with the Greenfield torch on the small generator and latterly to a shortage of experimental time. Not only are the results limited in number but the results for the neutral atom lines are inexplicable as can be seen from Table 157 which is a summary of the relevant parts of Tables 102, 112, 122, 137 and 154.

Table 157. Changes in Optimised Conditions on going from Nebuliser No. 1 to Nebuliser No. 2. Scott Torch. Argon Coolant.

Element.	Na	Cs	Al	Ba	V
State.	U_1	U_3	U_1	V_1	V_1
Wavelength Å.	5896	4555	3961	4554	3093
Conc. p.p.m.	1	1	1	1	1000
Power.	increased.	increased.	increased.	decreased.	decreased
Plasma Gas Flow.	decreased.	decreased.	decreased.	decreased.	decreased
Nebuliser Gas Flow.	decreased.	decreased.	decreased.	decreased.	decreased
Coolant Gas Flow.	increased.	similar.	increased.	decreased.	decreased
Height of Observation.	increased.	similar.	increased.	similar.	decreased
Plasma Length.	increased.	increased.	-	decreased.	similar.
x	similar.	decreased.	decreased.	decreased.	similar.
b	similar.	increased.	increased.	decreased.	similar.
a	similar.	similar.	similar.	similar.	similar.
$\frac{x - b}{b - a}$	similar.	decreased.	decreased.	increased.	similar.

The annular orifice of nebuliser No. 2 must have been smaller than that of nebuliser No. 1 since the nebuliser was passing over twice as much solution with a flow-rate of gas nearly half of that of nebuliser No. 1 at the same pressure. The gas velocity must have been higher and the droplets smaller.

With smaller droplets it might be expected that the power requirement would be lower as it would be easier to flash off the solvent. If the power is lower then a lower background might also be expected and hence a similar or higher signal to background would result.

This is confirmed by the limited results for ion lines given in Table 157 where every parameter moves in an explicable fashion. The power requirement is less which necessitates less plasma gas and coolant and, of course, the nebuliser gas is reduced by virtue of the smaller orifice in the nebuliser. Although the signal is reduced, as a result of the lower power, the background is reduced even more and hence an increased or similar ratio results.

However, the changes and results obtained for the neutral atom lines are inexplicable apart from some of the gas flows for which an explanation could be concocted. It must be stressed again that the information obtained is limited and no hard conclusions can be drawn.

There are further examples of anomalous behaviour on the part of the neutral atom lines. One such anomaly is shown in Table 158, which is a comparison of ratios and signals produced at two different concentrations of the same element. The optimised conditions for one concentration were found to be similar for the other concentration.

Table 158. A Comparison of Signal to Background Ratios and Net Signals obtained at different Concentrations. With Conditions Optimum for both Concentrations. Scott Torch.

Element.	Na	Al	V
Wavelength Å	5896	3961	3093
State.	U_1	U_1	V_1
$\frac{x-b}{b-a}$ at 1000 ppm.	27,245	35,151	1,395
x-b at 1000 ppm.	258,824	239,025	27,902
$\frac{x-b}{b-a}$ at 1 ppm	221	61	1.9
x - b at 1 p.p.m.	1550	342	

Since the ionisation potential of argon is higher than those of the elements of interest here, it might be expected at low concentrations, that the partial pressure of the analyte would be such that the electron density would be low, favouring an equilibrium shift to the right and a reduced emission from the neutral atoms. At high concentrations the electron density would be higher, favouring an equilibrium shift to the left enhancing the emission from the neutrals. In the case of ion lines it would be expected that a low concentration would favour enhanced emission. In the case of the vanadium ion line in Table 157 this occurs. However, for the atom lines the reverse of the expected is true. Again it must be stressed that the evidence is limited.

As indications of how difficult a line is to excite it was thought reasonable to use the excitation potential for neutral lines and the sum of excitation and ionisation potentials for ion lines. These are simple and useful indicators, although it is realised that it is not rigorously correct to use them. (The emission from an excited state of an ionic line is proportional to

$$\frac{e^{-(E_i + E_{ex})/KT}}{n_e + A\, e^{-E_i/KT}}$$

where E_i and E_{ex} are respectively the ionisation and excitation potentials, n_e is the electron density and A is a constant depending upon temperature. Thus if the temperature is not too high and the ionisation potential not too low the second term in the denominator will be negligible. Under these circumstances the expression is equivalent to Boltzmann's Law with $E_i - E_{ex}$ as the effective excitation energy).

Although the quantity optimised was the net signal to background ratio and not the signal, it is to be expected that the optimum ratio should be obtained at a higher power for lines difficult to excite.

Assume for the moment that the system is in L.T.E. The background, if due to the argon continuum, will increase with temperature. So will the intensity of the line until the norm temperature is reached. It seems reasonable to expect the signal to background ratio for a given element to increase until the sensitivity curve begins to flatten out close to the norm temperature. Thus it might be expected that higher temperatures would be required for the more difficult lines and this will be achieved with higher power.

Fig. 98 shows that there is a convincing correlation between E_{ex} or $E_i + E_{ex}$ and optimised power (temperature) for the Greenfield torch operating with a nitrogen coolant. On the evidence, two different lines are obviously required for neutral atoms and ions. The two lowest points, marked with arrows, correspond to the lowest settings of the generator and the indications were that the optimum powers were lower than this. The range of optimum powers thus lies between something less than 0.8 kW for sodium to 2.6 kW for Zn 3072 and Al 2816.

Fig. 99 shows the corresponding results with the Scott torch. Here there is no correlation that can be believed for neutral atoms and a possible correlation for ion lines. Once again neutral atoms seem to behave differently in an all argon system. (An attempt was also made to correlate the optimum power for the neutral and ion lines with the norm temperature of the elements investigated. No convincing correlation was found for the neutral atoms on any of the three systems. There was some evidence of a correlation with the ion lines).

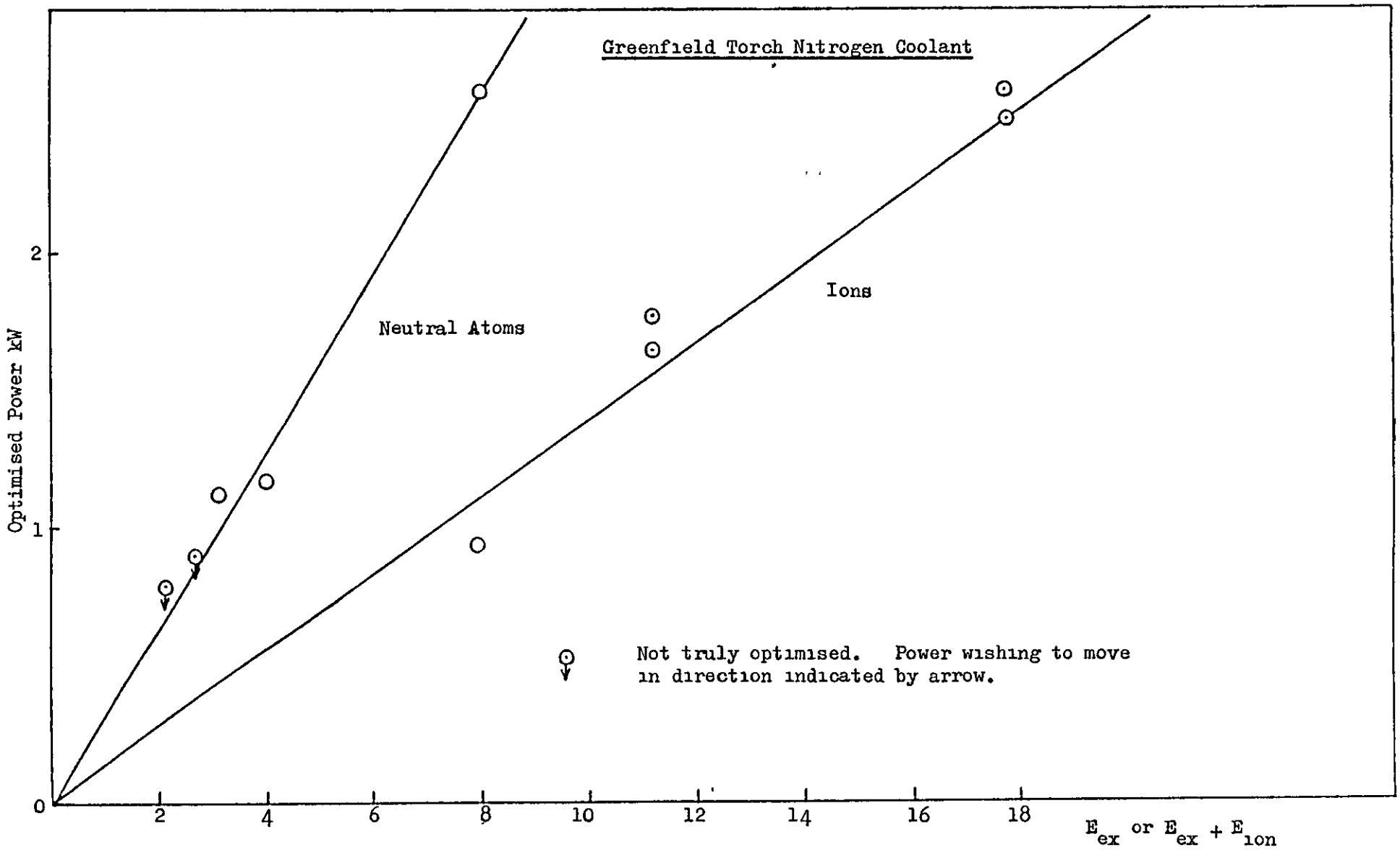

Fig. 98. Plot of optimised power for neutral atom lines and for ion lines versus E_{ex} or $E_{ex} + E_{ion}$ for the nitrogen cooled Greenfield torch.

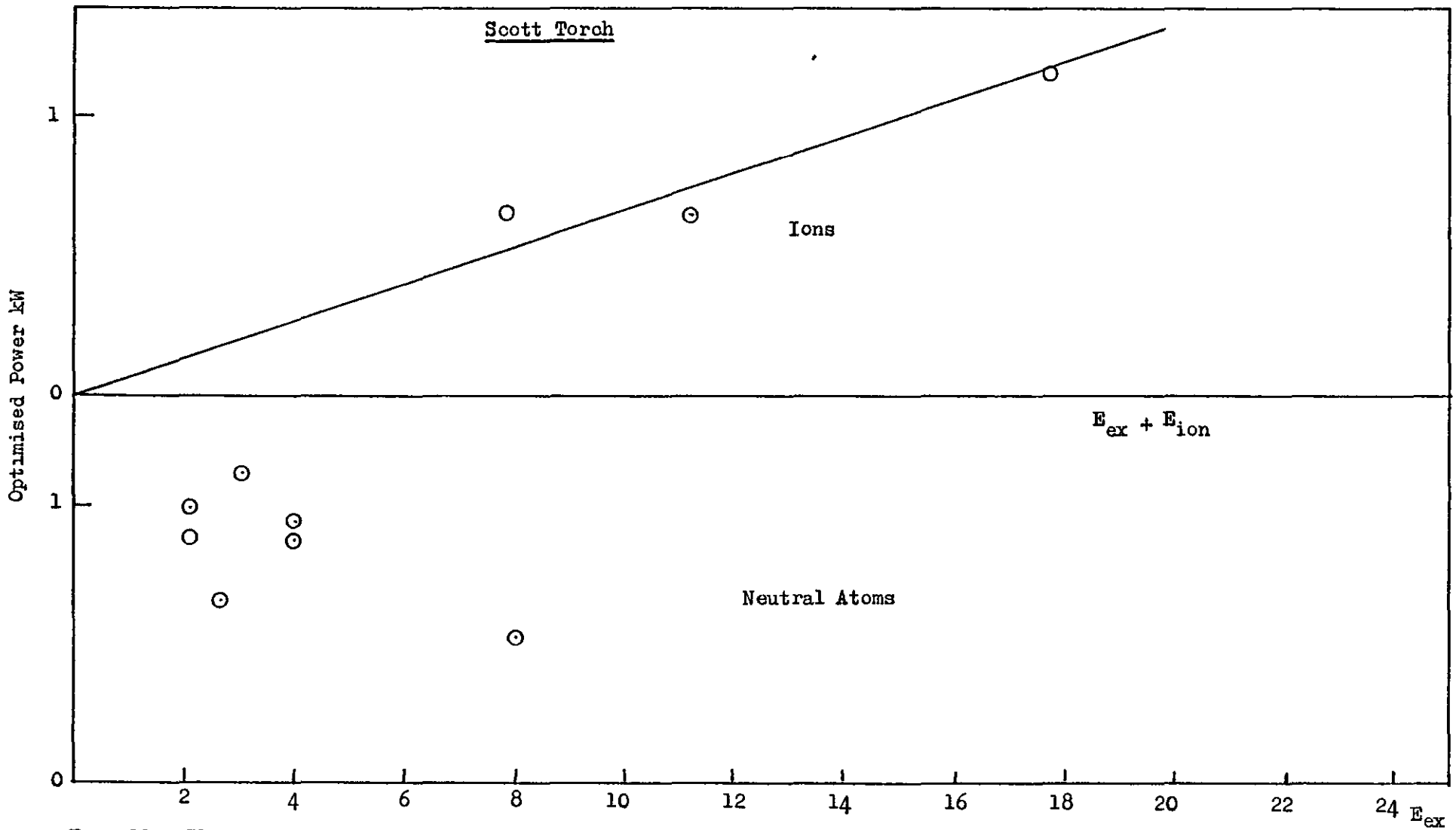

Fig. 99. Plot of optimised power for neutral atom lines and for ion lines versus E_{ex} or $E_{ex} + E_{ion}$ for the argon cooled Scott torch.

It had been hoped that the set of optimisations carried out on the Greenfield torch with argon coolant would allow it to be seen whether the difference was due to the nature of the coolant gas, or to the difference in torches. Unfortunately, six of the eight spectral lines required a lower power than could be achieved. The only line that was strictly optimised with power was the Al 2816Å, while the optimum power for the Zn 3072Å lay between 1.88 and 1.83 kW, these being respectively the lowest power on the large generator and the highest power on the small generator. (These results gave support to the belief in the effectiveness of the optimisation procedure). There is, therefore, no direct evidence to show whether the cell design or the nature of the coolant gas is responsible for the difference in behaviour of the two systems. It is tempting to speculate that the gas is the determining feature and more will be said of this in the concluding chapter.

Table 158 compares the net ratios obtained from the optimised conditions for the three systems.

Table 159. Values of $\frac{x - b}{b - a}$ Obtained from Optimised Conditions for Three Plasma Systems.

Element.	State.	Wavelength Å	Solution conc. p.p.m.	Scott Torch Ar Coolant.	Greenfield Torch N_2 Coolant.	Greenfiel Torch Ar Coolan
Na	U_1	5896	1	205	96*	50*
Cs	U_3	4555	1000	129	343*	95*
Al	U_1	3961	1	17	108	18*
Zn	U	3076	1000	15.6	11.5†	17.7*
Zn	U	3072	1000	1.09	1.35	0.94*
Ba	V_1	4554	1	232	339	146*
V	V_1	3093	1000	1340	765†	1277*
Al	V_2	2816	1000	0.70	1.28	0.62

* True optimisation not reached.

† Interference from N_2 bands.

The values marked with a star are not true optimisations in the sense that some variable had reached its limit before the ratio had peaked. The most common cause of this was the limited range of the power settings, but on occasions values of plasma gas flows and nebuliser flows were indicated that resulted in the plasma being extinguished or becoming unstable.

Although seven out of eight values for the Greenfield torch with an argon coolant suffer from these limitations, and have values which are strictly undetermined, it appears that better values are obtained with a nitrogen coolant than with argon. The two exceptions were Zn 3076 and V 3093. It was suspected that the reason for this might be due to the second positive emission system from the N_2 molecule.

Spectra were photographed from plasmas with nitrogen and argon coolants and weak lines or possibly band heads were visible at those wavelengths where nitrogen was used. They were not visible when an argon coolant was used. In this experiment no solution was aspirated, as strong OH bands in this region might have masked the lines sought. Thus it is felt justifiable to claim that unless there is interference from molecular emission, a plasma with a nitrogen coolant gives a better signal to background ratio than one with an argon coolant, at least for the Greenfield torch and over the wavelength range covered. This improved signal to background ratio, where it occurs, is brought about by a reduction in background, probably due to the smaller plasma that results from a nitrogen cooled system, and a larger signal.

Other generalizations which can be made about the comparisons of the three systems are that the volume of gas consumption tends to increase with increasing power, the length of the plasma tends to increase with power in the optimised systems and the position of preferred observation height tends to be closer to the plasma in the optimised systems and particularly with the nitrogen system.

CHAPTER 11.

CONCLUSIONS AND SUGGESTIONS FOR FUTURE WORK.

Although the early work using the profile meter rapidly showed the deficiencies of the method of signal measurement it did show that the gross signal increased with power in a way which would be consistent with a Boltzman type of excitation. It also established a close connection between optimum viewing position and the power generated in the plasma. This power, of course, controlled the size, heat content and to some extent the temperature of the plasma.

Before proceeding with the measurement of the signals, an examination was made of the noise in the system and of the figures of merit that could be used to compare the various plasmas. A Fourier analysis of the measured signals showed that the noise on the signals was low frequency noise of the type known as pink and proportional to the signal. This conclusion was confirmed by plotting the standard deviation against the signal. The slope of the line was 0.9, certainly closer to the expected slope of 1.0, which would denote proportionality, than 0.5 which would be indicative of the more general square root relationship. A further confirmation was obtained by comparing the signals from two solutions of iron differing in concentration and in exposure by a factor of ten. Neither set of results included the ratio $\sqrt{10}$ and therefore a square root dependence on the signal to noise is excluded.

Since a square root dependence would be expected from the statistical irregularities of the quantised signal, the proportionality exhibited must be due to other variations superimposed on the signal. These could be in gas-flows, nebuliser performance, power stability and impedance. An investigation into the source of this noise,

with a view to its eventual elimination, would be very fruitful as it may well lead to a great increase in the precision of inductively coupled plasma emission spectroscopy, (I.C.P. - O.E.S.).

An examination of the various figures of merit that could be used to compare plasmas led to the following conclusions. The ratio of the spectral radiances of the signal and the background radiation emanating from a plasma is a good indicator of the merit of that plasma and is independent of the spectrometer. The net ratio of signal to background radiation, as measured on a spectrometer, is proportional to the ratio of spectral radiances and is a good indicator of the relative merits of two or more plasmas when the signal to background ratios of all are measured on the same spectrometer. The detection limit is not independent of the spectrometer and can be degraded by the opto-electrical properties of the photomultiplier and the electrical properties of the associated circuitry.

The replacing of the profile meter with a D.V.M. and measuring the potential drop across, in the first case, a 1M ohm resistor and later across a 10M ohm resistor did not increase the measuring accuracy sufficiently to obtain any useful data, but the introduction of an emitter follower impedance changer did enable some data to be obtained. These data confirmed early results that the signals received are a function of height of observation of the tail-flame of the plasma and the power in the plasma. It also showed that the optimum viewing position moved closer to the plasma as the power was increased, which fact led to a hypothesis of which more will be reported later in the chapter. The emission from the sodium 5890Å line increased with power, when observed at a constant height above

the plasma, and finally passed through a maximum, unlike the emission from the two zinc lines, 3072Å and 3076Å, which did not pass through a maximum. This led to a conjecture that the norm temperature had been reached for sodium. However, this was discounted as the maxima at various heights had different values and the value was still increasing as the height of observation moved nearer to the plasma with increasing power. Another conjecture was made that changes in partial pressure of the analyte in the tail-flame could account for the discrepancies. The argument is not very convincing and further investigation could give a greater insight into plasma diagnostics.

The net ratio increased with power and reached a maximum for sodium at modest powers. In the case of zinc 3072Å the net ratio was still increasing at very high powers. In contrast the net ratio from the zinc 3076Å was constant over a wide range of power, starting at low powers and extending to high power, and exhibiting evidence of numerous ridges on the contour map. There was also evidence of two temperature maxima. These ridges were even more pronounced in the case of the boron 2497Å line, although evidence of a maximum at high power occurred. The accuracy of measurement was still not good enough and doubts were beginning to be felt whether the emission, height, power, relationships could be taken in isolation to compare plasmas, as they were probably part of a five dimensioned space model which could not be visualised. A further attempt was made to improve the data for boron, by resorting to integration with a greatly improved measuring set. The presence of ridges on the contour map for net signal were confirmed and the presence of twin peaks on the contour map for net ratio established. This type of

phenomenon could well explain some of the conflicting reports on operating conditions which have appeared in the literature.

One observation, that the optimum viewing height moved closer to the plasma the higher the power, led to the development of a model to explain this curious feature. It was suggested that the analyte reached its maximum temperature whilst still within or close to the end of a long high powered plasma, whereas it reached its maximum temperature more in the tail-flame of a short low-powered plasma. In order to support this model, measurements were made of the excitation temperature of the analyte T_{ex}, along the tail-flame and upto the end of the plasma tunnel, and calculations were then made of the kinetic temperature, T_k, of the analyte, within the tunnel, by using Jakob's equation for heat transfer within a tube furnace. The agreement obtained was remarkably good.

The implication of these results is that there is good agreement between T_{ex} and T_k and therefore the nitrogen cooled plasma is in L.T.E. It is not, however, a rigorous proof that this state exists.

The next stage in the work was to establish a method of working which accounted for all the variables in the system. There were coolant, plasma and nebuliser gas flows, height of observation and power in the plasma. It had been established that all these variables were interelated. Different methods of optimising were tried; these included Factorial Design and Simplex methods. Neither of these was very successful. One difficulty with both these methods is that two discrete levels of each variable have to be chosen. If the difference between the two levels is small, the effect may be swamped by errors of measurement, while if too high, the points may lie on slopes on either side of the maximum. Both cases give rise to apparently capricious results. It was found that the Alternating

Variable Search method was more successful. This method is simply to maximise the ratio when changing one variable at a time. This sequence may have to be repeated many times. Under some circumstances the optimisation converges very quickly, although when diagonal ridges occur the convergence can be slow and require many cycles.

The real advantage is that the variables can be changed quickly and continuously over a wide range and the effect can be seen quickly so the problem of choosing appropriate discrete levels does not occur.

After proving the system worked by using two channels of the Polychromator and an X-Y recorder to measure the signal and the background simultaneously, a Signal Divider network was constructed. Unfortunately, because of the noise in the system, heavy damping had to be used with the result that the sequence was not obtained quite instantaneously. However, it enabled the work to continue.

This optimisation of variables is a potential area of research with a view to automation of the procedure. Quite clearly the tedious and time consuming manual optimisation described in this thesis could be controlled by a micro computer and servo-mechanisms. The resultant fast optimisation of the variables would lead to improved working as the prevailing practice in most laboratories is to carry out a superficial optimisation which the experience of this work shows, must often be far from the true optimum conditions.

A look was also taken at the profile of the tail-flame of the plasma using quartz optical fibres to examine an image of the plasma tail-flame. It was found that the highest signal to background ratio was to be found in a vertical area 7 mm high and 0.7 mm wide. It was inferred that a vertical slit would give better signal to background

ratios than would a horizontal slit and this was confirmed by rotating the image with a Dove prism. Further investigation may well show that a cylindrical lens filling the width of a horizontal slit with an image of a small central part of the tail-flame may give the best result.

The main part of this work lay in comparing the net signal to background ratios of three plasma systems on one spectrometer. The three systems were the Scott torch with argon coolant and the Greenfield torch with argon and nitrogen coolants. High and low power generators were used as necessary, in the hope that they would give the power range required. Since the Meinhard nebuliser is normally used with the Scott torch and because it was known to be efficient, it was used with the three systems.

A surprising discovery was that the Scott spray-chamber, which is normally used with the Scott torch, gave worse signal to background ratios than did the cyclone chamber normally used with the Greenfield torch. The reason for this was that, because of a greater transfer efficiency, a similar, or greater, amount of solute was carried to the plasma at a slower rate by the cyclone chamber. This is probably a function of the surface to volume ratio of the two chambers and could bear further investigation, as could the seemingly impossible discovery that the uptake-rate of the nebuliser was less when spraying into free air than when spraying into either of the two chambers.

The central question (what is the optimum wattage necessary to do useful analytical work?) has not been answered in a completely unambiguous fashion. The Scott torch was found to require powers ranging from 0.53 to 1.21 kW, when a series of lines varying in difficulty of excitation were optimised for signal to background ratio.

However the same set of lines gave, in five cases out of eight and with powers varying from less than 0.79 upto 2.6 kW, better signal to background ratios on the Greenfield torch with nitrogen coolant. Of the other three cases, two of the lines were subject to molecular interference and the other was not truly optimised since the optimisation required a lower power than could be obtained from either generator. The Greenfield torch with an argon coolant could not be optimised in most cases as the power could not be reduced sufficiently for the gas flows required. However, in one case a power of 3.92 kW was required, at another 1.86 kW and it may be said that the bottom end was <1.39 kW. At the two powers where optimisation was achieved the net ratios were similar to those obtained with the Scott torch.

It can be surmised that similar net ratios would be obtained with both torches when each is run with the same coolant gas and that the power required is only a function of the size of the torch. It must be emphasised that attempts to run the Scott torch with a nitrogen coolant were unsuccessful and it is not known whether or not the net ratios would have been higher even had this been possible. The power controlling factor is the energy that is required to dissociate and ionise the nitrogen, and although the gas flows may be lower in a Scott torch there is little doubt that a nitrogen cooled plasma, if such were possible, would require more power than the argon cooled Scott torch.

The nitrogen cooled plasma is smaller than the argon cooled plasma, a fact that undoubtedly leads to lower background radiation. It may be noted that other gases, such as hydrogen, put an even greater thermal pinch onto the argon plasma and may well lead to even lower background radiation. This fact has been partially investigated by the author and

there is evidence that improved signal to background ratios could result from the use of hydrogen.

This work has taken account of an intrinsic property of the plasma which is measured by the net signal to background ratios. No account has been taken of the other properties of the plasma which are power dependent such as convenience of operation, dissociation of molecules and ionisation. These dependencies are little known and are waiting to be investigated in a rigorous fashion.

On the question of choice of torch, it was observed that the injector of the Scott torch, which is an integral part of the torch, was much more readily blocked by aerosols of high solute content, such as 1% w/v aluminium nitrate than was the Greenfield torch. It has also been reported by Browner [78] that a low powered system with a Scott torch was easily blocked by carbon when organic solvents were nebulised through it. In this author's experience no such blockage occurs with the large torch operating at high power.

Browner [78] also reported the presence of a green hue, denoting Swann bands, in his low powered system. This hue is absent when high power is used nor are the C-C bands visible in the spectrum obtained from such a system. This has nothing to do with the type of torch, but is an example of dissociation of molecules by the use of high power.

Thus in answer to the question of the optimum wattage necessary to do useful work, it is possible to say that the operating power depends

[78] R.F.Browner, The XXIst Colloquium Spectroscopicum Internationale and 8th International Conference on Atomic Spectroscopy, Cambridge, United Kingdom, July, 1979.

on the type of torch which is used and that depends on the use to which it is to be put and the effect which is desired. With the present state of the art and assuming that the full power of the technique is to be exploited, this author believes that 4-5 kW in the plasma is a reasonable compromise.

In conclusion, the interesting differences in behaviour between the argon cooled Scott torch and the nitrogen cooled Greenfield torch, apparent when an attempt was made to correlate the E_{ex} or $E_i + E_{ex}$ and the optimised power and also the generally anomalous behaviour of the neutral atom lines in other respects, leads to the speculation that a different mode of excitation is operating in the divergent cases.

The quite convincing correlation for both neutral and ion lines which was apparent with the nitrogen cooled torch was consistent with a Boltzmann type of excitation as was the correlation with the ion lines in the Scott torch. The neutral atom lines do not seem to correlate with E_{ex} at all when excited by the argon cooled plasma of the Scott torch and this could be due to a very different type of excitation.

It has been postulated [79] that some excited argon atoms do not spontaneously return to the ground state through a radiative transition but remain in the metastable state. The excitation energy is then transferred by a process known as Penning [79] ionisation:

[79] J.Robin., 3rd Congress. int Spectrom. Absorpt. et Fluoresc. Atomiques, Paris, 1971, Methodes Physiques d'Analyse (special issue, 3rd C.I.S.A.F.A.).

$$Ar^{Meta} + X \longrightarrow \begin{matrix} Ar + X^{+*} + e \\ \searrow \\ Ar + X^{+} + e \end{matrix}$$

The argon metastables have excitation energies around 11 ev and are thus able to excite ion lines. It is thus possible that this type of excitation may increase the population of ions, excited or otherwise, and as a consequence perturb the equilibria between the excited levels and between ionisation states. Thus it may be expected that less power will be required to excite some lines than would normally be the case.

This is only a hypothesis and the evidence is limited; the work which has been done, although time consuming and tedious, only points the way to further investigation and the accumulation of much more data - preferably by a fully automated computer controlled system.